Species specific nitrogen isotope analysis by NanoSIMS

Dissertation

zur Erlangung des akademischen Grades
'doctor rerum naturalium (Dr. rer. nat.)' der Fachbereiche:
08 - Physik, Mathematik und Informatik
09 - Chemie, Pharmazie und Geowissenschaften
10 - Biologie und der Universitätsmedizin

vorgelegt von
Kexue Li
Max Planck Graduate Center
Johannes Gutenberg-Universität Mainz

verfasst am Max-Planck-Institut für Chemie

Datum der mündlichen Prüfung: 13. Oktober 2015

I hearby declare that I wrote the dissertation submitted without any unauthorised external assistance and used only sources acknowledged in the work. All textual passages which are appropriated verbatim or paraphrased from published and unpublished texts as well as all information obtained from oral sources are duly indicated and listed in accordance with bibliographical rules. In carrying out this research, I complied with the rules of standard scientific practice as formulated in the statutes of the Johannes Gutenberg University, Mainz, to ensure standard scientific practice.

August 3, 2015
Kexue Li

Abstract

The atmospheric cycling of reactive nitrogen is a focus of both scientific and policy concern, because of the importance of reactive nitrogen in controlling the formation of tropospheric ozone. Atmospheric reactive nitrogen also plays a role in the formation of particulate matter and its long range transport modifies the global carbon cycle by providing nitrogen fertilization to remote ecosystem. Measurements of stable nitrogen isotope ratios ($^{15}N/^{14}N$) offer a means of discriminating sources of nitrogen, and reactions involved in reactive nitrogen cycling via their specific isotopic signatures.

In this thesis, I demonstrate that Nano Secondary Ion Mass Spectrometry (NanoSIMS) can be used to differentiate different nitrogen containing species commonly observed in atmospheric aerosol particles, with sub-micrometer spatial resolution, on the basis of the relative intensity of secondary ion signals, both in negative and positive secondary ion mode without the need to chemically or physically separate the samples. Compounds tested include nitrate, nitrite, ammonium salts, urea, amino acids, biological tissue and imidazole. I show that NO_2^- secondary ion is unique to the decomposition of nitrate and nitrite salts while NH_4^+ secondary ion is unique to samples containing ammonium ions or amino groups, but were not observed in biological tissue. CN^- signals are obtained from all nitrogen bearing compounds but relative signal intensities are highest for organic nitrogen containing compounds.

I further demonstrate that stable isotope ratios can be measured accurately and precisely using the $^{15}N^{16}O_2^- / ^{14}N^{16}O_2^-$ - molecular ion ratio on pure nitrate salts ($NaNO_3$ and KNO_3) deposited on gold foils. The precision of long term measurements on the in-house $NaNO_3$ standard is ± 0.6 ‰ for a raster size of 5×5 μm^2. The difference in the matrix specific instrumental mass fractionation (IMF) between $NaNO_3$ and KNO_3 is 7.1 ± 0.9 ‰. The secondary ion $^{23}Na^{12}C_2^-$ can be a serious interference when the $^{15}N^{16}O_2^-$ molecular ion is used to measure the nitrogen isotope composition of sodium nitrate, which is internally mixed with carbon containing compounds or deposited on carbon containing sample substrates.

Even in the absence of this interference (KNO_3) the presence of carbon in aerosol-like mixture samples leads to a matrix effect which can be quantified by $\delta^{15}N_{bias} = (101 \pm 4) \cdot f - (101 \pm 3)$ ‰, where $f = {}^{14}N^{16}O_2^- / ({}^{14}N^{16}O_2^- + {}^{12}C^{14}N^-)$.

There is neither a matrix effect induced by the presence of variable N/C ratios, nor do interferences complicate the analysis when the $^{12}C^{15}N^- / ^{12}C^{14}N^-$ molecular ion ratio is used to determine the isotopic signature of nitrate. Using $^{14}N^{16}O_2^-$ as mask mass can make these

measurements species specific for nitrate and depositing the sample on a carbon containing sample substrate can enhance the signal intensity for pure nitrate particles.

Zusammenfassung

Der atmosphärische Kreislauf reaktiver Stickstoffverbindungen beschäftigt sowohl die Naturwissenschaftler als auch die Politik. Dies ist insbesondere darauf zurückzuführen, dass reaktive Stickoxide die Bildung von bodennahem Ozon kontrollieren. Reaktive Stickstoffverbindungen spielen darüber hinaus als gasförmige Vorläufer von Feinstaubpartikeln eine wichtige Rolle und der Transport von reaktivem Stickstoff über lange Distanzen verändert den biogeochemischen Kohlenstoffkreislauf des Planeten, indem er entlegene Ökosysteme mit Stickstoff düngt. Die Messungen von stabilen Stickstoffisotopenverhältnissen ($^{15}N/^{14}N$) bietet ein Hilfsmittel, welches es erlaubt, die Quellen von reaktiven Stickstoffverbindungen zu identifizieren und die am Stickstoffkeislauf beteiligten Reaktionen mithilfe ihrer reaktionsspezifischen Isotopenfraktionierung genauer zu untersuchen.

In dieser Doktorarbeit demonstriere ich, dass es möglich ist, mit Hilfe von Nano-Sekundärionenmassenspektrometrie (NanoSIMS) verschiedene stickstoffhaltige Verbindungen, die üblicherweise in atmosphärischen Feinstaubpartikeln vorkommen, mit einer räumlichen Auflösung von weniger als einem Mikrometer zu analysieren und zu identifizieren. Die Unterscheidung verschiedener stickstoffhaltiger Verbindungen erfolgt anhand der relativen Signalintensitäten der positiven und negativen Sekundärionensignale, die beobachtet werden, wenn die Feinstaubproben mit einem Cs^+ oder O^- Primärionenstrahl beschossen werden. Die Feinstaubproben können direkt auf dem Probenahmesubstrat in das Massenspektrometer eingeführt werden, ohne chemisch oder physikalisch aufbereited zu werden. Die Methode wurde Mithilfe von Nitrat, Nitrit, Ammoniumsulfat, Harnstoff, Aminosären, biologischen Feinstaubproben (Pilzsporen) und Imidazol getestet. Ich habe gezeigt, dass NO_2 Sekundärionen nur beim Beschuss von Nitrat und Nitrit (Salzen) mit positiven Primärionen entstehen, während NH_4^+ Sekundärionen nur beim Beschuss von Aminosäuren, Harnstoff und Ammoniumsalzen mit positiven Primärionen freigesetzt werden, nicht aber beim Beschuss biologischer Proben wie z.B. Pilzsporen. CN^- Sekundärionen werden beim Beschuss aller stickstoffhaltigen Verbindungen mit positiven Primärionen beobachtet, da fast alle Proben oberflächennah mit Kohlenstoffspuren kontaminiert sind. Die relative Signalintensität der CN^- Sekundärionen ist bei kohlenstoffhaltigen organischen Stickstoffverbindungen am höchsten.

Darüber hinaus habe ich gezeigt, dass an reinen Nitratsalzproben ($NaNO_3$ und KNO_3), welche auf Goldfolien aufgebracht wurden speziesspezifische stabile Stickstoffisotopenverhältnisse mithilfe des $^{15}N^{16}O_2^-$ / $^{14}N^{16}O_2^-$ - Sekundärionenverhältnisses genau und richtig gemessen werden können. Die Messgenauigkeit auf Feldern mit einer Rastergröße von 5×5 μm^2 wurde anhand von Langzeitmessungen an einem hausinternen $NaNO_3$ Standard als ± 0.6 ‰ bestimmt. Die Differenz

der matrixspezifischen instrumentellen Massenfraktionierung zwischen $NaNO_3$ und KNO_3 betrug 7.1 ± 0.9 ‰. $^{23}Na^{12}C_2^-$ Sekundärionen können eine ernst zu nehmende Interferenz darstellen wenn $^{15}N^{16}O_2^-$ Sekundärionen zur Messung des nitratspezifischen schweren Stickstoffs eingesetzt werden sollen und Natrium und Kohlenstoff im selben Feinstaubpartikel als interne Mischung vorliegt oder die natriumhaltige Probe auf einem kohlenstoffhaltigen Substrat abgelegt wurde. Selbst wenn, wie im Fall von KNO_3, keine derartige Interferenz vorliegt, führt eine interne Mischung mit Kohlenstoff im selben Feinstaubpartikel zu einer matrixspezifischen instrumentellen Massenfraktionierung die mit der folgenden Gleichung beschrieben werden kann: $\delta^{15}N_{bias} = (101 \pm 4) \cdot f - (101 \pm 3)$ ‰, mit $f = {}^{14}N^{16}O_2^- / ({}^{14}N^{16}O_2^- + {}^{12}C^{14}N^-)$.

Wird das $^{12}C^{15}N^-$ / $^{12}C^{14}N^-$ Sekundärionenverhältnis zur Messung der stabilen Stickstoffisotopenzusammensetzung verwendet, beeinflusst die Probematrix die Messungsergebnisse nicht, auch wenn Stickstoff und Kohlenstoff in den Feinstaubpartikeln in variablen N/C–Verhältnissen vorliegen. Auch Interferenzen spielen keine Rolle. Um sicherzustellen, dass die Messung weiterhin spezifisch auf Nitratspezies eingeschränkt bleibt, kann eine $^{14}N^{16}O_2^-$ Maske bei der Datenauswertung verwendet werden. Werden die Proben auf einem kohlenstoffhaltigen, stickstofffreien Probennahmesubstrat gesammelt, erhöht dies die Signalintensität für reine Nitrat-Feinstaubpartikel.

Contents

Abstract v
Zusammenfassung vii
Acknowledgement ix
Contents xi
1 Introduction 1
1.1 The nitrogen cycle 1
1.2 Tropospheric processing of N_r and global climate change 3
1.2.1 Atmospheric N_r emission and processing 3
1.2.2 Impact via controlling tropospheric ozone formation 5
1.2.3 Impact on aerosol formation, properties and global climate change 6
1.2.4 Impact via influencing the carbon cycle 7
1.3 Nitrogen isotopes in atmospheric aerosol 9
1.3.1 Nitrogen isotopes 9
1.3.2 Nitrogen isotopes in the environment 9
1.4 Research objectives and thesis outline 14
2 Preparation of aerosol samples and standards 15
2.1 Sample preparation 15
2.1.1 Bulk samples pressed into gold foil 15
2.1.2 Aerosol-like mixture sample preparation 17
2.2 Description and composition of N isotope standards 20
3 Recognition of different N-bearing species in the NanoSIMS 23
3.1 Introduction 23
3.2 Materials and Methods 25
3.3 Results and Discussion 26
3.3.1 Mass spectra of nitrate and nitrite species 26
3.3.2 Mass spectra of ammonium containing inorganic salts 28
3.3.3 Speciation of nitrogen containing compounds using a combination of positive and negative mass spectra 30
3.3.4 Speciation of nitrogen containing compounds using negative secondary ion mass

spectra 32
3.3.5 Speciation of nitrogen containing compounds using positive secondary ion mass spectra 33
3.3.6 Feasibility study for speciated isotope analysis 34
3.4 Conclusions 35
4 Stable N isotope analysis of nitrate by NanoSIMS using the $^{15}N^{16}O_2^-$ / $^{14}N^{16}O_2^-$ - ratio. 37
4.1 Introduction 37
4.2 Materials and Methods 38
4.2.1 Experimental conditions and NanoSIMS analysis 38
4.2.2 Heterogeneous samples 39
4.2.3 NanoSIMS image data processing 42
4.3 Nitrogen isotope measurements in bulk nitrates 45
4.3.1 Influence of experimental parameters 45
4.3.2 Results and discussion 55
4.3.3 Conclusions 59
4.4 Nitrogen isotope measurements on aerosol-like mixture samples 61
4.4.1 IMF in $\delta^{15}N$ calculation 61
4.4.2 Results 61
4.4.3 Discussion 67
4.4.4 Conclusions 73
5 Stable N isotope analysis of nitrate by NanoSIMS using the $^{12}C^{15}N^-$ / $^{12}C^{14}N^-$ - ratio 75
5.1 Introduction 75
5.1.1 Secondary ion CN^- in SIMS analysis 75
5.1.2 Further exploration of nitrate species N isotope measurement 76
5.2 Experimental 77
5.2.1 Sample preparation 77
5.2.2 NanoSIMS analysis 77
5.2.3 Data processing 78
5.3 Results and discussion 81

5.3.1 Matrix effect induced by presence of carbon 81
5.3.2 $^{14}N^{16}O_2^-$ mask levels 81
5.4 Conclusion and future experiments 83
6 Conclusions: Main findings and outlook 85
Abreviations 89
List of tables 91
List of figures 93
Bibliography 97
Appendix 115
A Programming work based on MATLAB 115
A.1 Calculation of molecule masses program 115
A.2 Isotope mode NanoSIMS data processing program 119
A.2.1 Program interfaces and operations 119
A.2.2 Main mathematical calculations 126
A.3 Image mode NanoSIMS data processing program 128
A.3.1 Reading data and initial settings 129
A.3.2 Single im file calculation 135
A.3.3 Auto im file calculation 141
A.3.4 ROI mask calculation 141
A.3.5 Result file processing 141
B Details of all analysis spots on bulk standards, isotope ratio measured by $^{15}N^{16}O_2^-$ / $^{14}N^{16}O_2^-$ 149
C Details of all analysis spots on aerosol-like mixture standards, isotope ratio measured by $^{15}N^{16}O_2^-$ / $^{14}N^{16}O_2^-$ 179
D Details of all analysis spots on aerosol-like mixture standards, isotope ratio measured by $^{12}C^{15}N^-$ / $^{12}C^{14}N^-$ 183
Curriculum vitae 189

1 Introduction

1.1 The nitrogen cycle

The global nitrogen cycle plays a central role in sustaining life on the Earth. On a global scale a major fraction of the nitrogen is present in the form of inert N_2 gas, which is not biologically available to most organisms and does not participate in atmospheric reactions. Therefore, the global biogeochemical nitrogen cycle usually focuses on the N_r (reactive nitrogen) available in the system. An important key aspect of the global nitrogen budget is the conversion of inert N_2 gas to N_r. In preindustrial times, most of the conversion took place in the form of biological nitrogen fixation. Table 1-1 lists the main sources of fixed nitrogen worldwide. Annually about 413 Tg yr^{-1} of nitrogen is fixed by natural and anthropogenic activities and processed chemically and physically (Fowler et al., 2013). After nitrogen is fixed to N_r, it is inter-converted in the environment into different forms by steps of transformations, causing multiple effects in the atmosphere, terrestrial, freshwater and marine ecosystems. Some nitrogen containing compounds, e.g. isocyanic acid and hydrogen cyanide, also severely impact human health (Galloway et al., 2003). The lifetime of N_r in the atmosphere varies between a few weeks (NO_y, NH_x < 1 month) and more than a century (N_2O > 100 years). In terrestrial ecosystems the usual lifetime is a few decades. The average life time of species such as dead soil organic matter, plant N, microbes, ammonium and ammonia, is less than 10-50 years, with the exception of peatlands where the lifetime can extend to 10^2-10^3 years. The lifetime of N_r in the ocean is poorly constraint, however, it is probably longer than in terrestrial ecosystems, namely, 10-100 years (Fowler et al., 2013).

The nitrogen cycle consists of the following main processes:

- Biological Nitrogen Fixation (Postgate 1998): $N_2 + 3H_2 \rightarrow 2NH_3$.
- Industrial N fixation (Galloway et al., 2008): conversion of N_2 into NH_3 by the Haber–Bosch process.
- Nitrification (Verstraete and Focht 1977): $2NH_3 + e^- + 3O_2 \rightarrow 2NO_2^- + 2H_2O + 2H^+$, $2NO_2^- + O_2 \rightarrow 2NO_3^-$.
- Denitrification (Verstraete and Focht 1977, Freyer et al., 1993): $2NO_3^- + 12H^+ + 10e^- \rightarrow N_2 + 6H_2O$.
- Other reactions include assimilation, ammonification and the annamox reaction.
- Physical processes affecting the nitrogen cycle include volatilization, weathering of rocks, runoff and leaching (Sutton et al., 2011).

1. INTRODUCTION

Human activities have greatly modified the global nitrogen cycle. From Table 1-1 it can be seen that mankind is responsible for half of the total fixed nitrogen (210 Tg yr^{-1}) both through the industrial production of nitrogen fertilizer (reduced nitrogen) and as a byproduct of fuel combustion (oxidized nitrogen). The industrial production of nitrogen fertilizer has immensely benefited global food production. About half of global human population depends on the increased production of agricultural cops, due to the use of nitrogen fertilizer (De Vries et al., 2009). On the other hand, human fixation of nitrogen affects human health via aerosols and ozone formation (Cohen et al., 2005). Terrestrial ecosystems can be modified resulting in loss in biodiversity (Bobbink et al., 2010) and climate can be changed (Erisman et al., 2013). 40-50 Tg yr^{-1} anthropogenic emission of N_r are transferred from the land to the ocean and 30 Tg yr^{-1} are transferred from the atmosphere to the ocean. However, so far very few international regulations attempting to regulate and reduce the transfer of N_r to oceans are in place (Fowler et al., 2013).

Table 1-1. A summary of sources of fixed nitrogen from Fowler et al. (2013). *: biomass combustion and soil NO emissions are coming from existing N_r, they do not count towards total nitrogen fixation.

sources			**N_r emission (Tg yr^{-1})**
natural	biological fixation	terrestrial ecosystems	58, with a range 40-100
		marine ecosystems	140 ± 50
		total biological fixation	*198*
	lightning		5
	total natural sources		203 ± 50
anthropogenic	oxidized nitrogen	fossil fuel combustion	30
		biomass combustion*	5
		soil NO emissions*	5
		total oxidized nitrogen	*40*
	reduced nitrogen	industrial production	120
		biological nitrogen fixation in cropland	60
		total reduced nitrogen	*180*
	total anthropogenic nitrogen fixation		210
total			**413**

1.2 Tropospheric processing of N_r and global climate change

1.2.1 Atmospheric N_r emission and processing

Figure 1-1 illustrates the global atmospheric processing of N_r including the main sources, chemical pathways, products and the magnitudes of the fluxes (Fowler et al., 2013). Anthropogenic N_r emissions increase every year, dominated by agricultural activities. The using of fossil fuel is also playing an important role, especially for the application of new biofuels adding a rapidly changing dimension (Galloway et al., 2008), as NO_x emissions from biodiesel are higher. The emissions of N_r to atmosphere from agriculture are mainly in the form of ammonia (NH_3), while combustion related emissions are in the form of nitrogen oxides (NO_x = NO + NO_2). Approximately 87.5 % NO_x emission (35 Tg N yr^{-1}) and 58 % NH_3 emission (40 Tg N yr^{-1}) are triggered by human activities. The transportation and processing of N_r in the atmosphere generates secondary pollution, as NO_x emissions feed tropospheric ozone formation and play an important role in the radical chemistry in the atmosphere, in particular at night. Moreover, NO_x and NH_3 play an important role in the formation of secondary aerosols like ammonium nitrate (NH_4NO_3) and ammonium sulfate $(NH_4)_2SO_4$ (Kendall and McDonnell 1998, Fowler et al., 2013). The main reaction pathways of primary pollutants NO_x and other nitrogen oxide compounds are shown in Figure 1-2.

While research has already been done on inorganic N_r, only recently scientific interest focussed on organic N_r. Evidence that organic reactive nitrogen may play an important role has accumulated over the years (Neff et al., 2002, Cornell et al., 2003) but its quantitative importance to total airborne nitrogen (20 – 40 % of total particulate nitrogen), has only recently been appreciated (Freyer 1991, Cape et al., 2011). The role of organic N_r in the Earth system is poorly constrained. Sources and reactions leading to its formation, its role in particle nucleation, health effects, its contribution to brown carbon and its role in the long-range transport are less well understood and direct measurements of individual species are just started (Sutton et al., 2011).

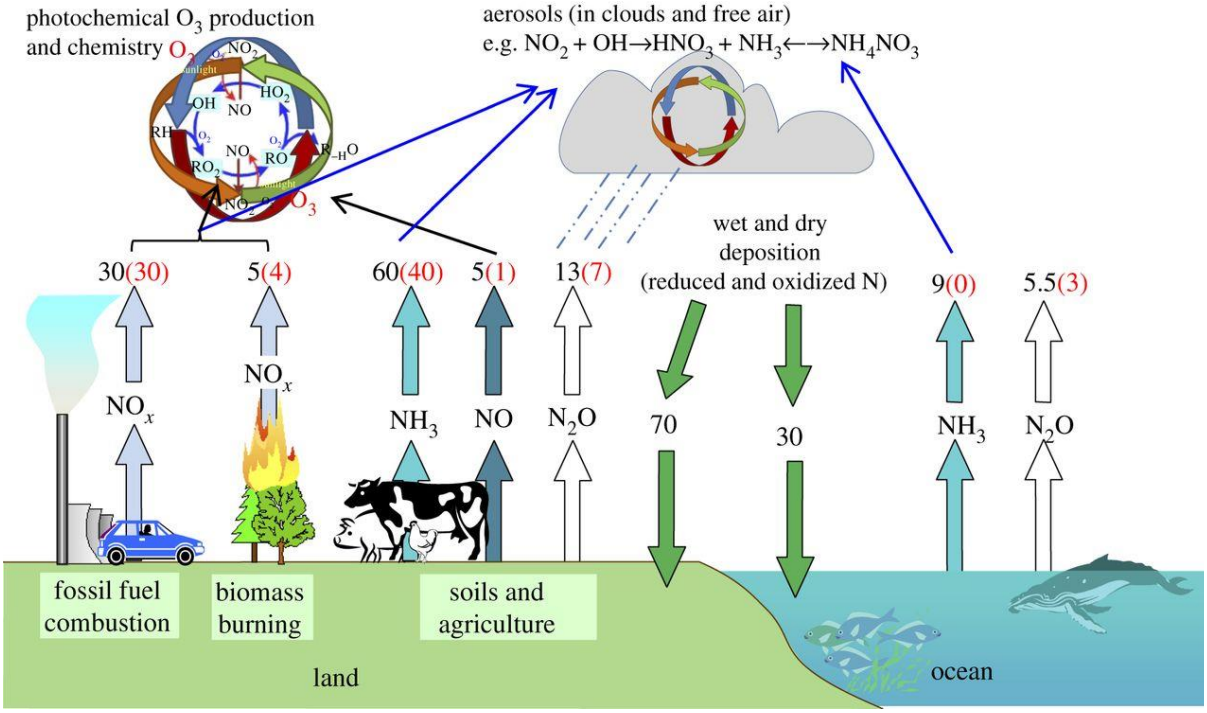

Figure 1-1. The global atmospheric processing of N_r, illustrating the main sources, the main chemical pathways and products, and the magnitudes of the fluxes (units Tg yr^{-1}). The emission flux values in black are the total fluxes while the red values indicate the anthropogenic contribution. Figure taken from (Fowler et al., 2013).

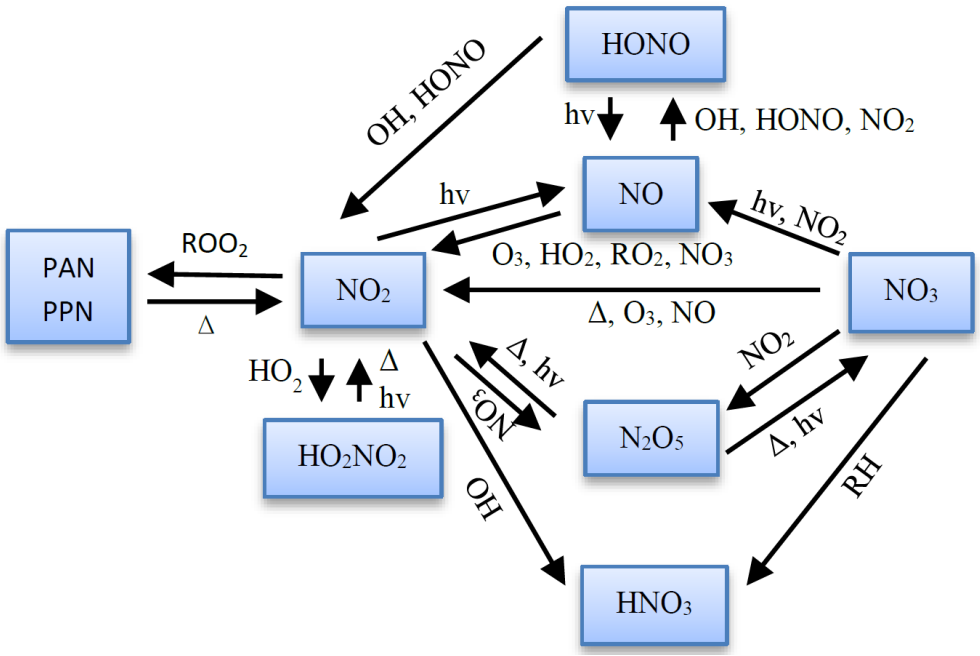

Figure 1-2. Illustration of the interaction between the various nitrogen oxide compounds in the troposphere. Δ represents energy leading to thermal degradation, hv solar radiation leading to photo dissociation and RH a hydrocarbon reacting with the specie in questing. PPN is a notation for peroxy propionyl nitrate, but includes also other peroxy nitrates. Figure taken from (Derwent and Hertel 1998).

1.2.2 Impact via controlling tropospheric ozone formation

According to the IPCC report (AR4, chapter 7) tropospheric ozone is the third most important global warming radiative forcing (first CO_2 and second CH_4) (Solomon et al., 2007). In near surface of the Earth, tropospheric ozone also effects human health, forest ecosystems and agricultural crops (National Research Council (U.S.). Committee on Tropospheric Ozone Formation and Measurement. 1991).

In the presence of NO_x, ozone is produced by photochemical oxidation of CO, CH_4 and non-methane VOCs (volatile organic compounds) in the troposphere (Heaton 1984, Seinfeld and Pandis 2012). In sunlight (wavelengths < 424 nm), ozone is produced via the reactions:

$$NO_2 + h\nu \rightarrow NO + O(^3P) \qquad \text{Reaction 1-1}$$

$$O(^3P) + O_2 + M \rightarrow O_3 + M \qquad \text{Reaction 1-2}$$

Reaction 1-2 is the major ozone source in the atmosphere. However, alongside O_3, NO is produced in Reaction 1-1 and reacts rapidly with ozone in Reaction 1-3 making a null cycle. M stands for a molecule or atom which is not transformed during reaction but required to absorb excess energy, e.g. of an activated intermediate state. $O(^3P)$ stands for the ground state of oxygen atom.

$$O_3 + NO \rightarrow NO_2 + O_2 \qquad \text{Reaction 1-3}$$

Considering Reaction 1-1 and Reaction 1-2, net ozone production occurs whenever NO is converted to NO2 without consuming ozone. This happens, whenever NO is oxidized to NO_2 via HO_2 or organic peroxy radicals, which form during the reaction of VOC or CO with the OH radical, i.e. whenever Reaction 1-3 is bypassed and instead Reaction 1-4 to Reaction 1-6 occur:

$$VOC + OH \rightarrow VOC' + H_2O \qquad \text{Reaction 1-4}$$

$$VOC' + O_2 \rightarrow VOC'' + HO_2 \qquad \text{Reaction 1-5}$$

$$HO_2 + NO \rightarrow NO_2 + OH \qquad \text{Reaction 1-6}$$

In situ chemical production of O_3 results primarily from the reaction of peroxy radicals with NO: HO_2 + NO (70 %) but RO_2 + NO (20 %) is an important second source of ozone (Seinfeld and Pandis 2012). Depending on the precursor VOC, both VOC' and VOC'' in Reaction 1-4 and Reaction 1-5 can be organic peroxy radicals (RO_2). Hence, the reaction chain initiated by Reaction 1-4 can result in the production of more than one ozone molecule.

Ozone chemistry shows a complex and highly non-linear dependence on NO_x mixing ratios. Due to the competition for the hydroxyl radical between NO_x and VOCs in Reaction 1-4 and Reaction 1-7, the ratio of VOC/NO_x and their concentrations controls ozone formation in the troposphere. Figure 1-3 illustrates the dependence of O_3 production on the initial mixtures of NO_x

and VOC in an ozone isopleth plot. In a NO_x limited ozone production regime more, NO_x emissions will increase ozone production via the reaction channels outlined above. However, in a NO_x rich environment (VOC-limited ozone production) more NO_x, which is generally emitted from its sources in the form of NO, will titrate ozone (trough Reaction 1-3) and will subsequently be remove from the system through the terminal reaction outlined below obstructing the further production of ozone.

$$NO_2 + HO + M \rightarrow HNO_3 + M \qquad \text{Reaction 1-7}$$

Because NO_x gets cycled back and forth between NO and NO_2 in O_3 generation, NO_x can be viewed as the catalyst in O_3 formation and its emissions strongly affect the ozone production efficiency (OPE) (Seinfeld and Pandis 2012). Hydroxyl radical also plays a key role during O_3 formation and without ozone there would be no OH radicals.

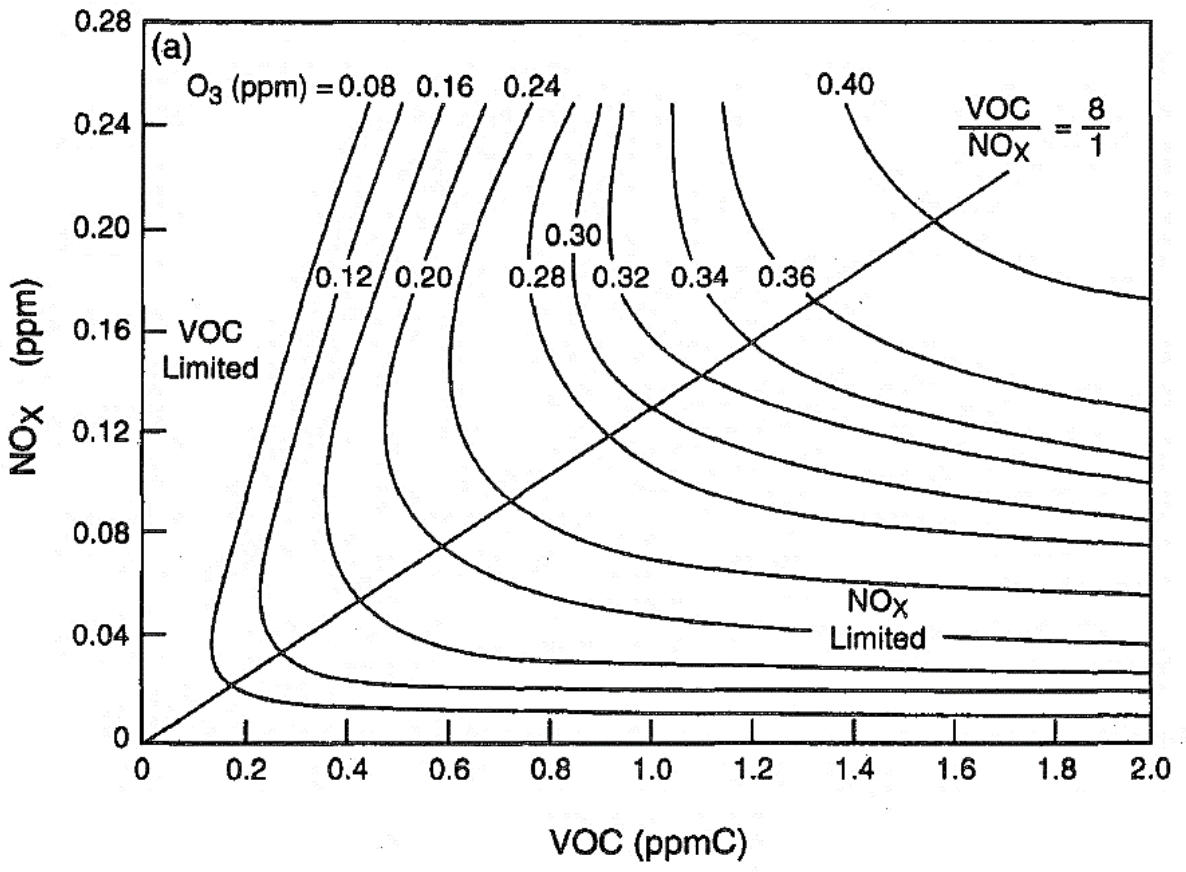

Figure 1-3. Two dimensional ozone isopleths generated from initial mixtures of NO_x and VOC based on EKMA model. Figure taken from Finlaysonpitts and Pitts (1993).

1.2.3 Impact on aerosol formation, properties and global climate change

The reactions between gas phase NH_3 and gas phase acids generate new aerosol particles. NH_3

also can condense onto existing atmospheric particles and modifies their ability to seed cloud droplets. Sulfate and nitrate aerosols form in the presence of ammonium. The irreversible reaction between NH_3 (g) and H_2SO_4 (g) has two steps (Hov et al., 1994):

$$NH_3\,(g) + H_2SO_4(g) \rightarrow NH_4HSO_4(p) \qquad \text{Reaction 1-8}$$

$$NH_3(g) + NH_4HSO_4\,(g) + M \rightarrow (NH_4)_2SO_4(p) + M \qquad \text{Reaction 1-9}$$

The reaction with HNO_3 depends on temperature and humidity (Stelson et al., 1979, Stelson and Seinfeld 1982):

$$NH_3(g) + HNO_3\,(g) \leftrightarrow NH_4NO_3(p) \qquad \text{Reaction 1-10}$$

Besides the reactions with H_2SO_4 and HNO_3, NH_3 may also react with HCl and form NH_4Cl (Pio and Harrison 1987):

$$HNO_3(g) + NaCl\,(p) \rightarrow NaNO_3(p) + HCl(g) \qquad \text{Reaction 1-11}$$

$$NH_3(g) + HCl\,(g) \leftrightarrow NH_4Cl\,(p) \qquad \text{Reaction 1-12}$$

Emissions of NO_x increased the production of ozone leading to a positive radiative forcing of climate, however via the effect of ozone on the OH radical formation they generate indirect negative radiative forcing by shortening the atmospheric lifetime of CH_4 (Prather 2002). Other indirect climate cooling effects induced by NO_x emissions include the increasing biogenic organic aerosol production caused by increasing amounts of ozone and NO_3 radicals (Kanakidou et al., 2000). Both NO_x and ammonia cause a direct negative radiative forcing by contributing to the formation of secondary sulfate and nitrate aerosols. Figure 1-4 shows the magnitude of the radiative forcing estimates in the past (1950 & 1980), currently (2011) and summarizes uncertainties for the main drivers of climate change (Stocker et al., 2013). Nitrate and sulfate aerosols are promoting to aerosol cooling. Previous studies and the recent IPCC report showed that ammonium and nitrate containing aerosol have a negative radiative forcing depending on the size of particles. The radiative forcing amounts to -0.22 Wm^{-2} for fine mode nitrate aerosols (Adams et al., 2001) and -0.02 Wm^{-2} for coarse mode nitrate aerosols (Jacobson 2001). Due to its short life time in atmosphere, ammonium nitrate aerosol is a locally important aerosol species (Veefkind et al., 1996, Haffner et al., 1997).

1.2.4 Impact via influencing the carbon cycle

Ammonium and NO_x are removed from the atmosphere by dry and wet deposition. NO_x in atmosphere is oxidized to HNO_3 by OH collected in droplets and on existing aerosol surfaces, NO_3 (nitrate radical) and N_2O_5 are converted to HNO_3 (Dentener and Crutzen 1993, Jacob 2000). The major sink is via wet deposition. With the increase of the atmospheric deposition or direct fertilization by N_r, biological carbon fixation is increased by accelerating plant growth (Vitousek

2004). Anthropogenic NO_x emissions could also relieve the nutrient constraint on CO_2 fertilization (Menon et al., 2007). However, high ozone levels, caused by N_r have a disadvantageous influence on plant growth, as ozone interferes with the plants control on stomata opening, closing and the energy metabolism of plants (Ollinger et al., 2002, Holland and Carroll 2003). It is estimated that carbon fixation was reduced by 18 to 20 Tg C yr^{-1} CO_2 since 1950 due to the effect of ozone in the USA (Felzer et al., 2004).

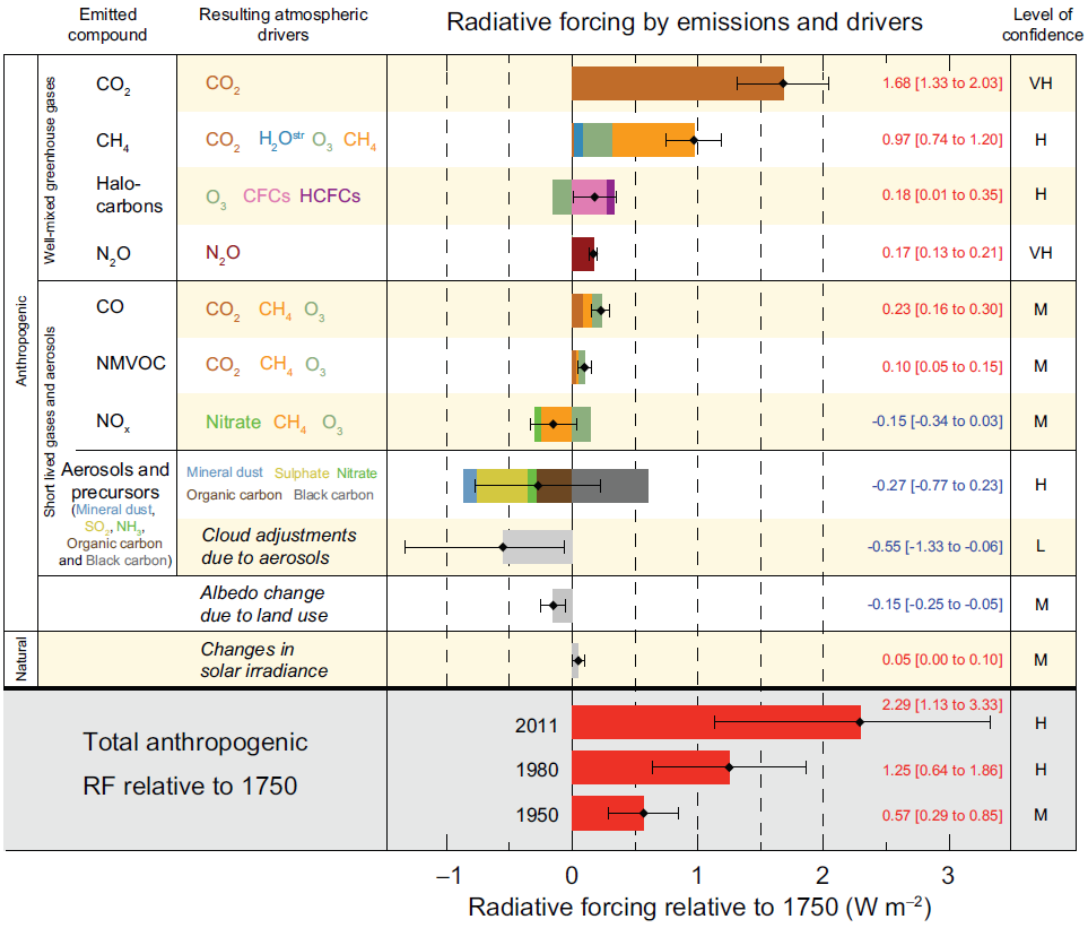

Figure 1-4. Radiative forcing estimates in 2011 and aggregated uncertainties for the main drivers of climate change. Values are global average radiative forcing (RF14), partitioned according to the emitted compounds or processes that result in a combination of drivers. The best estimates of the net radiative forcing are shown as black diamonds with corresponding uncertainty intervals; the numerical values are provided on the right of the figure, together with the confidence level in the net forcing (VH – very high, H – high, M – medium, L – low, VL – very low). Total anthropogenic radiative forcing is provided for three different years relative to 1750. From (Stocker et al., 2013).

1.3 Nitrogen isotopes in atmospheric aerosol

1.3.1 Nitrogen isotopes

Nitrogen (N) has two naturally occurring stable isotopes – one with a relative atomic mass of 14 (^{14}N) and the other of 15 (^{15}N). The most common ^{14}N has abundance in N_2 gas of 99.63% (Junk and Svec 1958, Mariotti 1983).

Nitrogen isotope ratios are measured as δ^{15}N:

$$\delta^{15}N_{air} = \left[\frac{\left(\frac{n(^{15}N)}{n(^{14}N)}\right)_{sample}}{\left(\frac{n(^{15}N)}{n(^{14}N)}\right)_{air}} - 1 \right] \times 1000 \ (‰) \qquad \text{Equation 1-1}$$

where n is the number of atoms.

The two isotopes of nitrogen exhibit different properties with regard to their reaction kinetics and thus, depending upon the nature of their respective formation processes and that of their precursors, the isotopic composition of particular species will be different. Isotopic fractionation can be described by the isotopic enrichment factor α and, in delta notation (isotopic separation factor), ε (‰):

$$\alpha_{15} = \frac{\left(\frac{n(^{15}N)}{n(^{14}N)}\right)_{product}}{\left(\frac{n(^{15}N)}{n(^{14}N)}\right)_{reactant}} \ , \ \varepsilon_{product-reactant} = (\alpha_{15} - 1) \times 1000 \ (‰) \qquad \text{Equation 1-2}$$

Value of α is characteristic for different reactions. E.g., in the atmosphere the isotopic separation factor of temperature dependent equilibrium reaction between NH_3 (g) and NH_4^+ (aq) is between +33.5 ‰ (70 °C) and +45.5 ‰ (23 °C) (Li et al., 2012). So, determining the value of α and its dependency on the conditions of reactions (e.g. pressure, temperature and humidity) is essential for the use of stable isotope techniques to understand the chemistry of nitrogen in the atmosphere.

1.3.2 Nitrogen isotopes in the environment

Figure 1-5 shows the major N_r sources, transportation pathways and processes. Table 1-2 gives the stable nitrogen isotope characteristics. Major potential sources of nitrogen pollution in the atmosphere commonly have characteristic ^{15}N/^{14}N ratios. Although data for the different forms and emission sources of nitrogen compounds are presently limited, it appears that they may be distinguishable on the basis of their isotopic composition (Freyer and Aly 1974, Kreitler 1979, Heathon 1986), in particular if the isotopic composition of gas phase compounds and particulate

phase compounds are monitored simultaneously. Stable nitrogen isotope ratios can be measured for all phases of atmospheric nitrogen. For inorganic nitrogen compounds, bulk isotope analyses have been used, e.g. to distinguish between agricultural and non-agricultural ammonia sources (Jickells et al., 2003) and to detect individual NO_x sources in aerosol samples (Yeatman et al., 2001, Elliott et al., 2007, Felix et al., 2012). However, for organic N, the results from nitrogen isotopic studies have so far not been successful at identifying sources of organic N. The challenge is the separation of the inorganic and organic components. Another challenge in using stable isotopes to study processes in the atmosphere is that all chemical reactions and physical phase transfers in the atmosphere can lead to isotope fractionation, in particular if the process does not go to completion. For most relevant reactions, the isotope fractionation factors have not been established through lab studies so far.

Heaton et al. (1997) reported a fractionation of $\varepsilon_{NH_4-NH_3}$ = +33 ‰ for Reaction 1-8 and Reaction 1-9 combined and a equilibrium constant of $\varepsilon_{NH_4NO_3-HNO_3}$ = +21 ‰ for Reaction 1-10, but did not investigate the influence of the reaction conditions in the isotope fractionation (temperature, relative humidity & pressure). In fact the study does not even report the temperature at which the experiment was conducted. The isotopic fractionation for the equilibrium between $NH_{3\,(aq)} - NH_4^{+}{}_{(aq)}$ is the most comprehensively studied reaction. A temperature dependent enrichment of the heavier ^{15}N in NH_4^+ ranging from +45.4 ± 0.6 ‰ at 23°C to +33.5 ± 0.6 ‰ at 70°C was found for this reaction in a recent study (Li et al., 2012). Previous experiments had yielded values ranging from +30.1 ‰ to +37.8 ‰ for the $NH_{3\,(g)} - NH_{3\,(aq)} - NH_4^+$ system at 23°C (Urey 1947, Scalen 1959). There are no studies investigating the effect of any other chemical reaction on the isotopic signature of NH_4^+ in the literature.

Freyer et al. (1993) investigated the dependency of the measured isotopic signature of NO_2 on the NO_2/NO_x ratio under ambient conditions with $NO_x >> O_3$ and found an isotope exchange equilibrium constant of +21.6 ± 1.5 ‰ for the isotope exchange between NO and NO_2, which is slightly lower than the isotope exchange constant of +28.6 ± 2 ‰ (Begun and Melton 1956) and +24 ± 2 ‰ (Brown and Drury 1968) established in early lab studies and significantly lower compared to theoretical calculations of +40 ‰ (Spindel 1954, Begun and Fletcher 1960, Richet et al., 1977). For the oxidation of NO_2 to HNO_3, Freyer et al. (1991) estimated a fractionation of -3 ‰ based on simple theoretical considerations, while a large positive fractionation of +55 ‰ at 0 °C between NO_2^- (aq) and HNO_3^- (aq) was found in aquous phase experiments (Brown and Drury 1967). An even larger positive fractionation of +74 ‰ at 0°C for the fractionation between NO_2 (g) and HNO_3 (aq) (Begun and Fletcher 1960) and +86 ‰ at 0°C for the fractionation between NO

(g) and HNO_3 (aq) (Stern et al., 1961) was estimated based on theoretical calculations. Between HNO_3 (aq) and particle phase NO_3^-, a large enrichment of the heavier ^{15}N in HNO_3 (aq) contradicts ambient data by Elliot et al. (2009), who showed that $\delta^{15}N$ of NO_3^- in particles is +1 ‰ to +12 ‰ heavier than the simultaneously collected HNO_3 (g) while the NO_3^- (aq) is isotopically lighter. The latter support the estimates by Freyer et al. (1991), which predict an enrichment of the lighter isotope in NO_3^- (aq). In the light of contradicting results from previous studies detailed understanding of the isotope fractionation during many of the reactions depicted in Figure 1-2 are lacking and lab studies performed under conditions that mimic the ambient atmosphere and also consider oxidation on aerosol surfaces are urgently required.

Almost all nitrogen isotope analyses described above were performed on bulk samples. For aerosol isotope analyses, they lost all information regarding the morphology and mixing state of the particles of interest, and provided results averaged over a large number of particles. Species specific single particle nitrogen isotope analysis can be a powerful tool for future atmospheric nitrogen aerosol research. The work presented here is the first step in this direction, which will employ the NanoSIMS ion probe technique to explore whether it is possible to measure separate isotope ratios for different nitrogen species on a single particle level, especially to distinguish organic and inorganic particles. Then, in combination with characterizing isotopic signatures of different nitrogen species and studying the isotope fractionation during the most important reactions in the lab, it will be possible to investigate reactions of different nitrogen species from individual atmospheric aerosol particles.

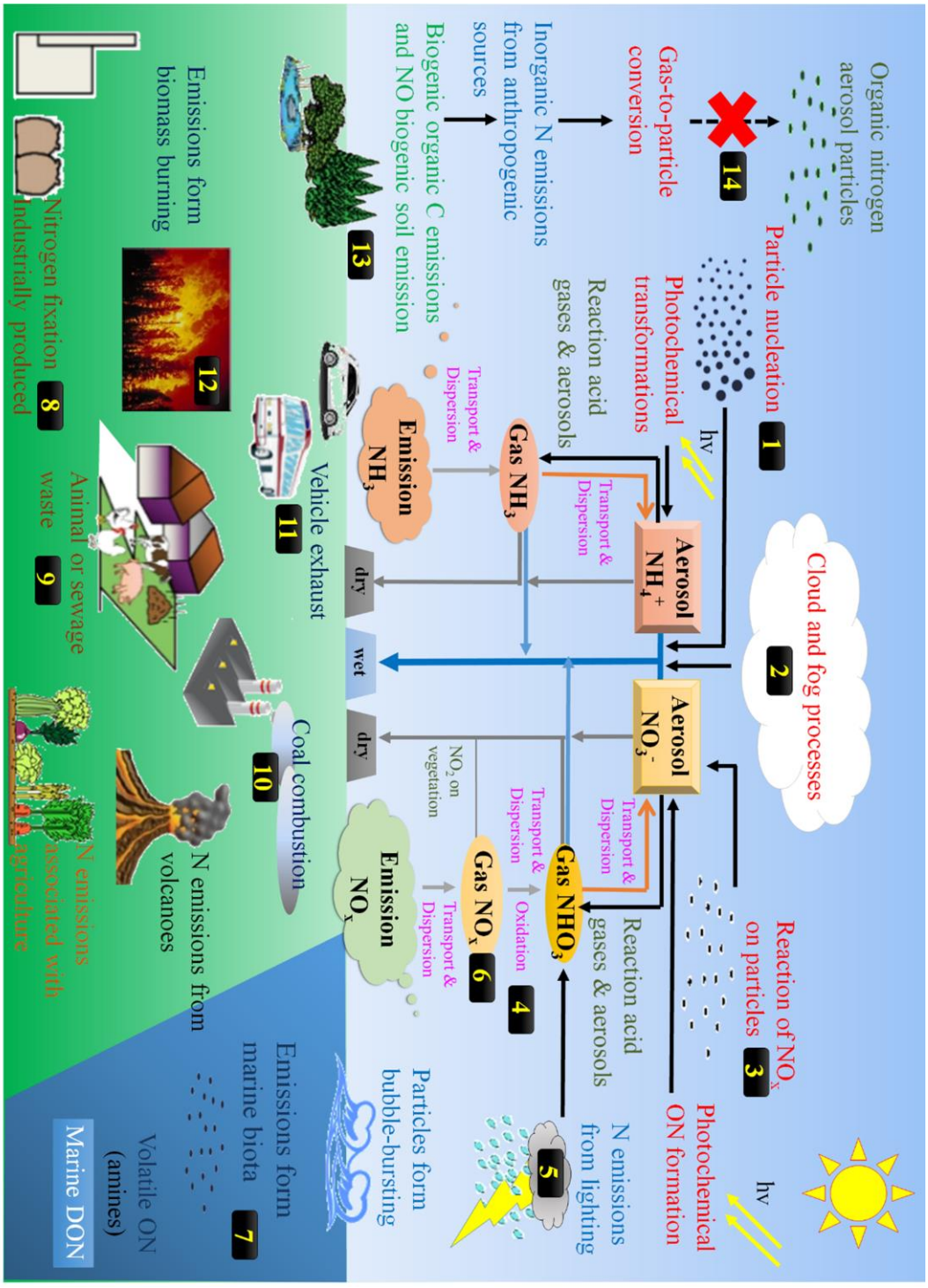

Figure 1-5. The stable nitrogen isotope characteristics of major potential sources, transportation pathways and processes. Different sources and processes (indicated by numbers) are characterized by specific N isotopic signatures (see Table 1-2).

Table 1-2. The stable nitrogen isotope characteristics in Figure 1-5.

No.	Nitrogen isotope characteristics	References
①	Particle nucleation: Particle phase NO_3^- is +1 ‰ to +12 ‰ heavier compared to simultaneously collected gas phase HNO_3 with larger differences observed in colder months.	(Freyer 1991, Elliott et al., 2009)
②	Cloud and fog processes: $NH_{3(gas)} \leftrightarrow NH_4^+{}_{(aq)}$ isotopic separation factors $\varepsilon_{NH_3-NH_4^+}$ = +35.5 ‰ ~ +45.5 ‰ temperature dependent. Ambient $NO_3^-{}_{(aq)}$ is -12 ‰ ~ 0 ‰ compared to simultaneously collected $HNO_{3\ (gas)}$, larger differences in colder months.	(Li et al., 2012, Elliott et al., 2009)
③	Reaction of NO_x on particles: Atmospheric NO_2 is -20 ‰ lighter ^{15}N than particle phase NO_3^- .	(Freyer 1991, Elliott et al., 2009)
④	Oxidation reaction of NO_x: In NO_2 + OH +M → HNO_3 +M, $\varepsilon_{HNO_3-NO_2}$ = -2.9 ‰.	(Freyer 1991, Ammann et al., 1999)
⑤	NO_x emissions from lightning: Due to high temperature involved in lightning, $\varepsilon_{NO_x-N_2}$ = 0 ‰.	(Wada and Hattori 1990)
⑥	Atmospheric gaseous NO_x: $\varepsilon_{HNO_3-NO_2}$= +28 ‰ in equilibrium reactions between NO and NO_2.	(Freyer et al., 1993, Elliott et al., 2009)
⑦	Emissions from marine biota: $\varepsilon_{N_r-N_2}$= 0 ‰ and water column denitrification $\varepsilon_{N_2-N_r}$= +20 ~ +30 ‰	(Wada et al., 1991)
⑧	Fertilizers: Industrial atmospheric nitrogen fixation of nitrate and ammonium have no nitrogen isotope fractionation;	(Heaton et al., 1986)
⑨	Nitrate in animal or sewage waste of water shows an isotope fractionation in the range of +10 ~ +20 ‰ in process $CO(NH_2)_2 \rightarrow NH_3 \leftrightarrow NH_4^+ \rightarrow NO_3^-$.	(Kreitler and Jones 1975, Kreitler 1979)
⑩	Coal combustion: $\delta^{15}N_{air}$ of NO_x from U.S. power plants is about +9 ‰ ~ +26 ‰.	(Felix et al., 2012)
⑪	NO_x from vehicle fossil fuel combustion: $\delta^{15}N_{air}$ of NO_x from vehicle exhausts ranges from -13 ‰ ~ -2 ‰, +5.7 ‰ on highway in the Swiss Middle Land, +3.8 ‰ roadside vegetation.	(Moore 1977, Heaton 1990, Ammann et al., 1999, Pearson et al., 2000)
⑫	Biomass burning: Lab experiments show that particles have N that is on average 6.6 ‰ (ranging from -1.3 ‰ to 13.1 ‰) heavier than the of vegetation burned.	(Turekian et al., 1998)
⑬	Biogenic soil emission: NO emitted from fertilized soils has a $\delta^{15}N_{air}$ range of -49‰ ~ -20‰.	(Li and Wang 2008)
⑭	Nitrogen isotope fractionations during reactions of NO_x with VOC and NH_3 gas with glyoxal are completely unknown, hence it is hard to identify the sources of the organic nitrogen and its transportation based on the isotopic signature.	

1.4 Research objectives and thesis outline

The main objectives of this study are:

1. To develop a new method to separate different nitrogen bearing species, including organic and inorganic species by applying the NanoSIMS ion probe technique and to investigate the possibility of measuring species specific nitrogen isotope compositions by NO_2^-, CN^- and NH_4^+ secondary ions.
2. To work out procedures that permit N isotope compositions of nitrate species measured by $^{15}N^{16}O_2^-/^{14}N^{16}O_2^-$ and $^{12}C^{15}N^-/^{12}C^{14}N^-$ secondary ion ratios with the NanoSIMS; this requires a detailed understanding of instrumental mass fractionation (IMF), matrix effects, and potential isobaric interferences.
3. To use $^{15}N^{16}O_2^-/^{14}N^{16}O_2^-$ and $^{12}C^{15}N^-/^{12}C^{14}N^-$ secondary ion ratios to measure micrometer-sized aerosol-like nitrate samples with the NanoSIMS.

The thesis is organized as follows:

Chapter 1: The introduction and overview of the thesis.

Chapter 2: Describes the method of bulk sample and aerosol-like mixture sample preparation. Gives informations on the nitrogen bearing standards used in this study, including in-house and known isotope composition standards.

Chapter 3: Recognition of different N-bearing species in the NanoSIMS. Feasibility study for speciated isotope analysis using NO_2^-, NH_4^+ and CN^- secondary ion ratios.

Chapter 4: Stable N isotope analysis of nitrate with the NanoSIMS using the $^{15}N^{16}O_2^-/^{14}N^{16}O_2^-$ - ratio. In bulk nitrate species analysis, exploration of experimental parameters and investigation of the matrix dependence of IMF between pure sodium nitrate and potassium nitrate. Determination of the precision and accuracy of this method. In aerosol-like sample analysis, identification of potential interferences and investigation of the matrix effect induced by the presence of variable N/C ratios.

Chapter 5: Use the $^{12}C^{15}N^-/^{12}C^{14}N^-$ - ratio to measure aerosol-like samples and to investigate the matrix effect induced by the presence of variable N/C ratios.

Chapter 6: Summary and discussion of the main findings.

Appendix A: Programing work related to my thesis.

Appendix B-D: Details of data.

2 Preparation of aerosol samples and standards

2.1 Sample preparation

2.1.1 Bulk samples pressed into gold foil

Agglomerates of grains of the in-house and isotope standards were pressed into ultra-clean gold foils using the methodology described in (Winterholler et al., 2008). Each sample holder contains several different standards; more details are shown in Table 2-1. After pressing the samples into the gold foils, grain agglomerates measured several square millimeters for each standard, see Figure 2-1. Subsequently, the mount was gold coated (Sputter coater Baltec SCD-050, sputter time = 120 s, sputtering current = 60 mA) to ensure sufficient surface conductivity of these larger area samples. The gold-coat thickness is about 70 nm. In order to investigate the dependence of the matrix specific IMF on the N/C ratio, carbon and nitrate mixture samples were prepared in that several pressed nitrate standard samples were coated with carbon (Quorum Q150TE, carbon coat thickness is about 20 nm). However, the heterogeneity of the amount of carbon deposited caused by the grainy nature of the standards led to variations in the thickness of the carbon coat on the edges of grains and this resulted in analytical challenges as the N/C ratio at the site of analysis was variable. Therefore, an aerosol generator was subsequently used (see section 2.1.2) to prepare standards with a well constrained N/C ratio.

Sodium nitrate and potassium nitrate grains were successfully pressed into gold foil and measured by NanoSIMS. Ammonium nitrate and calcium nitrate could not be introduced into the NanoSIMS. Ammonium nitrate was pressed into gold foil successfully at ambient temperature and pressure, but evaporated under high vacuum conditions in the NanoSIMS. Due to calcium nitrate deliquesce at low relative humidity (Al-Abadleh et al., 2003), it absorbs moisture from the air and becomes a droplet during sample preparation. The calcium nitrate droplet reacted with the adjacent samples and contaminations on the NanoSIMS holder before it eventually dried in the airlock. However, the dried droplet is then not gold coated and non-conductive. Even the preparation of a gold mount containing only calcium nitrate was not successful. Therefore, calcium nitrate could not be analyzed in the NanoSIMS.

2. PREPARATION OF AEROSOL SAMPLES AND STANDARDS

Table 2-1. Inorganic and organic standards used in this study. Standards which have the same product No. or lot No. are considered to have the same isotope composition. The nitrogen isotope compositions of in house standards #1, #2, and #3 were measured by an accredited laboratory (Iso-Analytical Limited, UK). ∗ is product Number. A few grams of sodium nitrite and ammonium nitrate were borrowed from other labs and production and lot No. information is missing.

Sample	Molecular formula	Purchased from:	Lot No.	$\delta^{15}N_{air}$ (‰)
Inorganic				
USGS35	$NaNO_3$	Isotope Hydrology Laboratory of the International Atomic Energy Agency, Vienna, Austria		2.7
IAEA-NO-3	KNO_3	Isotope Hydrology Laboratory of the International Atomic Energy Agency, Vienna, Austria		4.7
sodium nitrate 1[#1]	$NaNO_3$	VWR International BVBA, Leuven, Belgium	27955.238*	16.54 ± 0.43
sodium nitrate 2[#2]	$NaNO_3$	VWR International BVBA, Leuven, Belgium	27955.295*	14.19 ± 0.39
potassium nitrate[#3]	KNO_3	VWR International BVBA, Leuven, Belgium	26869.291	5.43 ± 0.20
sodium nitrite	$NaNO_2$			
calcium nitrate	$Ca(NO_3)_2$	Merck KGaA, Darmstadt, Germany	A0398121 319	
ammonium nitrate	NH_4NO_3			
ammonium sulfate	$(NH_4)_2SO_4$	Serva Electrophoresis GmbH, Heidelberg, Germany	110931	
Organic				
α-D-Glucose	$C_6H_{12}O_6$	Slgma-Aldrich Chemie GmbH, Steinbeim, Germany	STBC5226V	
urea	$CO(NH_2)_2$	Merck KGaA, Darmstadt, Germany	K44209987320	
cysteine	$C_3H_7NO_2S$	National Institute of Standards and Technology (NIST), Gaithersburg, USA	SRM 143d	
citric acid	$C_6H_8O_7$	Acros Organics, Ceel, Belgium	A0311494	
L(+)-Ascorbic acid	$C_6H_8O_6$	Acros Organics, Ceel, Belgium	A0268579	
Benzylimidazole	$C_{10}H_{10}N_2$	Biomol Research Labs, Inc. USA	P5730c	

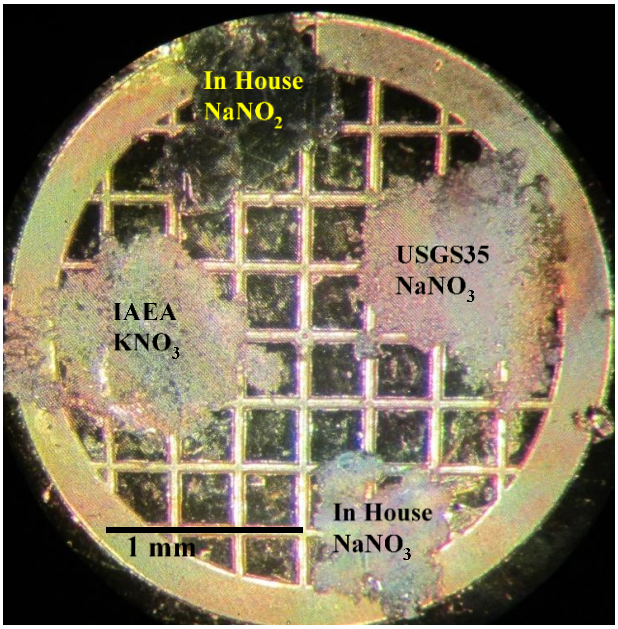

Figure 2-1. Standard grains pressed into a gold foil.

2.1.2 Aerosol-like mixture sample preparation

To investigate the matrix specific IMF of the nitrogen isotopes caused by the presence of carbon and the formation of CN^- molecular ions, standards with variable but known N/C ratio and known nitrogen isotopic composition were required.

The apparatus used to make aerosol-like mixture samples is shown in Figure 2-2: Milli-Q water was produced by PURELAB Option-Q and re-cleaned by PURELAB UHQ before the aerosol solution was made. Nitrate salts ($NaNO_3$ and KNO_3) and organic carbon samples (glucose) were dissolved by Milli-Q water. All solutions have certain nitrogen to carbon atom ratios. The concentration of the sum of the two solutes was kept constant at 20 g/L to ensure a homogeneous grain size. The appropriate mixing ratio for a target N/C ratio was calculated as follows: Each glucose molecule (molecular mass = 180) has six carbon atoms and each sodium nitrate molecule (molecular mass = 85) has one nitrogen atom. If the target N/C-ratio is 1, the mixture is prepared by dissolving 3.69 g of $NaNO_3$ (0.043 mol of N atoms) and 1.31 g glucose (0.043 mol of C atoms) in 250 ml Milli-Q water.

Before and after preparing each aerosol sample, the whole system was cleaned for 1 hour by Milli-Q water. Each sample was collected for about 10 to 25 minutes depending on the N/C ratio of the different solutions. For example, whenever the solution had a high salt content and contained less organic materials (high N/C ratio), the collection time was shorter as large salt particles crystalize readily upon drying the aerosol. Samples with more organic material on the other hand

(low N/C ratio) were found to display delayed drying, a behavior which has been previously reported for mixtures of organic and inorganic aerosol in chamber studies, and formed a larger number of small particles or large flat droplets (Smith et al., 2012). In order to ensure a sufficient number of large particles, the collection time was longer. All solutions in this experiment are summarized in Table 2-2.

An build in-house atomizer was used to generate aerosol: 2 bar (N_2 5.0 Nitrogen) expanded through a small orifice to form a high velocity gas jet, which atomized the liquid as it was sucked up from a reservoir. Only fine spray leaves the atomizer as large droplets are removed by impaction on the wall facing the jet. PFA fittings were used for all connections. The flow rate of N_2 in these experiments was 2000 ml/min. The aerosol passed through an aerosol drier containing silica gel and the dried aerosol was collected directly on a substrate. Four different substrates were tested in this study:

1) Gold coated nuclepore filter: Whatman Nuclepore Polycarbonate Track-Etched Membranes Filter with 0.2 μm pores;

2) Silver filter: Sterlitech Silver Membrane Filter with 0.2μm pores;

3) Silicon wafer;

4) Gold foil.

Nuclepore filter and silver filter were mounted in a filter holder when collecting aerosols. Silicon wafer and gold foil were fixed to a single stage impactor for aerosol collection described in (Pöhlker et al., 2012). SEM (Scanning electron microscope) images in Figure 2-3 show aerosols collected on these four substrates. Good conductivities and flat surfaces of substrates are crucial for NanoSIMS analysis.

Gold coated nuclepore filters are easy to handle and mount. It has emerged as the substrate of choice for sulfur isotope analysis of individual aerosol grains (Winterholler et al., 2008, Harris et al., 2013, Harris et al., 2014). Unfortunately, it was found that the $^{23}Na^{12}C_2^-$ ion can interfere with the detection of the $^{15}N^{16}O_2^-$ ions, see section 4. Since sodium is ubiquitous in aerosol samples and carbon is present in the nuclepore filter, gold coated nuclepore filters were found to be an unsuitable substrate for measuring the nitrogen isotopic composition of nitrate samples using the $^{15}N^{16}O_2^-/^{14}N^{16}O_2^-$ molecular ion ratio.

Silver filters display good conductivity, but their surface has a complex topography, which can lead to variations in the angular component of the momentum of secondary ions exiting the sample surface. Moreover, it was found that mixtures displaying delayed drying were not retained on the sample surface, but migrated into the interior of the silver membrane. Therefore, this substrate is not suitable for aerosol experiments.

Table 2-2. Concentrations of solutions used to make aerosol-like mixture samples.

sample	**Sodium nitrate ($NaNO_3$)**	**2-Deoxy-D-glucose ($C_6H_{12}O_6$)**	
molar mass	85.00	180.16	
N or C atom number	1	6	
Samples	N/C	$NaNO_3$ (g/L)	2-Deoxy-D-glucose ($C_6H_{12}O_6$) (g/L)
$NaNO_3$-glucose-1	0.1	4.41	15.59
$NaNO_3$-glucose-2	0.5	11.72	8.28
$NaNO_3$-glucose-3	1	14.78	5.22
$NaNO_3$-glucose-4	1.5	16.19	3.81
$NaNO_3$-glucose-5	2	17.00	3.00
$NaNO_3$-glucose-6	5	18.68	1.32
$NaNO_3$-glucose-7	infinity	20	0

sample	Potassium nitrate (KNO_3)	2-Deoxy-D-glucose ($C_6H_{12}O_6$)	
molar mass	101.11	180.16	
N or C atom number	1	6	
samples	N/C	KNO_3 (g/L)	2-Deoxy-D-glucose ($C_6H_{12}O_6$) (g/L)
KNO_3-glucose-1	0.1	5.03	14.97
KNO_3-glucose-2	0.5	12.54	7.46
KNO_3-glucose-3	1	15.42	4.58
KNO_3-glucose-4	2	17.41	2.59
KNO_3-glucose-5	5	18.88	1.12
KNO_3-glucose-6	infinity	20	0

Gold foils provide the perfect substrate for samples. They are conductive and flat in the vicinity of the grains (center of the foil), however, the cost of experiment is high. Moreover, mounting the foils after sample collection imposes several challenges. The gold foil is easy to bend and the cut edge of the foil can protrude above the sample holder by several hundred micrometers, unless the foils are very carefully mounted. Therefore, gold foil was used only to test critical interferences described in chapter 4.

Silicon wafers are flat, conductive and easier to mount than gold foils. Unfortunately, $^{29}Si^{18}O^-$ ions originating from the sampling substrate interfere with the detection of the $^{15}N^{16}O_2^-$ ions. This interference is discussed in detail in chapter 4. High mask levels and advanced plane-wise image processing (see Chapter 4) must be applied to the data for samples on silicon wafers.

Keeping in mind all constraints, gold coated nuclepore filters, gold foils and silicon wafers

were used for the experiments and usable data were obtained for all three substrates with potassium nitrate carbon mixtures. The same holds for sodium nitrate - carbon mixtures on gold foils and silicon wafers.

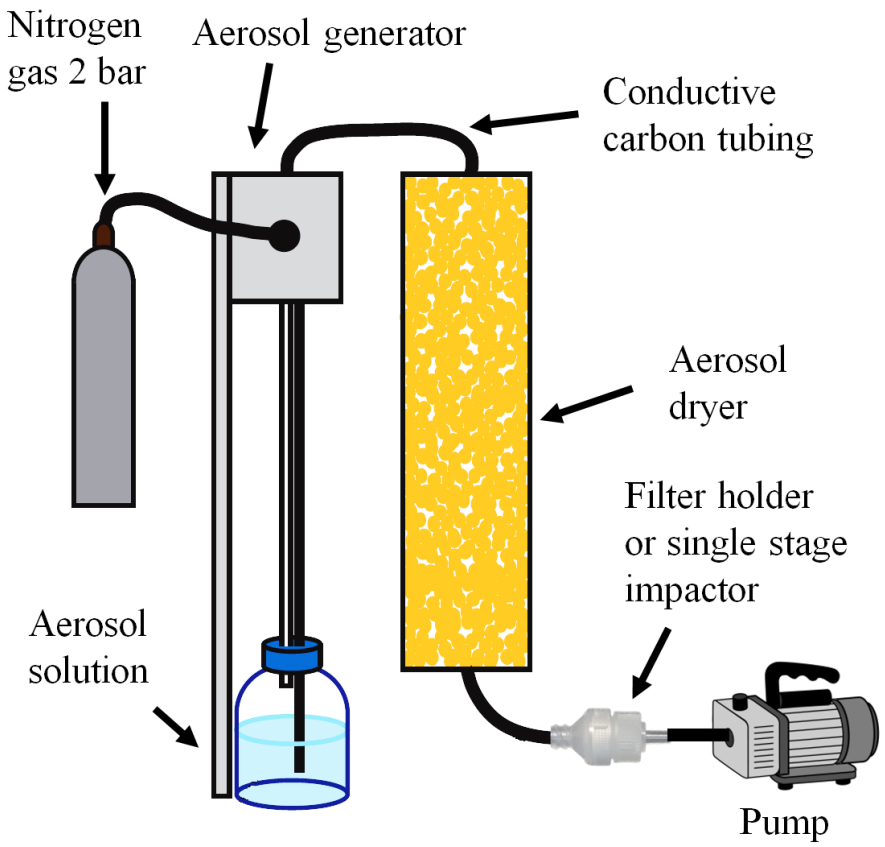

Figure 2-2. Experimental set-up used to produce aerosol-like mixture samples, consisting of organic carbon and nitrate salts.

2.2 Description and composition of N isotope standards

USGS35 (sodium nitrate) and IAEA-NO-3 (potassium nitrate) were obtained from Isotope Hydrology Laboratory of the International Atomic Energy Agency, Vienna, Austria. USGS35 was produced by J.K. Böhlke, S.J. Mroczkowski and T.B. Coplen, U.S. Geological Survey, Reston, USA (Bohlke et al., 2003). The certified isotope composition of this standard is $\delta^{15}N_{air}$ N_2 = +2.7 ‰. IAEA-NO-3 was prepared by A. Mariotti, Université Pierre et Marie Curie, Paris, France, between 1983 and 1985 (Gonfiantini 1984, Hut 1987). Its $\delta^{15}N_{air}$ N_2 = +4.7 ‰ was determined using data from an inter laboratory comparison (Bohlke et al., 1993).

Two in-house sodium nitrate standards and one in-house potassium nitrate standard were measured for their N isotope compositions in an accredited laboratory (Iso-Analytical Limited, UK) by EA-IRMS (Elemental Analyser Isotope Ratio Mass Spectrometry): In-house $NaNO_3$ #1has $\delta^{15}N_{air}$ = 16.54 ± 0.43 ‰, in-house $NaNO_3$ #2 $\delta^{15}N_{air}$ = 14.19 ± 0.39 ‰ and in-house KNO_3 $\delta^{15}N_{air}$ = 5.43 ± 0.20 ‰.

These in-house standards were used to prepare aerosol-like mixture samples of known N/C ratio and known nitrogen isotopic composition (Table 2-2) as described in section 2.1.

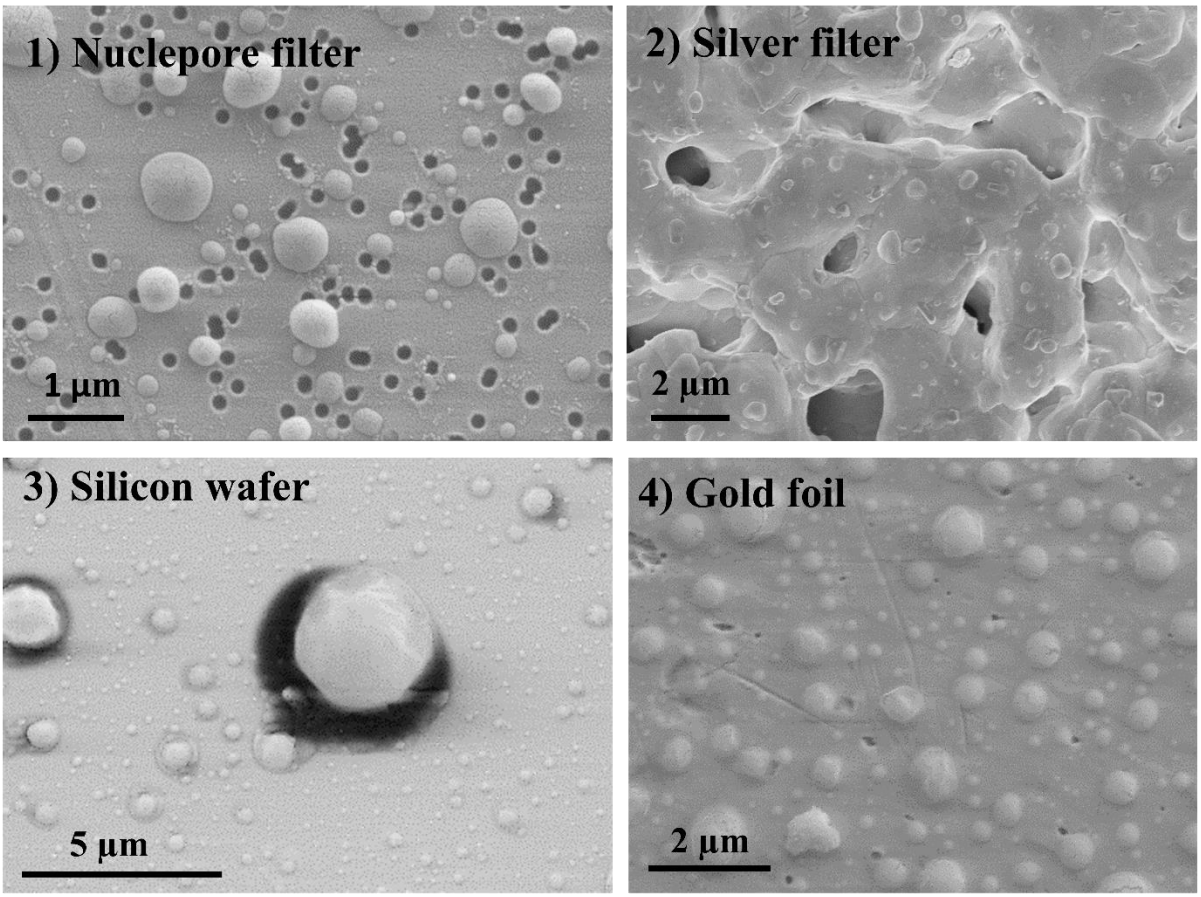

Figure 2-3. SEM images of aerosol-like samples collected on 1) Whatman Nuclepore Polycarbonate Track-Etched Membranes Filter with 0.2 µm pores; 2) Sterlitech Silver Membrane Filter with 0.2µm pores; 3) Silicon wafer; 4) Gold foil.

.

3 Recognition of different N-bearing species in the NanoSIMS

3.1 Introduction

The atmospheric cycling of N_r is a focus of both scientific and policy concern, because of the importance of N_r in controlling the formation of tropospheric ozone. Atmospheric N_r also plays a role in the formation of particulate matter and its long range transport modifies the global carbon cycle by providing nitrogen fertilization to remote ecosystem (Galloway et al., 2008, Compton et al., 2011). Measurements of stable nitrogen isotope ratios offer a means of discriminating sources of nitrogen, and reactions involved in N_r cycling via their specific isotopic signatures (Brown 1968a, Akhtar et al., 1979, Elliott et al., 2007, Li et al., 2012, Xiao et al., 2012). The potential of using the stable nitrogen isotopic signatures of airborne particles to deepen our understanding of the sources, reactivity, transport and removal of atmospheric nitrogen species has been recognized for a long time (Elliott et al., 2007, Widory 2007). Its application to real world samples has, however, suffered due to multiple analytical challenges.

Firstly, many conventional methods require large bulk samples. The analysis of species specific nitrogen isotopic signatures of nitrate aerosol via the microbial denitrification, the most sensitive technique currently in use, typically requires several μg of material (20-60 nmol NO_3^-) which corresponds to 10^7 accumulation mode aerosol particles (Elliott et al., 2007). Since atmospheric particles are chemically and morphologically heterogeneous, such an average signature is of limited use. Single particle analysis has the potential to overcome these restrictions in the interpretation of results.

Secondly, separation of different inorganic and organic nitrogen bearing species to obtain species specific isotopic signatures represents an analytical challenge. N_r includes contributions from nitrate salts, ammonium salts and organic nitrogen. All these species have different sources and are cycled via different reaction pathways. The sealed tube combustion method provides a single isotope signature for the total nitrogen in the sample (Widory 2007, Kundu et al., 2010), which is challenging to interpret. Separation of ammonium and nitrate ions via distillation or ion exchange chromatography involves an intensive, time consuming sample preparation and requires mg of samples material (Freyer 1978, Heaton 1987, Jia and Chen 2010, Kawashima and Kurahashi 2011). The denitrifier method which converts nitrate and nitrite to N_2O (gas) is fast and requires

only small samples, but recently its specificity has been questioned (Wankel et al., 2010) and the correction of the contribution of the mass independent oxygen isotope anomaly (Alexander et al., 2009) to m/z 45 & 46, which varies as a function of the oxidation pathway that produced the nitrate aerosol, often relies on unverified assumptions (Elliott et al., 2007, Wankel et al., 2010).

Even on a single particle scale, different sources of N_r are frequently found internally mixed in the same particle. Therefore, the isotopic signature of the total nitrogen present in an individual particle, which can be easily obtained using the CN^- molecular ion signal, is of limited use in understanding atmospheric nitrogen sources and the isotopic fingerprints of nitrogen cycling (Cape et al., 2011).

NanoSIMS has proven to be useful for studying isotopic signatures of individual atmospheric particles (Winterholler et al., 2006, Winterholler et al., 2008, Harris et al., 2013). Several previous studies demonstrated that the intensity of secondary ions in negative ion mode and their ratios can be successfully used to classify aerosol particles into broad classes without a corresponding microscopy image. The secondary ion signals of $^{16}O^-$, $^{12}C_2^-$, $^{12}C^{14}N^-$ and $^{32}S^-$ were used to identify soot, coated soot, organic aerosol, inorganic aerosol, primary biological aerosol and mineral dust particles from a NanoSIMS secondary ion image (Harris et al., 2013, Harris et al., 2014) and $^{12}C^-$, $^{16}O^-$, $^{12}C^{14}N^-$, $^{32}S^-$ and $^{35}Cl^-$ were used to separate particles from background and pollution episodes (Ghosal et al., 2014).

In this section, I demonstrate that NanoSIMS can be used to identify different nitrogen containing species commonly observed in atmospheric aerosol particles on the basis of the relative intensity of secondary ion signals, both in negative and positive secondary ion mode without the need to chemically or physically separate the samples.

Nitrogen bearing species that occur in atmospheric aerosol particles including inorganic species such as nitrates, ammonium containing salts like ammonium sulfate, ammonium nitrate and ammonium chloride, organonitrates (Farmer et al., 2010, Cape et al., 2011), amides (Bentz et al., 1994, Peterson et al., 2006, Cape et al., 2011), amines (Murphy et al., 2007, Martin et al., 2010, Hanson et al., 2011) and imidazoles (Kampf et al., 2012, Zarzana et al., 2012). NanoSIMS can be used to differentiate between these species with the help of $^{12}C^-$, $^{16}O^-$, $^{12}C^{14}N^-$ and $^{14}N^{16}O_2^-$ secondary ion signals under Cs^+ bombardment in negative ion mode and with the help of the intensity of the $^{14}NH_4^+$, $^{14}NH_3^+$, $^{14}NH_2^+$ and $^{14}NH^+$ molecular ion signals under O^- bombardment in positive secondary ion mode.

I also demonstrate that certain molecular ions can potentially be used to investigate the species specific nitrogen isotopic composition of individual aerosol particles. These include the $^{14}N^{16}O_2^-$ signal, which is specific to nitrate/nitrite and the $^{14}NH_4^+$ signal, which is specific to ammonium

containing particles and particles with amino groups. The $^{12}C^{14}N^-$ signal can potentially be used to study the isotopic composition of the total organic and inorganic nitrogen present in an individual aerosol particle.

3.2 Materials and Methods

Measurements were performed with the Cameca NanoSIMS 50 ion probe at MPIC (Max Planck Institute for Chemistry) in Mainz (Figure 3-1). This type of secondary ion mass spectrometer is characterized by high lateral resolution (down to 50 nanometers for Cs^+ primary ions and 200-300 nanometers for O^- primary ions), high detection efficiencies for secondary ions, and simultaneous measurement of up to five different masses via a multi-collection system. These features permit to analyze micrometer- and submicron-sized nitrogen-bearing aerosol particles individually for elemental and isotopic compositions.

Detailed information about the NanoSIMS 50 is given in the paper by (Hoppe et al., 2013). Here, I will give only a brief introduction. The NanoSIMS 50 has two primary ion sources: the $CsCO_3$ source produces a beam of positively charged cesium primary ions (Cs^+) and the duoplasmatron source together with a Wien filter produces a beam of negatively charged oxygen ions (O^-). Primary ions are accelerated by a potential of +/- 8 kV in the source, to a potential of -/+ 8 kV at the surface of the sample, thus impacting the sample with an energy of 16 keV (Hoppe et al., 2013). Before hitting the sample surface, the primary beam is trimmed by an aperture D1 of variable size. Then it is focused by the EOP lens to its final spot size on the sample surface (cf. Fig. 3 in Hoppe et al. 2013).

Secondary ions are transferred to a double-focusing mass spectrometer. Two apertures entrance slit (ES) and aperture slit (AS) were set to cut the secondary beam and to limit its angular dispersion. Then the beam went through an electrostatic Spherical Sector (SS100), where the secondary ions are dispersed according to energy and deviated onto an energy slit of variable width, which used to trim the beam and reduce its energy bandwidth to 20 eV. Five electron multipliers are placed in the local plane of the magnet and four of these are moveable on trolleys. (cf. Figure. 3 in Hoppe et al. 2013)

The important settings:

In one setup, negative secondary ions $^{12}C^-$, $^{12}C^{14}N^-$, $^{16}O^-$, $^{14}N^{16}O_x^-$ (x = 1, 2, 3) were measured using the cesium primary ion source. Aperture D1 was set to D1-2 (300 μm), which gave a primary ion current of about 4 pA. Entrance slit and aperture slit were set to 20×140 μm^2 (ES-4) and 150×150 μm^2 (AS-3), respectively. Energy bandwidth was set to 20 eV.

In a second setup, positive secondary NH_x^+ (x = 1, 2, 3, 4) ions were measured using the duoplasmatron primary ion source. Aperture D1 was set to D1-2 (300 µm), which gave a primary ion current of about 40 pA. Entrance slit and aperture slit were set to 20×140 μm^2 (ES-4) and 80×80 μm^2 (AS-4), respectively. Energy bandwidth was set to 20 eV.

A set of in-house standards of different nitrogen bearing species listed in Table 2-1 were used to demonstrate how different nitrogen bearing species can be differentiated using their secondary ion signals. These standards included sodium nitrate, sodium nitrite, ammonium sulfate, glucose, urea, cysteine, citric acid, and benzylimidazole which were pressed into gold foils as described in section 2.1.1.

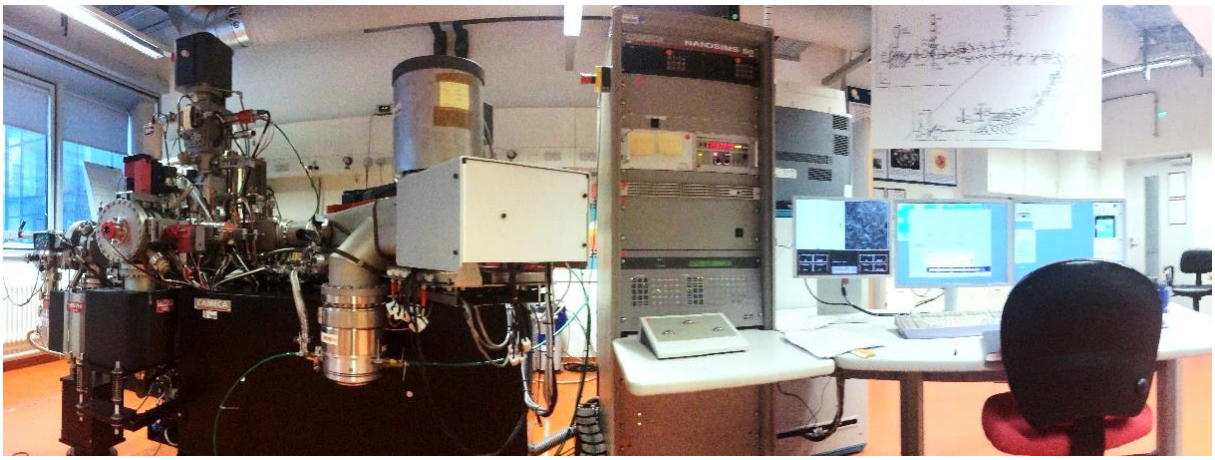

Figure 3-1. The Cameca NanoSIMS 50 ion probe at the Max Planck Institute for Chemistry in Mainz, Germany.

3.3 Results and Discussion

3.3.1 Mass spectra of nitrate and nitrite species

Benz et al. (1994) were the first to report that $^{16}O_2^-$ and $^{14}N^{16}O_x^-$ were the major ions observed while sputtering sodium nitrate with Ar^+. The same study reported that most of these molecular ions were uniquely associated with inorganic nitrates and nitrite and could be used to separate the same from organic nitrogen compounds and ammonium containing inorganic salts. The decomposition patterns of nitrate and nitrite caused by primary ions in SIMS analysis was reported by (Groenewold et al., 1997, Van Stipdonk et al., 2000). The intensities of secondary ions $^{14}N^{16}O_x^-$ depend on the energy deposition of the primary ion beam. Figure 3-2 shows the seconday ion intensity of $^{14}N^{16}O_x^-$ measured in NanoSIMS with the setting described above. In this study the secondary ion $^{14}N^{16}O_2^-$ signal has the hightest intensity, while Groenewold et al. (1997) using static SIMS reported much higher $^{14}N^{16}O_3^-$ secondary ion signals and van Stipdonk et al. (2000) reported

a dependence of the $^{14}N^{16}O_2^-$ / $^{14}N^{16}O_3^-$ ratio on the primary ion energy and primary ion dose.

The ratio of $^{14}N^{16}O^-$ / $^{14}N^{16}O_2^-$ and $^{14}N^{16}O_3^-$ / $^{14}N^{16}O_2^-$ are 12.8 % and 11.4 %, respectively for sodium nitrate; 30.0 % and ~0 % for sodium nitrite, respectively. Very few counts of the $^{14}N^{16}O_3^-$ molecular ion were observed for sodium nitrite, which indicats that the $^{14}N^{16}O_3^-$ is not formed in the reaction zone above the sample, but only produced by direct sputtering of samples containing $^{14}N^{16}O_3^-$ ions. This is useful to separate nitrate and nitrite salts during NanoSIMS analysis. However, the $^{14}N^{16}O_3^-$ secondary ion is unsuitable for high precision stable isotope analysis for two reasons. Firstly, it is impossible to bring two detectors close enough together for simultaneous analysis of $^{14}N^{16}O_3^-$ and $^{15}N^{16}O_3^-$. Measurements in peak jumping mode are undesirable on aerosol particles as they carry a much larger measurement uncertainty. Secondly, the signal intensity is lower. Considering the constraints imposed by the small sample size available in most aerosol particles, precise analysis will usually be difficult due to the low signal intensity. In order to measure the nitrogen isotope ratio with higher precision, the species with the larger secondary ion yield was chosen for measuring the species specific nitrogen isotopic composition of nitrate containing salts. The same species was also chosen as the most suitable species to detect nitrate/nitrite containing salts in atmospheric aerosol samples.

Figure 3-3 shows $^{14}N^{16}O_2^-$ is unique for nitrate and - to some extent - for nitrite species. Even urea, cysteine and ammonium sulfate have nitrogen and oxygen atoms, yet the signal of $^{14}N^{16}O_2^-$ is very low. This indicates that $^{14}N^{16}O_2^-$ does not form above the sample.

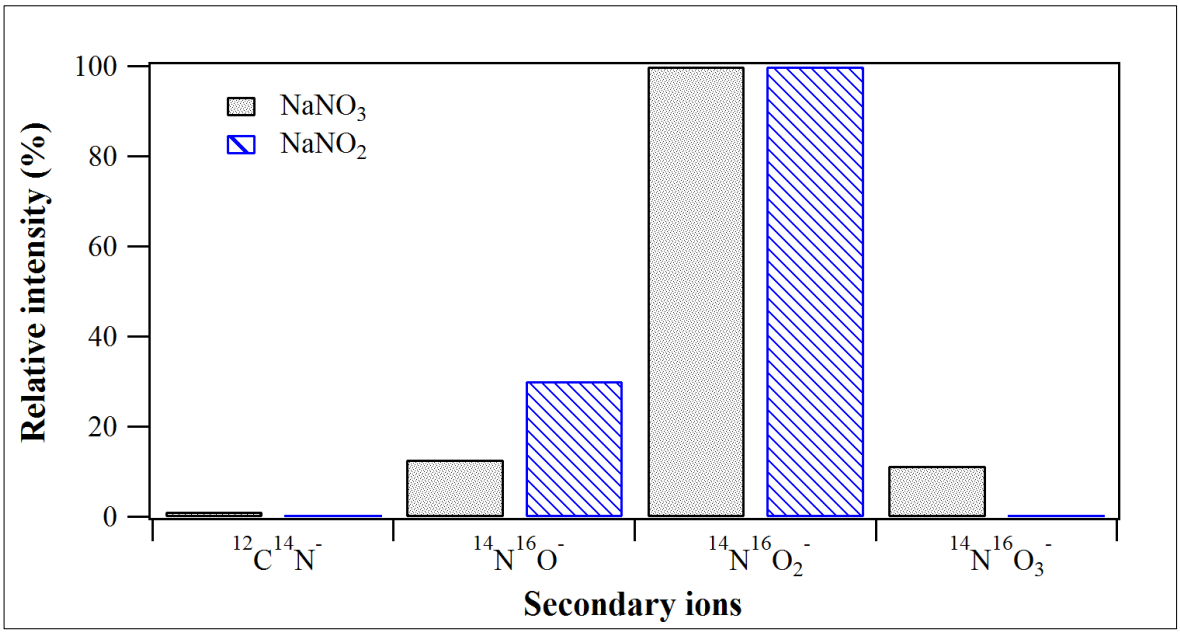

Figure 3-2. Relative intensities of secondary ions $^{12}C^{14}N^-$, $^{14}N^{16}O^-$, $^{14}N^{16}O_2^-$ and $^{14}N^{16}O_3^-$ in sodium nitrate and sodium nitrite samples. The maximum signal $^{14}N^{16}O_2^-$ is normalized to 100%.

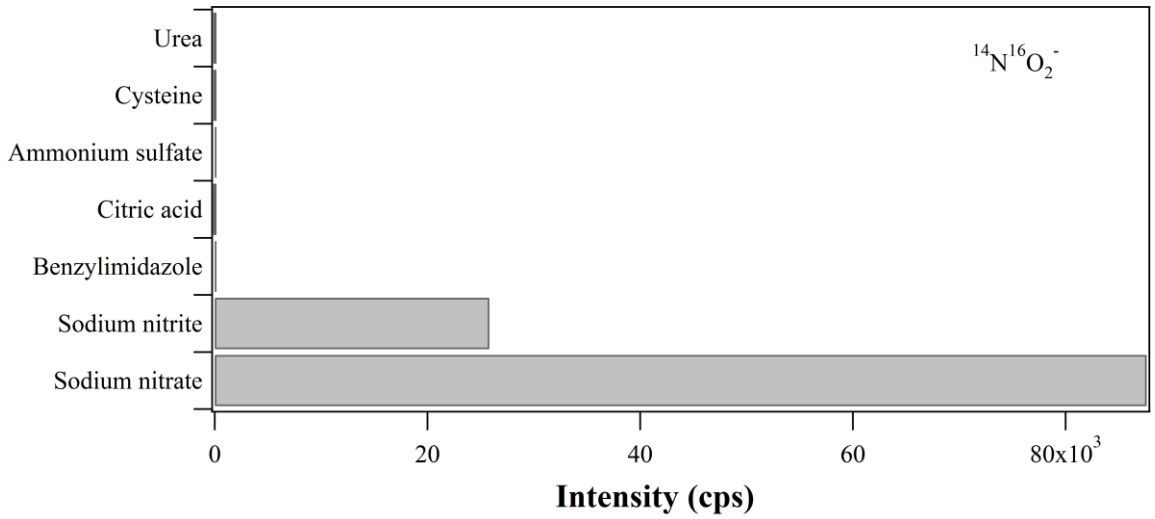

Figure 3-3. $^{14}N^{16}O_2^-$ ion intensities in different samples.

3.3.2 Mass spectra of ammonium containing inorganic salts

Only few studies so far reported measuring ammonium containing salts using SIMS. Previous researchers reported that ammonium salts can be identified by their positive secondary ion mass spectra which displays a cascade of NH_x^+ (x = 1, 2, 3, 4) with decreasing signal intensity (Bentz et al., 1994). They also reported that the same fragmentation pattern is not observed in organic amino compounds. NH_4^+, NH_3^+ and NH^+ molecular ions were observed in fine mode aerosol samples using TOF-SIMS (Faude and Goschnick 1997, Van Ham et al., 2000). These authors used multivariate cluster analysis to group aerosol particles into different chemical groups based on their secondary ion signal intensities. However, both studies did not report detailed mass spectra.

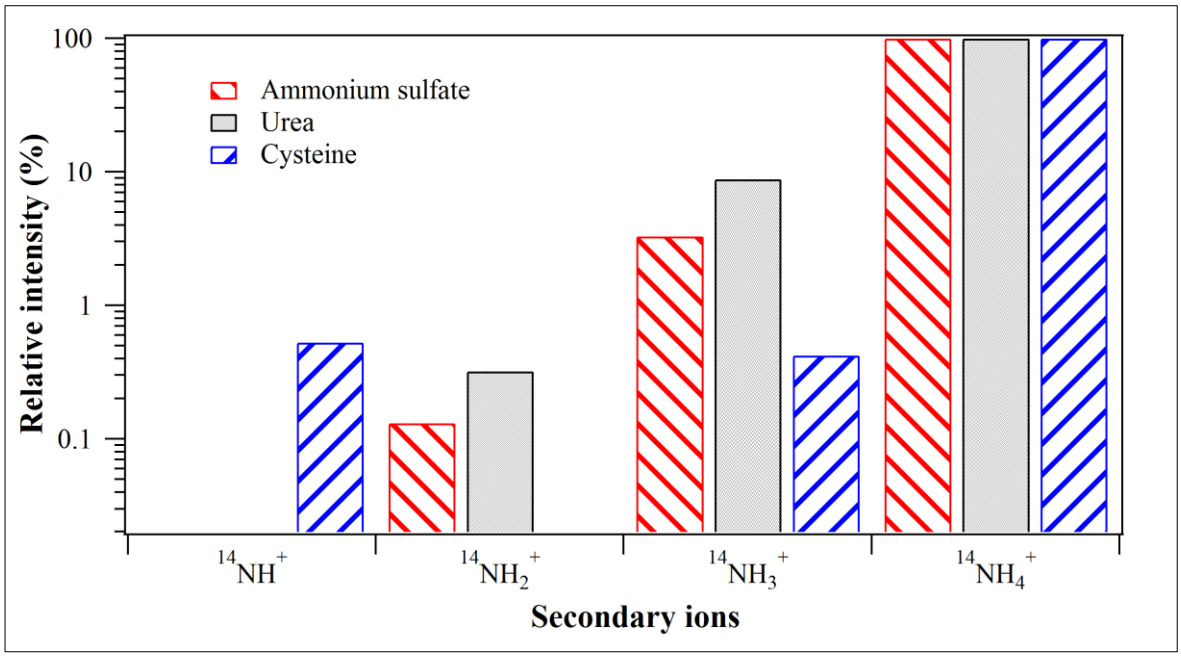

Figure 3-4. Relative intensities of secondary ions $^{14}NH^+$, $^{14}NH_2^+$, $^{14}NH_3^+$ and $^{14}NH_4^+$ in ammonium sulfate, urea and cysteine. The maximum signal $^{14}NH_4^+$ is normalized to 100%. Note that the Y axis is a logarithmic scale.

Figure 3-4 shows that in dynamic SIMS, with the tuning as described above, $^{14}NH_4^+$ has an higher intensity than $^{14}NH^+$, $^{14}NH_2^+$ and $^{14}NH_3^+$. This pattern is observed both for inorganic ammonium salts and organic amino groups in urea and in an amino acid, cysteine. The absolute signal intensity for positive secondary ions is lower for the organic compounds, but in contrast to the results reported by Bentz et al. (1994) under Ar^+ bombardement we do find these molecular ions even in organic compounds and find that $^{14}NH_4^+$ is the molecular ion with the highest signal intensity. Note that the Y axis has a logarithmic scale.

$^{14}NH_4$ groups do not exist in urea and cysteine molecules but $^{14}NH_4^+$ still has the highest secondary ion signal compared to other $^{14}NH_x^+$ species ($^{14}NH^+$, $^{14}NH_2^+$, $^{14}NH_3^+$). This indicates $^{14}NH_4^+$ can be formed during the sputtering process or as a result of collisions in the plasma above the sample surface. However, this process seems to be limited to pure amino acid samples. In Figure 3-5, primary biological aerosol particles – fungal hyphae, which do contain amino acids in the form of complex proteins, did not display this behavior and had no $^{14}NH_4^+$ secondary ion signal. Similarly, $^{14}NH_4^+$ were absent in sodium nitrate, nitrite and benzylimidazol. $^{14}NH_4^+$ was used to identify inorganic ammonium and organic amino group containing species in this study. However, the behavior of primary biological particles indicates that in real world aerosol this molecular ion may be more selective and may be species for ammonium salts.

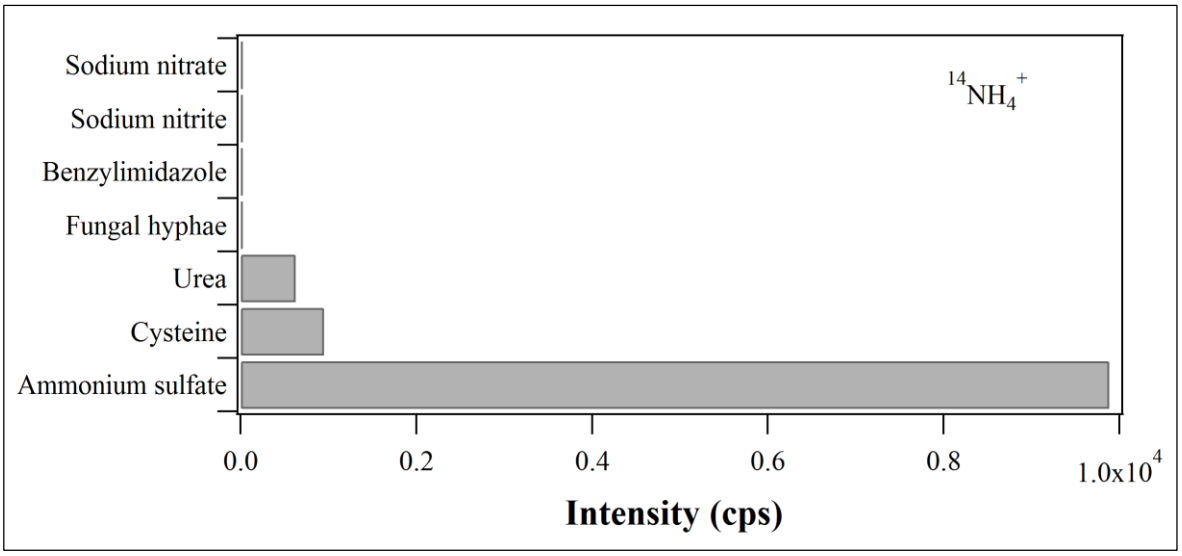

Figure 3-5. $^{14}NH_4^+$ ion intensities in different samples.

3.3.3 Speciation of nitrogen containing compounds using a combination of positive and negative mass spectra

The presence of organic nitrogen containing compounds in atmospheric aerosol has been confirmed by several researchers. Two recent studies reported the presence of organonitrates in secondary organic aerosol using AMS (Farmer et al., 2010, Nguyen et al., 2011) after the presence of such compounds in aerosol particles had been suggested from TOF-SIMS studies (Faude and Goschnick 1997). Several studies reported the presence of fatty acid amides on the surface of combustion particles (Peterson and Tyler 2002, Peterson and Tyler 2003) and amines are frequently found in fine mode aerosol (Smith et al., 2010, Hanson et al., 2011), in particular in rural regions. Imidazoles form during photochemical aging or as a product of aqueous phase reactions.(Kampf et al., 2012, Zarzana et al., 2012). Bentz et al. (1994) used 3-D plots depicting the secondary ion signals of $^{16}O_2^-$, $^{12}C^{14}N^-$ and m/z 42 to separate different nitrogen containing species. M/z 42 can arise from $^{12}C^{14}N^{16}O^-$, $^{12}C_2H_2{}^{16}O^-$ and $^{12}CH_2{}^{14}N_2^-$.

For large size aerosols (diameter > 1μm), I find that in samples where the same area can be analysed twice, once using negative secondary ions and once using positive secondary ions, combining the secondary ion signals of $^{12}C^{14}N^-$, $^{16}O^-$, $^{14}N^{16}O_2^-$, and $^{14}NH_4^+$ is most useful to separate different species, including organic nitrogen samples (cysteine, urea & benzylimidazole) and inorganic nitrogen samples (ammonium sulfate, sodium nitrate & sodium nitrite), based on the normalized heights of the secondary ion signals of these 4 species in the negative/positive secondary ion mode (Figure 3-6).

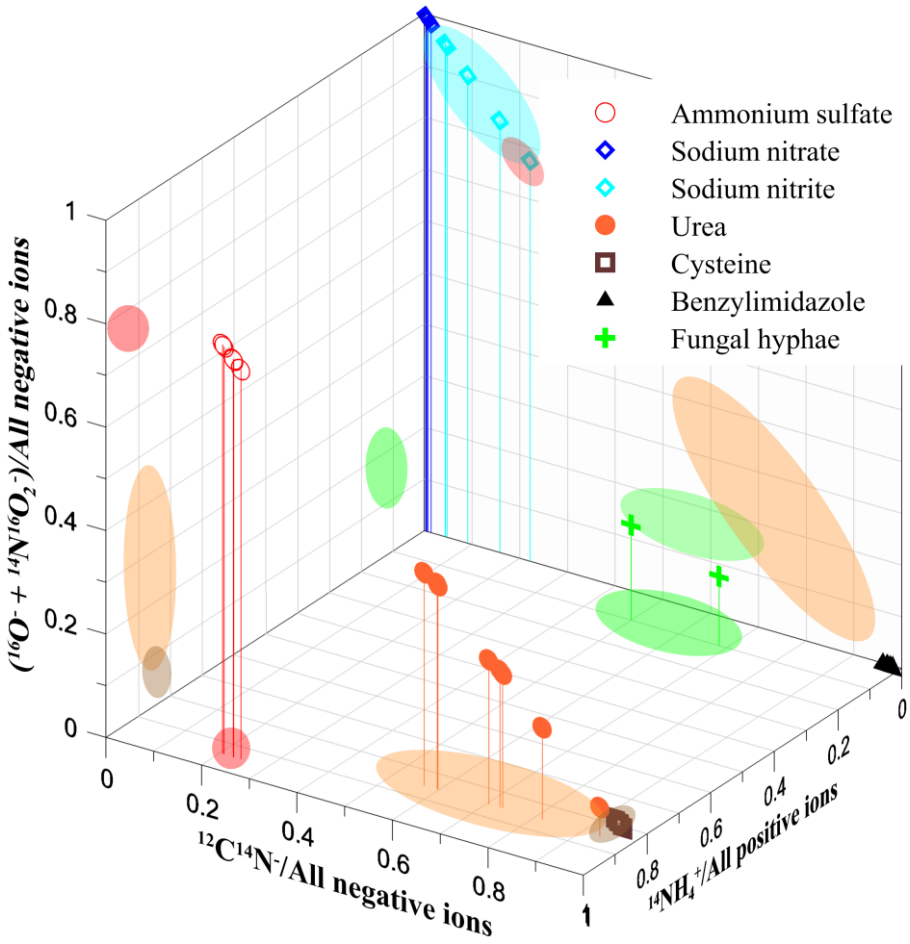

Figure 3-6. The distribution of different samples (sodium nitrite, sodium nitrate, ammonium sulfate, urea, cysteine, benzylimidazole and fungal hyphae) based on the normalized heights of the secondary ion signals of $^{12}C^{14}N^-$ / All negative ions, $^{14}NH_4^+$ / All positive ions and ($^{16}O^-$+ $^{14}N^{16}O_2^-$) / All negative ions. All negative ions = $^{16}O^-$ + $^{12}C^{14}N^-$ + $^{14}N^{16}O_2^-$; All positive ions = $^{14}NH^+$ + $^{14}NH_2^+$ + $^{14}NH_3^+$ + $^{14}NH_4^+$.

Samples containing ammino groups (urea and cysteine) and ammonium ions (ammonium sulfate) have high $^{14}NH_4^+$ signals. Sodium nitrate and sodium nitrite have high $^{16}O^-$ + $^{14}N^{16}O_2^-$ signals in Figure 3-6, and the $^{14}N^{16}O_2^-$ signal is unique to these species in Figure 3-3. Organic material: benzylimidazole, cysteine and urea show a high $^{12}C^{14}N^-$ signal while inorganic materials show a low $^{12}C^{14}N^-$ signal. So it is possible to distinguish the different particle types from a NanoSIMS analysis without chemical or physical separation. Fungal hyphae were plotted into Figure 3-6 to demonstrate that, despite the fact that the $^{14}NH_4^+$ has been observed in an individual pure amino acid (cysteine), the predominant signal for biological tissues is $^{12}C^{14}N^-$ and that the $^{14}NH_4^+$ signal is very low, due to the fact that the amino-acids are incorporated into larger chains in proteins (De Haan et al., 2009). In ambient aerosol $^{14}NH_4^+$ signals found to be characteristic of ammonium containing inorganic aerosol.

3.3.4 Speciation of nitrogen containing compounds using negative secondary ion mass spectra

For small size aerosols (diameter < 1 μm) and primary ion beam sensitive materials, e.g. ammonium sulfate, it is not possible to acquire two spectra: once using Cs^+ primary ions and once using O^- primary ions. In this case, it is necessary to identify the different species using only the relative intensities of different negative secondary ions ($^{12}C^-$, $^{16}O^-$, $^{12}C^{14}N^-$ and $^{14}N^{16}O_2^-$). This is particularly true if the isotopic signature is ultimately measured using $^{12}C^{14}N^-$ secondary ions, as this molecular ion forms irrespective of the speciation of the nitrogen in the original sample, as long as sufficient carbon is present. Since atmospheric aerosol usually consists of mixtures of organic and inorganic salts this is usually the case. Figure 3-7 shows the separation of different nitrogen bearing species using only negative ions. The following signals were measured in multi-collection mode: $^{12}C^-$, $^{16}O^-$, $^{12}C^{14}N^-$ and $^{14}N^{16}O_2^-$. The three axes show $^{12}C^-$ / All, $^{12}C^{14}N^-$ / All and $^{14}N^{16}O_2^-$ / All (All = $^{12}C^- + {}^{16}O^- + {}^{12}C^{14}N^- + {}^{14}N^{16}O_2^-$), respectively. Without $^{14}NH_4^+$ ions, one sample contains ammino groups - cysteine - is hard to be separate from another organic nitrogen containing compound which does not conatin ammino groups, benzylimidazole. However, when $^{12}C^-$ / All is plotted on a logarithmic scale of, cysteine has a one magnitude lower $^{12}C^-$ / All - ratio than benzylimidazole. Inorganic ammonium species have low $^{12}C^-$ signals and it is easy to seperated from nitrate species using the $^{12}N^{16}O_2^-$ signals. Glucose was also added in this plot and it has hightest $^{12}C^-$ / all values.

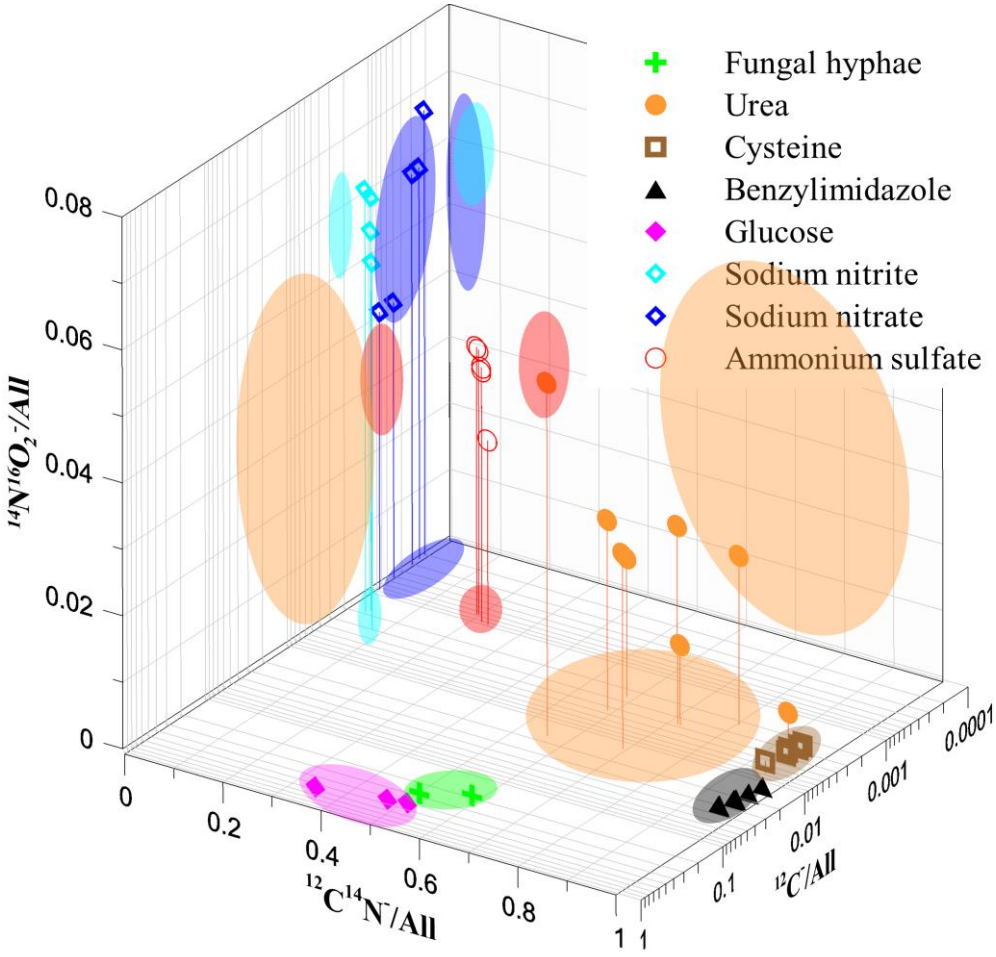

Figure 3-7. The distribution of different samples (sodium nitrite, sodium nitrate, ammonium sulfate, urea, cysteine, benzylimidazole, glucose and fungal hyphae) based on the normalized heights of the secondary ion signals of $^{12}C^{14}N^-$ / All, $^{12}C^-$ / All and $^{14}N^{16}O_2^-$ / All. $^{12}C^-$ / All is plotted in logarithmic scale. All = $^{12}C^-$ + $^{16}O^-$ + $^{12}C^{14}N^-$ + $^{14}N^{16}O_2^-$.

3.3.5 Speciation of nitrogen containing compounds using positive secondary ion mass spectra

For small size aerosols (diameter < 1 µm) and primary ion beam sensitive materials, positive secondary ion mass spectra were explored as well. As described above, $^{14}NH_x^+{}_{=1-4}$ secondary ions are unique for ammonium salts and amino groups, see Figure 3-5. Hence, in this section, only such species are investigated. Figure 3-8 shows the separation of ammonium ions or amino group containing samples, i.e. ammonium sulfate, urea and cysteine. The following signals were measured in multi-collection mode: $^{14}NH^+$,$^{14}NH_2^+$, $^{14}NH_3^+$ and $^{14}NH_4^+$. The three axes show $^{14}NH^+$ / All, $^{14}NH_3^+$ / All and $^{14}NH_4^+$ / All (All = $^{14}NH^+$ + $^{14}NH_2^+$ + $^{14}NH_3^+$ + $^{14}NH_4^+$). More than 88 % of $^{14}NH_x^+{}_{=1-4}$ secondary ions is present as $^{14}NH_4^+$ molecular ion but the species differ when it comes to the relative signal intensity of $^4NH_x^+{}_{=1-3}$ molecular ions. Among the three species, urea has the

highest ratio of $^{14}NH_3^+$ / All. The ratio of $^{14}NH^+$ /All from cysteine is more than one order of magnitude higher than from the others and it also has the highest ratio of $^{14}NH_4^+$ / All. Inorganic ammonium sulfate has the lowest ratio of $^{14}NH^+$ / All, but it has the highest secondary ion yield in $^{14}NH_x^+$=1-4.

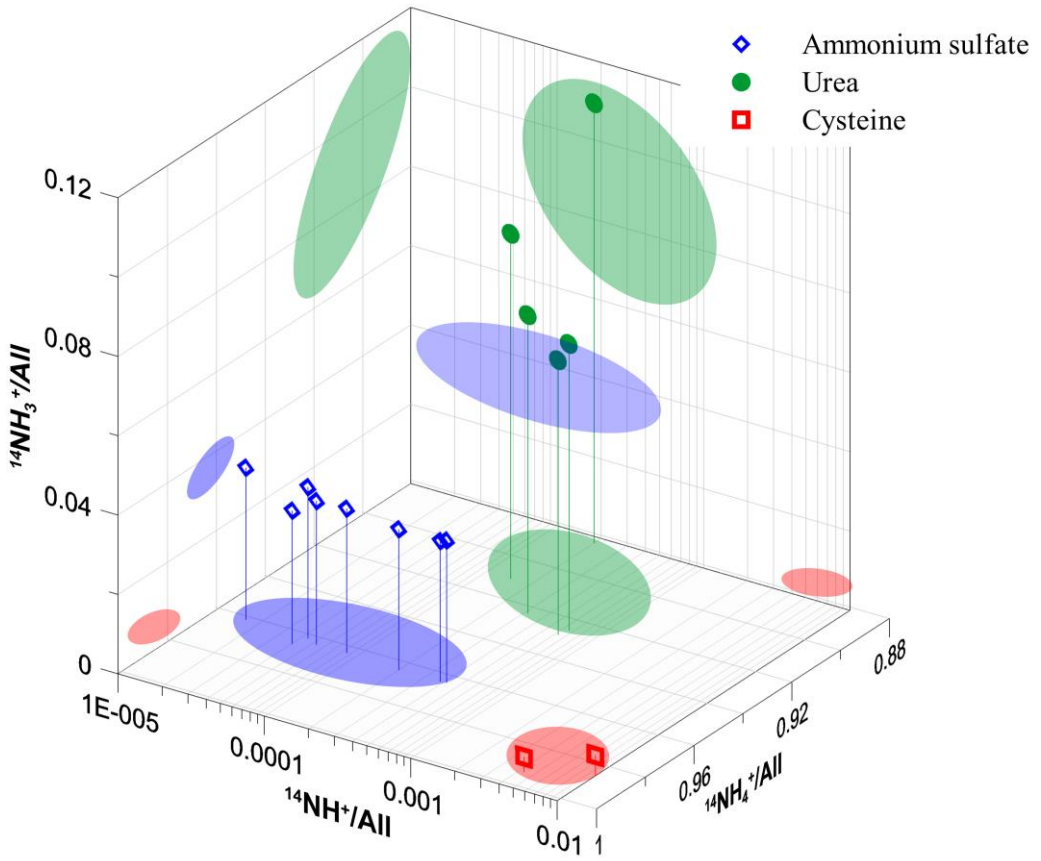

Figure 3-8. The distribution of different samples (ammonium sulfate, urea and cysteine) based on the normalized heights of the secondary ion signals of $^{14}NH^+$ / All, $^{14}NH_3^+$ / All and $^{14}NH_4^+$ / All. All = $^{14}NH^+ + ^{14}NH_2^+ + ^{14}NH_3^+ + ^{14}NH_4^+$.

3.3.6 Feasibility study for speciated isotope analysis

Different from previous methods (Boyd and Pillinger 1991, Boyd et al., 1994, Sigman et al., 2001, Coplen et al., 2004, Divers et al., 2014, Liu et al., 2014, Sofen et al., 2014) for nitrogen isotope analysis, in situ species specific nitrogen isotope analysis can be achieved at the micrometer and sub-micrometer scale and different N-bearing species are well separated by NanoSIMS analysis. With the NanoSIMS 5 masses can be collected simultaneously. So it is possible to distinguish N-bearing species by 4 different secondary ion species, while the nitrogen isotope ratio is measured using $^{12}C^{15}N^-$ / $^{12}C^{14}N^-$, $^{15}N^{16}O_2^-$ / $^{14}N^{16}O_2^-$ or $^{15}NH_4^+$ / $^{14}NH_4^+$. Uncorrected $\delta^{15}N$ was calculated by:

$$\delta^{15}N_{uncorrected} = \left(\frac{R_X}{\overline{R_X}} - 1\right) \times 1000\ (‰) \qquad \text{Equation 3-1}$$

where R_X represents $^{12}C^{15}N^-$ / $^{12}C^{14}N^-$, $^{15}N^{16}O_2^-$ / $^{14}N^{16}O_2^-$ or $^{15}NH_4^+$ / $^{14}NH_4^+$ molecular ion ratios. $\overline{R_X}$: Mean of individual R_x values.

Figure 3-9 demonstrates the results of a feasibility study for different N-bearing species. The $^{12}C^{15}N^-$ / $^{12}C^{14}N^-$ - ratio can be potentially used to determine the nitrogen isotopic composition of all types of samples, including those that do not contain carbon. Carbon contamination is ubiquitous and hence this isotope ratio can be used on all samples, though the counting statistical error on samples that do not contain carbon is poor. This can be remedied by carbon coating samples or depositing samples on a carbon containing substrate. The $^{15}N^{16}O_2^-$ / $^{14}N^{16}O_2^-$ - ratio can potentially be used to measure species specific nitrogen isotope ratios in nitrate/nitrite samples. The $^{15}NH_4^+$ / $^{14}NH_4^+$ - ratio, on the other hand, can potentially be used to measure species specific nitrogen isotope ratios in ammonium salts, urea and pure amino acids.

These initial results were used to optimize the analytical conditions to improve the precision and characterize the matrix specific IMF. This is described for NO_2 and CN in detail in chapters 4 and 5.

3.4 Conclusions

Secondary ion intensities of $^{14}N^{16}O_x^-$ species ($^{14}N^{16}O^-$, $^{14}N^{16}O_2^-$ and $^{14}N^{16}O_3^-$) in sodium nitrate and sodium nitrite samples were investigated by NanoSIMS. They are unique to the decomposition of nitrate and nitrite. $^{14}N^{16}O_2^-$ has the highest secondary ion yield, so it can potentially be used to to measure the nitrogen isotopic composition of nitrate and nitrite species in complex mixed ambient aerosols.

$^{14}NH_x^+$ secondary ions ($^{14}NH^+$, $^{14}NH_2^+$, $^{14}NH_3^+$ and $^{14}NH_4^+$) were unique to samples containing ammonium ions or amino groups, but were not observed in biological tissue. $^{14}NH_4^+$ has the highest secondary ion yield and can potentially be used to measure the nitrogen isotopic composition of ammonium salts and amines and amides in complex mixed ambient aerosol.

For coarse aerosols (diameter > 1 μm), different species, including organic and inorganic materials can be best separated in the NanoSIMS by measuring four secondary ions, $^{12}C^{14}N^-$, $^{16}O^-$, $^{14}N^{16}O^{2-}$, and $^{14}NH_4^+$ on the same area sequentially. For fine aerosols (diameter < 1 μm), the same feat can also be accomplised measuring the four secondary ions, $^{12}C^-$, $^{16}O^-$, $^{12}C^{14}N^-$ and $^{14}N^{16}O_2^-$ in negative secondary ion mode or using $^{14}NH^+$, $^{14}NH_2^+$, $^{14}NH_3^+$ and $^{14}NH_4^+$ in positive secondary ion mode.

My results indicate that stable nitrogen isotope ratio measurements can successfully be

performed using $^{12}C^{15}N^-$ / $^{12}C^{14}N^-$ - ratio on all samples. The $^{15}N^{16}O_2^-$ / $^{14}N^{16}O_2^-$ - ratio can potentially be used to measure species specific nitrogen isotope ratios in nitrate/nitrite samples and the $^{15}NH_4^+$ / $^{14}NH_4^+$ - ratio can potentially be used to measure species specific nitrogen isotope ratios in ammonium salts, urea and pure amino acids.

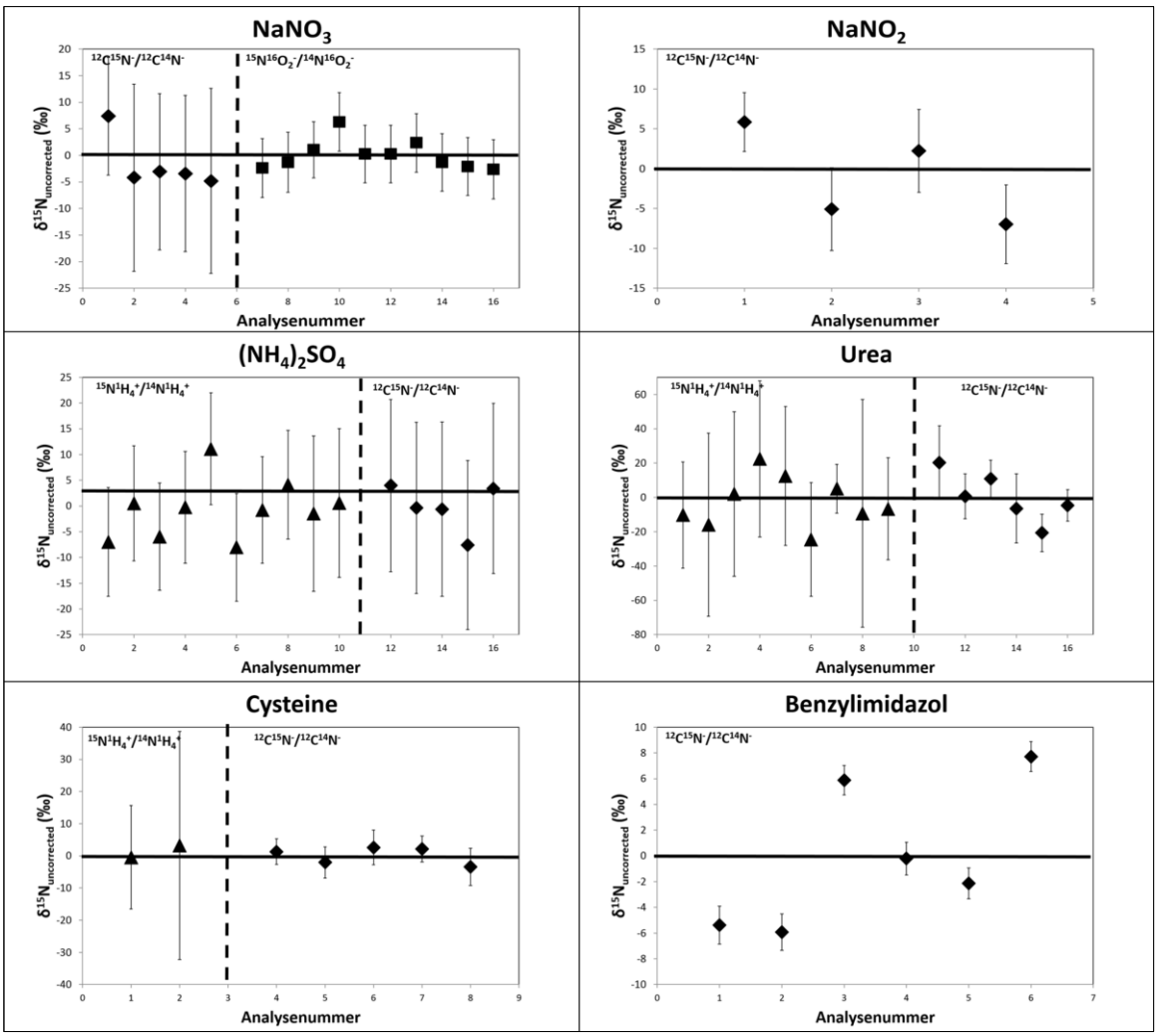

Figure 3-9. Stability of the $\delta^{15}N_{uncorrected}$ for different nitrogen containing compounds. Isotope ratio measurements were performed using $^{12}C^{15}N^-$ / $^{12}C^{14}N^-$ - ratios on all samples, $^{15}N^{16}O_2^-$ /$^{14}N^{16}O_2^-$ - ratios on nitrate samples and $^{15}NH_4^+$ / $^{14}NH_4^+$ - ratios on ammonium sulfate, urea and pure amino acid.

4 Stable N isotope analysis of nitrate by NanoSIMS using the $^{15}N^{16}O_2^-$ / $^{14}N^{16}O_2^-$ - ratio

4.1 Introduction

Nitrate is one of the major compounds of the suspended particulate matter in the atmosphere (Seinfeld and Pandis 2012). It has adverse effects on visibility, human health and ecosystems and causes acid rain (Milford and Davidson 1987, Compton et al., 2011, Sutton et al., 2011, Sofen et al., 2014). Nitrate aerosol, through its ability to scatter incoming solar radiation, has a negative radiative forcing and cools the climate (Van Dorland et al., 1997, Adams et al., 2001, Jacobson 2001, Adams and Seinfeld 2002, Martin et al., 2004, Schaap et al., 2004, Liao and Seinfeld 2005, Sutton et al., 2011). The climate consequences arising from the fertilization effect of nitrogen deposition and its influence on the carbon cycle is still hotly debated, but it is well known that N_2O emitted from fertilized soils is a potent climate gas (Compton et al., 2011, Gardenas et al., 2011, Zaehle et al., 2011).

In atmosphere, HNO_3 is formed by the reaction of NO_2 with OH. At night HNO_3 may also be produced from the reaction of NO_3 radicals with aliphatic hydrocarbons and aldehydes (Rollins et al., 2012, Seinfeld and Pandis 2012). Aerosol NO_3^- can be formed in aqueous phase aerosol by heterogeneous dissolution of HNO_3 and N_2O_5 (Seinfeld and Pandis 2012). In atmospheric aerosol particles nitrate is frequently found in the form of NH_4NO_3 which is formed by the reaction of HNO_3 with NH_3 (Buijsman et al., 1987, Seinfeld and Pandis 2012). HNO_3 can react with alkaline coarse-mode (> 1 μm) aerosols, e.g. $CaCO_3$, which is found in mineral dust (Krueger et al., 2004, Laskin et al., 2005, Laskin et al., 2005a, Hwang and Ro 2006), or sea salt NaCl (Zhuang et al., 1999, Coe et al., 2006, Hwang and Ro 2006, Saul et al., 2006) to form non-volatile coarse-mode NO_3^- species (Zhuang et al., 1999). It also frequently forms coarse mode KNO_3 when sufficient potassium derived from biomass combustion is present.

As described in chapter 3 for nitrate or nitrite salts, NO_2^- has a high secondary ion signal in the NanoSIMS. As nitrite is unstable in the atmosphere, in principle, the NO_2 signal can be used to measure species specific nitrogen isotope ratios in atmospheric nitrate aerosol. However, no one

has reported species specific nitrogen isotope analysis using these molecular ions in the literature so far. This chapter describes experiments to evaluate wether the $^{15}NO_2^-/^{14}NO_2^-$ - ratio can be used for species specific nitrogen isotope measurements. It furthermore discusses all potential interferances which complicate the succesfull application to atmospheric aerosol particles and investigates the matrix specific IMF in aerosol containing both nitrate and organic carbon.

4.2 Materials and Methods

4.2.1 Experimental conditions and NanoSIMS analysis

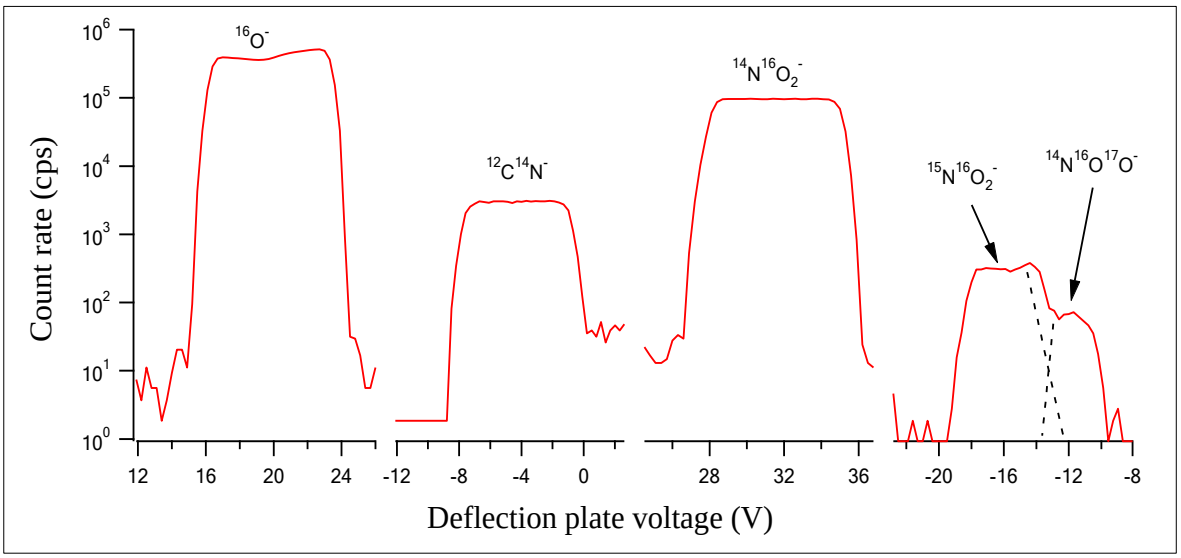

Figure 4-1: High-resolution mass spectra for mass regions 16, 26, 46 and 47. Entrance/exit slit setting: 20 µm/50 or 80 µm. All 4 masses can be obtained simultaneously in one measurement.

The description of the instrument and the most important settings were in section 3.2 . These settings resulted in a secondary ion transmission of ~10 - 35 % with the settings described above. Figure 4-1 shows the mass scans of peaks of interest for N isotope analysis.

The size of the analysis field over which the beam is scanned can affect the IMF. Since a certain number of counts have to be acquired for precise isotope measurements, small fields can promote the formation of craters, as the same small area is scanned repeatedly. On the other hand, on large fields charging may affect the IMF. To complicate matters further the sample roughness due to the grainy nature of the standards and the sample heterogeneity caused by a separation of organic and inorganic compounds during the crystallization of the aerosol can also affect the IMF. In order to investigate the effect of field size on the IMF, pressed bulk sodium and potassium nitrate standards were analyzed using three different field sizes. The measuring conditions were optimized

using three raster sizes 2 × 2 μm^2, 5 × 5 μm^2 and 10 × 10 μm^2. To keep the primary ion dose per unit area of sample per plane approximately equal, 64 × 64 pixels were set for 2 × 2 μm^2 scanning size and 128 × 128 pixels were set for 5 × 5 μm^2. Due to the much longer time (10 h for each sample) for a setting with 256 × 256 pixels for 10 × 10 μm^2 scanning size, the raster with 128 × 128 pixels was used instead. A residence time of 3000 μs/pixels was set for all measurements.

The IMF introduced by the presence of carbon in the sample was characterized using laboratory-generated aerosol-like particles. The method for producing these particles was described in great detail in chapter 2. Despite the fact that the nitrogen source in our aerosol-like mixtures was nitrate, in the presence of carbon, CN^- becomes the main nitrogen bearing molecular ion from the sample. Nevertheless, the $^{15}N^{16}O_2^-/^{14}N^{16}O_2^-$ - ratio is preferred for measuring the N-isotopic composition of nitrate even if the signal intensity is lower as the species is specific to nitrate. The CN^- molecular ion forms in the reaction zone above the sample because the C-N bond is energetically favored, while N-O bonds decompose under the primary ion bombardment. CN^- molecular ions have a short formation time and high ionization yield (Van Hardeveld et al., 1997). Hence, the presence of carbon can potentially influence the matrix specific IMF of nitrogen species, irrespective of whether the $^{15}N^{16}O_2^-/^{14}N^{16}O_2^-$ - or the $^{12}C^{15}N^-/^{12}C^{14}N^-$ - ratio is used to measure the isotopic composition. Carbon is a common element in atmosphere aerosol including organic (Jacobson et al., 2000) and inorganic materials (Gray et al., 1986) and carbon containing organic aerosol is coated onto or mixed with most particles. Therefore, it is extremely important to investigate the matrix specific IMF introduced by the presence of carbon for standards with known isotopic composition but variable N/C ratios.

While studying the matrix specific IMF of aerosol-like mixtures it was found that the sample substrate, too, plays an important role and can interfere with the measurement. Hence the IMF was studied on different sample substrates: gold foil, silver membrane filters, silicon wafers and gold coated nuclepore filers.

4.2.2 Heterogeneous samples

In previous SIMS studies, the N/C ratio was calculated from the secondary ion ratios CN^-/C^- (Van Zuilen et al., 2007, Thomen et al., 2014) and CN^-/C_2^- (Thomen et al., 2014). In these studies, nitrogen concentrations were low and carbon concentrations were high, i.e. nitrogen is the limiting species. These studies were conducted using standards of known chemical composition and the study showed that the $CN^-/(C^-$ or $C_2^-)$ - ratio can be used as a proxy for the N/C - ratio in the sample (on samples of known composition) with an appropriate calibration factor determined on a set of

standards (several standards with different known N/C - ratio) either using the $CN^-/(C^-$ or $C_2^-)$ – ratio. The conditions for this to be successful is that N<<C in the sample. As soon as N>C, i.e. nitrogen is no longer the limiting species, this no longer works. The $CN^-/(C^-$ or $C_2^-)$ – ratio cannot be used as proxy for the N/C ratio in our samples, as I also work with samples with N/C ratios >1 where C is the limiting factor.

In this study, two types of samples containing carbon are analyzed: Firstly, aerosol-like particles, a mixture of nitrates (sodium nitrate or potassium nitrate) with glucose. The two components are mixed in different proportions, resulting in a range of N/C ratios. Secondly, we studied carbon coated bulk nitrates. Initially, it was planned to use the theoretical N/C molar ratio (see table 2-2, chapter 2) of the aerosol-like mixture samples as proxy for the N/C ratio. However, it was found that the molar ratio of the mixture is a poor proxy for the true N/C ratio in the analysis field or sputtering spot. The reason is that each spot on each grain has a different real N/C ratio caused by the un-mixing of the salt and the organic carbon during crystallization, only the sample as a whole has the theoretical N/C ratio, i.e. the ratio in which the mixture has been prepared. Hence the true N/C ratio is different for each and every analysis field on the same sample. It also differs for different pixels within the same analysis field and changes from plane to plane for the same pixel. To investigate the influence of the presence of carbon on the IMF it is more crucial to ascertain the fractions of the nitrogen introduced into the sample in the form of nitrate, represented by NO_2^- and CN^- secondary ions for the specific spot. Therefore, the $^{14}N^{16}O_2^-$ / $^{12}C^{14}N^-$ - ratio is used to estimate the N (nitrate) / C (carbon atom) ratio of nitrite-glucose mixtures by calculating $^{14}N^{16}O_2^-$ / ($^{14}N^{16}O_2^-$ + $^{12}C^{14}N^-$), designated in the following as f. f does qualitatively correlate with the N/C - ratio but is not identical.

4.2.2.1 Aerosol-like particles

Figure 4-2 shows an SEM image and two NanoSIMS secondary ion images (^{14}N $^{16}O_2^-$, ^{12}C $^{14}N^-$) of laboratory-generated aerosol-like particles. The SEM image was taken after NanoSIMS analysis. From the secondary ion images it is clearly seen that the inorganic nitrate salt is concentrated in the center of particles, and is coated by organic glucose. Similar effects were observed in other laboratory studies (Pöhlker et al., 2014) and for ambient aerosols (Pöhlker et al., 2012). This behavior is characteristic for mixtures of inorganic salts and organic compounds in aerosol. The nitrogen to carbon ratio can be determined from the secondary ion ratio $^{12}C^{14}N^-/^{12}C^-$ in organic materials (Thomen et al., 2014) but as discussed above the fraction of the nitrate that is present in the form of NO_2^- as opposed to CN^- secondary ions is more crucial for studying the effect of the presence of carbon on the IMF and can be applied to all N/C - ratios including those >1.

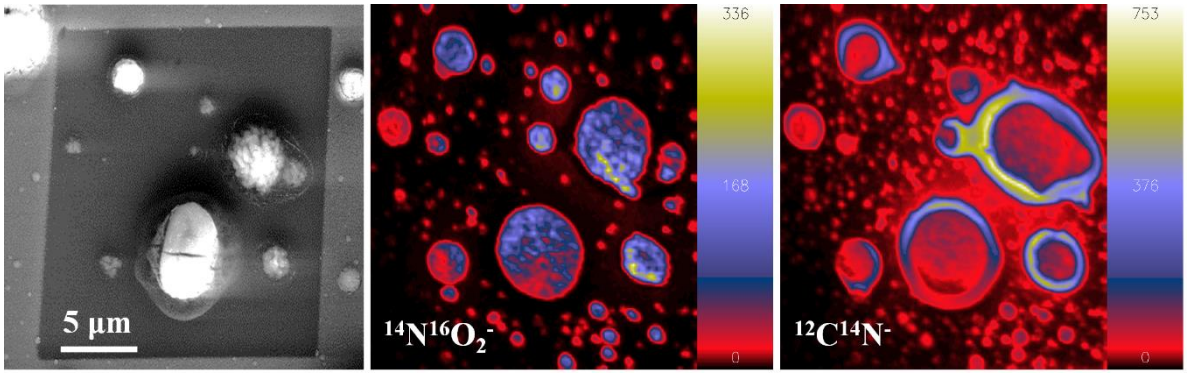

Figure 4-2. SEM image and NanoSIMS ion images of aerosol-like samples made by mixing potassium nitrate with glucose with N/C = 0.5. Raster size in the NanoSIMS ion images is 20×20 µm^2. SEM and NanoSIMS images are from the same position. SEM image was taken after NanoSIMS analysis.

4.2.2.2 Carbon coated bulk samples

Carbon coated bulk nitrates are not mixture samples. However, the collision cascade triggered by Cs^+ bombardment redistributes atoms in the upper layer of the sample and creates a mixed layer where carbon atoms and nitrate molecules co-occur. Moreover, at the edge of nitrate grains mixing of these two species also occurs. Figure 4-3 shows the images of carbon coated sodium nitrate analysis by NanoSIMS. The first and second row images are the data of 9th and 16th planes, respectively. In each row, secondary ion images of $^{12}C^{14}N^-$, $^{14}N^{16}O_2^-$ and the ratio image of $^{14}N^{16}O_2^-$ / $^{12}C^{14}N^-$ are shown. In the 9th plane, the carbon coating is still in the process of being sputtered away. Some grains of nitrate are already exposed resulting in an opposite distribution of $^{12}C^{14}N^-$ and $^{14}N^{16}O_2^-$ signals. This is also reflected in the ratio image that shows how a high heterogeneity. After further 7 planes of sputtering, the carbon coating has been sputtered away except the edge of raster area. Due to low electrical conductivity in the central area, very few $^{14}N^{16}O_2^-$ ions are being detected and charging stripes can be seen in the image. The $^{14}N^{16}O_2^-$ / $^{12}C^{14}N^-$ - ratio is still heterogeneous across the sample. By comparing the images in between the two planes, it can be seen that the $^{14}N^{16}O_2^-$ / $^{12}C^{14}N^-$ - ratio is highly heterogeneous for the same x-y coordinates and varies from plane to plane, which means the data processing should be performed for each plane individually.

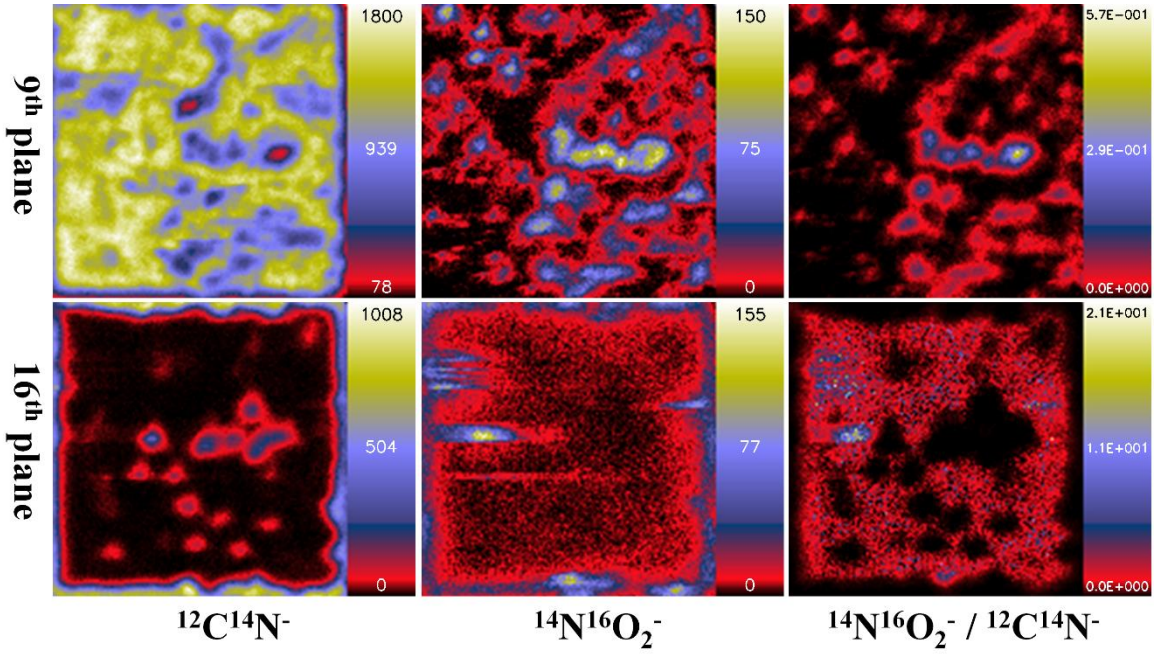

Figure 4-3. NanoSIMS ion images ($^{12}C^{14}N^-$ and $^{14}N^{16}O_2^-$) and ratio image ($^{14}N^{16}O_2^-/^{12}C^{14}N^-$) of carbon coated in-house sodium nitrate. Raster size is 5×5 µm^2. The first row and the second row are the data of the 9th and 16th planes, respectively.

4.2.3 NanoSIMS image data processing

The NanoSIMS analysis provides image data for up to five ion species as a function of sputter time (see Figure 4-3). Each image consists of a certain number of planes. Due to the heterogeneity of the samples describe above, in this study each plane of the $^{14}N^{16}O_2^-$ image was processed by defining a mask. This ensures that only areas with a $^{14}N^{16}O_2^-$ signal greater than a certain threshold value are considered for the data reduction. The threshold value is called mask level. Setting the mask level to 10 % means to select only the areas for which the $^{14}N^{16}O_2^-$ signal has an intensity larger than 10 % of the maximum intensity observed across all pixels in the analysis. After all planes of $^{14}N^{16}O_2^-$ data are calculated in this way, the total signal intensities of $^{15}N^{16}O_2^-$ and $^{14}N^{16}O_2^-$ are obtained. The ratio of $^{15}N^{16}O_2^-/^{14}N^{16}O_2^-$ is treated as the final isotope result. Figure 4-4 shows the data from one analysis calculated in this way. An aerosol-like potassium nitrate and glucose mixture with N/C = 0.1 was deposited on a silicon wafer. Images were recorded using a raster area of 10 × 10 µm^2 with 256 × 256 pixels² and a scanning speed of 1000 µs/pixel. Data was normalized to the maximum signal intensity (counts per second) observed in this analysis. $^{14}N^{16}O_2^-$ data from one plane are plotted in panel a), showing four nitrate grains. Three mask levels (10 % green plane, 20 % red plane and 30 % blue plane) were considered and are shown in panel b).

Panel c) shows the raw data without mask calculation. Panels d), e) and f) are the respective intensity plots after the mask levels were applied to all 75 planes separately. It can be seen from panels d), e) and f) that with the higher mask level, less areas with low secondary ion signal intensity were selected. Both, grain size and signal intensity were changing plane by plane. Due to the high glucose concentration in the sample, the potassium nitrate core was covered by glucose. In panel f), it is clear to see that, for grains 2 and 3, there is no data for the first 10 plans. After the glucose coating has been sputtered away, the size of grains 2 and 3 is growing from plain to plain. The size of grain 1 increases after about half of the analysis and grain 2 first becomes larger and then becomes smaller. If the material of the grain is easily sputtered away by the primary ion beam, the size and signal intensity will change dramatically from plane to plane. Therefore, using only one mask to quantify the IMF for the whole analysis may cause severe errors, if the IMF correction relies on determining the fraction of nitrogen present in the form of $^{14}N^{16}O_2^-$ as opposed to $^{12}C^{14}N^-$ accurately. The plane wise calculation method, which I incorporated into the NanoSIMS data analysis software, can trace the change in the composition and size of grains plane by plane, and it is very useful for measuring nitrate and glucose mixture grains. This method reduces the interference coming from background to a minimum, see section 4.4.3.2.

The heterogeneous mixing state of potassium nitrate and glucose causes discrepancies between the molar N/C ratio and the actual N/C ratio that vary from spot to spot and leads to variations in the results when different mask levels and calculation approaches are used. The $^{12}C^{14}N^-$ / $^{14}N^{16}O_2^-$ - ratio is affected as well. The numerical results of the data reduction procedure illustrated in Figure 4-4 are given in Figure 4-5, which shows the cumulated mass 26 ($^{12}C^{14}N^-$) and 46 ($^{14}N^{16}O_2^-$) ion intensities and f for four different mask levels.

A program was developed based on MATLAB to calculate single plane data with different parameters, e.g. 0 %, 10 %, 20 %, 30 % mask levels, automatically. More details about this program are given in appendix A.3

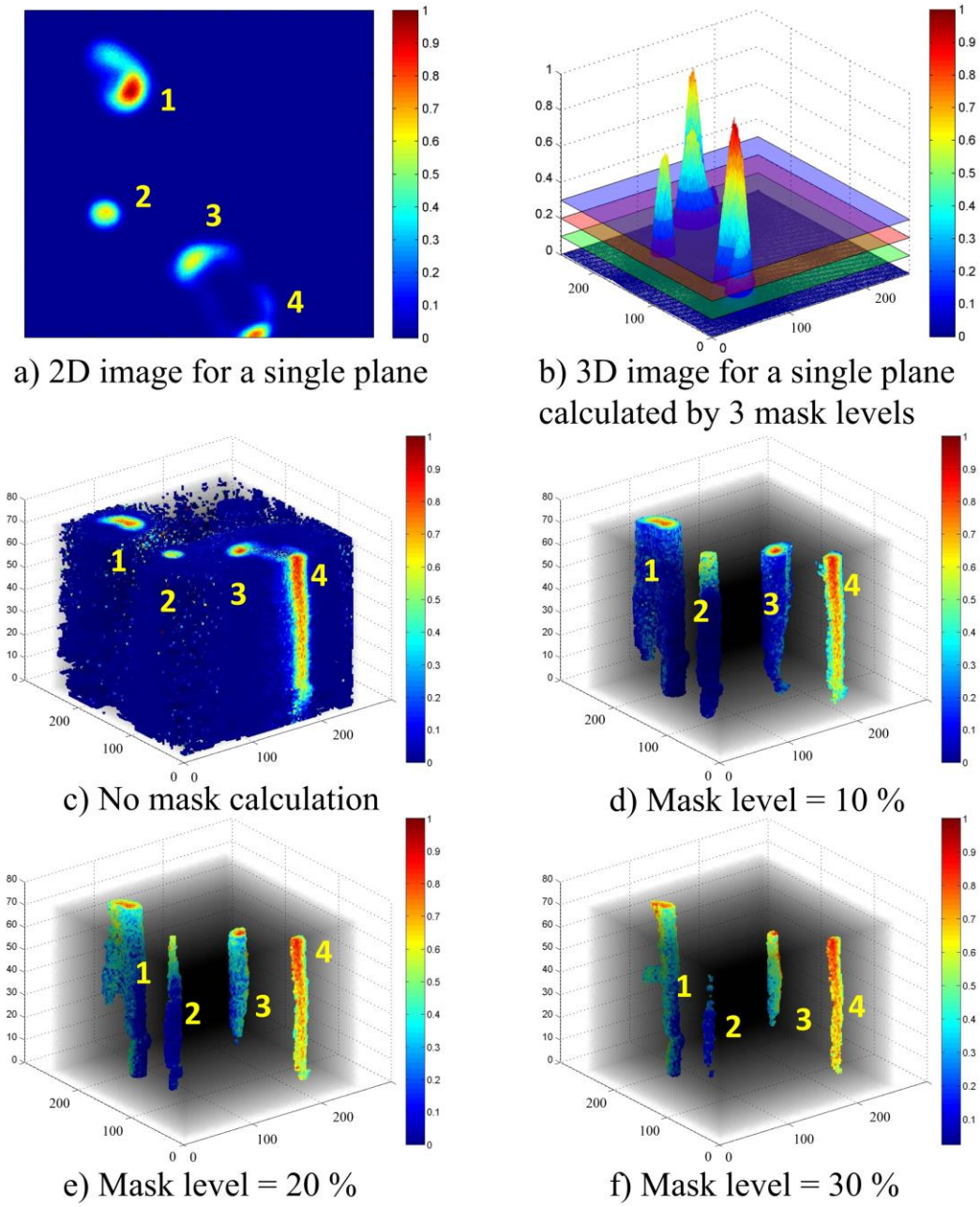

Figure 4-4. Illustration of the NanoSIMS ion image data reduction method used in this work. Sample: potassium and glucose aerosol-like mixture with N/C = 0.1 collected on a silicon wafer. Scanning area is 10 × 10 μm^2, 256 × 256 pixels^2, 75 planes. All data shown here are for mass 46 ($^{14}N^{16}O_2^-$). All signal intensities in each image were normalized to the highest intensity (= 1). In color scale, red (close to 1) means higher signal intensities than blue (close to 0). a) 2-D image of one single plane; b) 3-D image of the same data as in panel a) showing three different mask levels calculations (10 % mask level in green plane, 20 % mask level in red plane, 30 % mask level in blue plane). X and Y axis are pixel numbers and Z axis is the normalized signal intensity; c) no mask calculation; d) to f) single plane calculation results for all 75 planes using these three mask levels. X, Y axis are pixel numbers and Z axis is the plane number.

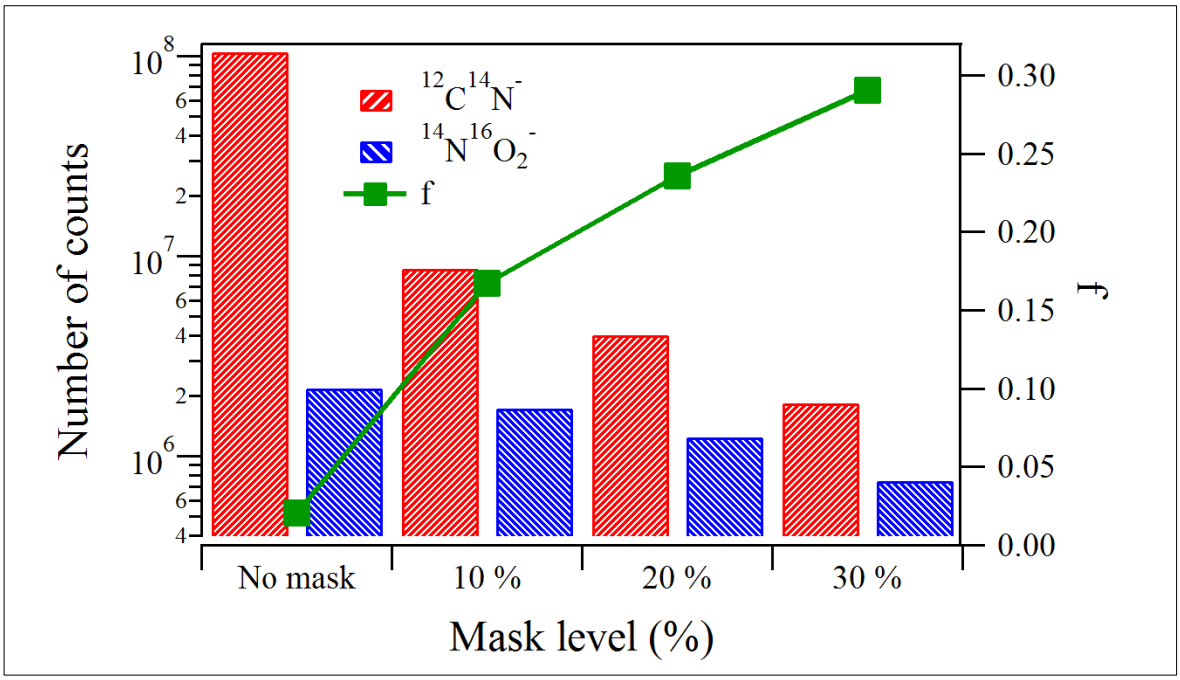

Figure 4-5. Cumulated ion intensities (left scale) for mass 26 ($^{12}C^{14}N^-$) and mass 46 ($^{14}N^{16}O_2^-$) of the four particles shown in Figure 4-4 for four different mask levels. The green squares represent f calculated from $^{14}N^{16}O_2^-$ / ($^{14}N^{16}O_2^-$ + $^{12}C^{14}N^-$) (right scale).

4.3 Nitrogen isotope measurements in bulk nitrates

Before attempting to measure the nitrogen isotopic signature using the $^{15}N^{16}O_2^-$/ $^{14}N^{16}O_2^-$ -ratio in aerosols, bulk nitrate standards pressed into gold foil were measured to explore factors that can influence the IMF, precision and accuracy.

4.3.1 Influence of experimental parameters

4.3.1.1 Raster area and pre-sputtering time

The nitrate salts used in this study (sodium nitrate and potassium nitrate), are non-conductive samples. Even when the standards are gold coated prior to the analysis, as soon as the gold-coating has been sputtered away, the center of the analysis field starts to charge. The consequence is that the center of the analysis field has a low secondary ion yield and potentially different IMF compared to the edge of the analysis field which has a high secondary ion yield. The ion yield of molecular secondary ions like $^{15}N^{16}O_2^-$ and $^{14}N^{16}O_2^-$ is more sensitive to charging compared to the secondary ion yield of atomic ions. Hence, optimizing the size of the measurement field is one of the critical parameters for isotope measurements.

A stable secondary ion signal is important for accurate and precise isotope measurements. After the gold-coat has been sputtered away and sufficient amount of Cs^+ has been deposited into the sample, a stable secondary ion signal can be obtained (Thomen et al., 2014), as long as crater effects and charging do not dominate. Whether a constant secondary ions count rate can be achieved, which effects accuracy and precision, depends on the size of the raster area, pre-sputtering time and primary ion beam current.

Pure nitrate samples were measured in ten NanoSIMS sessions, from August 2012 to December 2013. A total of 1243 spots were measured in two steps: 1) five sessions from August 2012 to January 2013, in which 2×2 μm^2, 5×5 μm^2 and 10×10 μm^2 raster areas were measured on three standards with different pre-sputtering times. The purpose was to identify the best raster area size and pre-sputtering time and to optimize the secondary ion count rate; 2) five sessions from June 2013 to December 2013 in which the instrument was operated using these optimized parameters to measure the isotope composition of in-house $NaNO_3$ #1, in preparation for using this in-house standard for aerosol-like mixture samples. In the same sessions the matrix dependent IMF between sodium nitrate and potassium nitrate was investigated.

Figure 4-6 shows the measured IMF of ^{15}N for pure nitrate standards. $\delta^{15}N_{bias}$ was calculated with reference to the average IMF factor α_{USGS35} for USGS35, see Equation 4-2.

$$\alpha_X = \frac{R_{X,SIMS}}{R_{X,true}} \qquad \text{Equation 4-1}$$

$$\delta^{15}N_{bias} = \left(\frac{\alpha_X}{\alpha_{USGS35}} - 1\right) \times 1000\ (‰) \qquad \text{Equation 4-2}$$

where $R = {}^{15}N^{16}O_2^- / {}^{14}N^{16}O_2^-$, X = USGS35, IAEA-NO-3 or in-house $NaNO_3$ #1.

This particular correction is not absolute but can be used to investigate the effect of instrumental conditions on the IMF and the matrix effect in this study.

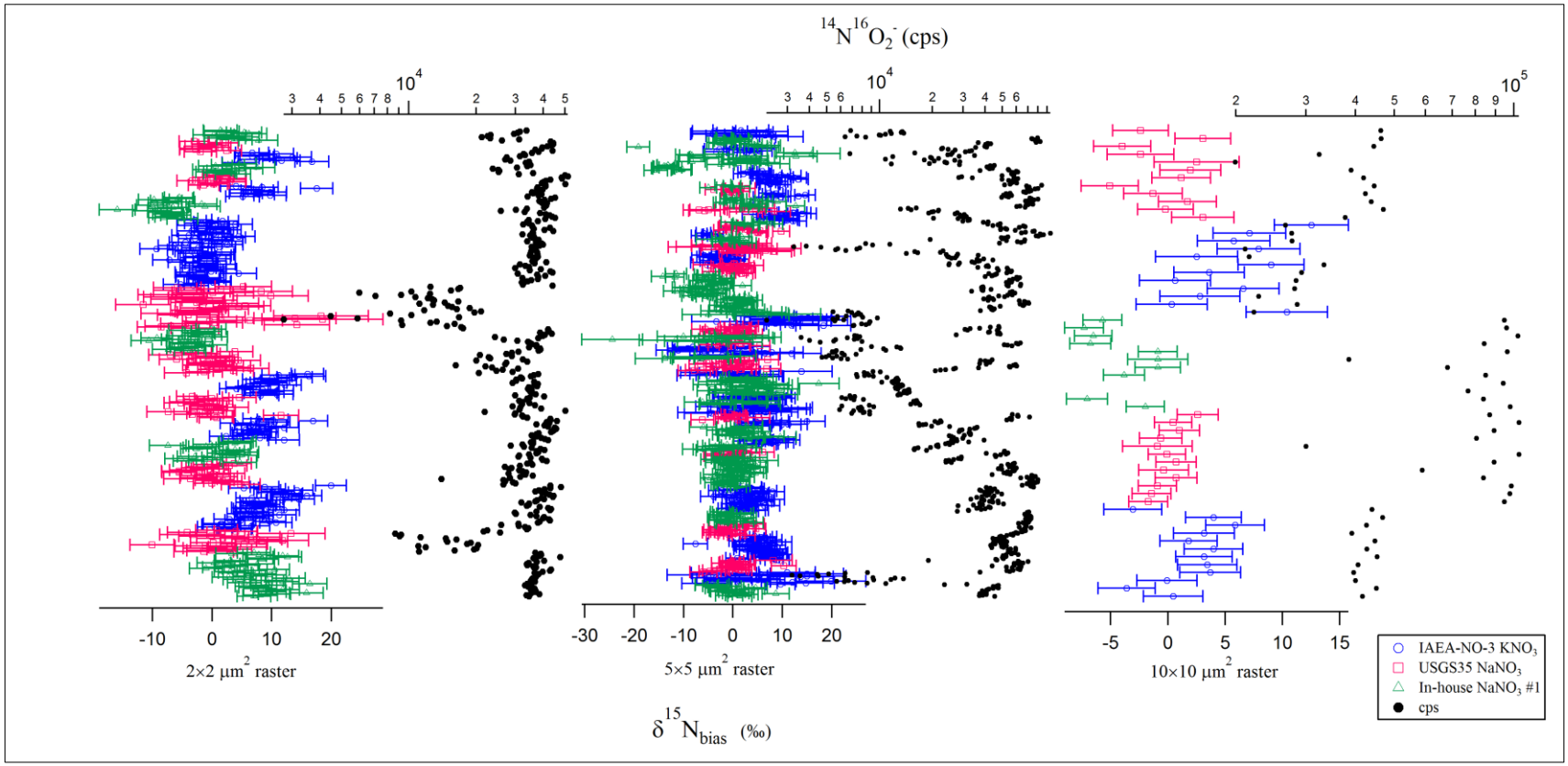

Figure 4-6. Relative IMF of 1243 spots measured from August 2012 to December 2013 in ten sessions for different raster areas. $\delta^{15}N_{bias}$ (lower axis) was calculated with reference to the IMF factor α_{USGS35} for USGS35. In the session December 2013 no USGS35 data were acquired. The in-house standard was used as the reference in this case to calculate the $\delta^{15}N_{bias}$ of KNO_3 in comparison to $NaNO_3$. Black dots are the secondary ion count rates of $^{14}N^{16}O_2^-$ (upper axis). Error bars are 1 σ.

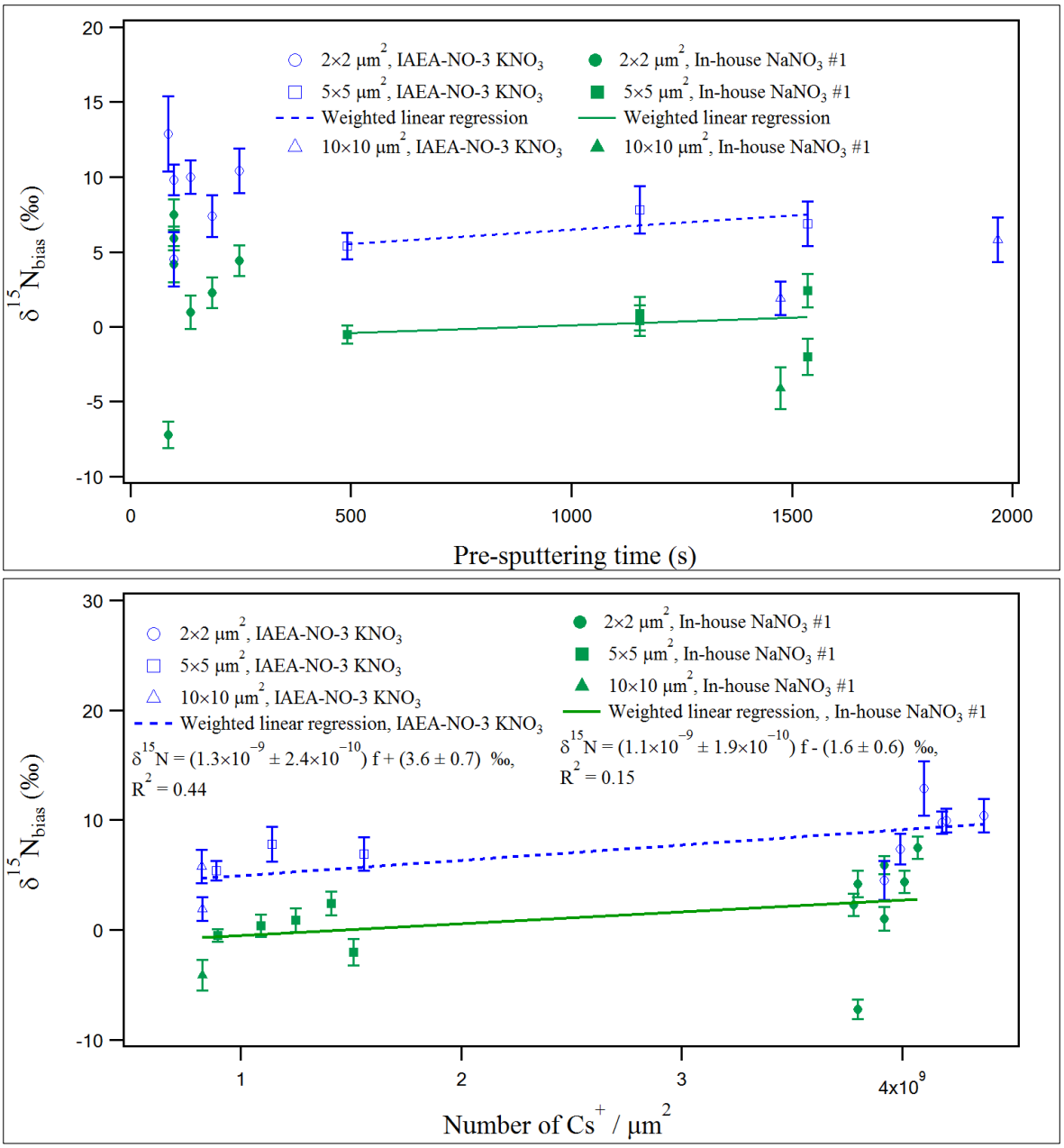

Figure 4-7. Dependence of $\delta^{15}N_{bias}$ for the in-house $NaNO_3$ #1 and the IAEA-NO-3 KNO_3 standards on pre sputtering time (top) and primary ion dose per square-micrometer (bottom) for three different raster areas: 2×2 µm², 5×5 µm² and 10×10 µm². Each data point in this plot was calculated according to Equation 4-2 using the USGS35 measurements recorded with the same pre-sputtering and analysis time. Error bars are 1 σ of the error of the mean.

Accuracy and precision displayed the following behavior with respect to the analysis field size and pre-sputtering time:

Influence of field size on accuracy and precision

2×2 µm² raster area: The small raster area is more sensitive to the varied topography of the

sample surface. A high density of primary ions is readily obtained and the gold coating on the sample surface is easily sputtered away. A long analysis time on a small field results in the formation of craters. The results, shown in Figure 4-7 top panel, demonstrate that the small fields are more sensitive with respect to different pre-sputtering times as compared to larger fields. They are also sensitive to differences in the ion dose per µm², obtained using the same pre-sputtering time, when the primary ion current drifts from analysis to analysis. Also, for very short pre-sputtering times, or poor instrument tuning, precision and accuracy on small fields are poor.

10×10 µm² raster area: It takes a very long time to sputter away the gold coating, and, consequently, the whole analysis takes too much time. Obtaining the same total primary ion dose while pre-sputtering on a 10 × 10 µm² area takes 4 times longer compared to a 5 × 5 µm² area and 25 times longer compared to a 2 × 2 µm² area. Only 60 spots were measured in one session. Since the larger analysis area does not bring any added value in terms of precision and accuracy, a shorter analysis time, which can only be obtained using a smaller area, is desirable.

5×5 µm² raster area: Compared to the other two raster settings, a 5×5 µm² raster area is the best choice, because: 1) for both standards, with a range of pre-sputtering times (500 s – 1500 s), the IMF is relatively stable, i.e. the amount of Cs^+ implanted prior to the start of the analysis does not influence the IMF too strongly; 2) The analysis time is acceptable compared to 10×10 µm² raster area; 3) The IMF is not affected by the complex topography of the sample surface as strongly as it is for 2 × 2 µm² fields.

Primary ion doses

Bombardment with primary ions does not only lead to sputter secondary ions, but also to a redistribution of sample atoms and massive changes of the samples surface. Primary ion induced matrix changes affect the secondary ion yields and signal stabilities (Breuer et al., 1997, Eckstein 2000). In this study, with the same primary current (typically 3 pA, i.e. 1.9 x 10^7 ions/s), different pre-sputtering times and raster areas cause different amounts of primary ions to be implanted per unit area of sample surface prior to commencing the analysis. The lower panel of Figure 4-7 shows the dependence of $\delta^{15}N_{bias}$ for the in-house $NaNO_3$ #1 standard and the IAEA-NO-3 KNO_3 standards on different primary ion doses for three different raster areas. It can be seen that samples receiving a higher primary ion dose tend to show a larger $\delta^{15}N_{bias}$ in favor of the heavier isotope ^{15}N. However, comparing the $\delta^{15}N_{bias}$ for the two standards shows that they have similar slopes within errors, which means the behavior is a function of primary ion dose only and not a function of the matrix. The reference USGS35, however, has a different dependence of matrix specific IMF on the primary ion dose than in-house sodium nitrate and IAEA-NO-3 potassium nitrate (see

section 4.3.1.3). The behavior should not be caused by crater effects, as deeper crater usually causes IMF favoring the lighter isotope, and USGS35 $NaNO_3$ is least prone to crater formation (Figure 4-10). It is possible that NO_2^- molecular ion formation depends on the number of multiple collisions in the collision cascade and faster ablation rates (nm/scanning frame) may favor greater stability of the $^{15}NO_2^-$ molecular ion. Both the IAEA-NO-3 and the in-house $NaNO_3$ show deeper craters and consequently faster ablation rates (nm/scanning frame) compared to USGS35 $NaNO_3$ and the effect is particularly pronounced for 2x2 μm² scanning fields.

Due to the facts that 1) the 2×2 μm^2 raster area analysis shows only a low stability of $\delta^{15}N_{bias}$ and that 2) the 10×10 μm^2 raster area analysis requires unreasonably long times to establish primary ion sputtering-implantation equilibrium, the 5×5 μm^2 raster area analysis was chosen as the best field size for further studies.

4.3.1.2 Influence of the secondary ion signal intensities and transmission

High mass resolution and high transmission for secondary ions make the NanoSIMS a powerful instrument for isotope measurement on small samples. However, low spot to spot reproducibility is one of the limitations for precise isotope measurement and the significant influence of the quasi-simultaneous arrivals (QSA) effect on the measurement result is one of the drawbacks of high transmission.

QSA

QSA is one of the limitations of isotope measurement by electron multipliers (Slodzian et al., 2001, Hoppe et al., 2013). Figure 4-8 shows the intensity ratio of secondary ions $^{14}N^{16}O_2^-$ over primary Cs^+ ions for three standards for the three raster sizes considered here. The data sequence is the same as the data in Figure 4-6.

As the abundance of $^{14}N^{16}O_2^-$ is 270 times larger than the abundance of $^{15}N^{16}O_2^-$, QSA affects mainly $^{14}N^{16}O_2^-$. A measured isotope ratio R_{meas} can be corrected by the equation: $R_{true} = R_{meas}/(1+\alpha \times K)$ if the major isotope is in the denominator, where K is the ratio of secondary over primary ions and α is a constant with a theoretical value of 0.5 (Slodzian et al., 2001). K is shown on the x axis in Figure 4-8. For all raster areas the differences of K for different measurements within a single session are less than 5×10^{-3}. This means the QSA effect will affect the final results by less than 2.5 ‰. This upper limit is comparable to the error of individual spot analyses (averaged about 3 ‰). Therefore, the QSA effect will not be considered for pure nitrate samples. However, if there are more significant differences in the count rates of different standards, e.g. in

the case of aerosol-like mixtures with different N/C-ratios, then a QSA correction may be required.

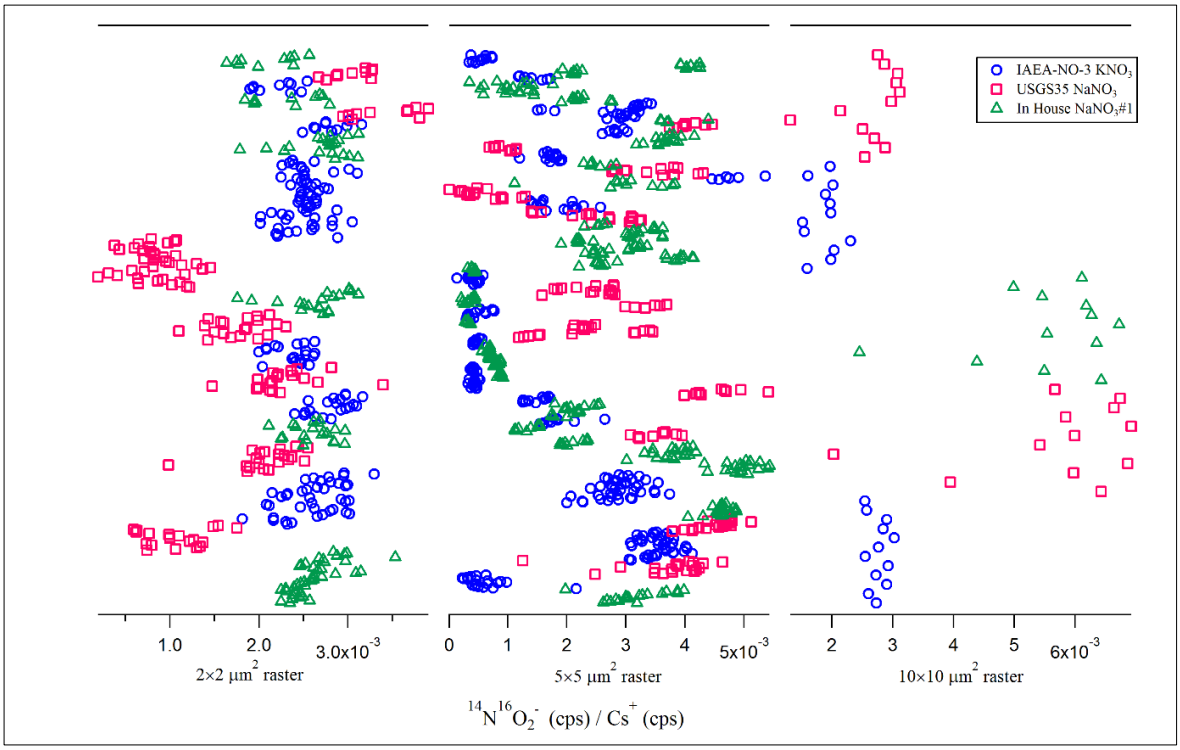

Figure 4-8. The ratio of secondary $^{14}N^{16}O_2^-$ over primary Cs^+ ion intensities for three standards and three raster areas. Measurement spots in this plot have the same sequence as in Figure 4-6. The Cs^+ count rate is calculated from the measured primary beam current, divided by 1.602×10^{-19} , and multiplied by the primary current reduction factor of 1.1×10^{-4} (D1-2, 300µm). Primary current is the average of currents before and after each spot measurement.

The challenges of low secondary ion count rates

In the first part of bulk analysis, August 2012 to January 2013, there were some measurements with very low count rates. These were excluded from the dataset above. Figure 4-9 top panel shows the $\delta^{15}N_{bias}$ increased sharply with the decreasing of the count rate for USGS35 and the in-house sodium nitrate standard. According to the previous discussion, QSA should not the main reason, because the maximum effect is less than 2.5 ‰, even for such a distinct drop in count rate. Considering the extremely low count rates ($^{14}N^{16}O_2^-$ < 7,000 cps, $^{15}N^{16}O_2^-$ < 26 cps), the influence of potential interferences and other effects is amplified. This point can be illustrated by introducing a constant hypothetical interference on the secondary ion signal of $^{15}N^{16}O_2^-$, which has a small count rate of 0.15 cps. The results were corrected for the measurements with low count rates (2×2 μm^2 raster area and 5×5 μm^2 raster area USGS35), by subtracting this hypothetical interference (see bottom panel in Figure 4-9). Compared to the original data, the $\delta^{15}N_{bias}$ becomes independent of the $^{14}N^{16}O_2^-$ count rate after subtracting the hypothetical interference. This indicates, that there

may indeed be an interference, that can possibly be a challenge while measuring the nitrogen isotope composition with a high precision and accuracy when the overall signal intensity is low.

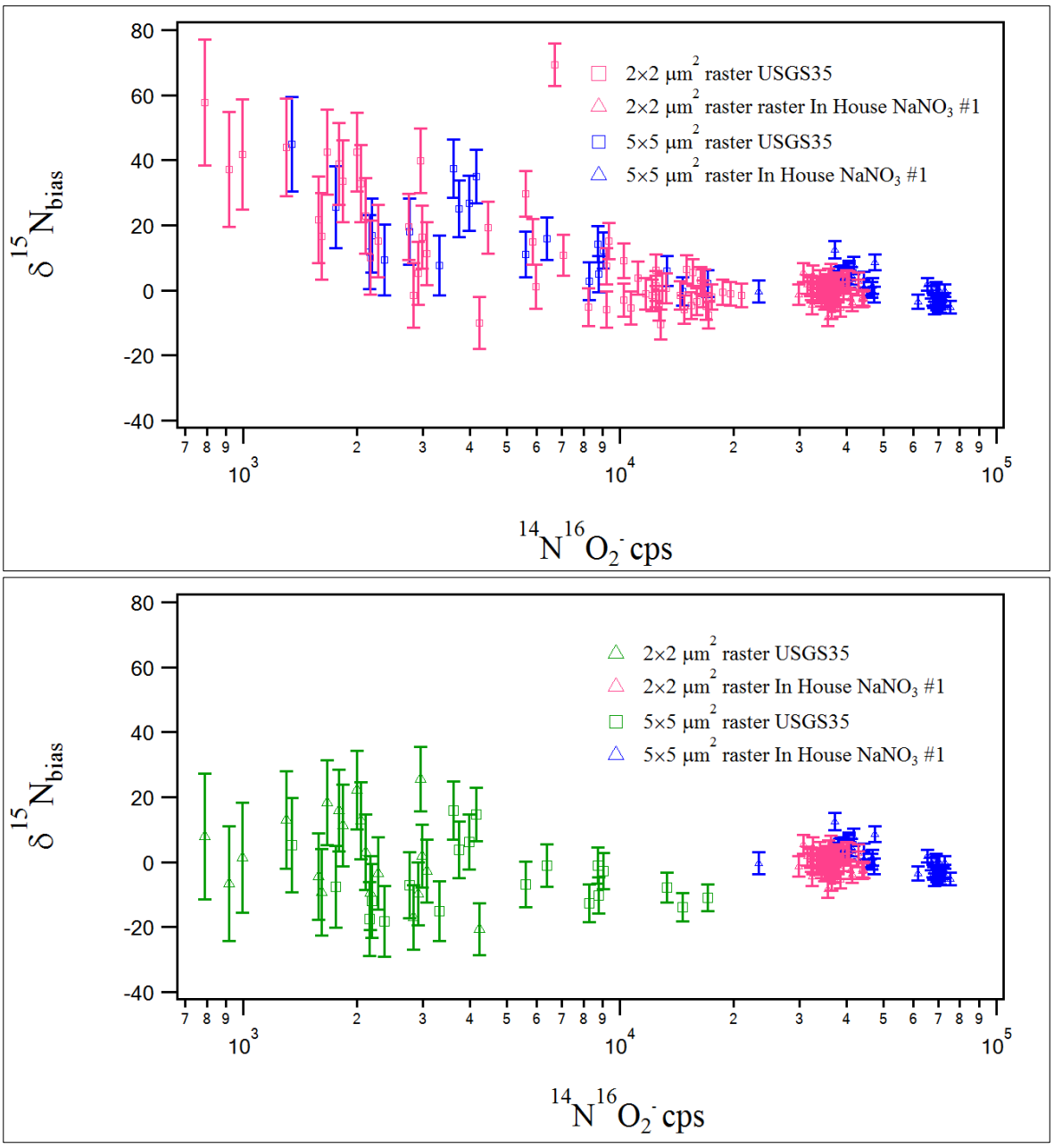

Figure 4-9. IMF against the count rate of the secondary ion $^{14}N^{16}O_2^-$. The data are from the October 2012 session. $\delta^{15}N_{bias}$ was calculated by using the data of USGS35 with count rate > 7,000 cps. Error bars are 1 σ. Top panel shows the raw data; bottom panel shows the data of 2×2 µm² raster area and 5×5 µm raster area after the data has been corrected by subtracting a hypothetical 0.15 cps interference on the secondary ion $^{15}N^{16}O_2^-$.

Figure 4-10. SEM images of standard IAEA-NO-3 KNO3, USGS35 $NaNO_3$ and in-house $NaNO_3$ #1 after NanoSIMS analysis in three raster areas. Primary ion beam current is about 2.7 pA. 64 × 64 pixels were set for 2 × 2 μm^2 scanning size and 128 × 128 pixels were set for 5 × 5 μm^2 and 10 × 10 μm^2 scanning size. A residence time of 3000 µs/pixels was set for all measurements. 80 planes were acquired for each spot.

4.3.1.3 Influence of ambient conditions on sample stability and isotopic composition

Most nitrate samples are relatively unstable materials chemically and physically. Chemically, the presence of a stronger acid, e.g. sulfuric acid can push the nitrate back into the gas phase if alkalinity is the limiting factor. Physically, nitrates activate readily at low relative humidity (RH), i.e. the sample preparation must take place in a laboratory with RH control and the samples need to be stored in a desiccator. The efflorescence behavior of nitrates is complex, in particular when there is some organic contamination (Tang and Munkelwitz 1994, Hoffman et al., 2004, Pöhlker et al., 2014). Extreme conditions in NanoSIMS, e.g. high vacuum and high energy Cs^+ ion bombardment, can be a potential challenge for high precision and accuracy isotope measurement on nitrate samples. It was found that sodium and potassium nitrate samples can be successfully prepared and introduced into the NanoSIMS while ammonium nitrate sublimates in the ultrahigh vacuum and calcium nitrate activates under laboratory conditions.

There are more additional challenges that become important when long time nitrate isotope measurements using the same set of standards are envisaged. Even after the $^{15}N^{16}O_2^-$ / $^{14}N^{16}O_2^-$ - ratio was successfully measured in the NanoSIMS for a certain nitrate and nitrite sample once, on the fresh sample, the deliquescence and efflorescence of these substances decrease the stability of the standards. The relative humidity in the lab was changing from 15% to 25 % RH and once the standard bottles have been opened while preparing samples for NanoSIMS analysis in the lab, the crystal structure of nitrate standards will change and a few monolayers of water will be coating the grains even at 15% RH. After putting the samples in the NanoSIMS, extreme vacuum conditions ($\sim 10^{-10}$ torr in analysis chamber) will completely dehydrate the standards. If the sample holder is taken out of the NanoSIMS, the standard will activate, or at least again acquire a coating of a few monolayers of water and also take up species from the gas phase in this process. When these changes accumulate over a long time, the consequence is a decreased life time of the standards. After more than a year's measurement, the standard USGS35 became less stable and it is became harder to get good results in the NanoSIMS. The standard does acquire some moisture while handling, and the degassing of this crystal water after introducing the sample into the NanoSIMS destroys the gold coating which results in charging. Stable and accurate isotope data is then difficult to obtain. A similar problem also occurred in two other standards, in sessions June 2013 to December 2013. After charging occurred, the samples were taken out of the NanoSIMS for a very brief time and were gold coated again to make them conductive. The deliquescence and efflorescence behavior varies between the different standards, e.g. sodium nitrate showed more deliquescence than potassium nitrate and the two different sodium nitrate standards also differ

because they have different grain sizes (Figure 4-10). This can cause different signal intensities, even within the same session, for different standards. The charging and topography of the surface, which can result when the gold coating is detached due to degassing, also leads to the bad peak shapes and reduces the mass resolution, due to variations in the angular component of the momentum of secondary ions exiting the sample surface. In this case the signal of $^{15}N^{16}O_2^-$ is easily interfered by the flank of $^{14}N^{16}O^{17}O^-$ (Figure 4-1) on some spots, while under good measurement conditions it is sufficiently separated from $^{15}N^{16}O_2^-$, which results in variable isotope ratios and a poor spot to spot variability.

4.3.1.4 Summary

The most important results can be summarized as follows:

1. 5×5 µm² raster area was chosen as the best field size.
2. Pre-sputtering time was initially set to 500 s and later reduced to 100 s, in order to make the analysis faster, as IMF for 5×5 µm² analysis fields is not sensitive to pre-sputtering time.
3. Only measurements with > 7,000 cps count rate of secondary ions $^{14}N^{16}O_2^-$ can be considered for the final results to avoid potential interferences.
4. Chemical and physical properties of nitrate salts should be considered during isotope analysis, e.g. the size of the grain, characteristic of deliquescence and efflorescence, when samples are moved between air and high vacuum conditions and the associated degassing/activation which damages the gold coating and reduces the conductivity and leads to uptake of gas phase species from the laboratory air.
5. IMF correction should be done in using standard bracketing mode to improve analysis accuracy.

4.3.2 Results and discussion

Additional analyses on pure nitrate samples were performed from June 2013 to December 2013 in five sessions to optimize the tuning parameters further. Only results obtained using 5×5 μm^2 raster area data are shown and discussed in this section. Section 4.3.2.1 investigates the precision and accuracy of nitrogen isotope analysis using the optimized conditions; section 4.3.2.2 investigates the matrix dependence of IMF for nitrate salts with different cations.

4.3.2.1 Analysis of in-house $NaNO_3$ sample using USGS35 $NaNO_3$ standard for IMF correction

Isotope ratios measured by NanoSIMS are always shifted from their true values due to IMF. Measurement of $\delta^{15}N$ values of unknowns requires that the IMF for N be measured accurately, which can only be done by repeat measurements of homogeneous standards with known N isotopic composition interspersed with analyses of unknowns (Hauri et al., 2002). In this section, standard USGS35 ($NaNO_3$, $\delta^{15}N_{air}$ = +2.7 ‰) was measured to determine the IMF in each measurement session which is calculated using the equation:

$$IMF_{USGS35} = \left(\frac{R_{USGS35,SIMS}}{R_{USGS35,true}} - 1 \right) \times 1000\ (‰) \qquad \text{Equation 4-3}$$

where $R = {}^{15}N^{16}O_2^- / {}^{14}N^{16}O_2^-$.

Table 4-1 lists the measured IMF of $\delta^{15}N$ in one year of NanoSIMS measurements. The apparent IMF ranges from -12.6 ± 4.9 ‰ to 11.3 ± 1.6 ‰ in these long-term measurements. Despite the fact that IMF can come from several stages during SIMS analysis (Winterholler et al., 2008), the absolute magnitude of the session to session change of the apparent IMF during measurements in multi collector mode is usually related to differences in the sensitivity of the electron multipliers recording the ^{14}N and the ^{15}N signal. This results in a change in the apparent IMF and this is the most frequent reason behind session to session changes in the apparent IMF. Since this electron multiplier effect is not related to a mass dependent fractionation caused by different trajectories of different m/z through the instrument and neither a mass independent effect related to the absolute count rate (dead time) or the secondary ions per primary ion impact (QSA effect) and affects all measurements within the same session equally, the relative difference between the IMF of two standards of different chemical composition (e.g., $NaNO_3$ and KNO_3), the matrix specific IMF, is usually much more stable than the absolute apparent IMF, see section 4.3.2.2. Differences in the kinetic energy and ejection angle of the secondary ions can result in different trajectories of secondary ions of different m/z through the mass spectrometer which can result in mass fractionation at different slits. This mass fractionation is mass dependent. The matrix specific IMF is the result of such differences in the kinetic energy or ejection angle of the secondary ions as a function of the sample matrix.

The in-house $NaNO_3$ #1 sample was measured with the same tuning conditions as standard USGS35 in the same measurement session. Consequently, the USGS35 standard can be used to correct the IMF for the in-house $NaNO_3$ #1. This isotopic signature of the in-house sample was measured as $\delta^{15}N_{air}$ = 16.6 ± 0.6 ‰ over all sessions with a session to session reproducibility of 1.3 ‰. The N isotopic composition of the in-house sample was determined independently by an

accredited laboratory (Iso-Analytical Limited, UK) as $\delta^{15}N_{air}$ = 16.54 ± 0.43 ‰. Hence, measurements on 5×5 µm^2 analysis fields provide excellent precision and accuracy.

Table 4-1. Measured IMF of $\delta^{15}N$ for UGSG35 $NaNO_3$ #1. 1σ is the error of the mean.

Measurement session	IMF (‰)	1 σ	Measurement session	IMF (‰)	1 σ	Measurement session	IMF (‰)	1 σ
08.2012	11.3	1.6	**11.2012**	-1.4	2.2	**08.2013**	-12	3.2
08.2012	9.2	0.6	**01.2013**	-5.7	1.1	**08.2013**	-11.8	0.9
09.2012	-2.2	0.6	**01.2013**	-2.5	0.8	**08.2013**	-8.3	1.3
09.2012	0.4	0.5	**01.2013**	-4	0.8	**09.2013**	-4.4	0.7
09.2012	2.4	0.8	**06.2013**	-12.4	1.2	**10.2013**	-12.1	2.8
09.2012	-3.9	0.8	**06.2013**	-12.6	4.9	**10.2013**	-11.9	0.8

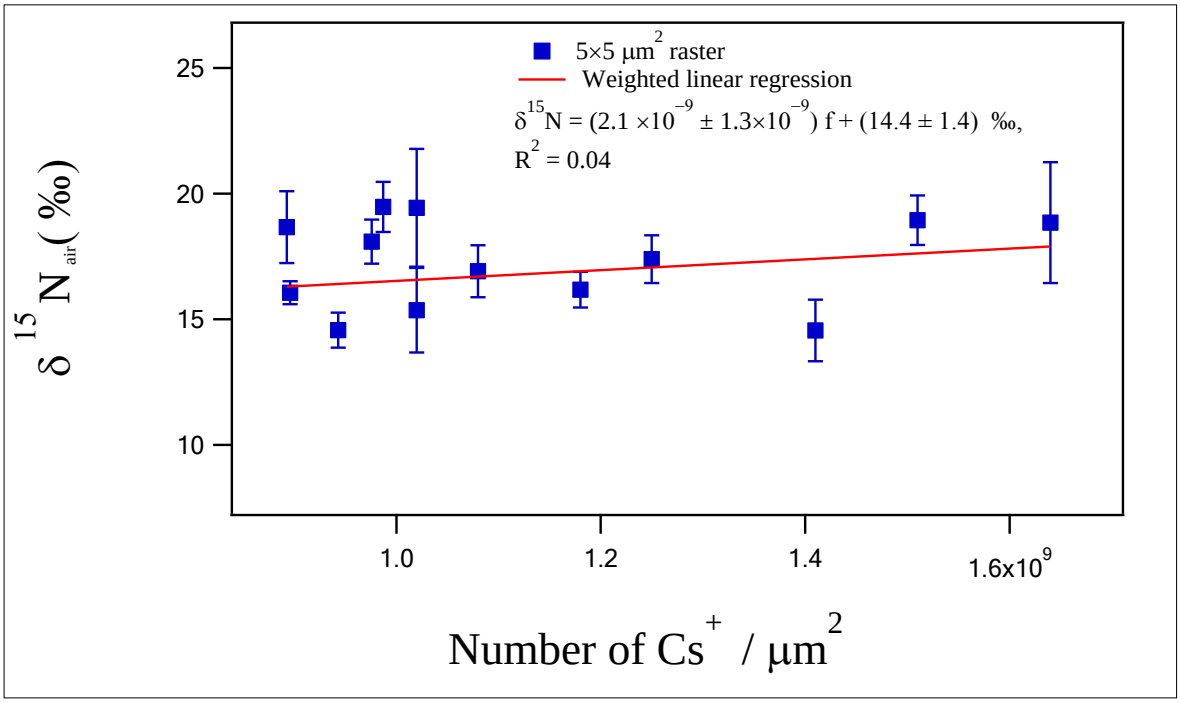

Figure 4-11. Results of N isotope analysis of in-house $NaNO_3$ #1 for different primary ion doses. The measured $^{15}N^{16}O_2^-$ / $^{14}N^{16}O_2^-$ ratio was corrected by IMF measured under the same conditions on USGS35. The primary ion dose was calculated from the number of Cs^+ ions, including pre-sputtering and analysis sputtering, impacting on the sample surface divided by the raster area. Only 5×5 µm^2 raster area data are shown here. Error bars are 1 sigma of the error of the mean of individual sessions.

Table 4-2. $\delta^{15}N_{air}$ of In-house $NaNO_3$ corrected by USGS35 $NaNO_3$ with raster area 5×5 μm^2. Spot to spot: spot-to-spot reproducibility.

Measurement session	Pre-sputtering time (s)	IMF factor	δ15N (‰)	1σ	Spot to Spot	Number of measurement spots
09.2012	492	0.99778	16.1	0.5	0.9	20
01.2013	1155	0.99426	16.9	1.0		10
01.2013	1155	0.99426	17.4	1.0		10
01.2013	1536	0.99474	18.9	1.0	0.7	10
01.2013	1536	0.99474	14.5	1.2		10
06.2013	100	0.98861	18.7	1.4		10
06.2013	200	0.98942	11.4	2.0	1.6	8
06.2013	1000	0.98768	18.8	2.4	3.3	10

4.3.2.2 Matrix dependence of the IMF

Nitrate aerosols in the atmosphere can be formed with different cations (Savoie and Prospero 1982, Wolff 1984, Kerminen et al., 1997). In order to measure the N isotope ratios in different nitrate salts, a good understanding of matrix effects, variations of the IMF between different nitrate salts, especially for $NaNO_3$ and KNO_3, is necessary. Matrix dependence of the IMF between the two standard samples $NaNO_3$ (USGS35) and KNO_3 (IAEA-NO-3) was investigated and calculated by:

$$\delta^{15}N_{bias} = \left(\frac{R_{IAEA-NO-3,SIMS}}{R_{IAEA-NO-3,true}} \times \frac{R_{USGS35,true}}{R_{USGS35,SIMS}} - 1\right) \times 1000\ (‰) \qquad \text{Equation 4-4}$$

where $R = {}^{15}N^{16}O_2^- / {}^{14}N^{16}O_2^-$. I.e., measurements on KNO_3 are corrected with the IMF correction factor inferred from the USGS35 standard. The results are shown in Figure 4-12. There is no strong relationship between matrix specific IMF and the primary ion dose implanted prior to commencing the measurement. For long-term measurements, $\delta^{15}N_{IMF\ KNO3}$ = 7.1 ± 0.9 ‰ with a session to session reproducibility of 1.5 ‰, respectively.

There is no previous study of the matrix dependent IMF for stable isotope analysis of nitrate using SIMS caused by the presence of different cations. Due to the difficulties of preparing samples and introducing them successfully into the ultrahigh vacuum in the NanoSIMS, only two standards were measured here: sodium nitrate and potassium nitrate.

Compared to similar studies by Winterholler et al. (2008) on sulfates that for different sulfates the IMF in the NanoSIMS depends on the ionic radius of the cations, these two salts have the same slope of the IMF as a function of the ionic radius of the cation (Figure 4-13). This indicates that

the processes governing the matrix specific IMF of nitrates and sulfates with the different cations are similar. It may also help to predict the matrix dependence of the IMF for different cations that may be encountered in atmospheric aerosols samples.

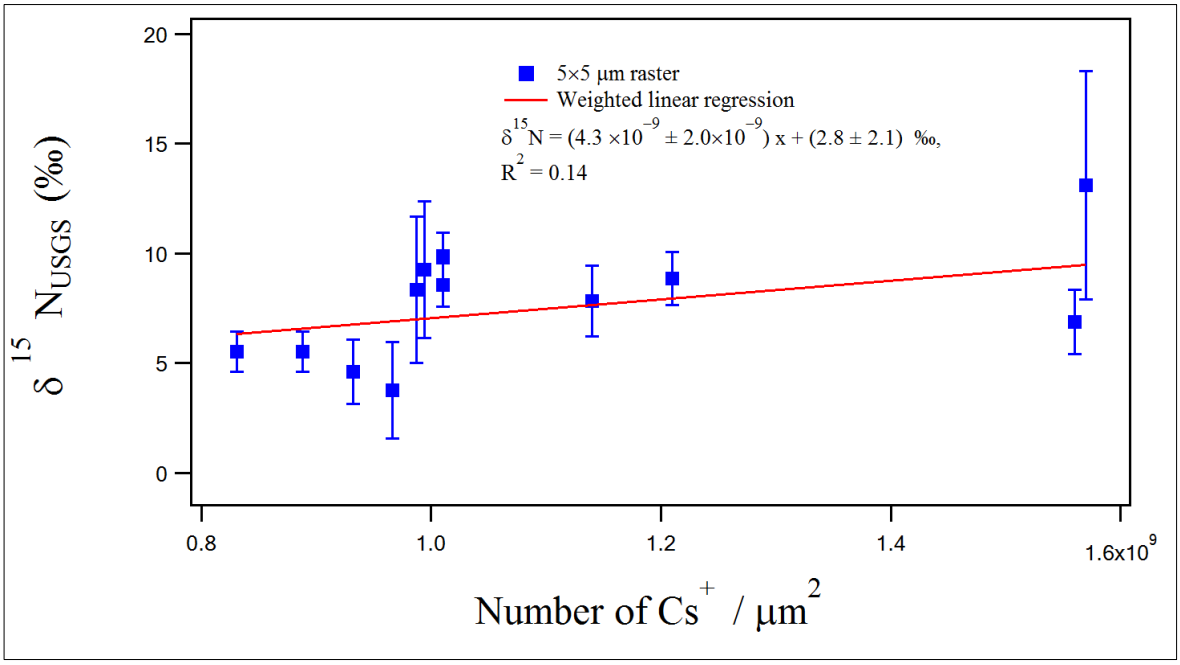

Figure 4-12. Matrix effect between $NaNO_3$ and KNO_3, calculated according to formula 4-4, for different primary ion doses (see legend to Figure 4-11). Only 5×5 µm raster area data are shown here. Error bars are1 sigma of the error of the mean.

4.3.3 Conclusions

Before attempting to measure $^{15}N^{16}O_2^-/^{14}N^{16}O_2^-$ ratios in nitrate containing aerosols-like mixtures, experimental parameters were optimized and the matrix dependence of IMF of pure nitrate samples was investigated. It was found that pure nitrate samples on gold foils can be analyzed with excellent precision and accuracy.

The time spent working on pure nitrate standards can be subdivided into two periods: The first period took 5 sessions from August 2012 to January 2013. The size of the analysis field and the pre-sputtering time was optimized. It was found that a 5×5 µm analysis field with 500 s pre-sputtering time is ideal, although IMF is not sensitive to pre-sputtering time and consequently the pre-sputtering time can be shortened further. It was also found that results obtained at low secondary ion count rate (< 7,000 cps) of $^{14}N^{16}O_2^-$ indicate the measurement may be affected by potential interferences. It was found that physical phase transitions while moving the sample from air to high vacuum conditions can compromise the conductive gold coating under certain

conditions. Multiple transfers can also compromise the sample chemically due to uptake of material from the gas phase during deliquescence. The second period took 5 sessions from June 2013 to December 2013. The optimized parameters were used to study the matrix specific IMF and determine the isotopic composition of the in-house standard.

After one year of measurement with the NanoSIMS, the results showed that the isotopic composition of pure nitrate salts ($NaNO_3$ and KNO_3) on gold foil can be measured accurately using the $^{15}N^{16}O_2^-$ / $^{14}N^{16}O_2^-$ secondary ion ratio. The precision of long term measurements on the in-house $NaNO_3$ sample is ± 0.6 ‰ for a raster size of 5×5 μm^2, which gave the best results. The accuracy obtained for this sample is better than 0.5 ‰. The difference in the matrix specific IMF between $NaNO_3$ and KNO_3 is 7.1 ± 0.9 ‰. The similarity of the matrix dependent of IMF on the ionic radius of the cations for sulfate and nitrate salts (Figure 4-13) indicates it should be possible to perform IMF correction on ambient nitrate aerosols which have different cations provided the samples can be introduced into the NanoSIMS successfully.

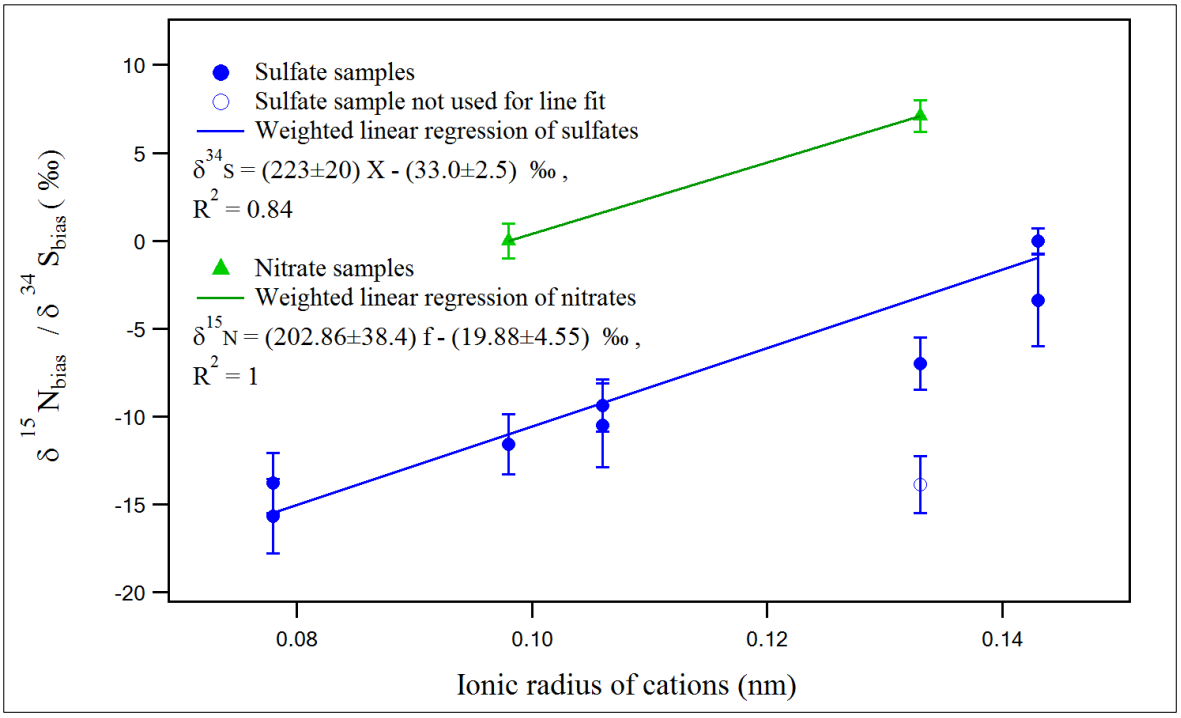

Figure 4-13. Dependence of $\delta^{34}S_{bias}$ and $\delta^{15}N_{bias}$ on the ionic radius of the cations of different sulfates and nitrates. Sulfates data are taken from previous research work (Winterholler et al., 2008) and the nitrate data are from this study. Due to unsuccessful analysis of calcium nitrate and ammonium nitrate by NanoSIMS, only two data points for sodium nitrate and potassium nitrate are available here. Blue and green lines are weighted linear regressions of sulfates data and nitrates data, respectively. Error bars are 1 sigma of the error of the mean.

4.4 Nitrogen isotope measurements on aerosol-like mixture samples

This section describes the analysis of sodium nitrate and potassium nitrate mixed with glucose in the form of aerosol-like samples, with variable N/C ratios. The purpose of these experiments is to explore the influence of the presence of carbon on the matrix dependence of the IMF for mixed aerosols.

Most results were obtained on two types of substrates: nuclepore filter and silicon wafer with two different collection techniques, filter collection and single stage impactor, respectively. Selected aerosol-like mixture samples were also deposited on gold foils using a single stage impactor after attempts to produce mixtures by carbon coating pure nitrate samples were found to not yield satisfactory results.

4.4.1 IMF in $\delta^{15}N$ calculation

All aerosol-like mixture samples were measured by NanoSIMS in image mode. The detailed data processing method is given in section 4.2.3 and the data processing program is described in section A.3 . Image data in each session was calculated with different mask levels: 0 %, 10 %, 20 % and 30 %. As described in section 4.2.3, single plane calculation together with high mask levels includes less background signals and focuses on more homogenous N/C ratio analysis areas. Hence, isotope ratios were calculated with a 30 % mask as function of the secondary ion ratio f. A weighted linear regression provides the fitting function:

$$R_{30\ \%\ mask\ level} = F(f) \qquad \text{Equation 4-5}$$

where $R = {}^{15}N^{16}O_2^- / {}^{14}N^{16}O_2^-$. In order to display the IMF induced by the presence of carbon, the isotope composition of the pure nitrate standard was defined as the zero point, i.e. $R_{30\ \%\ mask\ level} = F(1)$. Then the IMF of $\delta^{15}N$ is calculated by the equation:

$$\delta^{15}N = \left(\frac{R_{mixture\ aerosol,SIMS}}{R_{30\ \%\ mask\ level} = F(1)} - 1 \right) \times 1000\ (‰) \qquad \text{Equation 4-6}$$

where $R_{mixture\ aerosol,SIMS}$ is the measured isotope ratio of mixture particles.

4.4.2 Results

Two data sets are discussed in this section:

1. The first dataset was acquired for mixture samples containing sodium nitrate and glucose as a carbon source. The IMF was studied as a function of the N/C - ratio in the samples.

After good precision and accuracy were obtained while measuring the nitrogen isotopic composition of nitrate using the $^{15}N^{16}O_2^-$ / $^{14}N^{16}O_2^-$ - ratio on pure nitrate samples, in-house $NaNO_3$ #1 was used to generate aerosols-like mixture samples with glucose serving as a carbon source, to explore the matrix dependence of the IMF induced by the presence of carbon as a function of the N/C - ratio. Acquiring this data series took four experimental sessions (February 2013, March 2013, April 2013 and May 2013). The experiments included sample preparation, initial tests and three independent experiments. The results obtained are discussed in 4.4.1.1. The initial results on aerosol-like sodium nitrate - glucose mixtures showed that it is hard to control N/C ratios. Irrespective of the N/C ratio in the liquid aerosol, heterogeneous particles were formed. The N/C ratio in each of the particles varied from the coating (usually organic in nature) to the salt core. Moreover, IMF values were unreasonable high for low N/C ratios with low $^{15}N^{16}O_2^-$ ion signals. In the session June 2013, carbon coated bulk sodium nitrate and potassium nitrate pressed samples were analyzed, to establish whether the behavior is potentially caused by some contamination in the glucose. It was found that the IMF values were even more extreme for carbon coated $NaNO_3$.

2. The second dataset was acquired on potassium nitrate - glucose aerosol-like mixture samples and investigates the IMF of as a function of the N/C ratio.

   In order to find the reason behind the anomalous behavior of sodium nitrate and to get reproducible results, aerosol-like mixtures containing potassium nitrate and glucose were generated and collected on nuclepore filters and silicon wafers. Another four sessions (October 2013, November 2013, December 2013 and January 2014) were used to measure potassium nitrate mixture samples to understand their behavior. The data is summarized and described in section 4.4.1.2.

4.4.2.1 Sodium nitrate containing aerosol-like mixture samples with different N/C rations

Figure 4-14 shows the results of experiments performed on aerosol-like mixture samples containing a sodium nitrate and glucose mixture on different sample substrates. Top panel shows aerosols collected on nuclepore filter and bottom panel shows bulk sodium nitrate with carbon coating. Four mask levels (0 %, 10 %, 20 % and 30 %) were used to process NanoSIMS image data, for details see section 4.2.2. Higher mask level data has a larger f, due to the heterogeneous nature of the samples. Regions with high organic carbon and low nitrate content are excluded by applying the mask. With lower f, the $\delta^{15}N$ becomes very high, especially for carbon coated pure nitrate samples. Moreover, the slope of the weighted linear regressions is not comparable for aerosol-like mixture samples and carbon coated pure nitrate samples, -35± 22‰ and +1554 ± 22 ‰,

respectively.

A new secondary ion ratio f* = $^{14}N^{16}O_2^-$ / ($^{14}N^{16}O_2^-$ + $^{16}O^-$) was introduced to investigate whether loss of $^{14}N^{16}O_2^-$ explains the behavior (see section 4.4.1.2). Figure 4-15 shows $\delta^{15}N$ against f*. Top panel displays the results obtained on nuclepore filter and bottom panel shows the results from carbon coated pure nitrate samples. The $\delta^{15}N_{bias}$ values in top and bottom plots are the same as in Figure 4-14 top and bottom panels, respectively. Compared to f, f* increases only slightly when higher mask levels are used. However, the IMF of $\delta^{15}N$ shows no strong correlation with f*.

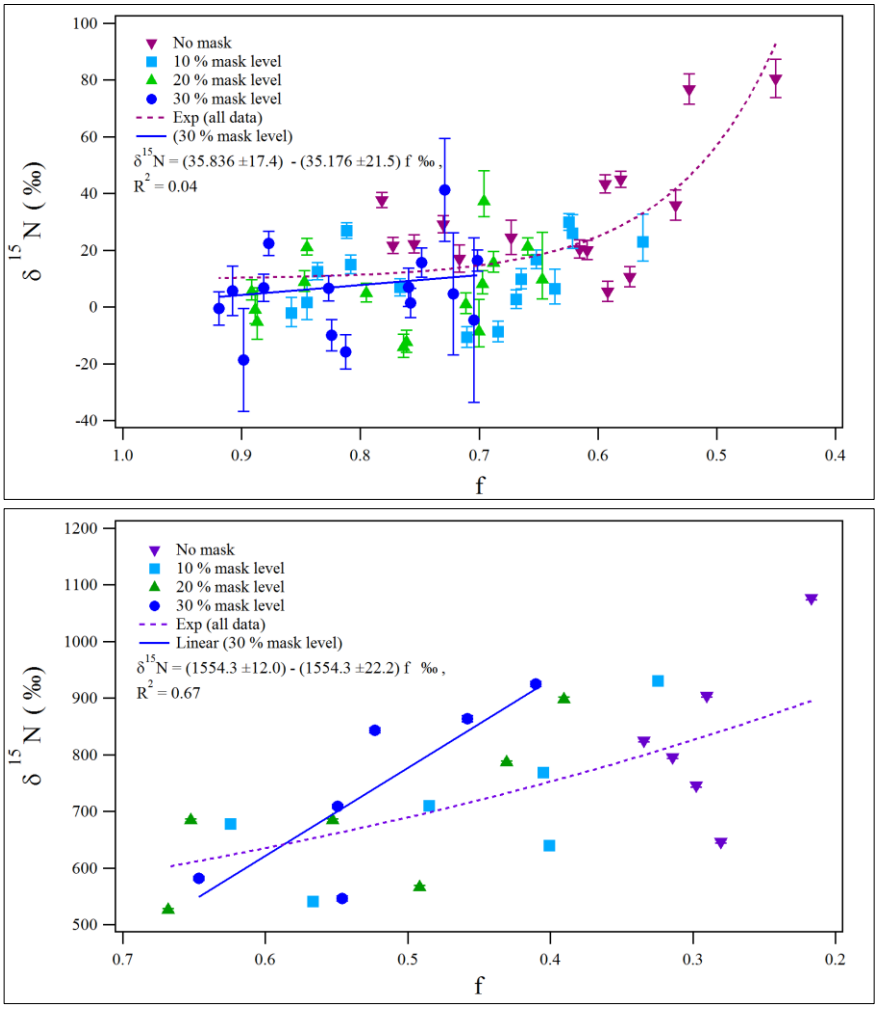

Figure 4-14. IMF introduced by the presence of carbon in sodium nitrate as the function of the secondary ion ratio f = $^{14}N^{16}O_2^-$ / ($^{14}N^{16}O_2^-$ + $^{12}C^{14}N^-$). Aerosol-like mixture samples collected on nuclepore filter (top). Samples with different N/C – ratios were produced from aqueous sodium nitrate and glucose solution as described in section 2.1.2. Carbon coated sodium nitrate (bottom). Variable pre-sputtering time was used which resulted in different values of f. Dashed line is the weighted exponential regression of all data. Solid line is the weighted linear regression of 30 % mask level data. Error bars are 1 σ of the error of the mean.

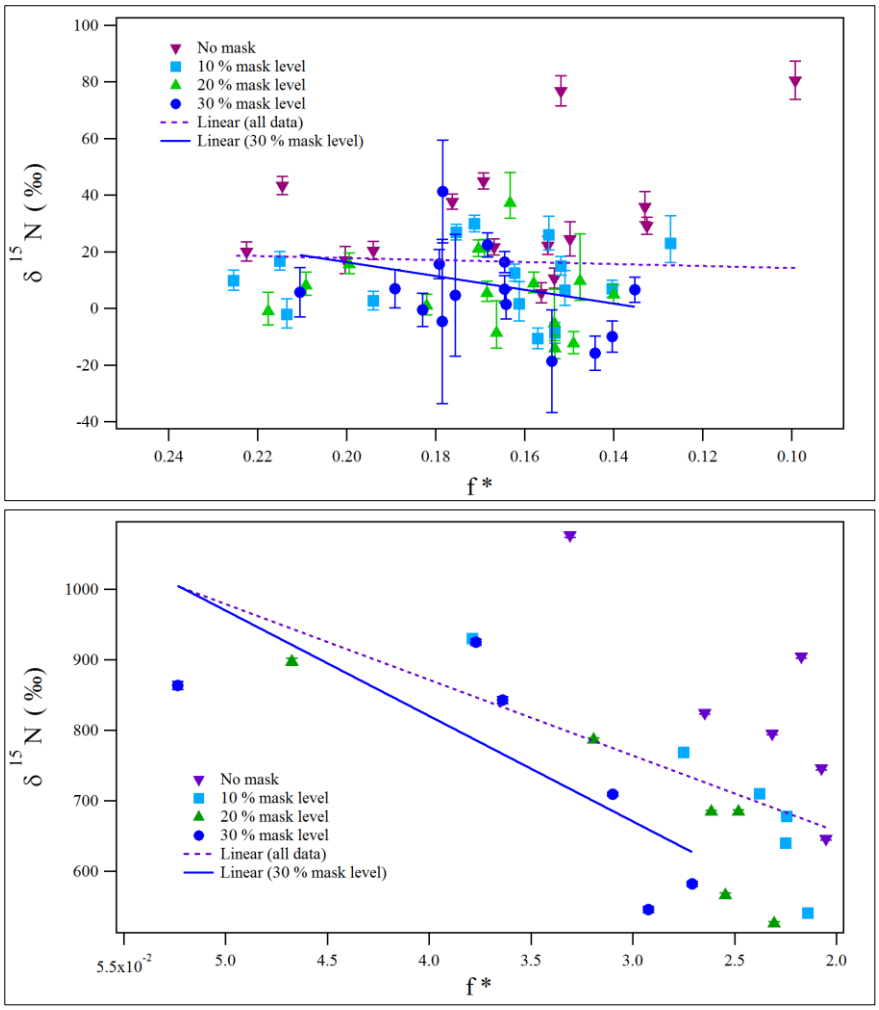

Figure 4-15. IMF of $^{15}N/^{14}N$ in C-bearing sodium nitrate as a function of the secondary ion ratio f* = $^{14}N^{16}O_2^-$ / ($^{14}N^{16}O_2^-$ + $^{16}O^-$). Aerosol-like mixture samples collected on nuclepore filters (top). Samples were produced from sodium nitrate and glucose. This figure shows the same data as Figure 4-14 (top). Carbon coated sodium nitrate (bottom). This figure shows the same data as Figure 4-14 (bottom). Dashed and solid lines are the weighted linear regressions of all data and 30 % mask level data, respectively. Error bars are 1 σ of the error of the mean.

4.4.2.2 Potassium nitrate containing aerosol-like mixture samples with different N/C rations

Figure 4-16 shows the results of aerosol-like mixture samples containing potassium nitrate collected on nuclepore filters (top), collected on silicon wafers (middle), and on gold foil with carbon coating (bottom). Four mask levels (0 %, 10 %, 20 % and 30 %) were used to process NanoSIMS image data, for details see section 4.2.2. Similar to the results on sodium nitrate containing aerosol-like mixture samples, a higher mask level results in a larger f. However, for the IMF, the behavior differs from that of sodium nitrate containing aerosol-like mixture samples. For potassium nitrate containing aerosol-like mixture samples with lower f, $\delta^{15}N$ becomes lower and the slopes of the weighted linear regressions are 110 ± 11 ‰, 48 ± 6 ‰ and 133 ± 30 ‰, for

nuclepore filter, and silicon wafers, and with carbon coating, respectively.

Figure 4-16 (top) and (bottom): The value of f increases sharply from no mask calculation to 10 % mask level. Between 10% to 30 % mask level, f increases slightly.

Figure 4-16 (middle): Differs from the other two plots in that the $\delta^{15}N$ values measured on silicon wafers decrease sharply when the mask level is increased from 0 % to 30 %, especially from 0 % to 10 %. The result obtained without any mask shows $\delta^{15}N$ tends to decrease with increasing f. However, when a 10% mask level is used, this trend changes its direction. IMF as a function of f no longer changes significantly when the mask level goes from 20% mask level to 30 % mask level. This difference in the behavior on this sample substrate is caused by an isobaric interference on $^{15}N^{16}O_2^-$ originating from the sample substrate (see section 4.4.2.3).

Due to the complex behavior of IMF as a function of f, other secondary ions related to the decomposition of nitrates were monitored from the second session onwards – $^{16}O^-$, was added to explore the behavior of IMF as decomposition of $^{14}N^{16}O_2^-$ will yield $^{14}N^{16}O^- + O^-$. The alternative secondary ion ratio $f^* = {}^{14}N^{16}O_2^- / ({}^{14}N^{16}O_2^- + {}^{16}O^-)$ was introduced to investigate whether loss of $^{14}N^{16}O_2^-$ explains the behavior. Figure 4-17 shows $\delta^{15}N$ against f*. Top panel shows the results measured on nuclepore filters and bottom panel shows the results from carbon coated pure nitrate samples. The $\delta^{15}N$ values in top and bottom panels are the same as in Figure 4-16 top and bottom panels, respectively. Compared to f, f* increases only slightly when higher mask levels are used. $\delta^{15}N$ shows a pronounced increase with increasing f* for very low f* values but no significant change with increasing f* for higher f* values. This transition between "low" and "high" f* occurs for different f* on different sample substrates indicating that for the IMF correction f is a much more suitable parameter compared to f*.

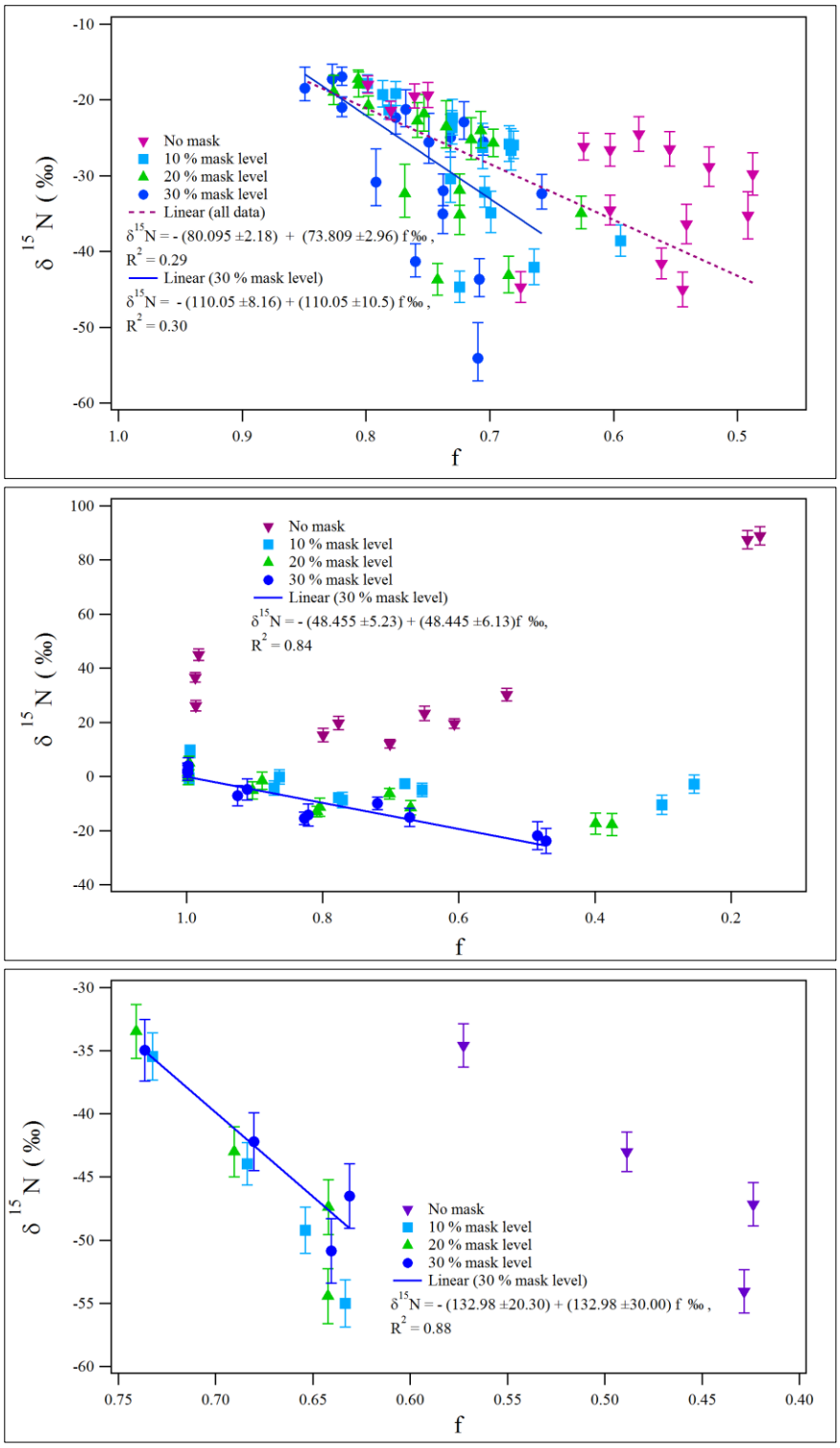

Figure 4-16. Variations in IMF introduced by the presence of carbon in potassium nitrate as function of secondary ion ratio $f = {}^{14}N^{16}O_2^- / ({}^{14}N^{16}O_2^- + {}^{12}C^{14}N^-)$. Aerosol-like samples collected on nuclepore filter (top). Samples were produced as aerosol-like mixtures with different N/C from potassium nitrate and glucose solution. Aerosol-like mixture samples collected on silicon wafers (middle). Samples were produced from potassium nitrate and glucose. Carbon coated potassium nitrate (bottom). The dashed line is the weighted linear regression of all data. The solid line is the weighted linear regression of 30 % mask level data. Error bars are 1 σ of the error of the mean. The isotope composition calculated at f = 1 was used as the reference. See Figure 4-14.

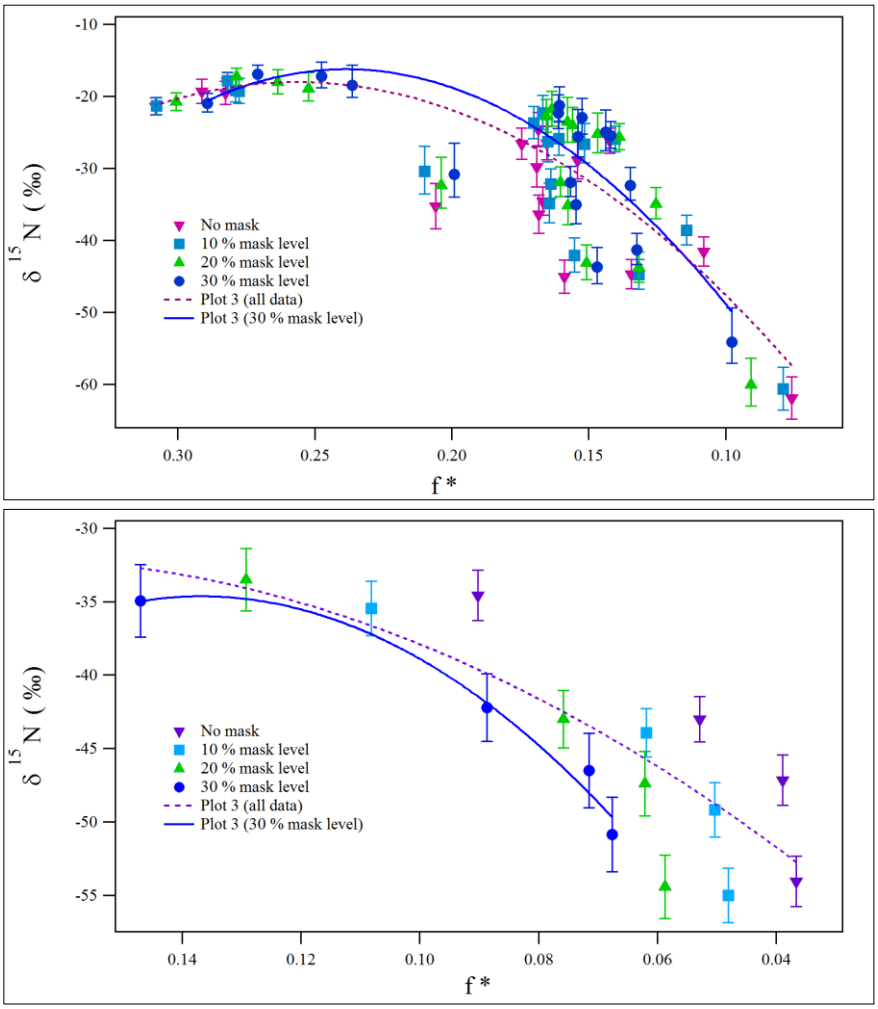

Figure 4-17. IMF in carbon bearing potassium nitrate as function of the secondary ion ratio f* = $^{14}N^{16}O_2^-/(^{14}N^{16}O_2^- + {}^{16}O^-)$. Aerosol-like mixture samples collected on nuclepore filters (top). Samples were produced from potassium nitrate and glucose. The same data as in Figure 4-16 (top) are shown. Carbon coated potassium nitrate (bottom). The same data as in Figure 4-16 (bottom) are shown. The dashed and solid lines are the weighted poly regressions with polynomial terms of order 3 of all data and 30 % mask level data, respectively. Error bars are 1 σ of the error of the mean.

4.4.3 Discussion

4.4.3.1 Isobaric interference on $^{15}N^{16}O_2^-$ from $^{23}Na^{12}C_2^-$ ions

Measured $\delta^{15}N$ values in sodium nitrate series experiments are highly variable for different f. When aerosols have low f and the absolute secondary ion signal is very low, the IMF gets much larger in favor of the heavier isotope ^{15}N. QSA effect could be excluded as the main reason because it can explain only up to 2.5 ‰ differences, see section 4.3.1.2. Another potential explanation is

that a very large nitrogen isotope fractionation happens during sputtering when CN^- molecular ions form. With more carbon being present, the CN^- signal intensity increases and less of the total nitrogen is present in the form of NO_2^-. During this process the remaining NO_2^- may be enriched in the heavy isotope ^{15}N if the CN^- formation favors the lighter isotope $^{12}C^{14}N^-$. However, opposite results were found during experiments on potassium nitrate glucose mixtures. Hence, a large isotope fractionation during CN^- formation should not be the main reason. As I discussed in section 4.3.1.2, several interfering ions with a mass close to that of $^{15}N^{16}O_2^-$ can lead to higher $\delta^{15}N$ (Figure 4-9), because with decreasing concentrations of sodium nitrate and increasing CN^- signals the secondary ion signal of $^{15}N^{16}O_2^-$ is very low and if unrecognized isobaric interferences exist, measured $\delta^{15}N$ values will be compromised. Considering that the $\delta^{15}N$ in sodium nitrate series results display an unreasonable high IMF and the results are in contrast to those of the potassium nitrate series, it is likely that the interfering ion contains a sodium atom. One potential candidate is $^{23}Na^{12}C_2^-$ which fall close to $^{15}N\ ^{16}O_2^-$ (mass difference is 0.00017 amu) and is unique to sodium nitrate - organic mixtures. To separate these two masses, more than 270,000 mass resolution power (MRP) would be needed, which is impossible to achieve with the NanoSIMS.

In order to pursue this possibility further, aerosol-like mixtures were placed on gold foils, which are essentially free of C, and on nuclepore filters, a C-bearing substrate. Figure 4-18 shows the results for $^{15}N^{16}O_2^-$ / $^{14}N^{16}O_2^-$ of the experiments I did in session February 2014 as function of $^{14}N^{16}O_2^-$ / ($^{14}N^{16}O_2^-$ + $^{12}C_2^-$). Secondary ions $^{23}Na^{12}C_2^-$ are formed by the combination of sodium ions and double carbon clusters. The newly performed analyses on potassium nitrate mixtures were conducted in the same manner as the analysis for sodium nitrate -glucose mixtures. While the major source of sodium is sodium nitrate, carbon may come either from the glucose or from nuclepore filters, which are made of polycarbonate. In the latter case, as soon as the gold-coating is sputtered away, carbon can be sputtered out, hence even the edge of pure salt particles on nuclepore filters can be problematic. When pure sodium nitrate is measured on clean gold foils, very little carbon is present. As soon as sodium and carbon co-exist in the sample or the sampling substrates contains carbon, the measured nitrogen isotope ratio increases as a function of carbon concentration. This indicates that the interfering ion is formed in the reaction zone above the sample. When pure sodium nitrate was measured on gold foil, carbon contamination can still affect the isotope ratio measured, but in this situation, the yield of secondary ion $^{15}N^{16}O_2^-$ is very high and the signal of $^{23}Na^{12}C_2^-$ very low, so the interference is not significant. If sodium nitrate glucose mixtures are measured on a nuclepore filter, which means a lot of carbon can be sputtered out, not only from the samples, but also from the filter, the measured isotope ratio can go up steeply. Figure 4-19 illustrates how the secondary ions yield and the ratio of the mass 47 ($^{15}N^{16}O_2^-$ + $^{23}Na^{12}C_2^-$) to

the mass 46 ($^{14}N^{16}O_2^-$) change over analysis time for a small sodium nitrate and glucose mixture grain sitting on a nuclepore filter. The red line is the measured isotope ratio and the green dashed line gives the true value of the isotope ratio in sodium nitrate. At the beginning, the carbon signal is low, so the interference is small compared to the $^{15}N^{16}O_2^-$ signal. But as more carbon in the sample and the sampling substrate comes out, the measured isotope ratio starts to leave the true value and increases. As soon as the gold-coating on the filter is sputtered away, the signal of mass 47 ($^{15}N^{16}O_2^- + {}^{23}Na^{12}C_2^-$) increases sharply. After 800 second sputtering, the $^{12}C_2^-$ signal continues to go up, but the signal on mass 47 starts to decrease. This is because the sample sputters away, which leads to a decrease of ^{23}Na and consequently $^{23}Na^{12}C_2^-$.

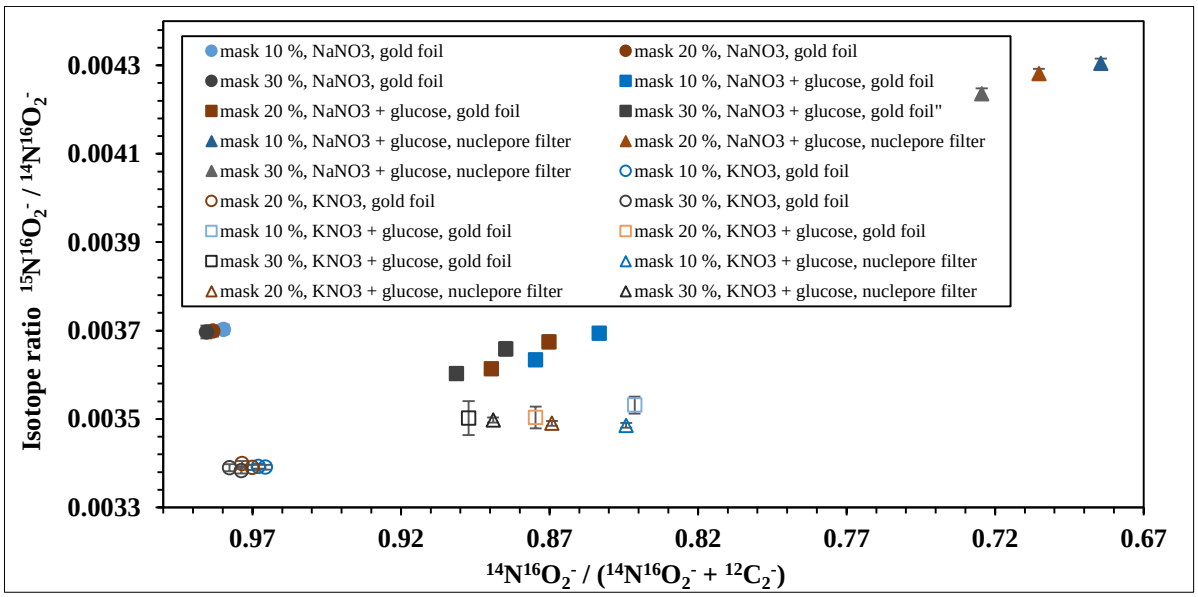

Figure 4-18. Nitrogen isotopes measured as $^{15}N^{16}O_2^-/^{14}N^{16}O_2^-$. KNO_3, $NaNO_3$, and their mixtures with glucose were transformed to aerosol, collected on gold foil and on nuclepore filter. Each sample was measured on a different mount. The type of substrate (nuclepore filter, gold foil), different heights of sample surfaces, and different tuning conditions can cause different IMF between individual analysis sessions. So the measured nitrogen isotope ratios between different samples are incomparable. Mask levels of 10 %, 20 % and 30 % were applied here in order to get different ratios of $^{14}N^{16}O_2^-/(^{14}N^{16}O_2^- + {}^{12}C_2^-)$, caused by inhomogeneity of mixture aerosols. Error bars are 1 sigma of the error of the mean.

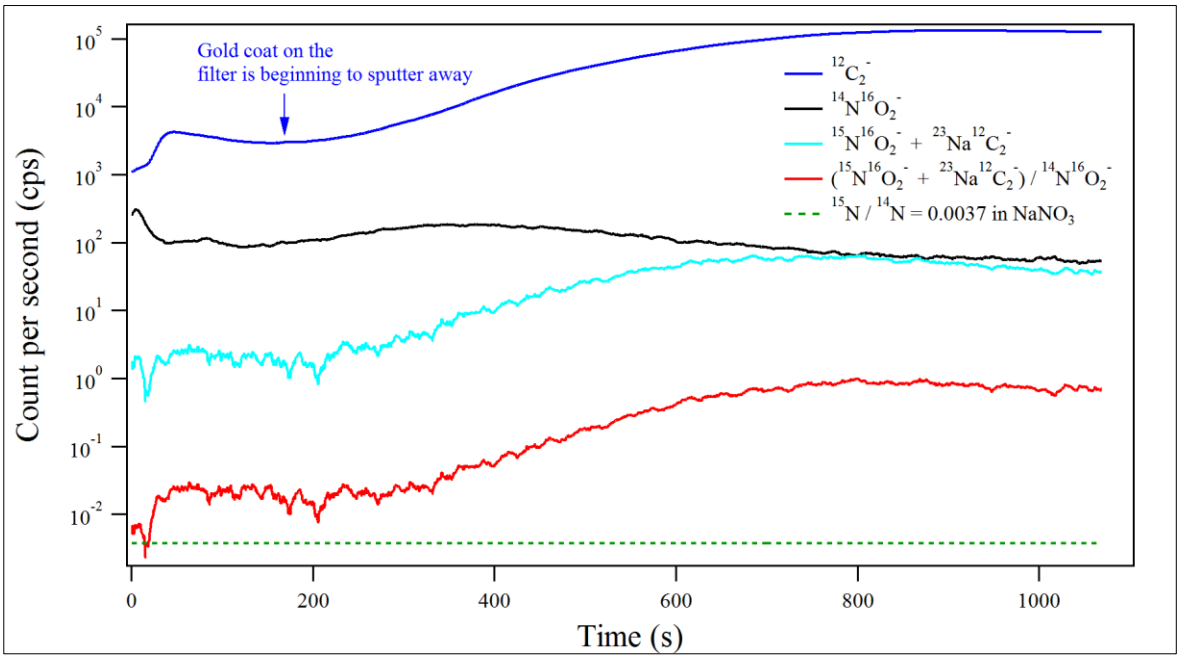

Figure 4-19: Ion intensities and the ratio of mass 47 ($^{15}N\ ^{16}O_2^- + {}^{23}Na\ ^{12}C_2^-$) to mass 46 ($^{14}N\ ^{16}O_2^-$) of a small grain (<200 nm) containing sodium nitrate and glucose with N/C = 0.5. Analysis time is 1080 seconds and raster area 2 × 2 µm^2. Green dashed line is the true value of the nitrogen isotope ratio in sodium nitrate.

4.4.3.2 Background interference from nuclepore filter and silicon wafer

While measuring aerosol samples on silicon wafers it was found that $^{29}Si^{18}O^-$ ions originating from the sampling substrate interfere with the $^{15}N^{16}O_2^-$ signal (mass difference: 0.014 amu). Although this interference is nominally largely separated at the MRP of 3000 used for this study, the tail of the high $^{29}Si^{18}O$ peak can still significantly contribute to the low $^{15}N^{16}O_2^-$ signal intensity. It was observed that the $^{15}N^{16}O_2^-$ / $^{14}N^{16}O_2^-$ ratio increased with more $^{29}Si^{18}O^-$ ions coming from Si wafer background. Different mask levels were used to avoid interfering $^{29}Si^{18}O^-$ ions coming from the Si substrate. Figure 4-16 middle panel shows the nitrogen isotope composition measured on a silicon wafer for aerosols consisting of potassium nitrate-glucose mixtures with different N/C-ratios, i.e. different f values. Using higher mask levels means data will be selected from the center area of the particle, and the interference of $^{29}Si^{18}O^-$ ions on the measured isotopic composition is reduced. As higher mask levels are used (30%), the isotope ratio for all analyses will fall onto the blue line, which is close to the true value, but values still vary as a function of f, possibly a matrix effect (see section 4.4.2.4). For a given analysis, a higher mask level increased the nitrogen to carbon ratio, because of the inhomogeneous nature and variations in the thickness of the aerosol grains. Typically there is more potassium nitrate in the center of the particle and more glucose at the edge, see section 4.2.3.

4.4.3.3 Matrix effect induced by presence of carbon

From section 4.4.3.1 it can be seen that measuring the nitrate specific nitrogen isotope ratio ($^{15}N^{16}O_2^-$ / $^{14}N^{16}O_2^-$ ratio) on samples which contain sodium and carbon simultaneously, it is hard to avoid the interference from $^{23}Na^{12}C_2^-$. Hence, the effect of carbon on the matrix dependent IMF in aerosol-like mixture samples was explored only on mixtures containing potassium nitrate and glucose. A 30 % mask level was used to calculate the final results. Potassium nitrate and glucose mixture aerosol-like samples were measured on two different substrates: silicon wafer and nuclepore filter. Carbon coated potassium nitrate was also measured using the same tuning conditions. Due to the fact that all measurements were made in different NanoSIMS sessions, the tuning conditions, in particular the sensitivity of the EMs used for detecting the two nitrogen isotope species, varied slightly from session to session. In order to discuss the matrix effect caused by different N/C ratios, the change in the absolute $^{15}N\ ^{16}O_2^-$ / $^{14}N\ ^{16}O_2^-$ ratio from session to session is not considered here. All linear regression functions in Figure 4-16 were forced to go through $\delta^{15}N = 0$ for f = 1 to calculate the isotope ratio that would have been measured for the tuning conditions of the individual session for a perfect sample, i.e. a pure nitrate sample in which no carbon exists. These values were used as reference and to calculate all other nitrogen isotope ratios using the Equation 4-6. Figure 4-20 shows there is a matrix dependence of the IMF due to the presence of carbon in potassium nitrate aerosol with different nitrogen to carbon ratio. The N isotope ratio decreases with increasing carbon content, not only in mixture aerosols but also in C-coated pure potassium nitrate samples. The weighted linear regression results given by all data is:

$$\delta^{15}N = (101 \pm 4) \cdot f - (101 \pm 3)\ ‰,\ R^2 = 0.51.$$

Considering only high concentration data (0.8 to 1), aerosol data are fitted very well with:

$$\delta^{15}N = (117 \pm 9) \cdot f - (117 \pm 8)\ ‰,\ R^2 = 0.91.$$

With higher carbon concentrations, i.e. lower f values, the scatter of $\delta^{15}N_{bias}$ increases, because of lower $^{15}N^{16}O_2^-$ and higher contribution of $^{23}Na^{12}C_2^-$ from contamination and background interference by $^{29}Si^{18}O^-$ from silicon wafer. When the sample substrate is a nuclepore filter, the CN^- signal and hence the calculated f can be affected by the background signal originating from the filter matrix. Carbon coated samples results at low f (= high CN^- signal) are very susceptible to even traces of nitrogen contamination from other sources that might be present in the carbon coating. Such traces can lower the f, as the CN^- signal will increase without NO_2 acting as a source of the nitrogen.

These data permit us to infer a matrix-specific IMF correction if a C-containing potassium nitrate- sample is measured. The nitrogen isotope composition in nitrate species can be calculated

by the following equation:

$$\delta^{15}N(x)_{air} = \left(\frac{(^{15}N/^{14}N)_x}{(^{15}N/^{14}N)_{air}} \times \frac{(^{15}N/^{14}N)_{IAEA-NO-3,true}}{(^{15}N/^{14}N)_{IAEA-NO-3,SIMS}} - 1\right) \times 1000 - (101 \pm 4)\, f + (101 \pm 3)\ ‰ \qquad \text{Equation 4-7}$$

where X refers to the unknown potassium nitrate sample measured by NanoSIMS, $(^{15}N/^{14}N)_{air}$ is the isotope composition of atmospheric N_2 (air), f = $^{14}N^{16}O_2^-$ / ($^{14}N^{16}O_2^-$ + $^{12}C^{14}N^-$), $^{15}N/^{14}N_{IAEA-NO-3,true}$ = 0.00369378 ($\delta^{15}N_{IAEA-NO-3}$ = +4.7 ‰) and $^{15}N/^{14}N_{IAEA-NO-3,SIMS}$ is the nitrogen isotope ratio of the KNO_3 standard measured with the NanoSIMS.

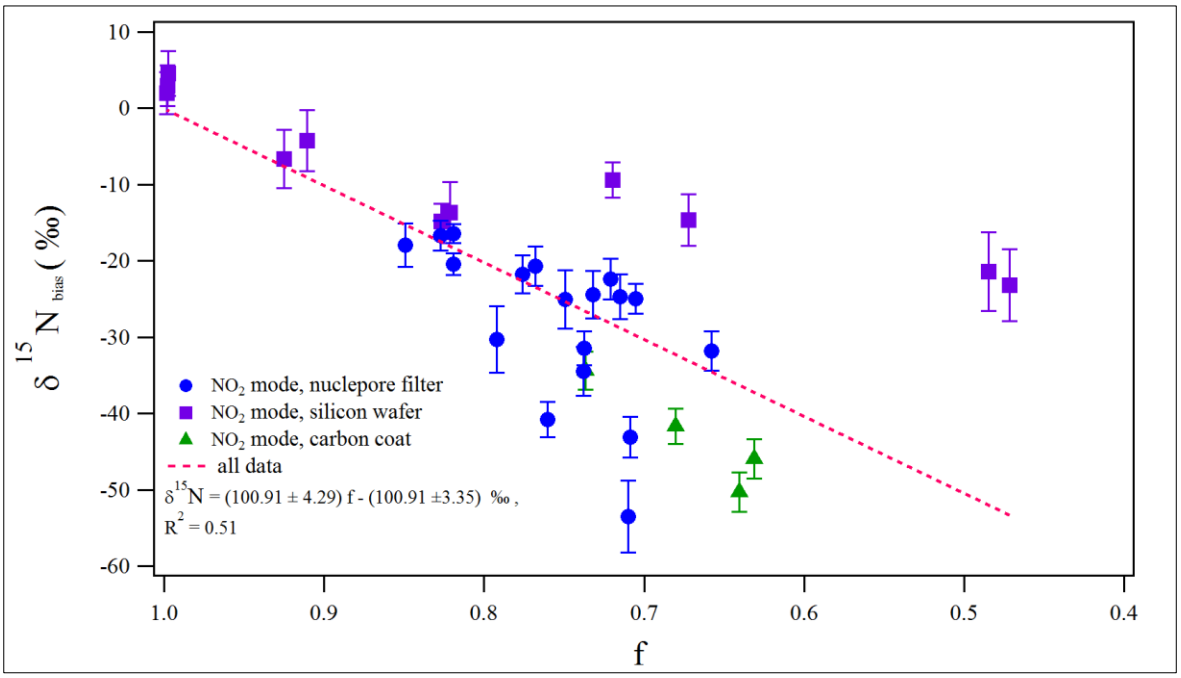

Figure 4-20. Matrix effect of nitrogen isotope measurements on C-containing potassium nitrate as function of f. Nitrogen isotope ratio measured as $^{15}N\ ^{16}O_2^-/^{14}N\ ^{16}O_2^-$; Error bars are 1 sigma of the error of the mean. Red dashed line is the weighted linear regression fitting results for all data.

A theoretical explanation for the matrix dependence of the IMF due to the presence of carbon in potassium nitrate is given here preliminary: A matrix with different N/C ratio can change the penetration range and the energy deposition efficiency of Cs^+ ions (Wittmaack 1981, Gnaser 2008). The presence of carbon can also change the nitrogen distribution among different species of secondary ions:

$$NO_3^- + e^- \rightarrow NO_2^- + O^- \qquad \text{Reaction 4-1}$$

$$NO_2^- + e^- \rightarrow NO^- + O^- \qquad \text{Reaction 4-2}$$

$$NO^- + C^- \rightarrow CN^- + O^- \qquad \text{Reaction 4-3}$$

$$NO_2^- + C^- \rightarrow CN^- + O_2^- \qquad \text{Reaction 4-4}$$

Reaction 4-1 and Reaction 4-2 show the decomposition of nitrate during Cs^+ primary ion sputtering, which provides free electrons, Reaction 4-3 and Reaction 4-4 are the formation of the CN^- ion. The CN^- ion may be formed when one carbon atom abstracts the nitrogen atom from NO^- or NO_2^- molecular ions. It has been shown that the formation of CN^- takes place in the reaction zone above the sample (McMahon et al., 2006). However, previous studies proposed recombination of monoatomic species and not abstraction to be the primary formation mechanism. I propose that the observed negative correlation between $\delta^{15}N$ and f can be explained by the fact that higher f indicates higher C concentration in reaction zone and $^{14}NO_2^-$ is lighter compared to $^{15}NO_2^-$ and has a slightly higher velocity. Therefore, it crosses the reaction zone above the sample more rapidly and is less likely to react with carbon and to form a CN^- molecular ion. However the results in chapter 5, which N isotope ratio measured by $^{12}C^{15}N^-$ / $^{12}C^{14}N^-$ don't show matrix effect on C-containing potassium nitrate and sodium nitrate, see chapter 5.

4.4.4 Conclusions

The secondary ion $^{23}Na^{12}C_2^-$ can be a serious interference when $^{15}N^{16}O_2^-$ is used to measure the nitrogen isotope composition of sodium nitrate-glucose mixtures. This is a potential problem when species specific measurements of the nitrogen isotope composition of nitrate are attempted on ambient aerosol particles, as sodium is ubiquitous in the atmosphere.

Potential interferences coming from different substrates were investigated as well. Nuclepore filter can be a problem when the carbon concentration in samples needs to be known accurately for IMF correction and silicon wafers affect the measurement of $^{15}N^{16}O_2^-$ directly through an interfering ion, $^{29}Si^{18}O^-$, hence high mask levels and accurate masks in the image analysis are a must. Single plane mask calculation and high mask level was used to minimize background interferences and to estimate the N/C ratio. Presence of aerosol-like carbon-containing potassium nitrate-glucose mixture samples leads to a matrix effect which can be quantified by $\delta^{15}N_{bias} = (101 \pm 4) \cdot f - (101 \pm 3)$ ‰. Even if these results show that the measurement precision is limited to ~5‰ (1σ), the method I developed is new and permits for the first time to measure the nitrate isotope composition by NanoSIMS. However, species specific isotope analysis using the NO_2^- molecular ion has limited scope in the field of aerosol sciences, as sodium-containing samples must be avoided. Unfortunately sodium is ubiquitous in aerosol particles. In the next chapter I will describe a measurement approach employing a NO_2 mask, but using the CN signal to measure the nitrogen isotopic signature of the nitrate, which offers a way forward for the real world application on ambient samples (i.e. works also on sodium nitrate).

5 Stable N isotope analysis of nitrate by NanoSIMS using the $^{12}C^{15}N^-$ / $^{12}C^{14}N^-$ - ratio

5.1 Introduction

5.1.1 Secondary ion CN^- in SIMS analysis

Nitrogen isotope measurements by SIMS are not straightforward because the positive secondary ion yield of N^+ is very low, and negative secondary ions do not form at all (Zinner et al., 1989, Hoppe et al., 2013). As mentioned above, section 4.1.2, the nitrogen isotope composition is usually measured by SIMS using the $^{12}C^{15}N^-/^{12}C^{14}N^-$ - ratio. A very intense CN^- signal is obtained in the presence of carbon (Zinner et al., 1989). It has been demonstrated that accurate isotope analysis using the $^{12}C^{15}N^-/^{12}C^{14}N^-$ - ratio is possible on a range of materials such as diamond (Boyd et al., 1992, Bulanova et al., 2002, Hauri et al., 2002), graphite (Mostefaoui et al., 2002, Mostefaoui et al., 2005, Marhas et al., 2008), and SiC (Zinner et al., 1989, Hoppe et al., 1994).

There are several limitations of nitrogen isotope measurements by $^{12}C^{15}N^-/^{12}C^{14}N^-$:

1. Interferences

   Zinner et al. (1989) show in Figure 3 potential peaks around two CN^- peaks at mass 26 and 27 obtained from 1-hydroxybenzotriazole and meteoritic SiC and demonstrated that $^{12}C^{14}N$ and $^{12}C^{15}N$ are easily resolved from carbon and carbon-hydrogen species in high mass resolving power ($m/\Delta m$) of ~6000. At these conditions $^{12}C^{15}N^-$ is also fully resolved from $^{13}C^{14}N^-$ which is about a factor of ~3 (= $(^{13}C/^{12}C)_{PDB}$ / $(^{15}N/^{14}N)_{air}$) higher than $^{12}C^{15}N^-$ for samples with close to terrestrial C and N isotopic compositions. However, boron is a ubiquitous contaminant and Hoppe et al. (2013) showed that no proper separation is achieved between $^{12}C^{15}N^-$ and $^{11}B^{16}O^-$ peaks in the NanoSIMS. Figure 5-1 shows the peak at mass 27 obtained using NanoSIMS on aerosol-like mixture samples. Here, no contribution from $^{11}B^{16}O$, which would fall between the $^{12}C^{15}N$ and $^{13}C^{14}N$ peaks, is apparent. Nevertheless, in order to ensure a proper measurement of the nitrogen isotope ratio in samples where $^{11}B^{16}O^-$ is present, recording the $^{12}C^{15}N^-$ intensity at ~1 V to the left of the $^{12}C^{15}N^-$ peak center is required.

2. Chemical bonding between carbon and nitrogen influences the CN^- secondary ion intensity. E.g., in 1-hydroxybenzotriazole hydrate ($C_6H_5N_3O \cdot H_2O$, N/C = 0.5) and thymine ($C_5N_2O_2H_6$, N/C = 0.4), the CN^-/C^- - ratio recorded by SIMS are ~3.3 and ~12, respectively (Zinner et al., 1989). Several materials, from nylon, abs, resinB to graphite, show a range of CN^-/C^- ratios from ~0 to ~4 (Thomen et al., 2014). Hence, it is hard to have quantitative nitrogen concentration measurements using CN^- and C^- signals only. Variable nitrogen abundances can be a problem for nitrogen isotope measurements, in particular when N>C. Zinner et al. (1989) demonstrated that the matrix effect on nitrogen isotope ratio measurements is less than 2 ‰ between 1-hydroxybenzotriazole hydrate and thymine. However, in this study, we study materials without chemical bonding between carbon and nitrogen in aerosol-like mixture samples, and include samples with N/C - ratios >1; consequently the partioning between different nitrogen bearing secondary ions could affect IMF.

So far, only few studies have demonstrated that precise and accurate nitrogen isotope analysis by SIMS is possible, e.g. on diamond (Bulanova et al., 2002, Hauri et al., 2002). In environmental science and biological science, labeled nitrogen is used to trace the nitrogen exchange in ecosystems and organisms and SIMS imaging of materials that are isotopically labeled with ^{15}N is straightforward (Hindie et al., 1992, Chandra 2004) and can be coupled to cell identity using fluorescent labeled dyes (Musat et al., 2008, Halm et al., 2009). NanoSIMS is widely applied in environmental microbiology and biogeochemistry and a ^{15}N label is often used for biological function research (Lechene et al., 2007, Popa et al., 2007). In cosmochemistry, the CN^- signal is used to measure nitrogen isotope ratios that differ from terrestrial nitrogen by up to 2 orders of magnitude (enrichments and depletions in ^{15}N; e.g., Hoppe et al., 1994). Due to the large nitrogen isotope abundance anomalies in these two applications that do not require high precision and accuracy, only few studies, mainly of geological materials, discussed IMF and potential matrix effects (Zinner et al., 1989, Bulanova et al., 2002, Hauri et al., 2002).

5.1.2 Further exploration of nitrate species N isotope measurement

Chapter 4 discusses species specific isotope analysis of nitrate using the NO_2^- molecular ions. However, this has limited scope in the field of aerosol sciences, as sodium-containing samples must be avoided. Unfortunately, sodium is ubiquitous in aerosol particles.

This chapter explores whether species specific N isotope measurement on nitrate using the CN^- signal offers a way forward for the real world application on ambient samples. Here, lab made aerosol-like mixture samples with sodium nitrate + glucose and potassium nitrate + glucose are

prepared, see section 2.1.2. The $^{12}C^{15}N^-/^{12}C^{14}N^-$ - secondary ion ratio is used for nitrogen isotope measurements with the NanoSIMS. Single plane mask calculation, based on $^{14}N^{16}O_2^-$, was used for data processing and it is shown that only the $^{14}N^{16}O_2^-$ mask can be used when specificity is envisaged. Matrix dependent IMF induced by carbon will be discussed.

5.2 Experimental

5.2.1 Sample preparation

Experiments in this chapter were performed in three NanoSIMS sessions: The experiment of aerosol-like potassium nitrate mixed with glucose on silicon wafer was finished in November 2013; the experiment of aerosol-like potassium nitrate mixed with glucose on nuclepore filter was finished in January 2014, and the experiments of aerosol-like sodium nitrate mixed with glucose, both on silicon wafer and nuclepore filter were finished in February 2015. The detailed description of the preparation of aerosol-like mixture samples has been discussed in chapter 2, section 2.1.2.

The average grain size of the powder nitrate standards USGS35 is less than 5 μm. Although these standards cannot be used to prepare aerosol-like mixtures, because the available amount is too small, individual grains can be analyzed with the NanoSIMS and compared with the results from similar sized lab made aerosols. In February 2015, individual grains of standards USGS35 was placed on silicon wafer and mounted along with aerosol samples. This is the first session in which single grain standards were used to calculate the IMF correction for aerosol-like samples.

5.2.2 NanoSIMS analysis

The specific NanoSIMS settings for CN^- ion isotope measurements were as follows.

Aperture D1 was set to 150 μm (D1-3) and the raster size was set to 5 × 5 μm^2, 128 × 128 pixels per frame. Depending on the size of particles, occasionally raster settings of 10 × 10 μm^2 were used with 256 × 256 pixels per frame, which resulted in a 4 times longer analysis time. This arrangement keeps the primary ion dose per square micrometer constant. A residence time of 3000 μs/pixels was set for all measurements. 30 frames were obtained on each spot. Entrance and aperture slits were set to 20×140 μm^2 (ES-4) and 80×80 μm^2 (AS-4), respectively. Energy bandwidth was set to 20 eV. The secondary ion transmission efficiency was ~ 10 - 35 % with these settings. Secondary ions of $^{12}C^-$, $^{16}O^-$, $^{12}C^{14}N^-$, $^{12}C^{15}N^-$ and $^{14}N^{16}O_2^-$ were simultaneously detected in five electron multipliers at high mass resolution ($M/\Delta M > 4000$ for $^{12}C^{15}N^-$). Figure 5-1 shows the mass scans of peaks monitored during isotope analysis.

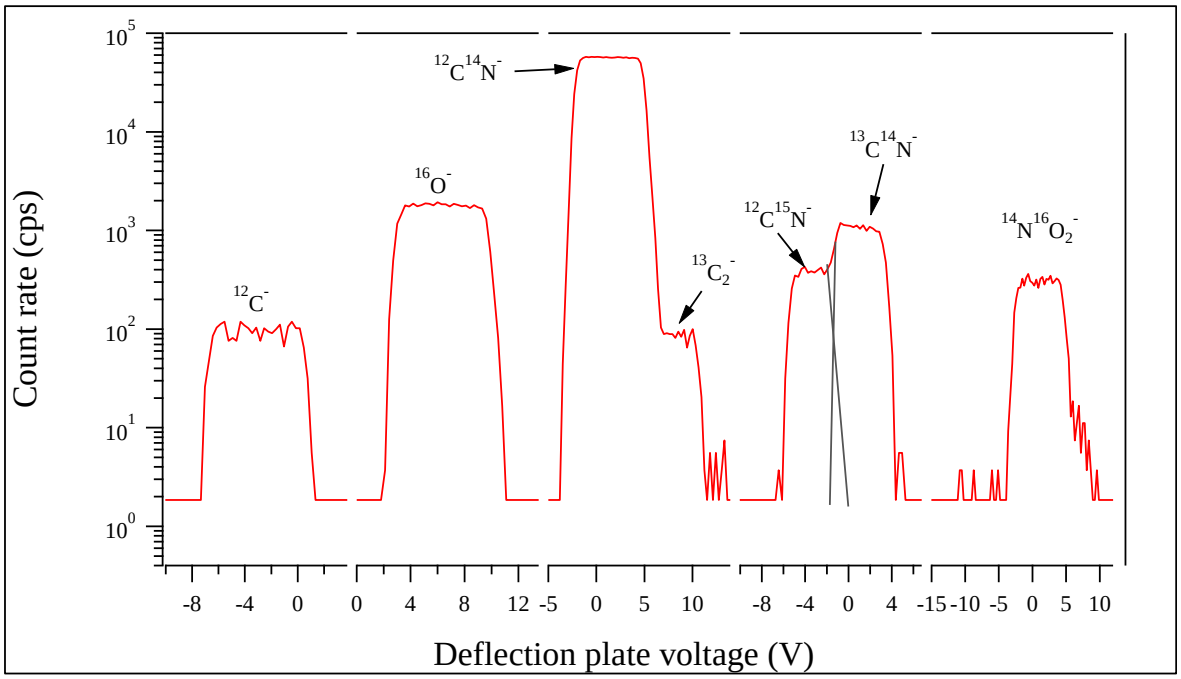

Figure 5-1. High-resolution mass spectra for mass regions 12 – $^{12}C^-$, 16 – $^{16}O^-$, 26 – $^{12}C^{14}N^-$, 27 – $^{12}C^{15}N^-$, 46 – $^{14}N^{16}O_2^-$. All 5 masses can be recorded simultaneously with the NanoSIMS.

5.2.3 Data processing

5.2.3.1 Mask calculation

Due to the highly heterogeneous nature of the samples (section 4.2.2), the 'smart mask' calculation procedure (section 4.2.3) was used for all image data processing. In this chapter, in order to analyze species specific isotope ratios for nitrate using the CN^- signal, the mask mass was set to the secondary ion $^{14}N^{16}O_2^-$ and the N isotope ratio was measured using the $^{12}C^{15}N^-/^{12}C^{14}N^-$ secondary ion ratio. In this case, the secondary ion used to measure the isotope ratio and the mask mass are different. Once a second source of nitrogen in the form of ammonia or organic nitrogen is present in the samples only the $^{14}N^{16}O_2^-$ mask will provide species specific results. Figure 5-2 gives examples of $^{14}N^{16}O_2^-$ mask calculations for two mask levels: 10 % and 30 %. The nuclepore filter has a complex CN^- signal background, which may complicate measurement of other species without a more specific mask mass (e.g. ammonium ions) on this substrate but the $^{14}N^{16}O_2^-$ - mask selects not only the nitrate grains. While a 10% mask level is very sensitive and includes smaller grains for which interferences from the substrate can be substantial, with a 30% mask level it is possible to efficiently exclude these smaller grains from the nuclepore filter.

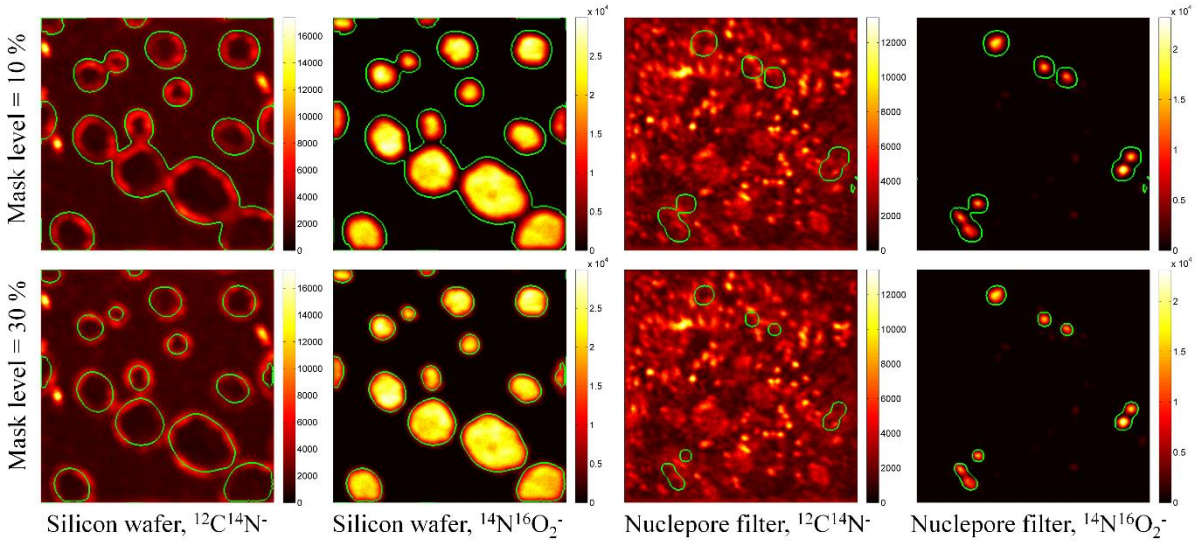

Figure 5-2. Secondary ion images of $^{12}C^{14}N^-$ and $^{14}N^{16}O_2^-$ from samples collected on silicon wafer and nuclepore filter, calculated with mask levels of 10 % and 30 % for $^{14}N^{16}O_2^-$, respectively. The sample was made from sodium nitrate and glucose, having N/C = 5. Raster size is 10 × 10 µm^2. Color bars represent secondary ion intensities (cps). Green lines are the borders of the selected analysis areas.

Similar to chapter 4 (section 4.2.2), f = $^{14}N^{16}O_2^-$ / ($^{14}N^{16}O_2^-$ + $^{12}C^{14}N^-$) was used as proxy for the N/C ratio in our samples. The matrix dependence of the IMF induced by the presence of carbon is investigated in section 5.3.1 as a function of f.

5.2.3.2 QSA correction

CN^- has a high secondary ion yield, making a proper QSA correction important. However, there is no publication investigating the QSA effect for CN^- secondary ions, so far. In this study, the theoretical value α = 0.5 was used for the QSA correction (see section 4.3.1.2). Figure 5-3 shows examples of results obtained before and after QSA correction. The $\delta^{15}N$ values of aerosol-like mixtures of potassium nitrate with glucose on silicon wafer were calculated without (α = 0) and with (α = 0.5) QSA correction. Figure 5-3 clearly shows that without QSA correction the measured $\delta^{15}N$ increased noticeable at high signal intensities, resulting from the significant reduction of the $^{12}C^{14}N^-$ signal. After applying the QSA correction, the $\delta^{15}N$ is stable within the error.

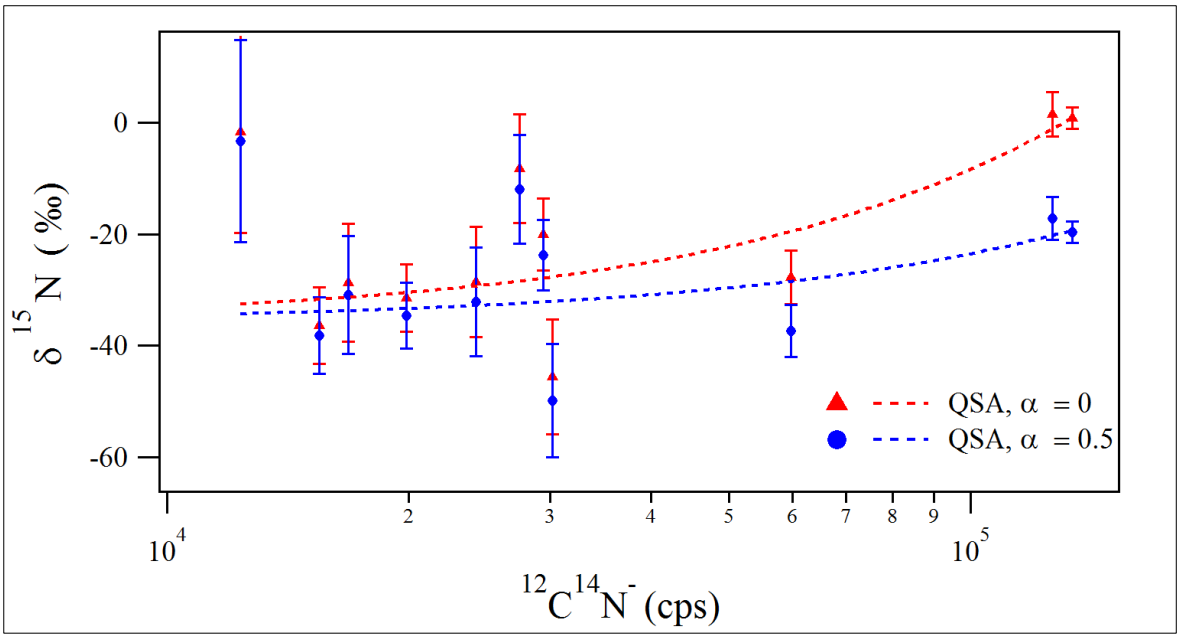

Figure 5-3. Example of QSA correction. Shown is the IMF ($\delta^{15}N = (R_{SIMS}/R_{true} - 1) \times 1000$) as a function of secondary ion intensity of $^{12}C^{14}N^-$. Samples are aerosol-like mixtures of potassium nitrate with glucose on silicon wafers. Red triangles show data without QSA correction ($\alpha = 0$) and blue circles show data after QSA correction ($\alpha = 0.5$). Dashed lines are weighted linear regressions. Error bars are 1 σ.

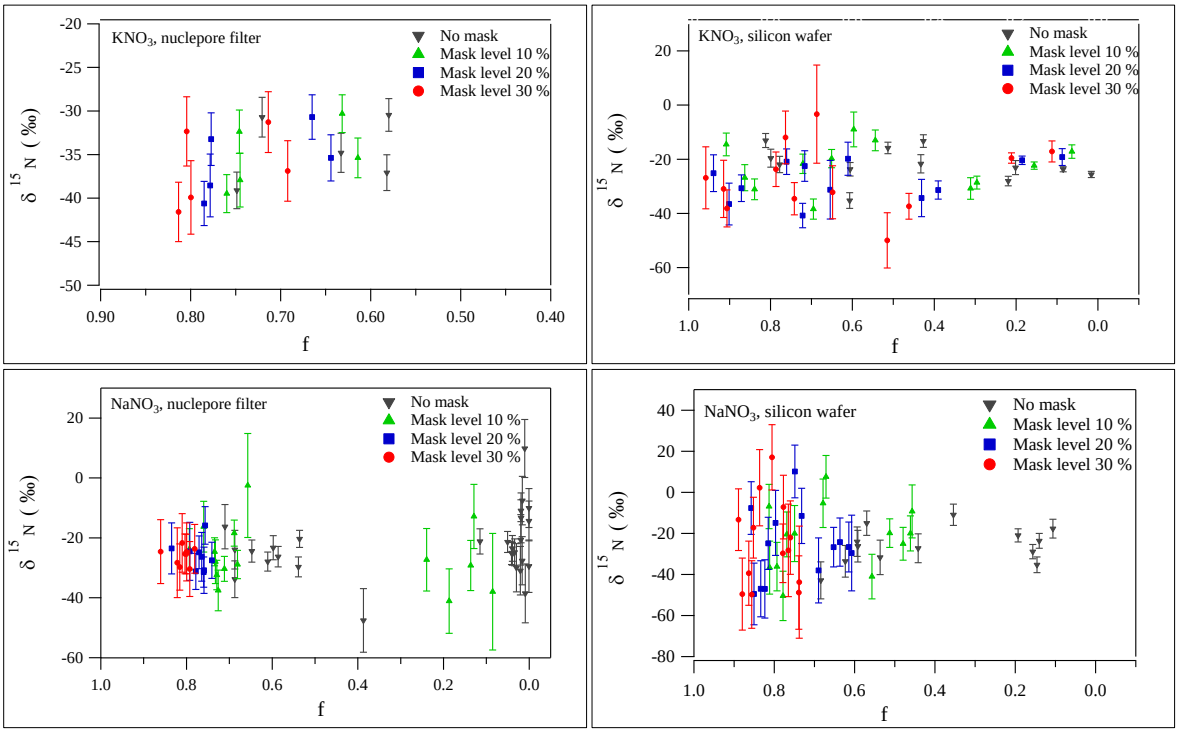

Figure 5-4. $\delta^{15}N$ inferred from $^{12}C^{15}N^-$ / $^{12}C^{14}N^-$ as a function of f and for different mask levels of $^{14}N^{16}O_2^-$. Top left, top right, bottom left and bottom right panels show results for aerosol-like mixture samples made from KNO_3 and glucose and from $NaNO_3$ and glucose on nuclepore filter and silicon wafer, respectively. QSA correction with $\alpha = 0.5$. $\delta^{15}N = (R_{SIMS}/R_{true} - 1) \times 1000$. Error bars are 1 σ.

5.3 Results and discussion

5.3.1 Matrix effect induced by presence of carbon

I investigated the matrix effect of N isotope measurements on aerosol-like mixture samples (KNO_3 + glucose, $NaNO_3$ + glucose) on nuclepore filter and silicon wafer as a function of f and different $^{14}N^{16}O_2^-$ mask levels. Figure 5-4 shows there is no clear matrix effect induced by the presence of carbon if N is measured as CN^-, regardless of the selected mask level, this differentiates isotope measurements using the $^{12}C^{15}N^-$ / $^{12}C^{14}N^-$ - ratio from those performed using the $^{15}N^{16}O_2^-$ / $^{14}N^{16}O_2^-$ secondary ion ratio (chapter 4). The results shown here indicate that the secondary ion ratio $^{12}C^{15}N^-$ /$^{12}C^{14}N^-$ can be used to measure the isotopic composition of nitrate species without a N/C ratio-dependent IMF correction and that the measurements can be meaningful and species specific if an NO_2^- mask is used to select the area of interest.

5.3.2 $^{14}N^{16}O_2^-$ mask levels

In this section, I explore how the use of different mask levels (no mask, mask 10 %, mask 20 % and mask 30 %) for the weighted average calculation affects the measurement results.

5.3.2.1 Potassium nitrate aerosol-like mixture samples

Experiments of potassium nitrate aerosol-like mixture samples were performed in two NanoSIMS analysis sessions. Unfortunately, standards with known isotopic composition were not measured in the same measurement session. Instead, the IMF reference isotope ratio was calculated by using the 30 % mask level on $^{14}N^{16}O_2^-$. Using a high mask level on the $^{14}N^{16}O_2^-$ signal restricts the calculation to nitrogen introduced into the sample as nitrate and decreases the effect of potential contaminations on the data analysis. The results are shown in Figure 5-5 A). Both on silicon wafer and nuclepore filter $\delta^{15}N_{bias}$ is very stable within errors for different mask levels.

Results for potassium nitrate aerosol-like mixture samples show species specific nitrogen isotope ratios can be measured using the CN^- signal, both on silicon wafer and on nuclepore filters, as long as NO_2^- is used as mask mass. In lab made samples, mask levels are not important, because N contamination and background are relative low, and nitrogen comes largely from nitrate. However, in aerosol samples collected in field campaigns, nitrogen can come from other species as well, e.g. ammonium and nitrogen-containing organics. Hence, high mask level calculations are needed to focus on only nitrate species.

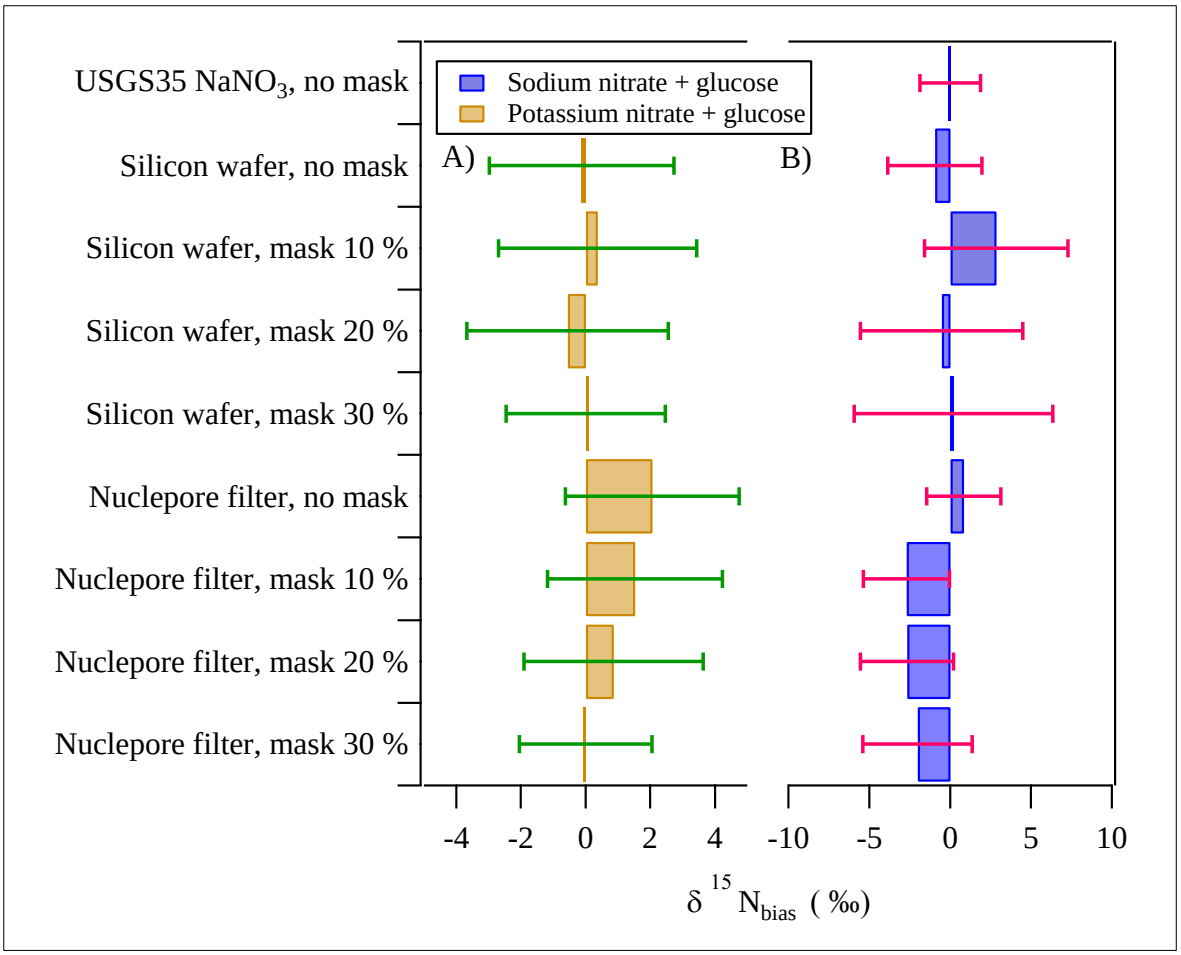

Figure 5-5. Weighted average $\delta^{15}N_{bias}$ results of aerosol-like mixture samples collected on nuclepore filter and silicon wafer with different mask levels for $^{14}N^{16}O_2^-$ in NanoSIMS images. A) experiments of potassium nitrate + glucose on these two substrates were performed in two NanoSIMS sessions. $\delta^{15}N_{bias}$ was calculated with reference to the IMF factor (R_{SIMS}/R_{true}) for the results of 30 % mask. B) experiments of sodium nitrate + glucose on these two substrates were performed in one NanoSIMS session. $\delta^{15}N_{bias}$ was calculated with reference to the IMF factor (R_{SIMS}/R_{true}) for USGS35, which was placed as individual grains on a silicon wafer. Error bars are 1 sigma of the error of the mean. The width of the yellow and blue boxes indicate the deviations from $\delta^{15}N_{bias} = 0$.

5.3.2.2 Sodium nitrate aerosol-like mixture samples

Experiments with sodium nitrate aerosol-like mixture samples were performed in one NanoSIMS session in February 2015, along with measurements of individual grains of standards USGS35 which were placed on a silicon wafer and measured on the same sample mount. USGS35 was used for IMF correction.

Figure 5-5 B shows the results of weighted average $\delta^{15}N_{bias}$ results of aerosol-like mixture samples of sodium nitrate mixed with glucose collected on nuclepore filter and silicon wafer for different $^{14}N^{16}O_2^-$ mask levels . Similarly to the results of potassium nitrate experiments, there is only a weak dependence on the mask level.

5.4 Conclusion and future experiments

Different from the results obtained from $^{15}N^{16}O_2^-/^{14}N^{16}O_2^-$, there is neither a matrix effect induced by the presence of variable N/C ratios, nor do interferences complicate determining the N isotope ratio using the $^{12}C^{14}N^-$ / $^{12}C^{15}N^-$ ratio. Using $^{14}N^{16}O_2^-$ as mask mass can make these measurements species specific for nitrate. For samples in which N only comes from nitrate, different $^{14}N^{16}O_2$ mask levels are not important. However, for multi-N-source samples containing ammonium ions or organic nitrogen, high mask levels should be used.

In future experiments, particles containing more than one N source, like mixtures of organic nitrogen with nitrate species or mixtures of ammonia species with nitrate species, should be considered. E.g. organic nitrogen mixed with inorganic (only nitrate) nitrogen in or organic nitrogen mixed with nitrate and ammonium in the same particle. Experiments using these types of mixture particles should be done in a follow-up study to ultimately establish whether measurements on real world aerosol samples can be successfully performed.

6 Conclusions: Main findings and outlook

In this thesis it has been demonstrated that Nano Secondary Ion Mass Spectrometry (NanoSIMS) can be used to differentiate different nitrogen containing species commonly observed in atmospheric aerosol particles, on the basis of the relative intensities of secondary ion signals, both in negative and positive secondary ion mode without the need to chemically or physically separate the samples. Compounds tested include nitrate, nitrite, ammonium salts, urea, amino acids, biological tissue and imidazole (Chapter 3). Standards and sample substrates used and the preparation methods employed are described in detail in chapter 2. In-house standards used in this study include inorganic species (sodium nitrate, sodium nitrite, potassium nitrate, calcium nitrate, ammonium nitrate and ammonium sulfate) and organic species (glucose, urea, cysteine, citric acid, ascorbic acid and benzylimidazole). Two standards with known N isotope composition having $\delta^{15}N$ values of +2.7 ‰ and +4.7 ‰ compared to N_2 in the air, respectively, were used in this study: USGS35 (sodium nitrate) and IAEA-NO-3 (potassium nitrate). I have shown that NO_2^- secondary ion is unique to the decomposition of nitrate and nitrite salts, while NH_4^+ secondary ion is unique to samples containing ammonium ions or amino groups, but were not observed in biological tissue. CN^- signals can be obtained from all nitrogen bearing compounds, but relative signal intensities are highest for organic nitrogen containing compounds. I have further demonstrated that stable N isotope ratios measured on in-house standards of unknown isotopic composition using the $^{12}C^{15}N^-$ / $^{12}C^{14}N^-$ - ratio (all nitrogen containing species), the $^{15}N^{16}O_2^-$ / $^{14}N^{16}O_2^-$ - ratio (nitrate and nitrite species) and the $^{15}NH_4^+$ / $^{14}NH_4^+$ - ratio (ammonium salts, amino acids and urea) are stable and sufficiently precise for nitrogen isotope analysis.

Chapter 4 describes the attempts to develop a new single particle technique for the analysis of species specific nitrogen isotope ratios on nitrate aerosol on a micrometer spatial resolution (coarse mode nitrate). The accuracy and precision has been extensively validated on a set of $NaNO_3$ and KNO_3 in-house standards and aerosol-like mixtures with variable N/C ratio in numerous sessions over a period of more than one year. Firstly, analysis conditions were optimized using pure nitrate salts ($NaNO_3$ and KNO_3) deposited on gold foil. It was found that accurate and precise measurements of the nitrogen isotopic composition can be performed using the $^{15}N^{16}O_2^-$ / $^{14}N^{16}O_2^-$ - ratio. The precision is ± 0.6 ‰ for long term measurements on the in-house $NaNO_3$ standard for a raster size of 5×5 μm^2 and the accuracy obtained for this sample is better than 0.5 ‰. The difference in the matrix specific IMF between $NaNO_3$ and KNO_3 is 7.1 ± 0.9 ‰ and the slope of the IMF as a function of the ionic radius of the cations was found to be similar to what was found for sulfate salts in a previous study.

However, while studying more complex aerosol-like mixture samples with different N to C atom ratios and experimenting with samples deposited on different substrates I found that the secondary ion $^{23}Na^{12}C_2^-$ can be a serious interference, when the $^{15}N^{16}O_2^-$ molecular ion is used to measure the nitrogen isotope composition while Na and C are present in the same analysis area. Moreover, even when KNO_3 samples, that do not suffer from this interference are analyzed, depositing the sample on Nuclepore filter can cause problems as the carbon concentration in samples needs to be known accurately for IMF correction. When silicon wafers are chosen as a sample substrate, the secondary ion $^{29}Si^{18}O^-$ coming from silicon wafers affects the measurement of the $^{15}N^{16}O_2^-$ molecular ion directly. A newly developed single plane data processing algorithm along with high mask levels allowed me to study the matrix effect induced by the presence of variable N/C ratios in the aerosol-like carbon-containing potassium nitrate-glucose mixture samples which I quantified as $\delta^{15}N_{bias} = (101 \pm 4) \cdot f - (101 \pm 3)$ ‰, where $f = NO_2^- / (NO_2^- + CN^-)$.

Since I found that measuring species specific isotope ratios for nitrate aerosol using the $^{15}N^{16}O_2^-$ / $^{14}N^{16}O_2^-$ - ratio is prone to interferences and more complex than anticipated, in Chapter 5, I investigated the option determining the nitrogen isotopic signature using the $^{12}C^{15}N^-/^{12}C^{14}N^-$ secondary ion ratio, while limiting the analysis area to nitrate by using a $^{14}N^{16}O_2^-$ mask. The results show that there is neither a detectable matrix effect induced by the presence of variable N/C ratios, nor do any interferences complicate determining the N isotope ratio measurement using the $^{12}C^{14}N^-/^{12}C^{15}N^-$ ratio. Using $^{14}N^{16}O_2^-$ as mask mass can make these measurements species specific for nitrate.

To make this work a success, I performed extensive programing work to develop a software that allows plane-wise image processing and isotope ratio calculations using NanoSIMS data. I summarized the programs that I wrote for this purpose in appendix A. Firstly, in order to estimate and find out potential interferences affecting certain masses in the NanoSIMS analysis, I wrote a small program to calculate all possible combinations of molecular ions that could potentially interfere with a given mass of interest, e.g. $^{15}N^{16}O_2^-$ at a certain mass resolving power. In addition, two new NanoSIMS data processing programs were written in the MATLAB language, based on the NanoSIMS data processing software written in the IDL language created by the NAMIP group at MPIC. One of these programs is used for isotope mode data processing. This software extracts all NanoSIMS conditions, parameters, and measured masses. This allows to rapidly assess how analytical conditions influence IMF. More than one thousand analysis points can be quickly processed and classified, binned, and plotted based on various analysis parameters, e.g. primary current, aperture settings, or lens settings (EOW and EOP). Automatic IMF and QSA corrections

can be applied and the results can be exported to an Excel file. The other program was created for the image processing of the aerosol-like mixture experiments. With this program, certain calculations are performed for large quantities of image data, e.g., single plane mask calculations at various mask levels and single plane QSA correction. A data filter and browser in this program provide fast plots to help data evaluation.

As species specific isotope analysis using the NO_2^- molecular ion has limited scope for the study of ambient aerosol particles, which frequently contain both sodium and carbon and hence suffer from the interference by $^{23}Na^{12}C_2^-$, future studies should focus on using CN^- secondary ion for the isotope analysis and different mask masses to make the measurement species specific (e.g. $^{14}N^{16}O_2^-$ for nitrate and $^{32}S^-$ for ammoniums sulfate). No serious interferences and matrix effects were found and I successfully measured the nitrogen isotope composition in nitrate species by using NO_2^- as mask. Follow-up experiments should be done in the future. Internally mixed particles containing more than one source of reactive nitrogen, like mixtures of organic nitrogen with nitrate species or mixtures of ammonia species with nitrate species, should be considered to ultimately establish whether measurements on real world aerosol samples can be successfully performed. The possibility of measuring the species specific N isotope composition of ammonium ions/amino groups using the NH_4^+ secondary ion should also be explored.

Abreviations

cps	Counts Per Second
D1	Aperture stop which limits the primary ion beam
EKMA	Empirical Kinetic Modeling Approach
EM	Electron Multiplier
EOP	Secondary electrode of the immersion lens E0 which focuses the primary ion beam on the sample
EOS	Third electrode of the immersion lens E0 which acts mainly on the secondary ion beam, and focuses extracted secondary ions
EOW	First electrode of the immersion lens E0 which acts mainly on the secondary ion beam and provides the sample HV
f	Secondary ion ratio of $^{14}N^{16}O_2^-$ / ($^{14}N^{16}O_2^-$ + $^{12}C^{14}N^-$)
f*	Secondary ion ratio of $^{14}N^{16}O_2^-$ / ($^{14}N^{16}O_2^-$ + $^{16}O^-$)
HMR	High Mass Resolution
IAEA	International Atomic Energy Agency
IDL	Interactive Data Language
im	Image data storage format in NanoSIMS 50
IMF	Instrumental Mass Fractionation
IPCC	Intergovernmental Panel on Climate Change
MATLAB	Matrix Laboratory
NO_x	Mono-nitrogen Oxides NO and NO_2
NO_y	Total reactive nitrogen, $NO_y = NO_x + HNO_3 + N_2O_5 + HONO + PAN$ + other organic nitrogen compounds
N_r	Reactive Nitrogen
PFA	Perfluoroalkoxy alkanes
QSA	Quasi Simultaneous Arrivals
SEM	Scanning Electron Microscope
SIBC	Secondary Ion Beam Centering
SIMS	Secondary Ion Mass Spectrometry
USGS	United States Geological Survey

VOC	Volatile organic compound

List of tables

Table 1-1. A summary of sources of fixed nitrogen from Fowler et al. (2013).. 2

Table 1-2. The stable nitrogen isotope characteristics in Figure 1-5. 13

Table 2-1. Inorganic and organic standards used in this study. 16

Table 2-2. Concentrations of solutions used to make aerosol-like mixture samples. 19

Table 4-1. Measured IMF of $\delta^{15}N$ for UGSG35 $NaNO_3$ #1.. 57

Table 4-2. $\delta^{15}N_{air}$ of In-house $NaNO_3$ corrected by USGS35 $NaNO_3$ with raster area 5×5 μm^2.. 58

Table A-1. An example of output results set with $^{15}N^{16}O_2$ as the reference mass 118

Table A-2. Option name with the description of x-axis in 'Create Chart' list. 124

Table A-3. Examples and descriptions of im file information in file database. 132

Table A-4. Examples and descriptions of measurement informations in im file database. 133

Table A-5. Examples and descriptions of calculation settings in im file database. 134

Table A-6. Descriptions of calculation settings.. 135

List of figures

Figure 1-1. The global atmospheric processing of N_r. 4

Figure 1-2. Illustration of the interaction between the various nitrogen oxide compounds in the troposphere.. 4

Figure 1-3. Two dimensional ozone isopleths generated from initial mixtures of NO_x and VOC based on EKMA model. 6

Figure 1-4. Radiative forcing estimates in 2011 and aggregated uncertainties for the main drivers of climate change. 8

Figure 1-5. The stable nitrogen isotope characteristics of major potential sources, transportation pathways and processes. 12

Figure 2-1. Standard grains pressed into a gold foil. 17

Figure 2-2. Experimental set-up used to produce aerosol-like mixture samples, consisting of organic carbon and nitrate salts. 20

Figure 2-3. SEM images of aerosol-like samples. 21

Figure 3-1. The Cameca NanoSIMS 50 ion probe at the Max Planck Institute for Chemistry in Mainz, Germany. 26

Figure 3-2. Relative intensities of secondary ions $^{12}C^{14}N^-$, $^{14}N^{16}O^-$, $^{14}N^{16}O_2^-$ and $^{14}N^{16}O_3^-$ in sodium nitrate and sodium nitrite samples. 27

Figure 3-3. $^{14}N^{16}O_2^-$ ion intensities in different samples. 28

Figure 3-4. Relative intensities of secondary ions $^{14}NH^+$, $^{14}NH_2^+$, $^{14}NH_3^+$ and $^{14}NH_4^+$ in ammonium sulfate, urea and cysteine. 29

Figure 3-5. $^{14}NH_4^+$ ion intensities in different samples. 30

Figure 3-6. The distribution of different samples (sodium nitrite, sodium nitrate, ammonium sulfate, urea, cysteine, benzylimidazole and fungal hyphae) based on the normalized heights of positive and negative secondary ion signals.. 31

Figure 3-7. The distribution of different samples (sodium nitrite, sodium nitrate, ammonium sulfate, urea, cysteine, benzylimidazole, glucose and fungal hyphae) based on the normalized heights of negative secondary ion signals 33

Figure 3-8. The distribution of different samples (ammonium sulfate, urea and cysteine) based on the normalized heights of tpositive secondary ion signals 34

Figure 3-9. Stability of the $\delta^{15}N_{uncorrected}$ for different nitrogen containing compounds.. 36

Figure 4-1: High-resolution mass spectra for mass regions 16, 26, 46 and 47.. 38

Figure 4-2. SEM image and NanoSIMS ion images of aerosol-like samples made by mixing potassium nitrate with glucose with N/C = 0.5.. 41

LIST OF FIGURES

Figure 4-3. NanoSIMS ion images ($^{12}C^{14}N^-$ and $^{14}N^{16}O_2^-$) and ratio image ($^{14}N^{16}O_2^-/^{12}C^{14}N^-$) of carbon coated in-house sodium nitrate.. 42

Figure 4-4. Illustration of the NanoSIMS ion image data reduction method used in this work. 44

Figure 4-5. Cumulated ion intensities (left scale) for mass 26 ($^{12}C^{14}N^-$) and mass 46 ($^{14}N^{16}O_2^-$) of the four particles shown in Figure 4-4 for four different mask levels.. 45

Figure 4-6. Relative IMF of 1243 spots measured from August 2012 to December 2013 in ten sessions for different raster areas. 47

Figure 4-7. Dependence of $\delta^{15}N_{bias}$ for the in-house $NaNO_3$ #1 and the IAEA-NO-3 KNO_3 standards on pre sputtering time (top) and primary ion dose per square-micrometer (bottom) for three different raster areas. 48

Figure 4-8. The ratio of secondary $^{14}N^{16}O_2^-$ over primary Cs^+ ion intensities for three standards and three raster areas. 51

Figure 4-9. IMF against the count rate of the secondary ion $^{14}N^{16}O_2^-$. 52

Figure 4-10. SEM images of standard IAEA-NO-3 KNO3, USGS35 $NaNO_3$ and in-house $NaNO_3$ #1 after NanoSIMS analysis in three raster areas. 53

Figure 4-11. Results of N isotope analysis of in-house $NaNO_3$ #1 for different primary ion doses. 57

Figure 4-12. Matrix effect between $NaNO_3$ and KNO_3, calculated according to formula 4-4, for different primary ion doses. 59

Figure 4-13. Dependence of $\delta^{34}S_{bias}$ and $\delta^{15}N_{bias}$ on the ionic radius of the cations of different sulfates and nitrates. 60

Figure 4-14. IMF introduced by the presence of carbon in sodium nitrate as the function of the secondary ion ratio f = $^{14}N^{16}O_2^- / (^{14}N^{16}O_2^- + ^{12}C^{14}N^-)$.. 63

Figure 4-15. IMF of $^{15}N/^{14}N$ in C-bearing sodium nitrate as a function of the secondary ion ratio f* = $^{14}N^{16}O_2^- / (^{14}N^{16}O_2^- + ^{16}O^-)$. 64

Figure 4-16. Variations in IMF introduced by the presence of carbon in potassium nitrate as function of secondary ion ratio f = $^{14}N^{16}O_2^- / (^{14}N^{16}O_2^- + ^{12}C^{14}N^-)$. 66

Figure 4-17. IMF in carbon bearing potassium nitrate as function of the secondary ion ratio f* = $^{14}N^{16}O_2^-/(^{14}N^{16}O_2^- + ^{16}O^-)$. 67

Figure 4-18. Nitrogen isotopes measured as $^{15}N^{16}O_2^-/^{14}N^{16}O_2^-$. KNO_3, $NaNO_3$, and their mixtures with glucose were transformed to aerosol, collected on gold foil and on nuclepore filter.. 69

Figure 4-19: Ion intensities and the ratio of mass 47 ($^{15}N\ ^{16}O_2^- + ^{23}Na\ ^{12}C_2^-$) to mass 46 ($^{14}N\ ^{16}O_2^-$) of a small grain (<200 nm) containing sodium nitrate and glucose with N/C = 0.5. 70

Figure 4-20. Matrix effect of nitrogen isotope measurements on C-containing potassium nitrate as function of f. 72

Figure 5-1. High-resolution mass spectra for mass regions 12 – $^{12}C^-$, 16 – $^{16}O^-$, 26 – $^{12}C^{14}N^-$, 27 – $^{12}C^{15}N^-$, 46 – $^{14}N^{16}O_2^-$. 78

Figure 5-2. Secondary ion images of $^{12}C^{14}N^-$ and $^{14}N^{16}O_2^-$ from samples collected on silicon wafer and nuclepore filter,

calculated with mask levels of 10 % and 30 % for $^{14}N^{16}O_2^-$. 79

Figure 5-3. Example of QSA correction. Shown is the IMF ($\delta^{15}N = (R_{SIMS}/R_{true} - 1) \times 1000$) as a function of secondary ion intensity of $^{12}C^{14}N^-$.. 80

Figure 5-4. $\delta^{15}N$ inferred from $^{12}C^{15}N^-$ / $^{12}C^{14}N^-$ as a function of f and for different mask levels of $^{14}N^{16}O_2^-$.. 80

Figure 5-5. Weighted average $\delta^{15}N_{bias}$ results of aerosol-like mixture samples collected on nuclepore filter and silicon wafer with different mask levels for $^{14}N^{16}O_2^-$ in NanoSIMS images.. 82

Figure A-1. The main interface of the isotope mode NanoSIMS data processing program. 120

Figure A-2. Advanced searching interface. 121

Figure A-3. Create chart list.. 121

Figure A-4. Exported chart by option 'Create chart' with the settings in Figure A-2. 122

Figure A-5. An example of export data in Excel file.. 123

Figure A-6. An example of 'Create Chart' option – 'Ref_cps/Cs_cps-IMF'.. 125

Figure A-7. Example of an auto IMF correction with the standard USGS35 ($NaNO_3$).. 126

Figure A-8. Image data input interface. 130

Figure A-9. im file organizing interface.. 131

Figure A-10. Calculation control interface. 132

Figure A-11. Single im file results interface.. 136

Figure A-12: Screenshots of the comparison of single plane mask calculation results (left plot, SinCal) and summary plane mask calculation results (right plot, SumCal). 137

Figure A-13. The comparison of single plane mask calculation results (upper plot, SinCal) and summary plane mask calculation results (lower plot, SumCal) in 3D cross-sectional plot. 138

Figure A-14. 3D cross-sectional plot interface. 139

Figure A-15. 2D single im file results browser. 140

Figure A-16. Schematic diagram of auto im file calculation. 142

Figure A-17. Time statistics of auto im file calculation. 142

Figure A-18. ROI mask maker. 143

Figure A-19. ROI mask previewer. 144

Figure A-20. An example of ROI mask setting result. 145

Figure A-21. Two results data filter. 146

Figure A-22. Results data browser. 147

Bibliography

Adams, P. J. and J. H. Seinfeld: Predicting global aerosol size distributions in general circulation models, Journal of Geophysical Research-Atmospheres, 107, D19, 2002.

Adams, P. J., J. H. Seinfeld, D. Koch, L. Mickley and D. Jacob: General circulation model assessment of direct radiative forcing by the sulfate-nitrate-ammonium-water inorganic aerosol system, Journal of Geophysical Research-Atmospheres, 106, D1, 1097-1111, 2001.

Akhtar, M. J., D. Axente and F. T. Bonner: Nitrogen isotope exchange between nitric and nitrous acids, The Journal of Chemical Physics, 71, 9, 3570-3572, 1979.

Al-Abadleh, H. A., B. J. Krueger, J. L. Ross and V. H. Grassian: Phase transitions in calcium nitrate thin films, Chemical Communications22, 2796-2797, 2003.

Alexander, B., M. G. Hastings, D. J. Allman, J. Dachs, J. A. Thornton and S. A. Kunasek: Quantifying atmospheric nitrate formation pathways based on a global model of the oxygen isotopic composition (Δ^{17}O) of atmospheric nitrate, Atmos. Chem. Phys., 9, 14, 5043-5056, 2009.

Ammann, M., R. Siegwolf, F. Pichlmayer, M. Suter, M. Saurer and C. Brunold: Estimating the uptake of traffic-derived NO_2 from N-15 abundance in Norway spruce needles, Oecologia, 118, 2, 124-131, 1999.

Audi, G., M. Wang, A. H. Wapstra, F. G. Kondev, M. MacCormick and X. Xu: The 2012 Atomic Mass Evaluation and the Mass Tables, Nuclear Data Sheets, 120, 1-5, 2014.

Begun, G. M. and W. H. Fletcher: Partition Function Ratios for Molecules Containing Nitrogen Isotopes, Journal of Chemical Physics, 33, 4, 1083-1085, 1960.

Begun, G. M. and C. E. Melton: Nitrogen Isotopic Fractionation between NO and NO_2 and Mass Discrimination in Mass Analysis of NO_2, Journal of Chemical Physics, 25, 6, 1292-1293, 1956.

Bentz, J. W. G., M. Fichtner, J. Goschnick and H. J. Ache: Depth-Resolved Speciation of Nitrogen-Compounds in Environmental Solids, Fresenius Journal of Analytical Chemistry, 349, 1-3, 205-207, 1994.

Berglund, M. and M. E. Wieser: Isotopic compositions of the elements 2009 (IUPAC Technical Report), Pure and Applied Chemistry, 83, 2, 397-410, 2011.

BIBLIOGRAPHY

Bevington, P. R. and D. K. Robinson. Data reduction and error analysis for the physical sciences. New York, McGraw-Hill. 1992.

Bobbink, R., K. Hicks, J. Galloway, T. Spranger, R. Alkemade, M. Ashmore, M. Bustamante, S. Cinderby, E. Davidson, F. Dentener, B. Emmett, J. W. Erisman, M. Fenn, F. Gilliam, A. Nordin, L. Pardo and W. De Vries: Global assessment of nitrogen deposition effects on terrestrial plant diversity: a synthesis, Ecological Applications, 20, 1, 30-59, 2010.

Bohlke, J. K., C. J. Gwinn and T. B. Coplen: New Reference Materials for Nitrogen-Isotope-Ratio Measurements, Geostandards Newsletter, 17, 1, 159-164, 1993.

Bohlke, J. K., S. J. Mroczkowski and T. B. Coplen: Oxygen isotopes in nitrate: new reference materials for O-18: O-17: O-16 measurements and observations on nitrate-water equilibration, Rapid Communications in Mass Spectrometry, 17, 16, 1835-1846, 2003.

Boyd, S. R. and C. T. Pillinger: Rubidium Sulfate Ammonium-Sulfate Solid-Solution - a Standard for Use during the Determination of Nitrogen Abundance and Isotopic Composition at the Ppm Level by Static-Vacuum Mass-Spectrometry, Analytical Chemistry, 63, 13, 1332-1335, 1991.

Boyd, S. R., C. T. Pillinger, H. J. Milledge, M. J. Mendelssohn and M. Seal: C-Isotopic and N-Isotopic Composition and the Infrared-Absorption Spectra of Coated Diamonds - Evidence for the Regional Uniformity of CO_2-H_2O Rich Fluids in Lithospheric Mantle, Earth and Planetary Science Letters, 109, 3-4, 633-644, 1992.

Boyd, S. R., A. Rejoumichel and M. Javoy: Noncryogenic Purification of Nanomole Quantities of Nitrogen Gas for Isotopic Analysis, Analytical Chemistry, 66, 9, 1396-1402, 1994.

Breuer, U., H. Holzbrecher, M. Gastel, J. S. Becker and H. J. Dietze: Comparative studies of SIMS and SNMS analyses during the build up of sputter equilibrium under oxygen and rare gas ion bombardment, Fresenius Journal of Analytical Chemistry, 358, 1-2, 47-50, 1997.

Brown, L. L. and J. S. Drury: Nitrogen-Isotope Effects in Reduction of Nitrate Nitrite and Hydroxylamine to Ammonia .I. In Sodium Dydroxide Solution with Fe (2), Journal of Chemical Physics, 46, 7, 2833-&, 1967.

Brown, L. L. and J. S. Drury: Exchange and Fractionation of Nitrogen Isotopes between NO and NO_2^-, Journal of Chemical Physics, 48, 3, 1400-&, 1968.

Brown, L. L., J.S. Drury: Exchange and Fractionation of Nitrogen Isotopes Between NO_2^- and NO_3, The Journal of Chemical Physics, 48, 3, 1399, 1968a.

Buijsman, E., H. F. M. Maas and W. A. H. Asman: Anthropogenic NH_3 Emissions in Europe, Atmospheric Environment, 21, 5, 1009-1022, 1987.

Bulanova, G. P., D. G. Pearson, E. H. Hauri and B. J. Griffin: Carbon and nitrogen isotope systematics within a sector-growth diamond from the Mir kimberlite, Yakutia, Chemical Geology, 188, 1-2, 105-123, 2002.

Cape, J. N., S. E. Cornell, T. D. Jickells and E. Nemitz: Organic nitrogen in the atmosphere — Where does it come from? A review of sources and methods, Atmospheric Research, 102, 1-2, 30-48, 2011.

Chandra, S.: Subcellular SIMS imaging of isotopically labeled amino acids in cryogenically prepared cells, Applied Surface Science, 231, 462-466, 2004.

Coe, H., J. D. Allan, M. R. Alfarra, K. N. Bower, M. J. Flynn, G. B. McFiggans, D. O. Topping, P. I. Williams, C. D. O'Dowd, M. Dall'Osto, D. C. S. Beddows and R. M. Harrison: Chemical and physical characteristics of aerosol particles at a remote coastal location, Mace Head, Ireland, during NAMBLEX, Atmospheric Chemistry and Physics, 6, 3289-3301, 2006.

Cohen, A. J., H. R. Anderson, B. Ostro, K. D. Pandey, M. Krzyzanowski, N. Kunzli, K. Gutschmidt, A. Pope, I. Romieu, J. M. Samet and K. Smith: The global burden of disease due to outdoor air pollution, Journal of Toxicology and Environmental Health-Part a-Current Issues, 68, 13-14, 1301-1307, 2005.

Compton, J. E., J. A. Harrison, R. L. Dennis, T. L. Greaver, B. H. Hill, S. J. Jordan, H. Walker and H. V. Campbell: Ecosystem services altered by human changes in the nitrogen cycle: a new perspective for US decision making, Ecology Letters, 14, 8, 804-815, 2011.

Coplen, T. B., J. K. Bohlke and K. L. Casciotti: Using dual-bacterial denitrification to improve delta N-15 determinations of nitrates containing mass-independent ^{17}O, Rapid Communications in Mass Spectrometry, 18, 3, 245-250, 2004.

Cornell, S. E., T. D. Jickells, J. N. Cape, A. P. Rowland and R. A. Duce: Organic nitrogen deposition on land and coastal environments: a review of methods and data, Atmospheric Environment, 37, 16, 2173-2191, 2003.

De Haan, D. O., A. L. Corrigan, K. W. Smith, D. R. Stroik, J. J. Turley, F. E. Lee, M. A. Tolbert, J. L. Jimenez, K. E. Cordova and G. R. Ferrell: Secondary Organic Aerosol-Forming Reactions of Glyoxal with Amino Acids, Environmental Science & Technology, 43, 8, 2818-2824, 2009.

De Vries, W., S. Solberg, M. Dobbertin, H. Sterba, D. Laubhann, M. van Oijen, C. Evans, P. Gundersen, J. Kros, G. W. W. Wamelink, G. J. Reinds and M. A. Sutton: The impact of nitrogen deposition on carbon sequestration by European forests and heathlands, Forest Ecology and Management, 258, 8, 1814-1823, 2009.

Dentener, F. J. and P. J. Crutzen: Reaction of N_2O_5 on Tropospheric Aerosols - Impact on the Global Distributions of Nox, O_3, and OH, Journal of Geophysical Research-Atmospheres, 98, D4, 7149-7163, 1993.

Derwent, R. and O. Hertel. Transformation of Air Pollutants. Urban Air Pollution — European Aspects. J. Fenger, O. Hertel and F. Palmgren, Springer Netherlands. 1: 137-159. 1998.

Divers, M. T., E. M. Elliott and D. J. Bain: Quantification of Nitrate Sources to an Urban Stream Using Dual Nitrate Isotopes, Environmental Science & Technology, 48, 18, 10580-10587, 2014.

Eckstein, W.: Oscillations of sputtering yield, Nuclear Instruments & Methods in Physics Research Section B-Beam Interactions with Materials and Atoms, 171, 4, 435-442, 2000.

Elliott, E. M., C. Kendall, E. W. Boyer, D. A. Burns, G. G. Lear, H. E. Golden, K. Harlin, A. Bytnerowicz, T. J. Butler and R. Glatz: Dual nitrate isotopes in dry deposition: Utility for partitioning NO_x source contributions to landscape nitrogen deposition, Journal of Geophysical Research-Biogeosciences, 114, 2009.

Elliott, E. M., C. Kendall, S. D. Wankel, D. A. Burns, E. W. Boyer, K. Harlin, D. J. Bain and T. J. Butler: Nitrogen Isotopes as Indicators of NOx Source Contributions to Atmospheric Nitrate Deposition Across the Midwestern and Northeastern United States, Environmental Science & Technology, 41, 22, 7661-7667, 2007.

Erisman, J. W., J. N. Galloway, S. Seitzinger, A. Bleeker, N. B. Dise, A. M. R. Petrescu, A. M. Leach and W. de Vries: Consequences of human modification of the global nitrogen cycle, Philosophical Transactions of the Royal Society B-Biological Sciences, 368, 1621, 2013.

Farmer, D. K., A. Matsunaga, K. S. Docherty, J. D. Surratt, J. H. Seinfeld, P. J. Ziemann and J. L. Jimenez: Response of an aerosol mass spectrometer to organonitrates and organosulfates and implications for atmospheric chemistry, Proceedings of the National Academy of Sciences of the United States of America, 107, 15, 6670-6675, 2010.

Faude, F. and J. Goschnick: XPS, SIMS and SNMS applied to a combined analysis of aerosol particles from a region of considerable air pollution in the upper Rhine valley, Fresenius Journal of Analytical Chemistry, 358, 1-2, 67-72, 1997.

Felix, J. D., E. M. Elliott and S. L. Shaw: Nitrogen Isotopic Composition of Coal-Fired Power Plant NO_x: Influence of Emission Controls and Implications for Global Emission Inventories, Environmental Science & Technology, 46, 6, 3528-3535, 2012.

Felzer, B., D. Kicklighter, J. Melillo, C. Wang, Q. Zhuang and R. Prinn: Effects of ozone on net primary production and carbon sequestration in the conterminous United States using a biogeochemistry model, Tellus Series B-Chemical and Physical Meteorology, 56, 3, 230-248, 2004.

Finlaysonpitts, B. J. and J. N. Pitts: Atmospheric Chemistry of Tropospheric Ozone Formation - Scientific and Regulatory Implications, Journal of the Air & Waste Management Association, 43, 8, 1091-1100, 1993.

Fitzsimons, I. C. W., B. Harte and R. M. Clark: SIMS stable isotope measurement: counting statistics and analytical precision, Mineralogical Magazine, 64, 1, 59-83, 2000.

Fowler, D., M. Coyle, U. Skiba, M. A. Sutton, J. N. Cape, S. Reis, L. J. Sheppard, A. Jenkins, B. Grizzetti, J. N. Galloway, P. Vitousek, A. Leach, A. F. Bouwman, K. Butterbach-Bahl, F. Dentener, D. Stevenson, M. Amann and M. Voss: The global nitrogen cycle in the twenty-first century, Philosophical Transactions of the Royal Society B-Biological Sciences, 368, 1621, 2013.

Freyer, H. D.: Seasonal trends of NH_4^+ and NO_3^- nitrogen isotope composition in rain collected at Jülich, Germany, Tellus, 30, 1, 83-92, 1978.

Freyer, H. D.: Seasonal variation of $^{15}N/^{14}N$ ratios in atmospheric nitrate species, Tellus, Series B, 43 B, 1, 30-44, 1991.

Freyer, H. D. and A. I. M. Aly: Nitrogen-15 Variations in Fertilizer Nitrogen, Journal of Environmental Quality, 3, 4, 405-406, 1974.

Freyer, H. D., D. Kley, A. Volzthomas and K. Kobel: On the Interaction of Isotopic Exchange Processes with Photochemical-Reactions in Atmospheric Oxides of Nitrogen, Journal of Geophysical Research-Atmospheres, 98, D8, 14791-14796, 1993.

Galloway, J. N., J. D. Aber, J. W. Erisman, S. P. Seitzinger, R. W. Howarth, E. B. Cowling and B. J. Cosby: The nitrogen cascade, Bioscience, 53, 4, 341-356, 2003.

Galloway, J. N., A. R. Townsend, J. W. Erisman, M. Bekunda, Z. Cai, J. R. Freney, L. A. Martinelli, S. P. Seitzinger and M. A. Sutton: Transformation of the Nitrogen Cycle: Recent Trends, Questions, and Potential Solutions, Science, 320, 5878, 889-892, 2008.

Gardenas, A. I., G. I. Agren, J. A. Bird, M. Clarholm, S. Hallin, P. Ineson, T. Katterer, H. Knicker, S. I. Nilsson, T. Nasholm, S. Ogle, K. Paustian, T. Persson and J. Stendahl: Knowledge gaps in soil carbon and nitrogen interactions - From molecular to global scale, Soil Biology & Biochemistry, 43, 4, 702-717, 2011.

Ghosal, S., P. K. Weber and A. Laskin: Spatially resolved chemical imaging of individual atmospheric particles using nanoscale imaging mass spectrometry: insight into particle origin and chemistry, Analytical Methods, 6, 8, 2444-2451, 2014.

Gnaser, H.: Isotopic fractionation of sputtered anions: C^- and C_2^-, Nuclear Instruments & Methods in Physics Research Section B-Beam Interactions with Materials and Atoms, 266, 1, 37-43, 2008.

Gonfiantini, R.: Iaea Advisory Group Meeting on Stable Isotope Reference Samples for Geochemical and Hydrological Investigations - Vienna, Austria, September 19-21, 1983, Journal of Hydrology, 72, 1-2, 205-205, 1984.

Gray, H. A., G. R. Cass, J. J. Huntzicker, E. K. Heyerdahl and J. A. Rau: Characteristics of Atmospheric Organic and Elemental Carbon Particle Concentrations in Los-Angeles, Environmental Science & Technology, 20, 6, 580-589, 1986.

Groenewold, G. S., J. E. Delmore, J. E. Olson, A. D. Appelhans, J. C. Ingram and D. A. Dahl: Secondary ion mass spectrometry of sodium nitrate: Comparison of ReO_4^- and Cs^+ primary ions, International Journal of Mass Spectrometry and Ion Processes, 163, 3, 185-195, 1997.

Haffner, H. T., M. Banger, M. Graw, K. Besserer and T. Brink: The kinetics of methanol elimination in alcoholics and the influence of ethanol, Forensic Science International, 89, 1-2, 129-136, 1997.

Halm, H., N. Musat, P. Lam, R. Langlois, F. Musat, S. Peduzzi, G. Lavik, C. J. Schubert, B. Sinha, J. LaRoche and M. M. M. Kuypers: Co-occurrence of denitrification and nitrogen fixation in a meromictic lake, Lake Cadagno (Switzerland), Environmental Microbiology, 11, 8, 1945-1958, 2009.

Hanson, D. R., P. H. McMurry, J. Jiang, D. Tanner and L. G. Huey: Ambient Pressure Proton Transfer Mass Spectrometry: Detection of Amines and Ammonia, Environmental Science & Technology, 45, 20, 8881-8888, 2011.

Harris, E., B. Sinha, D. van Pinxteren, J. Schneider, L. Poulain, J. Collett, B. D'Anna, B. Fahlbusch, S. Foley, K. W. Fomba, C. George, T. Gnauk, S. Henning, T. Lee, S. Mertes, A. Roth, F. Stratmann, S. Borrmann, P. Hoppe and H. Herrmann: In-cloud sulfate addition to single particles resolved with sulfur isotope analysis during HCCT-2010, Atmospheric Chemistry and Physics, 14, 8, 4219-4235, 2014.

Harris, E., B. Sinha, D. van Pinxteren, A. Tilgner, K. W. Fomba, J. Schneider, A. Roth, T. Gnauk, B. Fahlbusch, S. Mertes, T. Lee, J. Collett, S. Foley, S. Borrmann, P. Hoppe and H. Herrmann: Enhanced Role of Transition Metal Ion Catalysis During In-Cloud Oxidation of SO2, Science, 340, 6133, 727-730, 2013.

Hauri, E. H., J. Wang, D. G. Pearson and G. P. Bulanova: Microanalysis of delta C-13, delta N-15, and N abundances in diamonds by secondary ion mass spectrometry, Chemical Geology, 185, 1-2, 149-163, 2002.

Heathon, T. H. E.: Isotopic studies of nitrogen pollution in the hydrosphere and atmosphere a review, Chemical Geology (Isotope Geoscience Section), 87-102, 1986.

Heaton, T.: $^{15}N/^{14}N$ ratios of NOx from vehicle engines and coal-fired power stations, Tellus, Series B, 42 B, 3, 304-307, 1990.

Heaton, T., B. Spiro and S. M. C. Robertson: Potential canopy influences on the isotopic composition of nitrogen and sulphur in atmospheric deposition, Oecologia, 109, 4, 600-607, 1997.

Heaton, T., J. C. Vogel, G. Von la Chevallerie and G. Collett: Climatic influence on the isotopic composition of bone nitrogen, Nature, 322, 6082, 822-823, 1986.

Heaton, T. H. E.: Sources of the Nitrate in Phreatic Groundwater in the Western Kalahari, Journal of Hydrology, 67, 1-4, 249-259, 1984.

Heaton, T. H. E.: $^{15}N/^{14}N$ ratios of nitrate and ammonium in rain at Pretoria, South Africa, Atmospheric Environment (1967), 21, 4, 843-852, 1987.

Hertel, O., C. A. Skjoth, P. Lofstrom, C. Geels, L. M. Frohn, T. Ellermann and P. V. Madsen: Modelling nitrogen deposition on a local scale - A review of the current state of the art, Environmental Chemistry, 3, 5, 317-337, 2006.

Hindie, E., B. Coulomb, R. Beaupain and P. Galle: Mapping the Cellular-Distribution of Labeled Molecules by Sims Microscopy, Biology of the Cell, 74, 1, 81-88, 1992.

Hoffman, R. C., A. Laskin and B. J. Finlayson-Pitts: Sodium nitrate particles: physical and chemical properties during hydration and dehydration, and implications for aged sea salt aerosols, Journal of Aerosol Science, 35, 7, 869-887, 2004.

Holland, E. A. and M. A. Carroll: Atmospheric chemistry and the bioatmospheric carbon and nitrogen cycles, Interactions of the Major Biogeochemical Cycles, 61, 273-292, 2003.

Hoppe, P., S. Amari, E. Zinner, T. Ireland and R. S. Lewis: Carbon, Nitrogen, Magnesium, Silicon, and Titanium Isotopic Compositions of Single Interstellar Silicon-Carbide Grains from the Murchison Carbonaceous Chondrite, Astrophysical Journal, 430, 2, 870-&, 1994.

Hoppe, P., S. Cohen and A. Meibom: NanoSIMS: Technical Aspects and Applications in Cosmochemistry and Biological Geochemistry, Geostandards and Geoanalytical Research, 37, 2, 111-154, 2013.

Hov, O., B. A. Hjollo and A. Eliassen: Transport Distance of Ammonia and Ammonium in Northern Europe .1. Model Description, Journal of Geophysical Research-Atmospheres, 99, D9, 18735-18748, 1994.

Hut, G. Consultants' group meeting on stable isotope reference samples for geochemical and hydrological investigations. 1987.

Hwang, H. J. and C. U. Ro: Direct observation of nitrate and sulfate formations from mineral dust and sea-salts using low-Z particle electron probe X-ray microanalysis, Atmospheric Environment, 40, 21, 3869-3880, 2006.

Jacob, D. J.: Heterogeneous chemistry and tropospheric ozone, Atmospheric Environment, 34, 12-14, 2131-2159, 2000.

Jacobson, M. C., H. C. Hansson, K. J. Noone and R. J. Charlson: Organic atmospheric aerosols: Review and state of the science, Reviews of Geophysics, 38, 2, 267-294, 2000.

Jacobson, M. Z.: Global direct radiative forcing due to multicomponent anthropogenic and natural aerosols, Journal of Geophysical Research-Atmospheres, 106, D2, 1551-1568, 2001.

Jia, G. and F. Chen: Monthly variations in nitrogen isotopes of ammonium and nitrate in wet deposition at Guangzhou, south China, Atmospheric Environment, 44, 19, 2309-2315, 2010.

Jickells, T. D., S. D. Kelly, A. R. Baker, K. Biswas, P. F. Dennis, L. J. Spokes, M. Witt and S. G. Yeatman: Isotopic evidence for a marine ammonia source, Geophysical Research Letters, 30, 7, 27-21, 2003.

Junk, G. and H. J. Svec: The absolute abundance of the nitrogen isotopes in the atmosphere and compressed gas from various sources, Geochimica et Cosmochimica Acta, 14, 3, 234-243, 1958.

Kampf, C. J., R. Jakob and T. Hoffmann: Identification and characterization of aging products in the glyoxal/ammonium sulfate system - implications for light-absorbing material in atmospheric aerosols, Atmospheric Chemistry and Physics, 12, 14, 6323-6333, 2012.

Kanakidou, M., K. Tsigaridis, F. J. Dentener and P. J. Crutzen: Human-activity-enhanced formation of organic aerosols by biogenic hydrocarbon oxidation, Journal of Geophysical Research-Atmospheres, 105, D7, 9243-9254, 2000.

Kawashima, H. and T. Kurahashi: Inorganic ion and nitrogen isotopic compositions of atmospheric aerosols at Yurihonjo, Japan: Implications for nitrogen sources, Atmospheric Environment, 45, 35, 6309-6316, 2011.

Kendall, C. and J. J. McDonnell. Isotope tracers in catchment hydrology. Amsterdam; New York, Elsevier. 1998.

Kerminen, V. M., T. A. Pakkanen and R. E. Hillamo: Interactions between inorganic trace gases and supermicrometer particles at a coastal site, Atmospheric Environment, 31, 17, 2753-2765, 1997.

Kreitler, C. W.: Nitrogen-isotope ratio studies of soils and groundwater nitrate from alluvial fan aquifers in Texas, Journal of Hydrology, 42, 1-2, 147-170, 1979.

Kreitler, C. W. and D. C. Jones: Natural soil nitrate: the cause of the nitrate contamination of ground water in Runnels county, Texas, Ground Water, 13, 1, 53-62, 1975.

Krueger, B. J., V. H. Grassian, J. P. Cowin and A. Laskin: Heterogeneous chemistry of individual mineral dust particles from different dust source regions: the importance of particle mineralogy, Atmospheric Environment, 38, 36, 6253-6261, 2004.

Kundu, S., K. Kawamura, T. W. Andreae, A. Hoffer and M. O. Andreae: Diurnal variation in the water-soluble inorganic ions, organic carbon and isotopic compositions of total carbon and nitrogen in biomass burning aerosols from the LBA-SMOCC campaign in Rondônia, Brazil, Journal of Aerosol Science, 41, 1, 118-133, 2010.

Laskin, A., M. J. Iedema, A. Ichkovich, E. R. Graber, I. Taraniuk and Y. Rudich: Direct observation of completely processed calcium carbonate dust particles, Faraday Discussions, 130, 453-468, 2005.

Laskin, A., T. W. Wietsma, B. J. Krueger and V. H. Grassian: Heterogeneous chemistry of individual mineral dust particles with nitric acid: A combined CCSEM/EDX, ESEM, and ICP-MS study, Journal of Geophysical Research-Atmospheres, 110, D10, 2005a.

Lechene, C. P., Y. Luyten, G. McMahon and D. L. Distel: Quantitative imaging of nitrogen fixation by individual bacteria within animal cells (vol 317, pg 1563, 2007), Science, 318, 5850, 570-570, 2007.

Li, D. and X. Wang: Nitrogen isotopic signature of soil-released nitric oxide (NO) after fertilizer application, Atmospheric Environment, 42, 19, 4747-4754, 2008.

Li, L., B. S. Lollar, H. Li, U. G. Wortmann and G. Lacrampe-Couloume: Ammonium stability and nitrogen isotope fractionations for –NH_3(aq)–NH_3(gas) systems at 20–70°C and pH of 2–13: Applications to habitability and nitrogen cycling in low-temperature hydrothermal systems, Geochimica et Cosmochimica Acta, 84, 280-296, 2012.

Liao, H. and J. H. Seinfeld: Global impacts of gas-phase chemistry-aerosol interactions on direct radiative forcing by anthropogenic aerosols and ozone, Journal of Geophysical Research-Atmospheres, 110, D18, 2005.

Liu, D. W., Y. T. Fang, Y. Tu and Y. P. Pan: Chemical Method for Nitrogen Isotopic Analysis of Ammonium at Natural Abundance, Analytical Chemistry, 86, 8, 3787-3792, 2014.

Marhas, K. K., S. Amari, F. Gyngard, E. Zinner and R. Gallino: Iron and Nickel Isotopic Ratios in Presolar Sic Grains, Astrophysical Journal, 689, 1, 622-645, 2008.

Mariotti, A.: Atmospheric nitrogen is a reliable standard for natural 15N abundance measurements, Nature, 303, 5919, 685-687, 1983.

Martin, S. T., M. O. Andreae, D. Althausen, P. Artaxo, H. Baars, S. Borrmann, Q. Chen, D. K. Farmer, A. Guenther, S. S. Gunthe, J. L. Jimenez, T. Karl, K. Longo, A. Manzi, T. Muller, T. Pauliquevis, M. D. Petters, A. J. Prenni, U. Poschl, L. V. Rizzo, J. Schneider, J. N. Smith, E. Swietlicki, J. Tota, J. Wang, A. Wiedensohler and S. R. Zorn: An overview of the Amazonian Aerosol Characterization Experiment 2008 (AMAZE-08), Atmospheric Chemistry and Physics, 10, 23, 11415-11438, 2010.

Martin, S. T., H. M. Hung, R. J. Park, D. J. Jacob, R. J. D. Spurr, K. V. Chance and M. Chin: Effects of the physical state of tropospheric ammonium-sulfate-nitrate particles on global aerosol direct radiative forcing, Atmospheric Chemistry and Physics, 4, 183-214, 2004.

McMahon, G., H. F. Saint-Cyr, C. Lechene and C. J. Unkefer: CN^- secondary ions form by recombination as demonstrated using multi-isotope mass spectrometry of ^{13}C- and ^{15}N-Labeled Polyglycine, Journal of the American Society for Mass Spectrometry, 17, 8, 1181-1187, 2006.

Menon, S., K. L. Denman, G. Brasseur, A. Chidthaisong, P. Ciais, P. M. Cox, R. E. Dickinson, D. Hauglustaine, C. Heinze and E. Holland. Couplings between changes in the climate system and biogeochemistry, Ernest Orlando Lawrence Berkeley National Laboratory, Berkeley, CA (US). 2007.

Milford, J. B. and C. I. Davidson: The Sizes of Particulate Sulfate and Nitrate in the Atmosphere - a Review, Japca-the International Journal of Air Pollution Control and Hazardous Waste Management, 37, 2, 125-134, 1987.

Moore, H.: The isotopic composition of ammonia, nitrogen dioxide and nitrate in the atmosphere, Atmospheric Environment (1967), 11, 12, 1239-1243, 1977.

Mostefaoui, S., A. El Goresy, P. Hoppe, P. Gillet and U. Ott: Mode of occurrence, textural settings and nitrogen-isotopic compositions of in situ diamonds and other carbon phases in the Bencubbin meteorite, Earth and Planetary Science Letters, 204, 1-2, 89-100, 2002.

Mostefaoui, S., E. Zinner, P. Hoppe, F. J. Stadermann and A. El Goresy: In situ survey of graphite in unequilibrated chondrites: Morphologies, C, N, O, and H isotopic ratios, Meteoritics & Planetary Science, 40, 5, 721-743, 2005.

Murphy, S. M., A. Sorooshian, J. H. Kroll, N. L. Ng, P. Chhabra, C. Tong, J. D. Surratt, E. Knipping, R. C. Flagan and J. H. Seinfeld: Secondary aerosol formation from atmospheric reactions of aliphatic amines, Atmospheric Chemistry and Physics, 7, 9, 2313-2337, 2007.

Musat, N., H. Halm, B. Winterholler, P. Hoppe, S. Peduzzi, F. Hillion, F. Horreard, R. Amann, B. B. Jørgensen and M. M. M. Kuypers: A single-cell view on the ecophysiology of anaerobic phototrophic bacteria, Proceedings of the National Academy of Sciences of the United States of America, 105, 46, 17861-17866, 2008.

National Research Council (U.S.). Committee on Tropospheric Ozone Formation and Measurement. Rethinking the ozone problem in urban and regional air pollution. Washington, D.C., National Academy Press. 1991.

Neff, J. C., E. A. Holland, F. J. Dentener, W. H. McDowell and K. M. Russell: The origin, composition and rates of organic nitrogen deposition: A missing piece of the nitrogen cycle?, Biogeochemistry, 57, 1, 99-136, 2002.

Nguyen, T. B., J. Laskin, A. Laskin and S. A. Nizkorodov: Nitrogen-Containing Organic Compounds and Oligomers in Secondary Organic Aerosol Formed by Photooxidation of Isoprene, Environmental Science & Technology, 45, 16, 6908-6918, 2011.

Ollinger, S. V., J. D. Aber, P. B. Reich and R. J. Freuder: Interactive effects of nitrogen deposition, tropospheric ozone, elevated CO_2 and land use history on the carbon dynamics of northern hardwood forests, Global Change Biology, 8, 6, 545-562, 2002.

Pearson, J., D. M. Wells, K. J. Seller, A. Bennett, A. Soares, J. Woodall and M. J. Ingrouille: Traffic exposure increases natural N-15 and heavy metal concentrations in mosses, New Phytologist, 147, 2, 317-326, 2000.

Peterson, R. E., A. Nair, S. Dambach, H. F. Arlinghaus and B. J. Tyler: Characterization of individual atmospheric aerosol particles with SIMS and laser-SNMS, Applied Surface Science, 252, 19, 7006-7009, 2006.

Peterson, R. E. and B. J. Tyler: Analysis of organic and inorganic species on the surface of atmospheric aerosol using time-of-flight secondary ion mass spectrometry (TOF-SIMS), Atmospheric Environment, 36, 39-40, 6041-6049, 2002.

Peterson, R. E. and B. J. Tyler: Surface composition of atmospheric aerosol: individual particle characterization by TOF-SIMS, Applied Surface Science, 203, 751-756, 2003.

Pio, C. A. and R. M. Harrison: The Equilibrium of Ammonium-Chloride Aerosol with Gaseous Hydrochloric-Acid and Ammonia under Tropospheric Conditions, Atmospheric Environment, 21, 5, 1243-1246, 1987.

Pöhlker, C., J. Saturno, M. L. Kruger, J. D. Forster, M. Weigand, K. T. Wiedemann, M. Bechtel, P. Artaxo and M. O. Andreae: Efflorescence upon humidification? X-ray microspectroscopic in situ observation of changes in aerosol microstructure and phase state upon hydration, Geophysical Research Letters, 41, 10, 3681-3689, 2014.

Pöhlker, C., K. T. Wiedemann, B. Sinha, M. Shiraiwa, S. S. Gunthe, M. Smith, H. Su, P. Artaxo, Q. Chen, Y. F. Cheng, W. Elbert, M. K. Gilles, A. L. D. Kilcoyne, R. C. Moffet, M. Weigand, S. T. Martin, U. Poeschl and M. O. Andreae: Biogenic Potassium Salt Particles as Seeds for Secondary Organic Aerosol in the Amazon, Science, 337, 6098, 1075-1078, 2012.

Popa, R., P. K. Weber, J. Pett-Ridge, J. A. Finzi, S. J. Fallon, I. D. Hutcheon, K. H. Nealson and D. G. Capone: Carbon and nitrogen fixation and metabolite exchange in and between individual cells of Anabaena oscillarioides, Isme Journal, 1, 4, 354-360, 2007.

Postgate, J. R. Nitrogen fixation. Cambridge, U.K. ; New York, NY, USA, Cambridge University Press. 1998.

Prather, M. J.: Lifetimes of atmospheric species: Integrating environmental impacts, Geophysical Research Letters, 29, 22, 20-23, 2002.

Richet, P., Y. Bottinga and M. Javoy: Review of Hydrogen, Carbon, Nitrogen, Oxygen, Sulfur, and Chlorine Stable Isotope Fractionation among Gaseous Molecules, Annual Review of Earth and Planetary Sciences, 5, 65-110, 1977.

Rollins, A. W., E. C. Browne, K. E. Min, S. E. Pusede, P. J. Wooldridge, D. R. Gentner, A. H. Goldstein, S. Liu, D. A. Day, L. M. Russell and R. C. Cohen: Evidence for NO_x Control over Nighttime SOA Formation, Science, 337, 6099, 1210-1212, 2012.

Saul, T. D., M. P. Tolocka and M. V. Johnston: Reactive uptake of nitric acid onto sodium chloride aerosols across a wide range of relative humidities, Journal of Physical Chemistry A, 110, 24, 7614-7620, 2006.

Savoie, D. L. and J. M. Prospero: Particle-Size Distribution of Nitrate and Sulfate in the Marine Atmosphere, Geophysical Research Letters, 9, 10, 1207-1210, 1982.

Scalen, R. S.: The Isotopic Composition, Concentration and ChemicalState of the Nitrogen in IgneousRocks, 1959.

Schaap, M., M. van Loon, H. M. ten Brink, F. J. Dentener and P. J. H. Builtjes: Secondary inorganic aerosol simulations for Europe with special attention to nitrate, Atmospheric Chemistry and Physics, 4, 2004.

Seinfeld, J. H. and S. N. Pandis. Atmospheric chemistry and physics: from air pollution to climate change, John Wiley & Sons. 2012.

Sigman, D. M., K. L. Casciotti, M. Andreani, C. Barford, M. Galanter and J. K. Bohlke: A bacterial method for the nitrogen isotopic analysis of nitrate in seawater and freshwater, Analytical Chemistry, 73, 17, 4145-4153, 2001.

Slodzian, G., M. Chaintreau, R. Dennebouy and A. Rousse: Precise in situ measurements of isotopic abundances with pulse counting of sputtered ions, European Physical Journal-Applied Physics, 14, 3, 199-231, 2001.

Smith, J. N., K. C. Barsanti, H. R. Friedli, M. Ehn, M. Kulmala, D. R. Collins, J. H. Scheckman, B. J. Williams and P. H. McMurry: Observations of aminium salts in atmospheric nanoparticles and possible climatic implications, Proceedings of the National Academy of Sciences of the United States of America, 107, 15, 6634-6639, 2010.

Smith, M. L., A. K. Bertram and S. T. Martin: Deliquescence, efflorescence, and phase miscibility of mixed particles of ammonium sulfate and isoprene-derived secondary organic material, Atmospheric Chemistry and Physics, 12, 20, 9613-9628, 2012.

Sofen, E. D., B. Alexander, E. J. Steig, M. H. Thiemens, S. A. Kunasek, H. M. Amos, A. J. Schauer, M. G. Hastings, J. Bautista, T. L. Jackson, L. E. Vogel, J. R. McConnell, D. R. Pasteris and E. S. Saltzman: WAIS Divide ice core suggests sustained changes in the atmospheric formation pathways of sulfate and nitrate since the 19th century in the extratropical Southern Hemisphere, Atmospheric Chemistry and Physics, 14, 11, 5749-5769, 2014.

Solomon, S., Intergovernmental Panel on Climate Change and Intergovernmental Panel on Climate Change. Working Group I. Climate change 2007: the physical science basis: contribution of Working Group I to the Fourth Assessment Report of the Intergovernmental Panel on Climate Change. Cambridge; New York, Cambridge University Press. 2007.

Spindel, W.: The calculation of equilibrium constants for several exchange reactions of nitrogen-15 between oxy compounds of nitrogen, The Journal of Chemical Physics, 22, 7, 1271-1272, 1954.

Stelson, A. W., S. K. Friedlander and J. H. Seinfeld: Note on the Equilibrium Relationship between Ammonia and Nitric-Acid and Particulate Ammonium-Nitrate, Atmospheric Environment, 13, 3, 369-371, 1979.

Stelson, A. W. and J. H. Seinfeld: Thermodynamic Prediction of the Water Activity, NH_4NO_3 Dissociation-Constant, Density and Refractive-Index for the NH_4NO_3-$(NH_4)_2SO_4$-H_2O System at 25°C, Atmospheric Environment, 16, 10, 2507-2514, 1982.

Stern, M. J., L. N. Kauder and W. Spindel: Temperature dependence of the isotopic fractionation of nitrogen in the NO-NO-3 system, The Journal of Chemical Physics, 34, 1, 333-334, 1961.

Stocker, T., D. Qin, G. Plattner, M. Tignor, S. Allen, J. Boschung, A. Nauels, Y. Xia, V. Bex and P. Midgley. Climate Change 2013: The Physical Science Basis. Summary for Policymakers. Contribution of Working Group I to the Fifth Assessment Report of the Intergovernmental Panel on Climate Change. 27 p, Cambridge University Press, Cambridge, 2013.

Sutton, M. A., C. M. Howard, J. W. Erisman, G. Billen, A. Bleeker, P. Grennfelt, H. van Grinsven and B. Grizzetti. The European nitrogen assessment: sources, effects and policy perspectives. Cambridge, UK; New York, Cambridge University Press. 2011.

Tang, I. N. and H. R. Munkelwitz: Water Activities, Densities, and Refractive-Indexes of Aqueous Sulfates and Sodium-Nitrate Droplets of Atmospheric Importance, Journal of Geophysical Research-Atmospheres, 99, D9, 18801-18808, 1994.

Thomen, A., F. Robert and L. Remusat: Determination of the nitrogen abundance in organic materials by NanoSIMS quantitative imaging, Journal of Analytical Atomic Spectrometry, 29, 3, 512-519, 2014.

Turekian, V. C., S. M. , Donna Ballentine, Robert J. Swap, and M. Garstang: Causes of bulk carbon and nitrogen isotopic fractionations in the products of vegetation burns laboratory studies, Chemical Geology, 152, 12, 1998.

Urey, H. C.: The Thermodynamic Properties of Isotopic Substances, Journal of the Chemical SocietyMay, 562-581, 1947.

Van Dorland, R., F. J. Dentener and J. Lelieveld: Radiative forcing due to tropospheric ozone and sulfate aerosols, Journal of Geophysical Research-Atmospheres, 102, D23, 28079-28100, 1997.

Van Ham, R., A. Adriaens, L. Van Vaeck and F. Adams: TOF-SIMS, a new versatile technique for the analysis of environmental aerosols?, Journal of aerosol science, 31, 396-397, 2000.

Van Hardeveld, R. M., R. A. Van Santen and J. W. Niemantsverdriet: C-N coupling in reactions between atomic nitrogen and ethylene on Rh(III), Journal of Physical Chemistry B, 101, 40, 7901-7907, 1997.

Van Stipdonk, M. J., D. R. Justes, C. M. Force and E. A. Schweikert: Speciation of sodium nitrate and sodium nitrite using kiloelectronvolt energy atomic and polyatomic and megaelectronvolt energy atomic projectiles with secondary ion mass spectrometry, Analytical Chemistry, 72, 11, 2468-2474, 2000.

Van Zuilen, M. A., M. Chaussidon, C. Rollion-Bard and B. Marty: Carbonaceous cherts of the Barberton Greenstone Belt, South Africa: Isotopic, chemical and structural characteristics of individual microstructures, Geochimica et Cosmochimica Acta, 71, 3, 655-669, 2007.

Veefkind, J. P., J. C. H. vanderHage and H. M. tenBrink: Nephelometer derived and directly measured aerosol optical depth of the atmospheric boundary layer, Atmospheric Research, 41, 3-4, 217-228, 1996.

Verstraete, W. and D. Focht. Biochemical ecology of nitrification and denitrification. Advances in microbial ecology, Springer: 135-214. 1977.

Vitousek, P. M. Nutrient cycling and limitation: Hawai'i as a model system, Princeton University Press. 2004.

Wada, E. and A. Hattori. Nitrogen in the sea: forms, abundance, and rate processes, CRC press. 1990.

Wada, G., R. C. Aragones and H. Ando: Effect of Slow Release Fertilizer (Meister) on the Nitrogen Uptake and Yield of the Rice Plant in the Tropics, Japanese Journal of Crop Science, 60, 1, 101-106, 1991.

Wankel, S. D., Y. Chen, C. Kendall, A. F. Post and A. Paytan: Sources of aerosol nitrate to the Gulf of Aqaba: Evidence from $\delta^{15}N$ and $\delta^{18}O$ of nitrate and trace metal chemistry, Marine Chemistry, 120, 1-4, 90-99, 2010.

Widory, D.: Nitrogen isotopes: Tracers of origin and processes affecting PM_{10} in the atmosphere of Paris, Atmospheric Environment, 41, 11, 2382-2390, 2007.

Winterholler, B., P. Hoppe, M. O. Andreae and S. Foley: Measurement of sulfur isotope ratios in micrometer-sized samples by NanoSIMS, Applied Surface Science, 252, 19, 7128-7131, 2006.

Winterholler, B., P. Hoppe, S. Foley and M. O. Andreae: Sulfur isotope ratio measurements of individual sulfate particles by NanoSIMS, International Journal of Mass Spectrometry, 272, 1, 63-77, 2008.

Wittmaack, K.: A Unified Explanation for Secondary-Ion Yields and Mechanism of the Sims Matrix Effect - Comment, Journal of Applied Physics, 52, 1, 527-529, 1981.

Wolff, G. T.: On the Nature of Nitrate in Coarse Continental Aerosols, Atmospheric Environment, 18, 5, 977-981, 1984.

Xiao, H.-W., H.-Y. Xiao, A.-m. Long and Y.-L. Wang: Who controls the monthly variations of NH_4^+ nitrogen isotope composition in precipitation?, Atmospheric Environment, 54, 201-206, 2012.

Yeatman, S. G., L. J. Spokes, P. F. Dennis and T. D. Jickells: Comparisons of aerosol nitrogen isotopic composition at two polluted coastal sites, Atmospheric Environment, 35, 14, 2001.

Zaehle, S., P. Ciais, A. D. Friend and V. Prieur: Carbon benefits of anthropogenic reactive nitrogen offset by nitrous oxide emissions, Nature Geoscience, 4, 9, 601-605, 2011.

Zarzana, K. J., D. O. De Haan, M. A. Freedman, C. A. Hasenkopf and M. A. Tolbert: Optical Properties of the Products of alpha-Dicarbonyl and Amine Reactions in Simulated Cloud Droplets, Environmental Science & Technology, 46, 9, 4845-4851, 2012.

Zhuang, H., C. K. Chan, M. Fang and A. S. Wexler: Formation of nitrate and non-sea-salt sulfate on coarse particles, Atmospheric Environment, 33, 26, 4223-4233, 1999.

Zinner, E., T. Ming and E. Anders: Interstellar Sic in the Murchison and Murray Meteorites - Isotopic Composition of Ne, Xe, Si, C, and N, Geochimica Et Cosmochimica Acta, 53, 12, 3273-3290, 1989.

Appendix

A Programming work based on MATLAB

In this study, three programs were written based on MATLAB language to help data processing. The code of program 'Calculation of molecule masses program' is given in section A.1 Section A.2 and A.3 give brief introductions of NanoSIMS isotope mode and image mode data processing programs, respectively, which were written from September 2012 to October 2014, based on the NanoSIMS data processing software written in the IDL language created by the NAMIP group at MPIC. The total amount of code of the three programs, except comments and blank lines, is about 12,000 lines.

A.1 Calculation of molecule masses program

This program is used to calculate all possible molecular ions combined from the chart of nuclides that could potentially interfere with a given mass of interest at a certain mass resolving power. The masses of isotopes in this program are according to Atomic Mass Evaluation (Audi et al., 2014). Program code is shown here and Table A-1 gives an example of all possible molecule masses around $^{15}N^{16}O_2^-$ in a range of 46.98994 ± 0.0005 amu.

```
function IsotopeCombinationCal()

%==========================================================================
%   IsotopeCombinationCal function.
%
%   Input parameters:
%   base_mass is the mass of the reference ion, unit amu.
%   base_mass_str is the label of the reference ion.
%   delta_ gives the range ± delta_ give for searching posibile combinations.
%   isotope database: atmo isotope database.xlsx
%       Audi, G., M. Wang, A. H. Wapstra, F. G. Kondev, M. MacCormick and X. Xu (2014).
%       "The 2012 Atomic Mass Evaluation and the Mass Tables."
%       Nuclear Data Sheets 120: 1-5
%
%   Output:
%   An excel file named by base_mass_str.
%
%   Examples:
%
%   base_mass = 46.98993814; % set 15N 16O2 as the reference mass
%   base_mass_str = 'mass15N16O2';
%   delta_=0.0005; % Give the range of + - 0.0005 amu
%
%   Author: Kexue Li
```

```
%   January 2014
%==========================================================================

% Read isotope database file to MATLAB
[num, txt,raw] = xlsread('atmo isotope database.xlsx');
[m,n]=size(txt);
txt2=txt;
tem_iso='H';
k=1;ki=1;kii=1;
for i=2:m
    tem_mass=txt{i,2};
    tem_comp=txt{i,3};
    content_=find(tem_mass=='(');
    content_comp=find(tem_comp=='(');
    isotope_=txt{i,1};
    if ~isempty(content_)
        txt2(i,2)={tem_mass(1:content_-1)};
    end
    if ~isempty(content_comp)
        txt2(i,3)={tem_comp(1:content_comp-1)};
    elseif ~isempty(isotope_)
        txt2(i,3)={'1'};
    end

    if ~isempty(isotope_)
        tem_iso=isotope_;
    end
    % label isotopes, e.g. 1H, 2D, 3T, 4He,....
    txt2(i,1)={[num2str(round(str2num(txt2{i,2}))),tem_iso]};
end

% Select the less than 54 mass
txt3=txt2(2:54,1:3);
txt4=cell(53,30);
txt4(:,1:3)=txt3;
for j=2:10
    for jj=1:53
        txt4(jj,j*3-2)={[txt3{jj,1},num2str(j)]};
        txt4(jj,j*3-1)={str2num(txt3{jj,2})*j};
        txt4(jj,j*3)={str2num(txt3{jj,3})*str2num(txt3{jj,3})};
    end
end
for jjj=1:53
    txt4(jjj,2)={str2num(txt3{jjj,2})};
    txt4(jjj,3)={str2num(txt3{jjj,3})};
end

% Select mass 15N 16O2 as the reference mass
%%%%%%%%%%%%%%%%%%%%%%%%%%%%%%%%%%%%%%%%%%%%%%%%%%%%%%%%%%%%%%%%%%%%%%%
mass15n16o2 = txt4{13,2}+txt4{14,5};
mass14n16o2 = txt4{12,2}+txt4{14,5};
base_mass = mass15n16o2; % set 15N 16O2 as the reference mass
base_mass_str = 'mass15N16O2';
delta_=0.0005; % Give the range of searching + - 0.0005 amu
%%%%%%%%%%%%%%%%%%%%%%%%%%%%%%%%%%%%%%%%%%%%%%%%%%%%%%%%%%%%%%%%%%%%%%%

% main search body
for ii=1:10-1
    for ij=1:53-1
        mass1=txt4{ij,ii*3-1};
```

```
        if mass1<=base_mass
            for iii=1:10
                for iji=ij+1:53
                    mass2=txt4{iji,iii*3-1};
                    summass=mass1+mass2;
                    if summass <=delta_+base_mass;
                        absmass=summass-base_mass;
                        if abs(absmass)<=delta_
                            comp=txt4{ij,ii*3}*txt4{iji,iii*3};
                            result_str(k,:)=[{[txt4{ij,ii*3-2},' ',...
                                txt4{iji,iii*3-2}]},{summass},{absmass},{comp}];
                            k=k+1;
                        end
                        for iiii=1:10
                            for ijii=iji+1:53
                                mass3=txt4{ijii,iiii*3-1};
                                summass2=mass1+mass2+mass3;
                                if summass2 <=delta_+base_mass;
                                    absmass2=summass2-base_mass;
                                    if abs(absmass2)<=delta_
                                        % calculation relative composition
                                        comp=txt4{ij,ii*3}*txt4{iji,iii*3}*txt4{ijii,iiii*3};
                                        result_str2(ki,:)=[{[txt4{ij,ii*3-2},' ',...
                                            txt4{iji,iii*3-2},' ',txt4{ijii,iiii*3-2}]},...
                                            {summass2},{absmass2},{comp}];
                                        ki=ki+1;
                                    end
                                    for iiiii=1:10
                                        for ijiii=iji+1:53
                                            mass4=txt4{ijiii,iiiii*3-1};
                                            summass3=mass1+mass2+mass3+mass4;
                                            if summass2 <=delta_+base_mass;
                                                absmass3=summass3-base_mass;
                                                if abs(absmass3)<=delta_
                                                    comp1 = txt4{ij,ii*3};
                                                    comp2 = txt4{iji,iii*3};
                                                    comp3 = txt4{ijii,iiii*3};
                                                    comp4 = txt4{ijiii,iiiii*3};
                                                    comp=comp1*comp2*comp3*comp4;
                                                    result_str3(kii,:)=[{[txt4{ij,ii*3-2},...
                                                        ' ',txt4{iji,iii*3-2},...
                                                        ' ',txt4{ijii,iiii*3-2},' ',...
                                                        txt4{ijiii,iiiii*3-2}]},...
                                                        {summass3},{absmass3},{comp}];
                                                    kii=kii+1;
                                                end
                                            end
                                        end
                                    end
                                end
                            end
                        end
                    end
                end
            end
        end
    end
end

titlecell=[{'ion name'},{'mass(amu)'},{['delta with-',base_mass_str]},{'composition'}];
```

APPENDIX A

```
% write final results to a excel file
xlswrite(['allresults','-',base_mass_str],[titlecell;result_str;result_str2;result_str3])
```

Published with MATLAB® R2014a

Table A-1. An example of output results set for $^{15}N^{16}O_2$ as the reference mass in a range of 46.98994 ± 0.0005 amu. Molecular isotope abundances are calculated by multiplying the respective isotope abundances of each element.

Molecular mass	**Mass (amu)**	**Delta mass with $^{15}N^{16}O_2$**	**Isotope abundance**
15N 16O2	46.98994	0.00000	3.62233E-03
12C2 23Na	46.98977	-0.00017	9.78714E-01
1H4 43Ca	46.99007	0.00013	1.34969E-03
2D 13C 32S	46.98953	-0.00041	1.16885E-06
2D 17O 28Si	46.99016	0.00022	4.03015E-08
1H2 3He 42Ca	46.99030	0.00036	8.66781E-09
1H2 15N 30Si	46.98953	-0.00041	1.12523E-04
4He2 15N 24Mg	46.99036	0.00042	2.87523E-03
4He2 16O 23Na	46.98989	-0.00005	9.97567E-01
1H3 4He 40K	46.99008	0.00014	1.16973E-04
1H 3He 4He 39K	46.99016	0.00023	1.24951E-06
1H 3He 39K 4He	46.99016	0.00023	1.24951E-06
1H 4He 13C 29Si	46.99028	0.00034	5.01237E-04
1H 4He 14N 28Si	46.99043	0.00049	9.18766E-01
1H 4He 28Si 14N	46.99043	0.00049	9.18766E-01
1H 4He 29Si 13C	46.99028	0.00034	5.01237E-04

A.2 Isotope mode NanoSIMS data processing program

A.2.1 Program interfaces and operations

Data from isotope analysis were transferred to a database including NanoSIMS parameters shown in 'Analysis conditions' and 'Measurements' areas in Figure A-1. In this study, each analysis contains a certain number of measurements. And each measurement has its own parameters, e.g. primary current. The function "Search system" is used to find those analyses which have certain selected parameter values and to show them in the 'Analysis' list. All measurements in this particular analysis are shown in the 'Measurements' list. By selecting one 'analysis', the data and calculation results are shown in the 'Chart' part. The upper part of the chart shows the cps (counts per second) data, with the reference mass cps and total cps shown as yellow and green bars, respectively. Pink rectangles are the primary ion dose per square micrometer. RPS and ATPS are the averaged value of reference mass cps (red line) and total cps, respectively. Isotope data and calculation results are shown in the lower part of the chart. Each dot with error bar (1σ) is the result of one spot measurement. If the sample is a standard with known nitrogen isotope composition, the chart will give IMF results with error of the mean, spot to spot reproducibility, chi square and so on.

The advanced searching interface in Figure A-2 allows analysis data to be separated into different groups according to different parameters. 15 different parameters can be selected simultaneously. E.g. three groups were created for three different standards with 2×2 um^2 raster size in session 'EXP-8'.

Calculations can be controlled by the 'Create Chart' list (Figure A-3):

- 'Create Chart' option is used to plot a bar graph (see Figure A-4) to show isotope composition or IMF in a certain group. Single spot measurement results are shown with 1 σ error bars.
- 'Export Group Data' is used to export NanoSIMS data and calculation results to an Excel file. There are three sheets in this file. First sheet presents analysis information, including the main settings of the NanoSIMS (see Figure A-5 A). The second sheet presents the summary data of each analysis (see Figure A-5 B) and the last sheet contains all data of spot measurements.

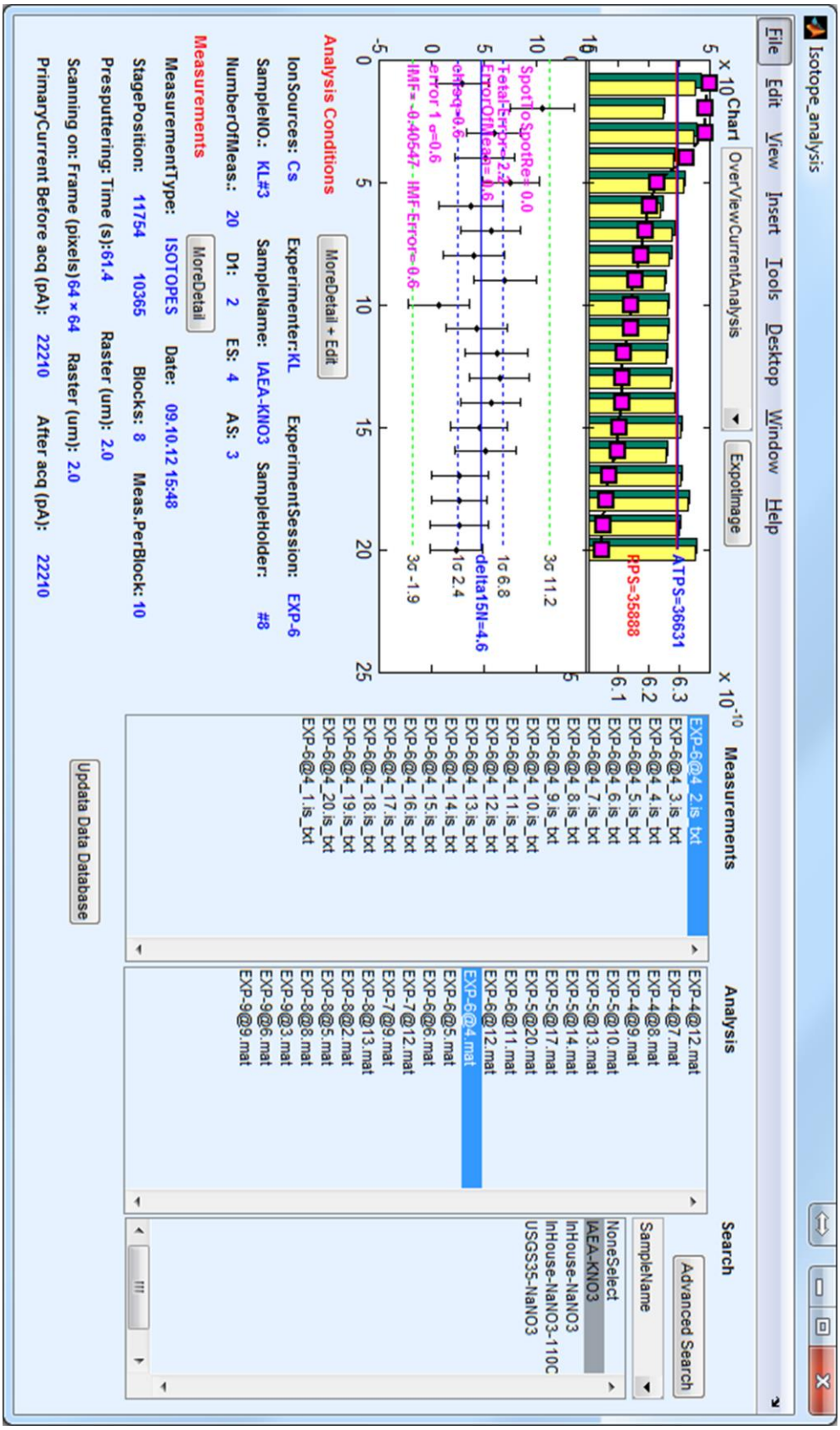

Figure A-1. The main interface of the isotope mode NanoSIMS data processing program.

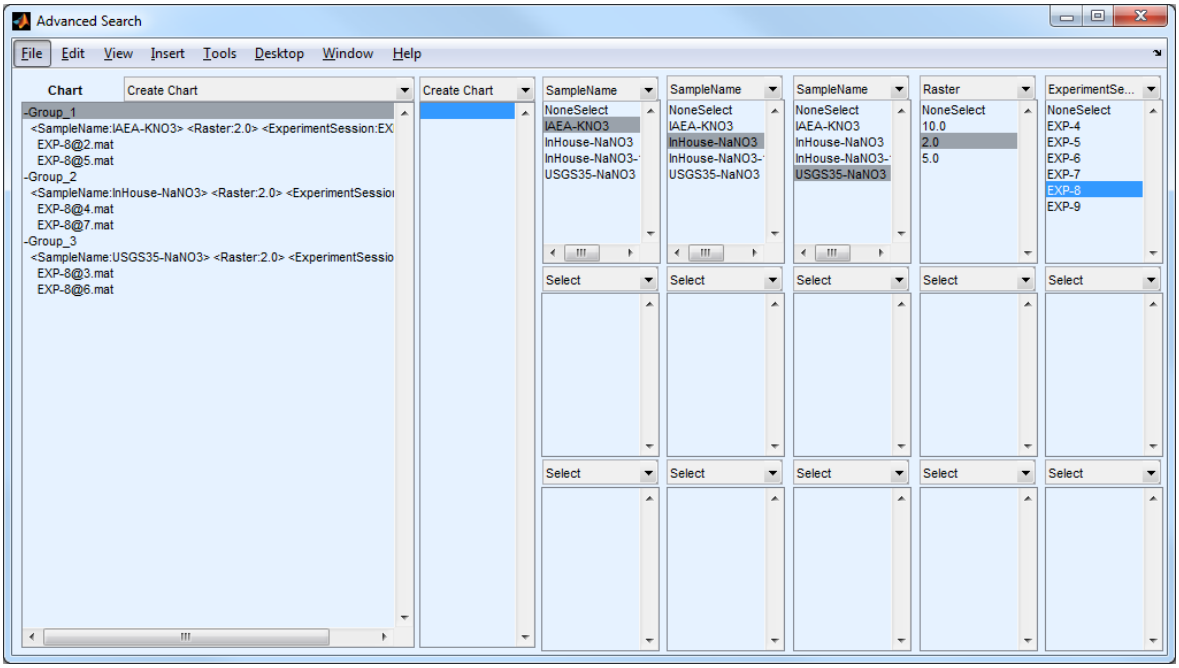

Figure A-2. Advanced searching interface.

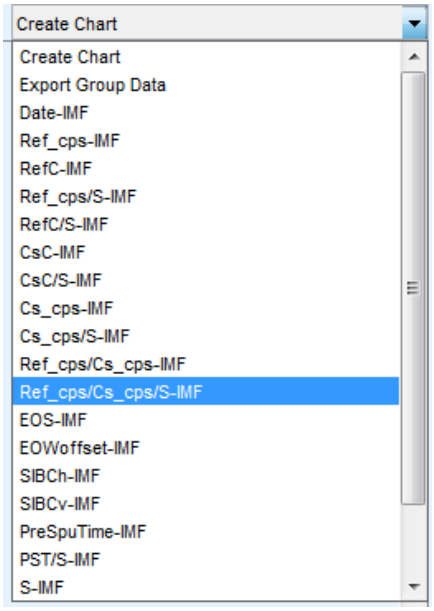

Figure A-3. Create chart list. Option 'Export Group Data' is used to export results to an Excel file, and other options are used to calculate and create the chart.

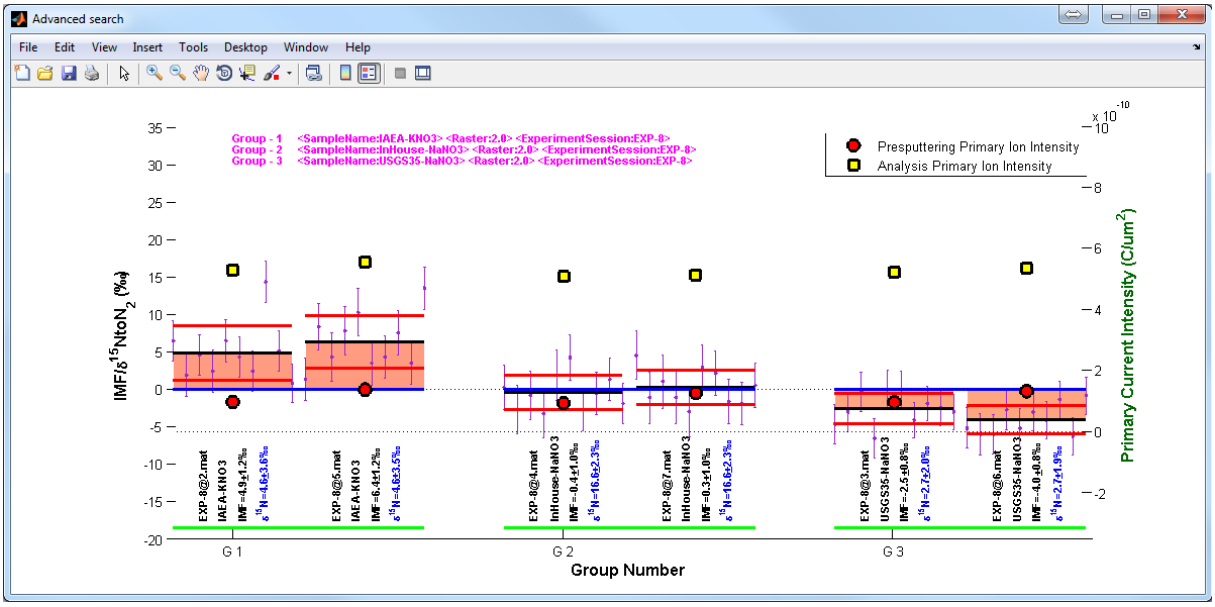

Figure A-4. Exported chart by option ‘Create chart’ with the settings in Figure A-2.

- The other options are used to plot IMF against other quantities which are summarized in Table A-2. Figure A-6 shows one example created by ‘Ref mass cps/Cs ion cps.

The auto IMF correction program is used to edit in-house samples and their isotopic standards to different correction groups according the analysis conditions. Then isotope ratios of in-house samples are corrected for IMF calculated from the standards in each group. R_n marks the reference standard where n connected by ‘_’ is the group number. Single letter n marks the sample in this correction group. Then the program corrects isotope compositions of samples using the calculated IMF of the standards. Figure A-7 shows one example of IMF correction. All corrected data and results can be exported to an Excel file in the form as shown in Figure A-4, as well.

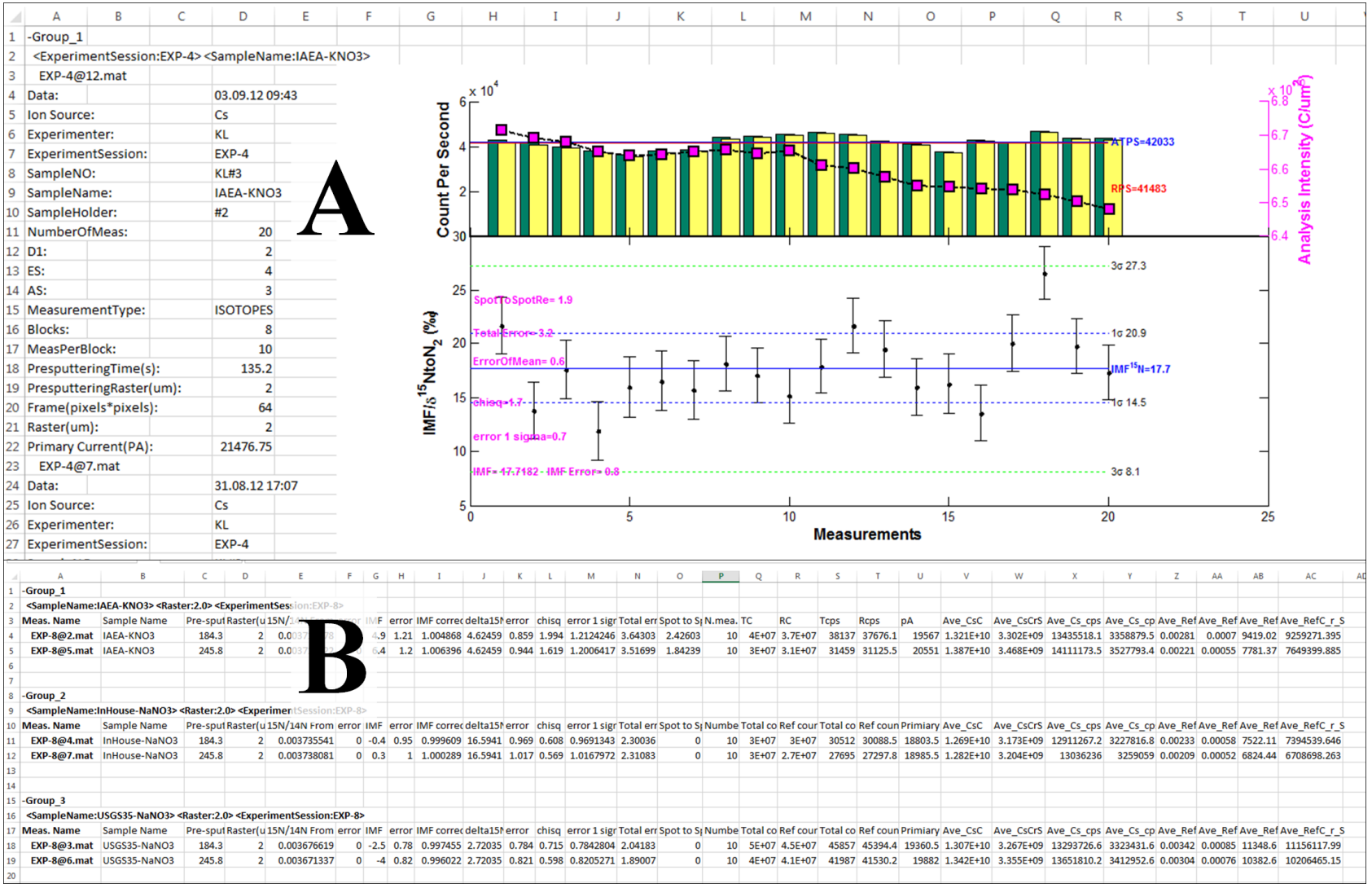

	A	B	C	D	E
1	-Group_1				
2	<ExperimentSession:EXP-4> <SampleName:IAEA-KNO3>				
3	EXP-4@12.mat				
4	Data:			03.09.12 09:43	
5	Ion Source:			Cs	
6	Experimenter:			KL	
7	ExperimentSession:			EXP-4	
8	SampleNO:			KL#3	
9	SampleName:			IAEA-KNO3	
10	SampleHolder:			#2	
11	NumberOfMeas:			20	
12	D1:			2	
13	ES:			4	
14	AS:			3	
15	MeasurementType:			ISOTOPES	
16	Blocks:			8	
17	MeasPerBlock:			10	
18	PresputteringTime(s):			135.2	
19	PresputteringRaster(um):			2	
20	Frame(pixels*pixels):			64	
21	Raster(um):			2	
22	Primary Current(PA):			21476.75	
23	EXP-4@7.mat				
24	Data:			31.08.12 17:07	
25	Ion Source:			Cs	
26	Experimenter:			KL	
27	ExperimentSession:			EXP-4	

	A	B	C	D	E	F	G	H	I	J	K	L	M	N	O	P	Q	R	S	T	U	V	W	X	Y	Z	AA	AB	AC
1	-Group_1																												
2	<SampleName:IAEA-KNO3> <Raster:2.0> <ExperimentSes																												
3	Meas. Name	Sample Name	Pre-sput	Raster(u	15N/		IMF	error	IMF correc	delta15N	error	chisq	error 1 sigr	Total err	Spot to S	N.mea.	TC	RC	Tcps	Rcps	pA	Ave_CsC	Ave_CsCrS	Ave_Cs_cps	Ave_Cs_cp	Ave_Ref	Ave_Ref	Ave_Ref	Ave_RefC_r_S
4	EXP-8@2.mat	IAEA-KNO3	184.3	2	0.0		4.9	1.21	1.004868	4.62459	0.859	1.994	1.2124246	3.64303	2.42603	10	4E+07	3.7E+07	38137	37676.1	19567	1.321E+10	3.302E+09	13435518.1	3358879.5	0.00281	0.0007	9419.02	9259271.395
5	EXP-8@5.mat	IAEA-KNO3	245.8	2	0.0		6.4	1.2	1.006396	4.62459	0.944	1.619	1.2006417	3.51699	1.84239	10	3E+07	3.1E+07	31459	31125.5	20551	1.387E+10	3.468E+09	14111173.5	3527793.4	0.00221	0.00055	7781.37	7649399.885
6																													
7																													
8	-Group_2																												
9	<SampleName:InHouse-NaNO3> <Raster:2.0> <Experimen																												
10	Meas. Name	Sample Name	Pre-sput	Raster(u	15N/14N From		error	IMF	error	IMF correc	delta15N	error	chisq	error 1 sigr	Total err	Spot to S	Numbe	Total co	Ref coun	Total co	Ref coun	Primiary	Ave_CsC	Ave_CsCrS	Ave_Cs_cps	Ave_Cs_cp	Ave_Ref	Ave_Ref	Ave_Ref	Ave_RefC_r_S
11	EXP-8@4.mat	InHouse-NaNO3	184.3	2	0.003735541		0	-0.4	0.95	0.999609	16.5941	0.969	0.608	0.9691343	2.30036	0	10	3E+07	3E+07	30512	30088.5	18803.5	1.269E+10	3.173E+09	12911267.2	3227816.8	0.00233	0.00058	7522.11	7394539.646
12	EXP-8@7.mat	InHouse-NaNO3	245.8	2	0.003738081		0	0.3	1	1.000289	16.5941	1.017	0.569	1.0167972	2.31083	0	10	3E+07	2.7E+07	27695	27297.8	18985.5	1.282E+10	3.204E+09	13036236	3259059	0.00209	0.00052	6824.44	6708698.263
13																													
14																													
15	-Group_3																												
16	<SampleName:USGS35-NaNO3> <Raster:2.0> <ExperimentSession:EXP-8>																												
17	Meas. Name	Sample Name	Pre-sput	Raster(u	15N/14N From		error	IMF	error	IMF correc	delta15N	error	chisq	error 1 sigr	Total err	Spot to S	Numbe	Total co	Ref coun	Total co	Ref coun	Primiary	Ave_CsC	Ave_CsCrS	Ave_Cs_cps	Ave_Cs_cp	Ave_Ref	Ave_Ref	Ave_Ref	Ave_RefC_r_S
18	EXP-8@3.mat	USGS35-NaNO3	184.3	2	0.003676619		0	-2.5	0.78	0.997455	2.72035	0.784	0.715	0.7842804	2.04183	0	10	5E+07	4.5E+07	45857	45394.4	19360.5	1.307E+10	3.267E+09	13293726.6	3323431.6	0.00342	0.00085	11348.6	11156117.99
19	EXP-8@6.mat	USGS35-NaNO3	245.8	2	0.003671337		0	-4	0.82	0.996022	2.72035	0.821	0.598	0.8205271	1.89007	0	10	4E+07	4.1E+07	41987	41530.2	19882	1.342E+10	3.355E+09	13651810.2	3412952.6	0.00304	0.00076	10382.6	10206465.15
20																													

Figure A-5. An example of export data in Excel file. A: analysis information. B: Analysis data and results.

Table A-2. Option name with the description of x-axis in 'Create Chart' list. * means the option can only be used if the mass settings contain $^{14}N^{16}O_2^-$ and $^{15}N^{16}O_2^-$ simultaneously and at least one of $^{12}C^-$, $^{16}O^-$ and $^{12}C^{14}N^-$.

option name	x-axis
Date-IMF	Experiment date and time
Ref_cps-IMF	Counts per second of reference mass (cps)
RefC-IMF	Total counts of reference mass (cps)
Ref_cps/S-IMF	The ratio of counts per second of reference mass over raster area (cps/μm^2)
RefC/S-IMF	The ratio of total counts of reference mass over raster area (cps/μm^2)
CsC-IMF	Cs^+ primary ion dose
CsC/S-IMF	The ratio of Cs^+ primary ion dose over raster area (Cs^+ dose/μm^2)
Cs_cps-IMF	Cs^+ primary ion dose per second (Cs^+ does/s)
Cs_cps/S-IMF	The ratio of Cs^+ primary ion dose per second over raster area (Cs^+ dose/s/μm^2)
Ref_cps/Cs_cps-IMF	The ratio of counts per second of reference mass over Cs^+ primary ion dose per second (cps/Cs^+ dose/s)
Ref_cps/Cs_cps/S-IMF	The ratio of counts per second of reference mass over Cs^+ primary ion dose per second over raster area (cps/Cs^+ dose/s/μm^2)
EOS-IMF	EOS setting in bits (immersion lens used to extract secondary ions)
EOWoffset-IMF	EOW offset voltage
SIBCh-IMF	Secondary ion beam centering setting in horizontal direction (bit)
SIBCv-IMF	Secondary ion beam centering setting in vertical direction (bit)
PreSpuTime-IMF	Pre-sputtering time (s)
PST/S-IMF	The ratio of pre-sputtering time over raster area (s/μm^2)
S-IMF	Raster area (μm^2)
NO2/(O+NO2)-IMF*	The ratio of secondary ions $^{14}N^{16}O_2^-/(^{16}O^- + ^{14}N^{16}O_2^-)$
NO2/(CN+NO2)-IMF*	The ratio of secondary ions $^{14}N^{16}O_2^-/(^{12}C^{14}N^- + ^{14}N^{16}O_2^-)$
NO2/(C+NO2)-IMF*	The ratio of secondary ions $^{14}N^{16}O_2^-/(^{12}C^- + ^{14}N^{16}O_2^-)$

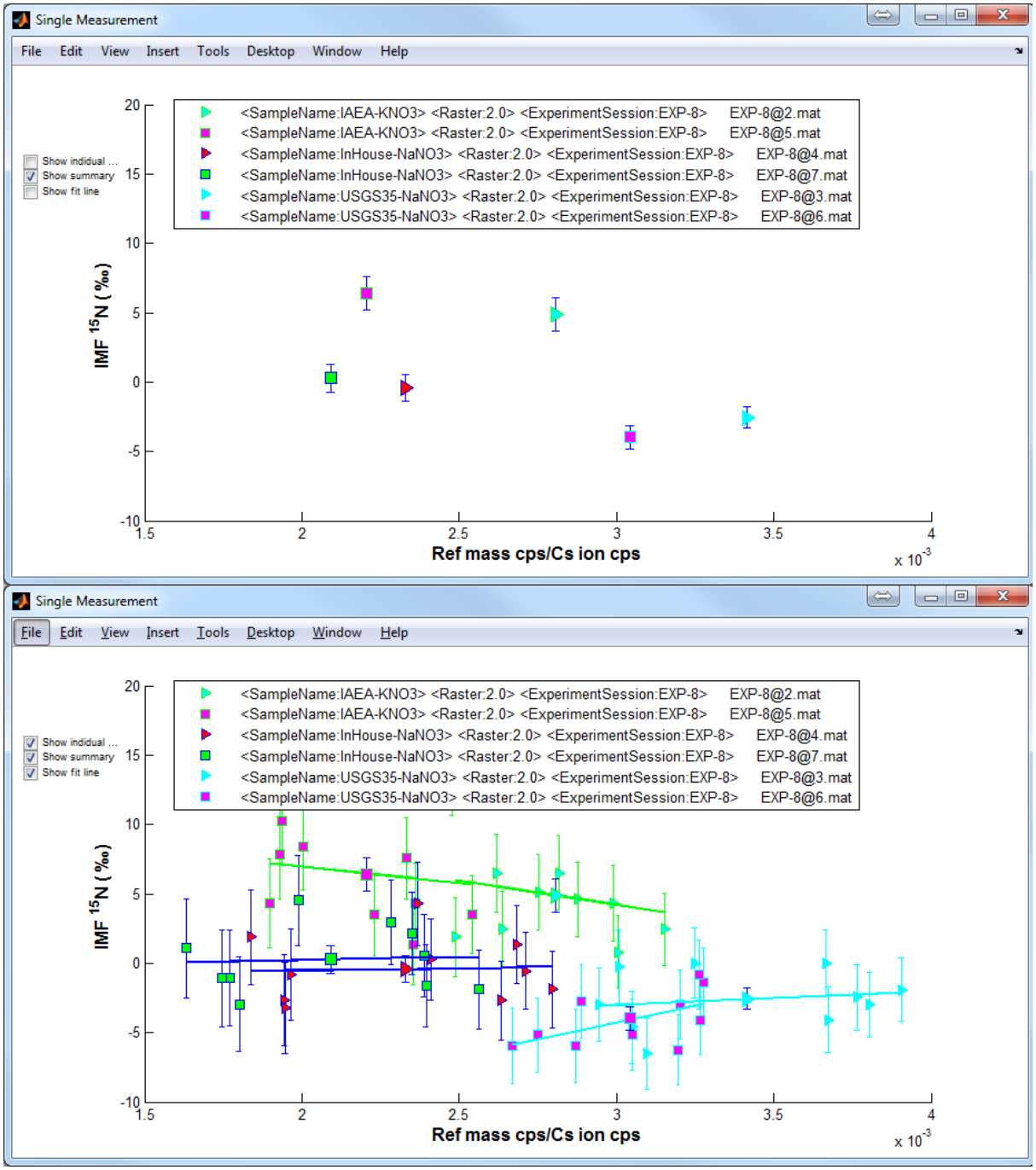

Figure A-6. An example of 'Create Chart' option – 'Ref_cps/Cs_cps-IMF'. X-axis is the ratio of counts per second of reference mass ($^{14}N^{16}O_2^-$) over Cs^+ primary ion dose per second and y-axis is the IMF of three standards. Upper chart shows the averaged results of analysis and the lower chart all measurement spots. Analysis errors are 1σ error of the mean and measurement spot errors are 1σ.

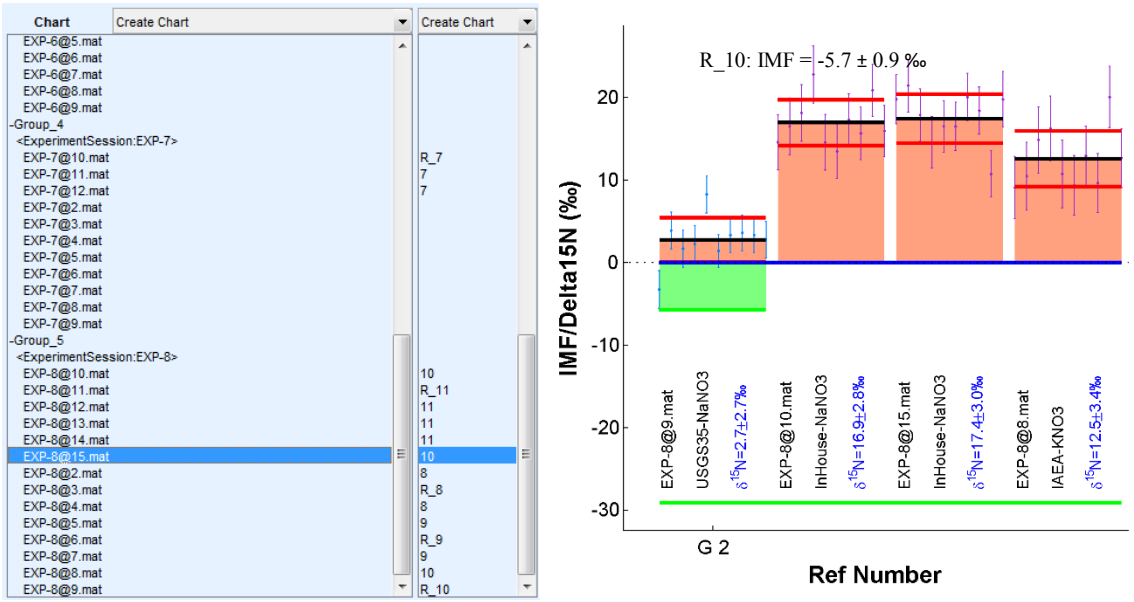

Figure A-7. Example of an auto IMF correction with the standard USGS35 ($NaNO_3$). Left figure shows the user interface to select the settings of IMF correction and right chart the results of group R_10. Analysis name, standard name and true isotope composition ($\delta^{15}N$) are shown below the bars. Green and orange bars represent the IMF of analysis and the true isotope composition, respectively. $\delta^{15}N$ in sample IAEA-KNO_3 is not corrected for the matrix effect between $NaNO_3$ and KNO_3. Errors of analysis are 1 σ error of the mean. Spot measurement errors are 1 σ.

A.2.2Main mathematical calculations

Statistical calculation

In this study the isotope ratio in each spot measurement is given by:

$$R_s = \frac{n(^{15}N)}{n(^{14}N)} \qquad \text{Equation A-1}$$

where n is the number of counts of nitrogen ions and R_s the isotope ratio measured by NanoSIMS. The counting statistical error is $\sqrt{n}$ according to Poisson distribution (Bevington and Robinson 1992, Fitzsimons et al., 2000) and the error of R_s is σ_s:

$$\sigma_s \approx R_s \cdot \sqrt{\frac{1}{n(^{14}N)} + \frac{1}{n(^{15}N)}} \qquad \text{Equation A-2}$$

All average calculations are weighted averages:

$$\overline{R_w} = \frac{\sum_{i=1}^{n} R_i/\sigma_{s,i}^2}{\sum_{i=1}^{n} 1/\sigma_{s,i}^2} \qquad \text{Equation A-3}$$

The error of weighted mean is:

$$\sigma_m = \frac{1}{\sqrt{\sum_{i=1}^{n} 1/\sigma_{s,i}^2}} \qquad \text{Equation A-4}$$

where $\sigma_{s,i}$ is the error of spot measurement i.

Spot to spot reproducibility is calculated by:

$$\sigma_{spot} = \sqrt{STD^2 - N * \sigma_m^2} \quad \text{Equation A-5}$$

$$STD = \sqrt{\frac{1}{n-1}} \sum_{i=1}^{n} \left(R_{s,i} - \overline{R_w}\right)^2 \quad \text{Equation A-6}$$

Chi square calculation:

$$\text{chisq} = \frac{\sum_{i=1}^{n} \left(R_{s,i} - \overline{R_w}\right)^2 \frac{1}{\sigma_{s,i}^2}}{(n-1) s_{\text{m}}^2 \sum_{i=1}^{n} \frac{1}{\sigma_{s,i}^2}} \quad \text{Equation A-7}$$

If chisq >1, the error of analysis will be multiplied by $\sqrt{chisq}$.

The procedures of IMF correction

- Firstly, calculate IMF correction factor:
  - If the data come from a standard, load true isotope ratio from database file:

    $\left({}^{15}N/{}^{14}N\right)_{Standard,true}$

    For the standards used in this study and their isotope compositions see Table 2-1.
  - Calculate the weighted average isotope ratio of all spot measurements for the standard by NanoSIMS analysis:

    $\left({}^{15}N/{}^{14}N\right)_{Standard,NanoSIMS}$
  - Get IMF factor:

    $$\alpha = \frac{\left({}^{15}N/{}^{14}N\right)_{Standard,NanoSIMS}}{\left({}^{15}N/{}^{14}N\right)_{Standard,true}} \quad \text{Equation A-8}$$

    $$IMF = (\alpha - 1) \times 1000\ (‰) \quad \text{Equation A-9}$$

    where, α is the IMF factor.
- Then, in-house sample isotope compositions are corrected by IMF
  - Calculate the weighted average isotope ratio of all spot measurements of in-house sample X:

    $\left({}^{15}N/{}^{14}N\right)_{X,NanoSIMS}$
  - Load true isotope ratio of N_2 in the air from database file:

    $\left({}^{15}N/{}^{14}N\right)_{N_2} = 0.0036533$ (Berglund and Wieser 2011)
  - IMF correction:

$$\delta^{15}N_X = \left(\frac{\left({}^{15}N/{}^{14}N\right)_{X,NanoSIMS}}{\left({}^{15}N/{}^{14}N\right)_{N_2}} \cdot \frac{1}{\alpha} \right) \times 1000\ ‰ \qquad \text{Equation A-10}$$

where $\delta^{15}N_X$ is the isotope composition compared to the air.

Primary ion dose per second calculation

$$A = \frac{I_{0,before} + I_{0,after}}{2} \times I_{Prim,D1-x} \times \frac{1}{e} \qquad \text{Equation A-11}$$

where A is the primary ion dose per second hitting to the sample surface; $I_{0,before}$ and $I_{0,after}$ are the primary currents measured before and after measurement, respectively; $I_{Prim,D1\text{-}x}$, is the primary current reduction factor when aperture D1 was set to x; $e = 1.602 \times 10^{-19}$.

QSA correction

The QSA correction setting can be changed via the program code in the function 'AnalysisesCalculate.m', line 202. It is calculated by:

$$R_{true} = \frac{R_{NanoSIMS}}{1 + \alpha \times K} \qquad \text{Equation A-12}$$

where R_{true} and $R_{NanoSIMS}$ are corrected and measured isotope ratio, respectively. K is the ratio of secondary ions over primary ions (Slodzian et al., 2001). α is the QSA factor and the default value in this program is 0.

A.3 Image mode NanoSIMS data processing program

Complex samples and analysis challenges are discussed in chapters 4 & 5. The heterogeneous mixture of aerosol-like particles causes high matrix differences even in one particle. Because nitrate samples are primary ion beam sensitive, particles are easily sputtered away and the size and composition (the ratio of nitrate salts and glucose in this study) changes plane by plane. Complex isobaric interferences were found for $^{15}N^{16}O_2^-$, i.e. $^{29}Si^{18}O^-$ from silicon wafer and a fatal interference from $^{23}Na^{12}C_2^-$. Sample topography and charging can cause changes of mass resolution power, hence signals $^{15}N^{16}O_2^-$ and $^{12}C^{15}N^-$ are easily interfered by the flank of $^{14}N^{16}O^{17}O^-$ and $^{13}C^{14}N^-$, respectively. For image data obtained by NanoSIMS measurements in complex situations, new types of calculations needed to be explored. E.g. single plane mask calculation at various mask levels and single pixel QSA correction for each plane. Measurement settings and parameters also need to be extracted and considered for data processing, e.g. primary current and aperture settings. This section gives a brief introduction into the image data processing program.

Image data are processed in the following steps:

- Firstly, the data input section reads im files (im: image data storage format in NanoSIMS 50). Im files can come from different NanoSIMS sessions and different file paths. File types can be multi plane im files and also single plane im files. The file organizing section is used to create a database for all im files including file informations, NanoSIMS measurement informations and calculation settings.
- The calculation section recognizes calculation settings according to the im file database, and then performs single im file and auto im files calculations. In single im file calculation, each plane is processed separately, including mask calculation, ratio mask f calculation, secondary ion intensities, isotope ratio calculation and QSA correction. The auto im file calculation is controlled by the calculation settings and each im file can be processed by single im file calculation automatically. In order to separate different types of ambient atmospheric particles in the future, users are allowed to select, calculate and store various separated analysis areas in one image analysis, manually and automatically.
- The data output section is used to store all settings (im file input, calculation and output settings), data results, figures and plots. Users can easily review and recalculate previous calculations. New session data can be added, calculated and compared, as well.
- After each data processing, huge amount of data are stored in Excel files; data filter and data browser permit to get a quick data analysis for further in-depth analysis.

The description of mathematical calculations used in this program are described in section A.2.2.

A.3.1Reading data and initial settings

Figure A-8 shows the interface of the data reading program, which was designed according to the NanoSIMS data processing software based on the IDL language created by the NAMIP group at the MPIC. ‘Input’ button is used to clean all the old files and to make a new im file list. ‘Add files’ is used to add new files to an existing file list, e.g. data from other analysis sessions stored in other folders. Initial input files are shown in the left file list; via select buttons files of interest can be put to the right side, then by clicking ‘Multi Img Calc’ button input files can be organized.

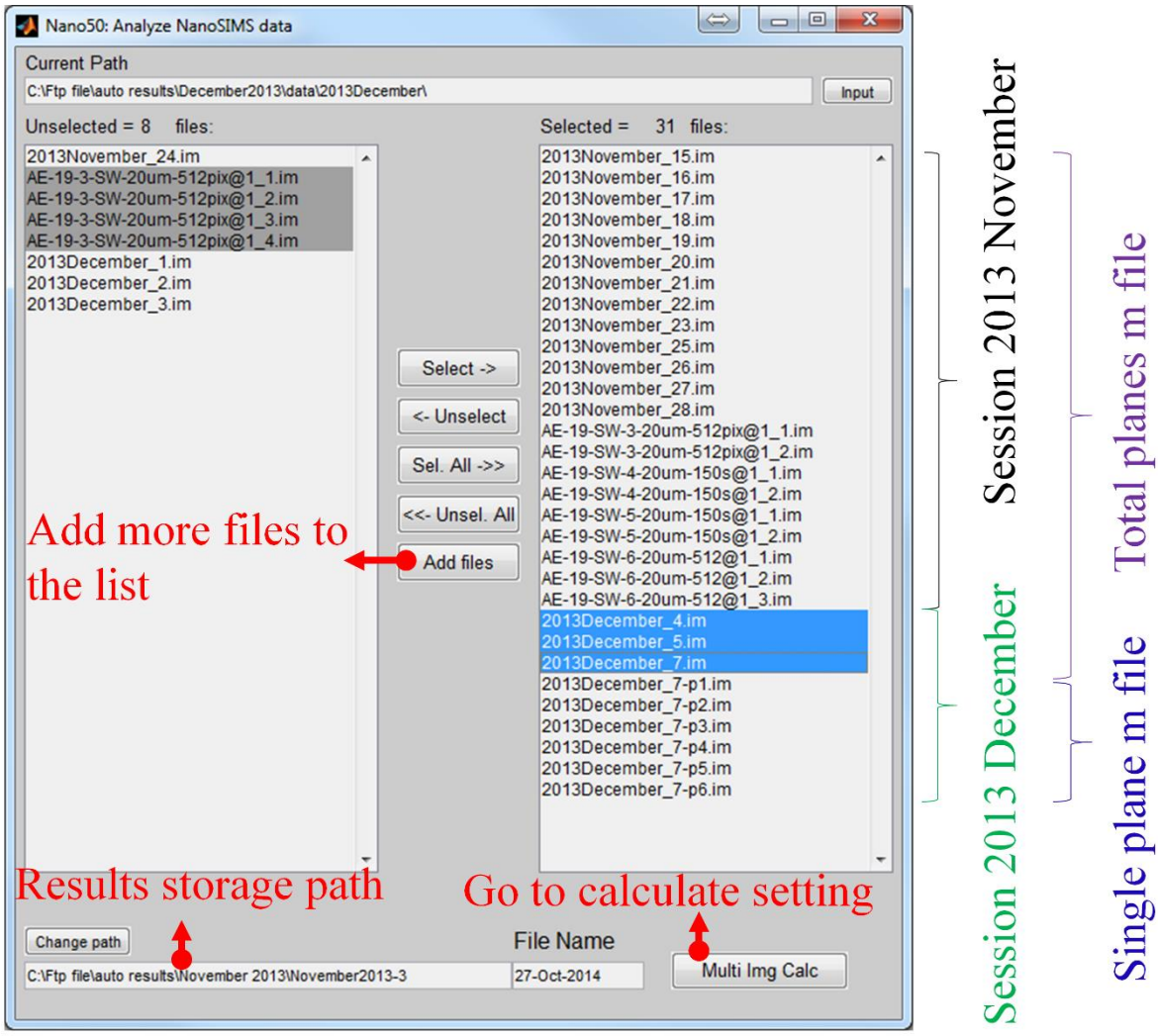

Figure A-8. Image data input interface.

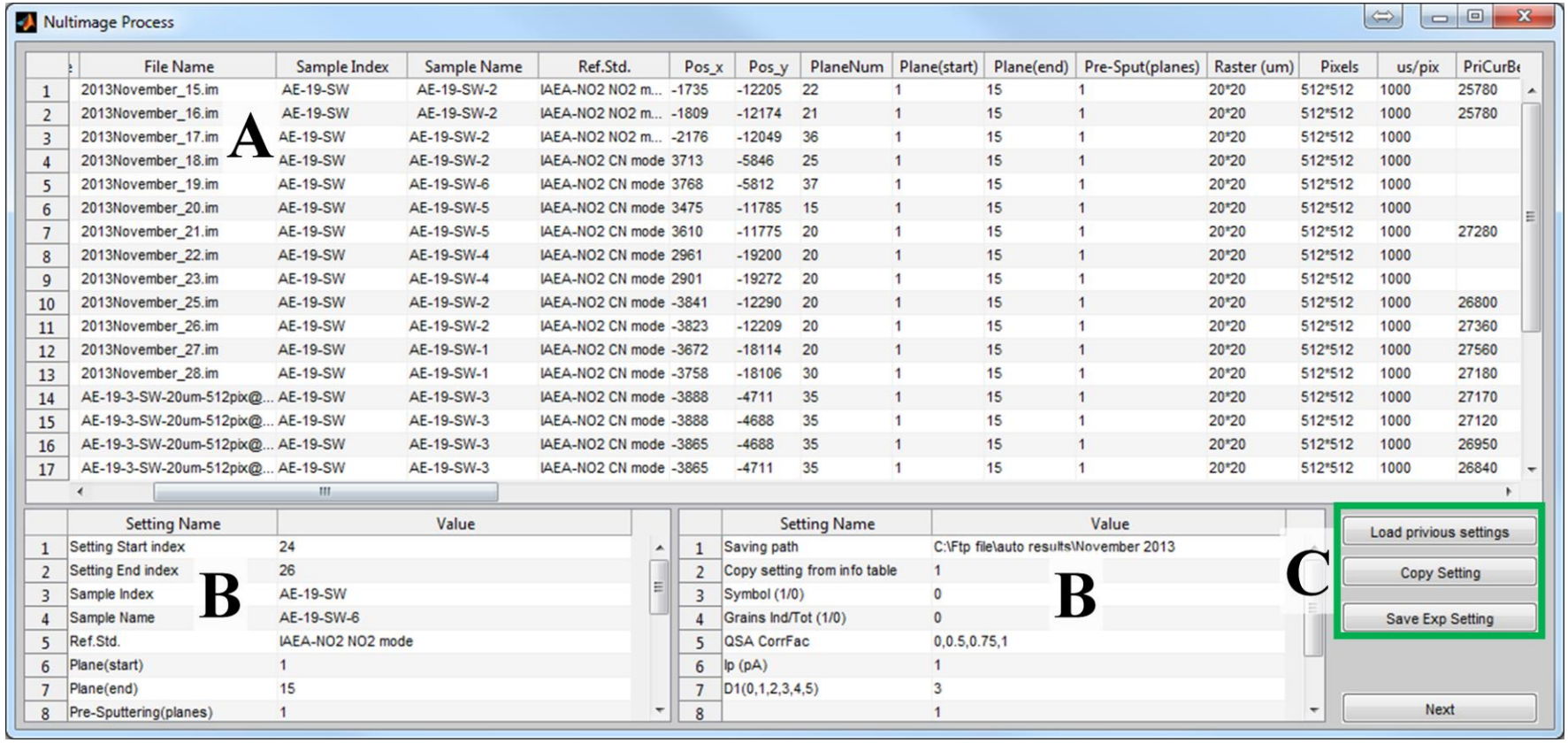

	File Name	Sample Index	Sample Name	Ref.Std.	Pos_x	Pos_y	PlaneNum	Plane(start)	Plane(end)	Pre-Sput(planes)	Raster (um)	Pixels	us/pix	PriCurBe
1	2013November_15.im	AE-19-SW	AE-19-SW-2	IAEA-NO2 NO2 m...	-1735	-12205	22	1	15	1	20*20	512*512	1000	25780
2	2013November_16.im	AE-19-SW	AE-19-SW-2	IAEA-NO2 NO2 m...	-1809	-12174	21	1	15	1	20*20	512*512	1000	25780
3	2013November_17.im	AE-19-SW	AE-19-SW-2	IAEA-NO2 NO2 m...	-2176	-12049	36	1	15	1	20*20	512*512	1000	
4	2013November_18.im	AE-19-SW	AE-19-SW-2	IAEA-NO2 CN mode	3713	-5846	25	1	15	1	20*20	512*512	1000	
5	2013November_19.im	AE-19-SW	AE-19-SW-6	IAEA-NO2 CN mode	3768	-5812	37	1	15	1	20*20	512*512	1000	
6	2013November_20.im	AE-19-SW	AE-19-SW-5	IAEA-NO2 CN mode	3475	-11785	15	1	15	1	20*20	512*512	1000	
7	2013November_21.im	AE-19-SW	AE-19-SW-5	IAEA-NO2 CN mode	3610	-11775	20	1	15	1	20*20	512*512	1000	27280
8	2013November_22.im	AE-19-SW	AE-19-SW-4	IAEA-NO2 CN mode	2961	-19200	20	1	15	1	20*20	512*512	1000	
9	2013November_23.im	AE-19-SW	AE-19-SW-4	IAEA-NO2 CN mode	2901	-19272	20	1	15	1	20*20	512*512	1000	
10	2013November_25.im	AE-19-SW	AE-19-SW-2	IAEA-NO2 CN mode	-3841	-12290	20	1	15	1	20*20	512*512	1000	26800
11	2013November_26.im	AE-19-SW	AE-19-SW-2	IAEA-NO2 CN mode	-3823	-12209	20	1	15	1	20*20	512*512	1000	27360
12	2013November_27.im	AE-19-SW	AE-19-SW-1	IAEA-NO2 CN mode	-3672	-18114	20	1	15	1	20*20	512*512	1000	27560
13	2013November_28.im	AE-19-SW	AE-19-SW-1	IAEA-NO2 CN mode	-3758	-18106	30	1	15	1	20*20	512*512	1000	27180
14	AE-19-3-SW-20um-512pix@...	AE-19-SW	AE-19-SW-3	IAEA-NO2 CN mode	-3888	-4711	35	1	15	1	20*20	512*512	1000	27170
15	AE-19-3-SW-20um-512pix@...	AE-19-SW	AE-19-SW-3	IAEA-NO2 CN mode	-3888	-4688	35	1	15	1	20*20	512*512	1000	27120
16	AE-19-3-SW-20um-512pix@...	AE-19-SW	AE-19-SW-3	IAEA-NO2 CN mode	-3865	-4688	35	1	15	1	20*20	512*512	1000	26950
17	AE-19-3-SW-20um-512pix@...	AE-19-SW	AE-19-SW-3	IAEA-NO2 CN mode	-3865	-4711	35	1	15	1	20*20	512*512	1000	26840

	Setting Name	Value
1	Setting Start index	24
2	Setting End index	26
3	Sample Index	AE-19-SW
4	Sample Name	AE-19-SW-6
5	Ref.Std.	IAEA-NO2 NO2 mode
6	Plane(start)	1
7	Plane(end)	15
8	Pre-Sputtering(planes)	1

	Setting Name	Value
1	Saving path	C:\Ftp file\auto results\November 2013
2	Copy setting from info table	1
3	Symbol (1/0)	0
4	Grains Ind/Tot (1/0)	0
5	QSA CorrFac	0,0.5,0.75,1
6	Ip (pA)	1
7	D1(0,1,2,3,4,5)	3
8		1

Figure A-9. im file organizing interface. A is the table of file database, Part B and Part C are used to edit table A.

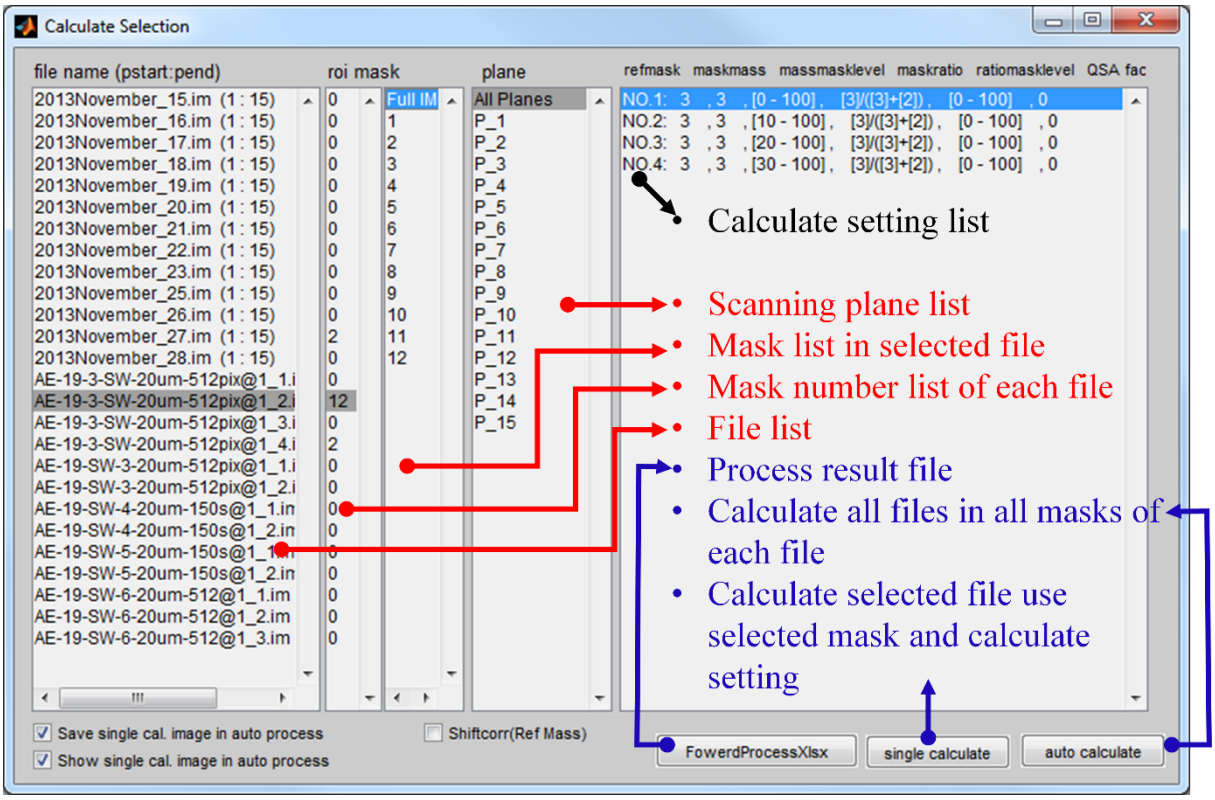

Figure A-10. Calculation control interface.

Table A-3. Examples and descriptions of im file information in file database.

Data file information	**Example**	**Description**
File Name	2013November_15.im	im file name of image data
Date and Time	30.11.13-03:01	Date and time of current measurement
Sample Index	AE-19-SW	Sample mount name
Sample Name	AE-19-SW-2	Sample name of current measurement
Ref.Std.	IAEA-NO-3	Reference standard with known isotope ratio
Data Address	N:\data\Aerosols\2013November\	The storage path of current im file

Table A-4. Examples and descriptions of measurement informations in im file database.

Measurement information	**Example**	**Description**
Analysis Name	IMAGE ACQUISITION	NanoSIMS analysis type
Pos_x	-1735	Measurement position x-axis (μm)
Pos_y	-12205	Measurement position y-axis (μm)
PlaneNum	22	Plane number of current measurement
Pre-Sput(planes)	1	Plane number of pre-sputtering
Raster (um)	20*20	Raster area (μm^2)
Pixels	512*512	Scanning pixels is 512 × 512
us/pix	1000	Sputtering time in each pixel is 1000 us/pix
PriCurBefore(pA)	25780	Before measurement, primary current was 25780 pA
PriCurAfter(pA)	25635	After measurement, primary current was 25635 pA
Dead Time (ns)	44	Electron multiplayer dead time is 44 ns.
Trolley 1	12C	Trolley 1 was set to mass ^{12}C
Trolley 2	12C 14N	Trolley 2 was set to mass $^{12}C^{14}N$
Trolley 3	14N 16O2	Trolley 3 was set to mass $^{14}N^{16}O_2$
Trolley 4	15N 16O2	Trolley 4 was set to mass $^{15}N^{16}O_2$
Trolley 5	unused	Trolley 5 was not used
D1	2	D1 Aperture was set to D1-2 (300μm)
EOS (bit)	2850	After centering, the value of EOS lens was 2850 bit.
BS_EOS	2865	Before centering, the value of EOS lens was 2865 bit.
SIBC_Hor (bit)	82	Secondary ion beam centering results: horizontal direction.
SIBC_V_P3B (bit)	917	Secondary ion beam centering results: vertical direction P3B
SIBC_V_P3H (bit)	917	Secondary ion beam centering results: vertical direction P3H
SIBC_V_P2B (bit)	2049	Secondary ion beam centering results: vertical direction P2B
SIBC_V_P2H (bit)	2022	Secondary ion beam centering results: vertical direction P2H
EOW_OffSet_num	8	Number of times of energy centering in current measurement
EOW_OffSet_m	12.1	The average of all energy centered values (bit)
EOW_OffSet_std	5.5	The standard deviation of all energy centered values (bit)

Table A-5. Examples and descriptions of calculation settings in im file database. * mask level calculation is described in section 4.2.3.

Calculation setting	Example	Description
Plane(start)	1	The No. of first calculated plane
Plane(end)	15	The No. of last calculated plane
Ref.Mass	3	Mass in the third trolley ($^{14}N^{16}O_2$) is set as reference mass
Mask Mass	3	Mass in the third trolley ($^{14}N^{16}O_2$) is set as mask mass
Mass Mask Level (%)*	0,10,20,30	Four mask levels are used, 0~100, 10~100, 20~100 and 30~100 %.
Ratio Mask	[3]/([3]+[2])	[trolley's No.], secondary ion ratio is calculated by $^{14}N^{16}O_2/(^{14}N^{16}O_2 + {}^{12}C^{14}N)$
Ratio Mask Level (%)*	0	No ratio mask calculation
QSA CorrFac	0, 0.5	QSA correction factors are set to 0 and 0.5

The interface of the data organizing interface is shown in Figure A-9. All informations for the input files are shown in part A – the file database, which contains im file informations (Table A-3), measurement informations (Table A-4) and calculation settings (Table A-5). Part B and part C are used to edit table A. The role of calculation settings are listed in Table A-6. Users are allowed to update the file database directly and via part B with the buttons in part C.

The calculation control interface is accessible after click the button 'Next', see Figure A-10. Five lists are used to control the calculation. 'File list' is used to select the im file. 'Mask number list' shows how many masks are in the current im file and it is also used to open the mask maker program, see section A.3.4. 'Mask list' is used to select certain masks (whole area or particle area). 'Plane list' is used to show all input planes of current im file. 'Calculation setting list' is used to select a certain calculation group.

Table A-6. The description of calculation settings. f([m],[n],[i]) is a defined function used to calculate image data, e.g. f = [m]/([n]+[m]). Tro No. is the No. of used trolley in NanoSIMS 50.

setting	reference mass	mask mass	ratio mask	mass/ratio mask level	QSA correction
m,n,i,j,k….	m,n,i,j,k…. (m,n,i,j,k = Tro No.)	m,n,i,j,k…. (m,n,i,j,k = Tro No.)	m,n,i,j,k…. (m,n,i,j,k = Tro No.)	m ~ 100 %, n ~ 100 %, i ~ 100 %, j ~ 100 %, k ~ 100 %…. (0<m,n,i,j,k<100)	m,n,i,j,k…. (0<m,n,i,j,k<1)
-m	×	×	×	0 ~ m% (0<m<100)	×
<m>	×	×	×	0 ~ 100/m %, 100/m ~ 100/m×2 %, 100/m×2 ~ 100/m×3 % …. 100/m× (m-1) ~ 100 %, (m = Positive integer)	×
[m:n]	×	×	×	m ~ n % (0 < m < n < 100)	×
f([m],[n],[i])	×	×	f([m],[n],[i]) (m,n,i,j,k = Tro No.)	×	×

A.3.2Single im file calculation

Figure A-11 shows the interface for the single im file calculation. All current im file informations are shown in text box A. Images are shown in area B, where the first row images are the measured NanoSIMS images, the second row images are the ratio images and the image in the third row is the multi-calculated image by the function f([m],[n],[i]) (m, n, i, j and k = Trolley No.). Each plane data is calculated separately and the weighted average results are summarized in area C and single plan results are shown in plot D. Two lists in area E are used to select the data shown here, including calculation method and plane No. In F area, the button ‘Export IMG’ is used to export images with color bar to a JPEG image file with a resolution of 600 dpi. Button ‘Show plot 3D’ is used to create a 3D cross-sectional plot, Figure A-14. Button ‘Show plotyy’ used to create single im file calculation result browser, Figure A-15.

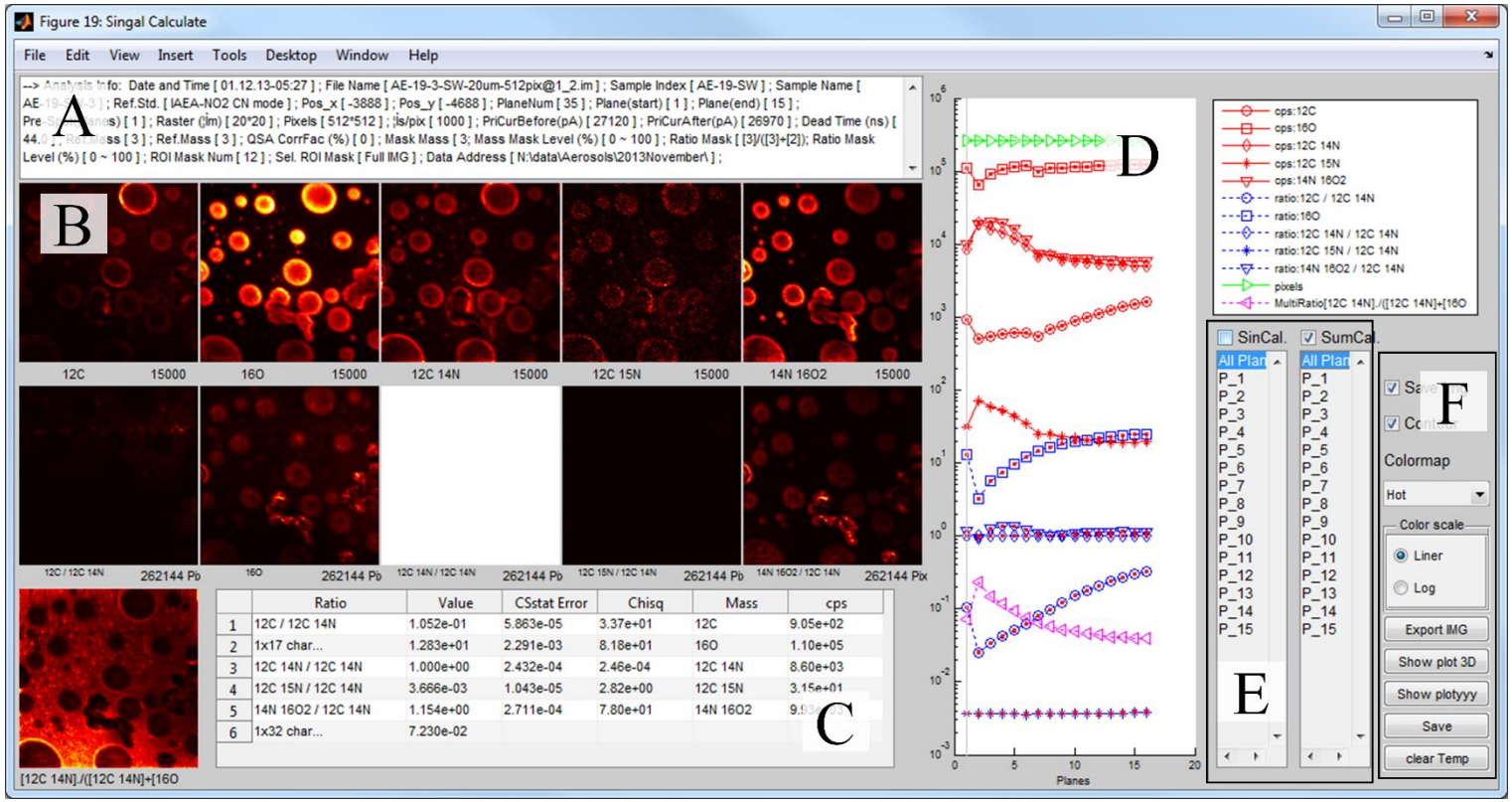

Figure A-11. Single im file results interface. A shows current file informations. B shows NanoSIMS images, ratio images and multi-calculated ratio images. C shows image calculation results. D is the plot of single plane results. The first spot data is the weighted average results, others are single plane data. Lists in area E control which calculation method and plane data are shown in areas A, B, C and D. Other control options are shown in F area.

There are two types of plane calculation methods in this program: One method is ‘SinCal’. Each plane has its own mask calculation. Final results are obtained by summarizing all independent plane results. Another method is called ‘SumCal’. Firstly, all planes are superimposed to a summarized image. Then a total mask is calculated for all single planes. This section gives an example for these two mask calculation methods in sample AE-19-SW-2, which is an aerosol-like sample, consisting of a mixture of potassium nitrate with glucose with a N/C ratio of 0.5 collected on silicon wafer. Figure A-12 shows two screenshots of area D and E in Figure A-11. Left and right plots show the results obtained by single plane mask calculation and the results obtained by summary plane mask calculation, respectively. The signal intensity of $^{15}N^{16}O_2^-$ in the left plot is more stable than that in the right plot. 3D cross-sectional plots, Figure A-13, gives more intuitive feeling of the difference. Upper and lower plots show the results obtained by single plane mask calculation and the results obtained by summary plane mask calculation, respectively. Compared to summary mask calculation, single plane mask calculation avoid lower signal intensity area and signal intensity is more stable, however it has a more fragmentary pixel distribution.

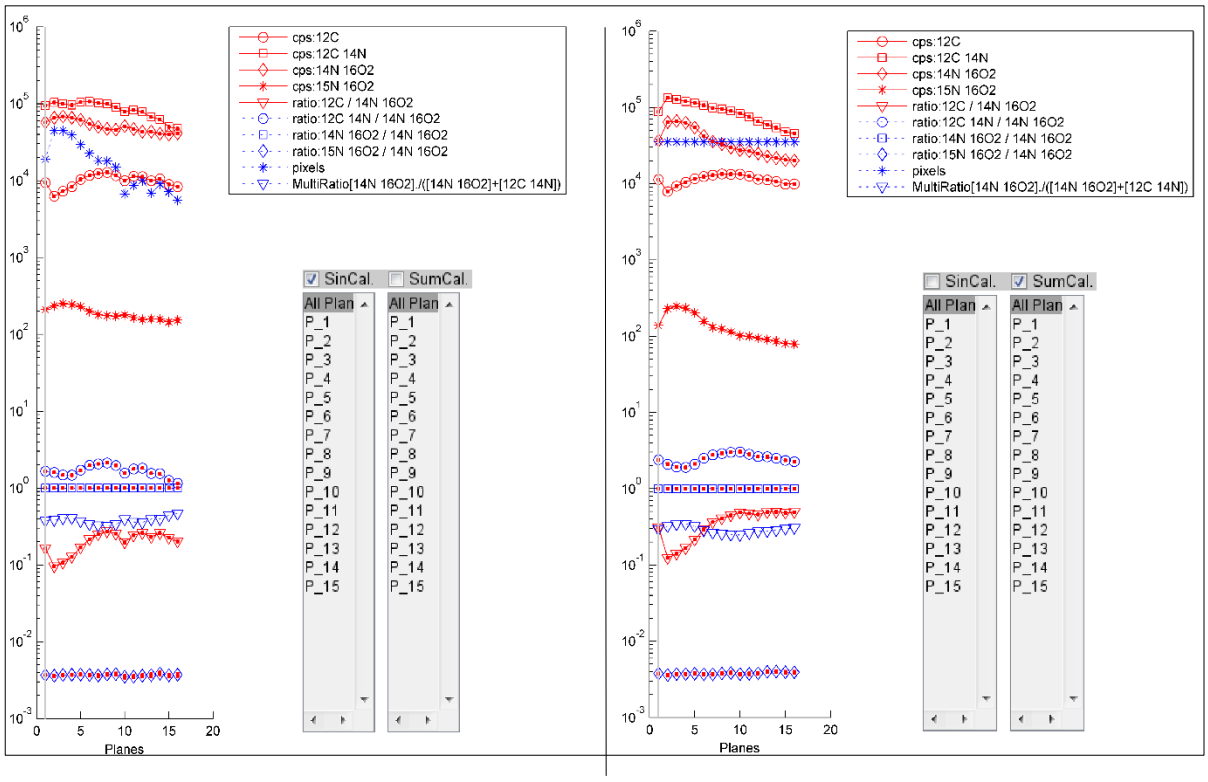

Figure A-12: Screenshots of the comparison of single plane mask calculation results (left plot, SinCal) and summary plane mask calculation results (right plot, SumCal). The first spot data is the weighted average results, others are single plane data. Gray solid line in plots mark the current plane data results.

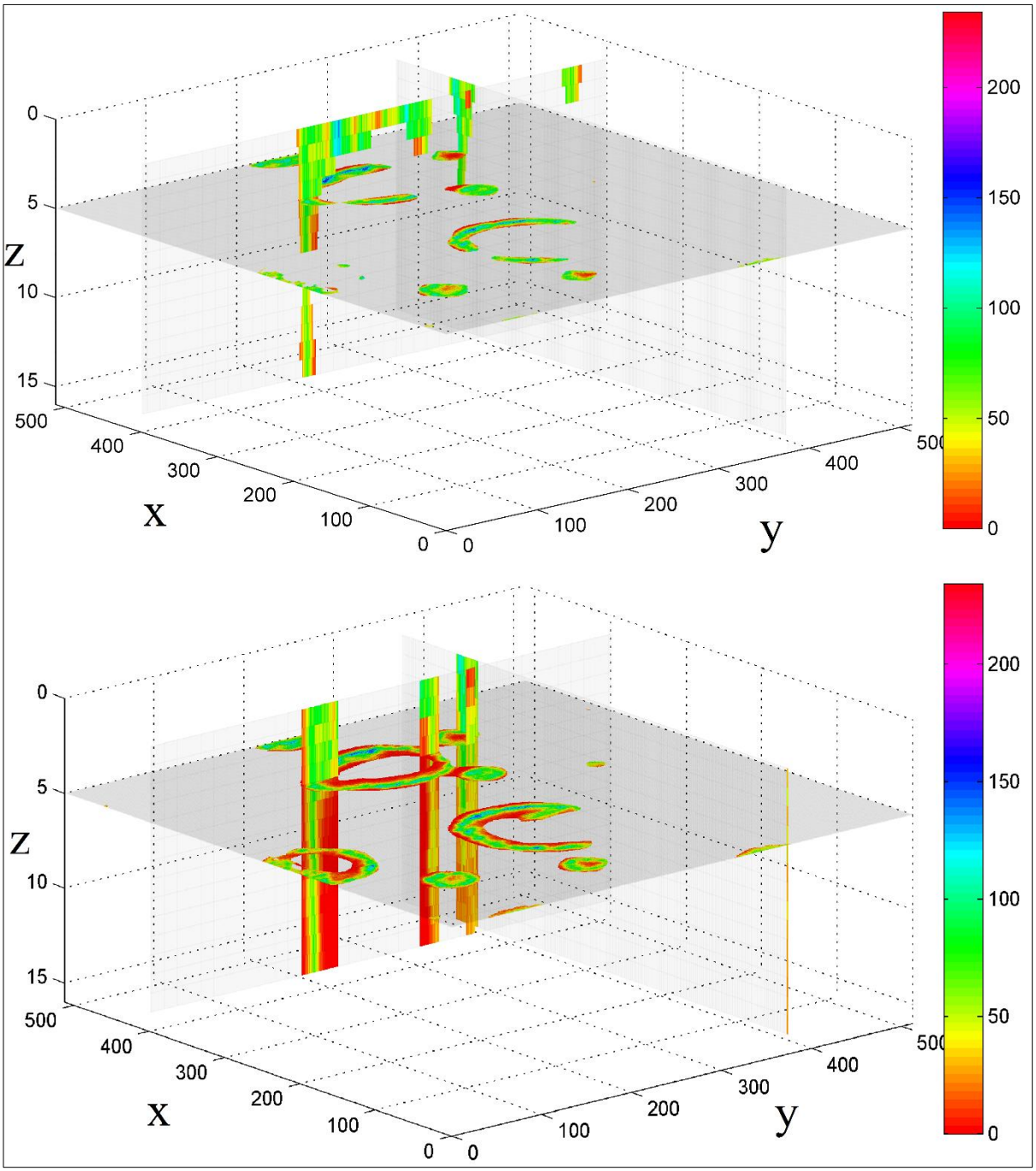

Figure A-13. The comparison of single plane mask calculation results (upper plot, SinCal) and summary plane mask calculation results (lower plot, SumCal) in 3D cross-sectional plot. x=400 and y=375 are the pixels No. z=5 is the plane No.

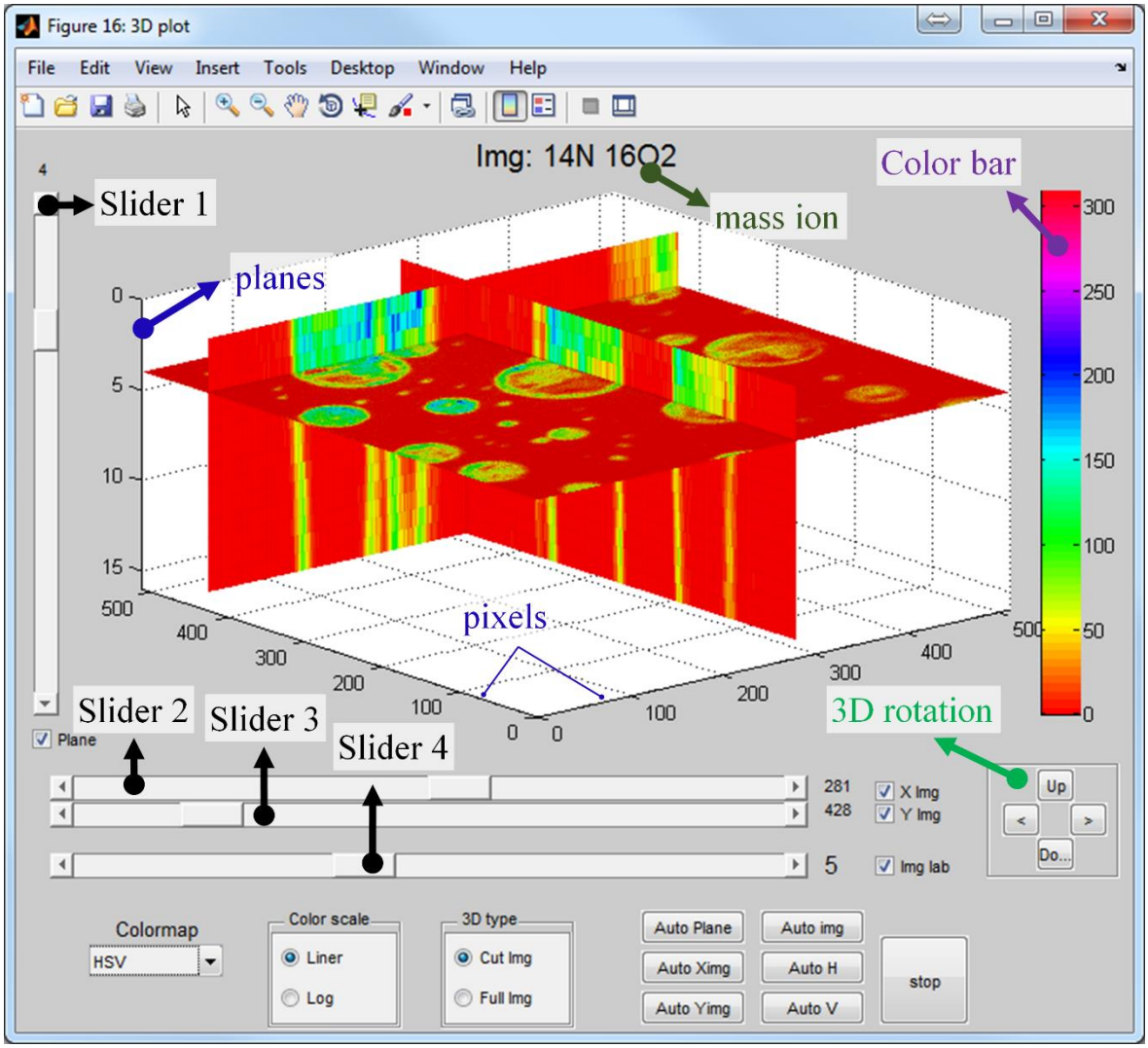

Figure A-14. 3D cross-sectional plot interface. Axis x and y are the pixels No. Axis z is the plane No. Slider 1, slider 2 and slider 3 are used to control z, x and y direction. Different images, e.g. ion images, ratio images and multi-ratio images, can be shown via change slider 4.

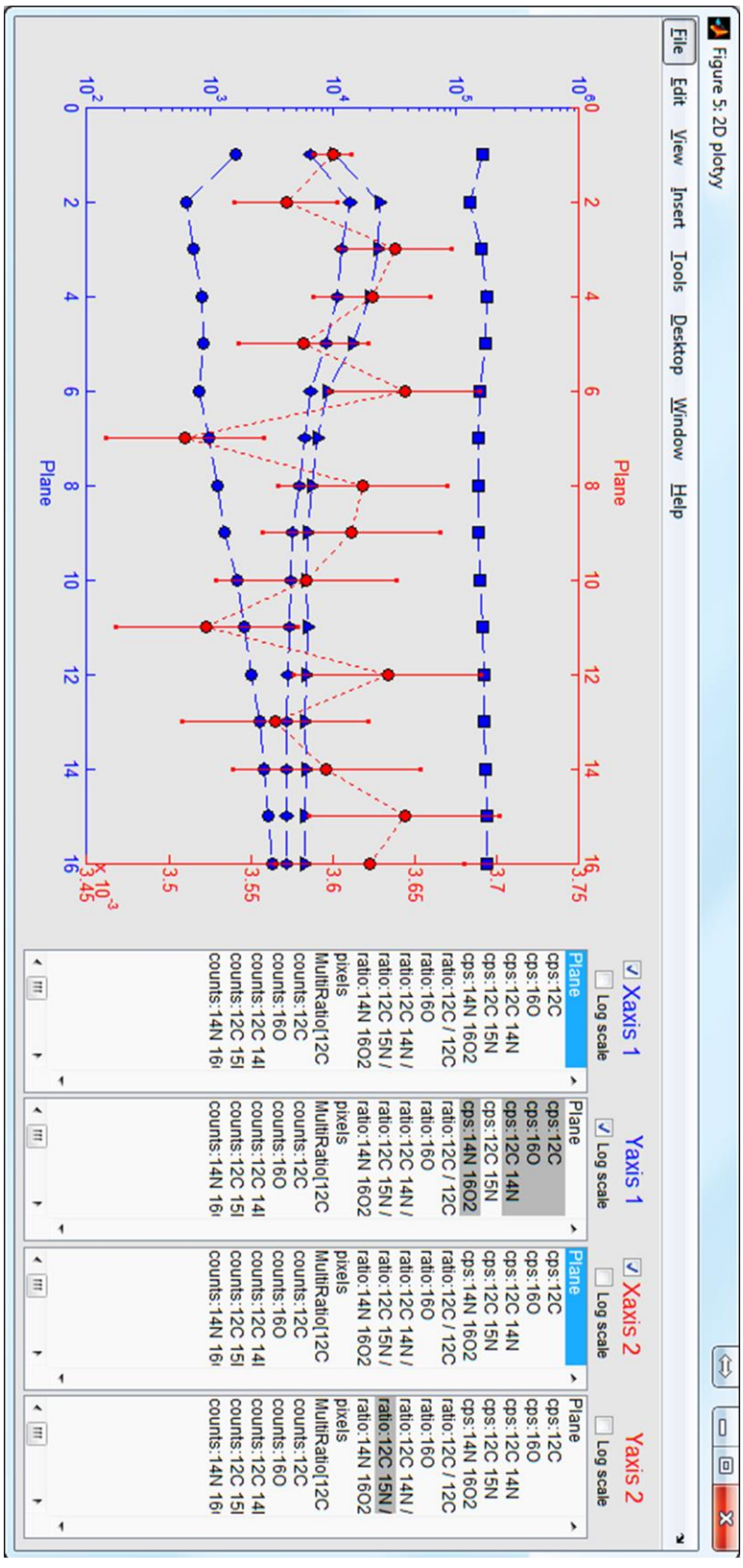

Figure A-15. 2D single im file results browser.

A.3.3 Auto im file calculation

Auto im file calculation is used to help users to get results more systematically and completely. Figure A-16 shows the calculation process. Input im files are organized to three different layers: image layer, mask layer (several independent areas in one image) and plane layer. Calculation settings, including reference mass, mask mass, mask level, ratio mask f, ratio mask level and QSA correction factor, are packaged to independent calculation groups. Based on single im file calculation, described above, each plane data is calculated for all calculation groups. Each single im file calculation has its own index number, which is the marker of storage address and used to search and forward analysis. All input im file informations, calculation settings and analysis parameters are saved in MATLAB format figure files, calculation results are automatically saved in an Excel file. A log file records the calculation index, date and time of each single im file calculation. All single im file calculation interfaces can be saved in bmp images. In the end of auto im file calculation, a time statistics plot is given for all single im file calculations, e.g. Figure A-17.

A.3.4 ROI mask calculation

ROI (regions of interest) mask calculation is quite useful for single particle analysis in one image. According to the NAMIP group software and based on ROI-Based processing functions in Image Processing Toolbox of MATLAB 2014a, this program was written and inserted into the single plane calculation program. The interface of ROI mask maker is shown in Figure A-18. According to the shape of the particles, button ‘Ellipse’, ‘Rectangle’ and ‘Free hand’ creates a draggable ellipse, rectangle and freehand region, respectively. Then, by clicking the ‘Save’ button, all created mask outlines can be seen in the ROI mask previewer, Figure A-19. Save all masks in this interface, mask information will be added to the calculation control interface ROI lists. Left figure in Figure A-20 gives an example after saving mask settings in Figure A-19. Right plot is the isotope ratio image calculated with the 11^{th} mask. All mask settings are automatically stored. Users can reopen and recalculate all mask regions.

A.3.5 Result file processing

Single plane calculation produces large amounts of data in one analysis session. Based on the image im file database in section A.3.1, a data filter lists all data properties (parameters and settings). Two independent filters, which have blue and red background, are shown in Figure A-21. After selecting checkboxes in front of interested data properties, the program examines all results and transfers filtered results to the data browser, see Figure A-22. The plots in blue and red colors

correspond to the data coming from blue and red background data filters. All searching informations are listed in textbox in blue and red, respectively. Select x (single choice available) and y (multiple choices available) axis options to plot data of interest.

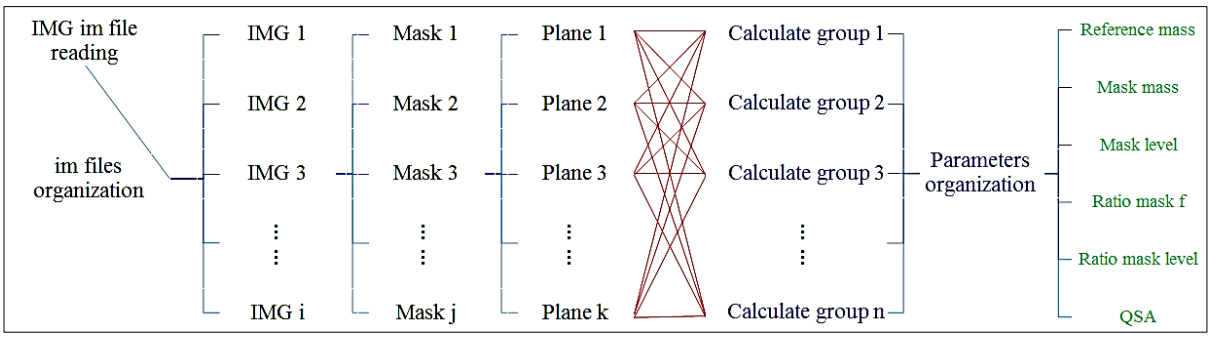

Figure A-16. Schematic diagram of auto im file calculation.

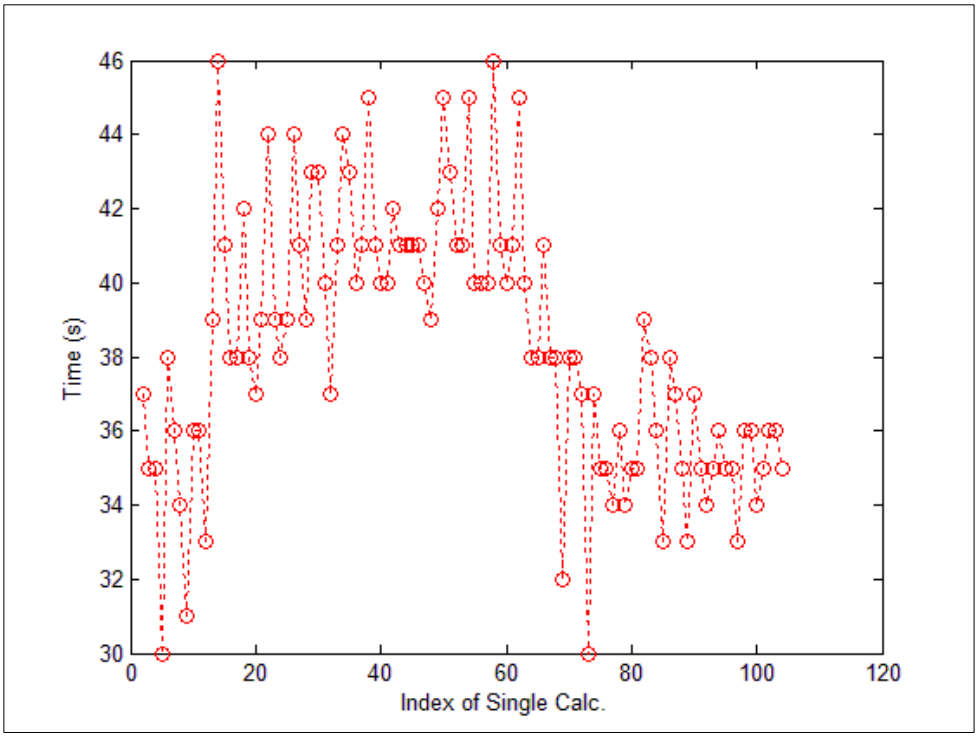

Figure A-17. Time statistics of auto im file calculation. Axis x is the index of single im file calculation and y axis is the consumed time (s) in each single im file calculation.

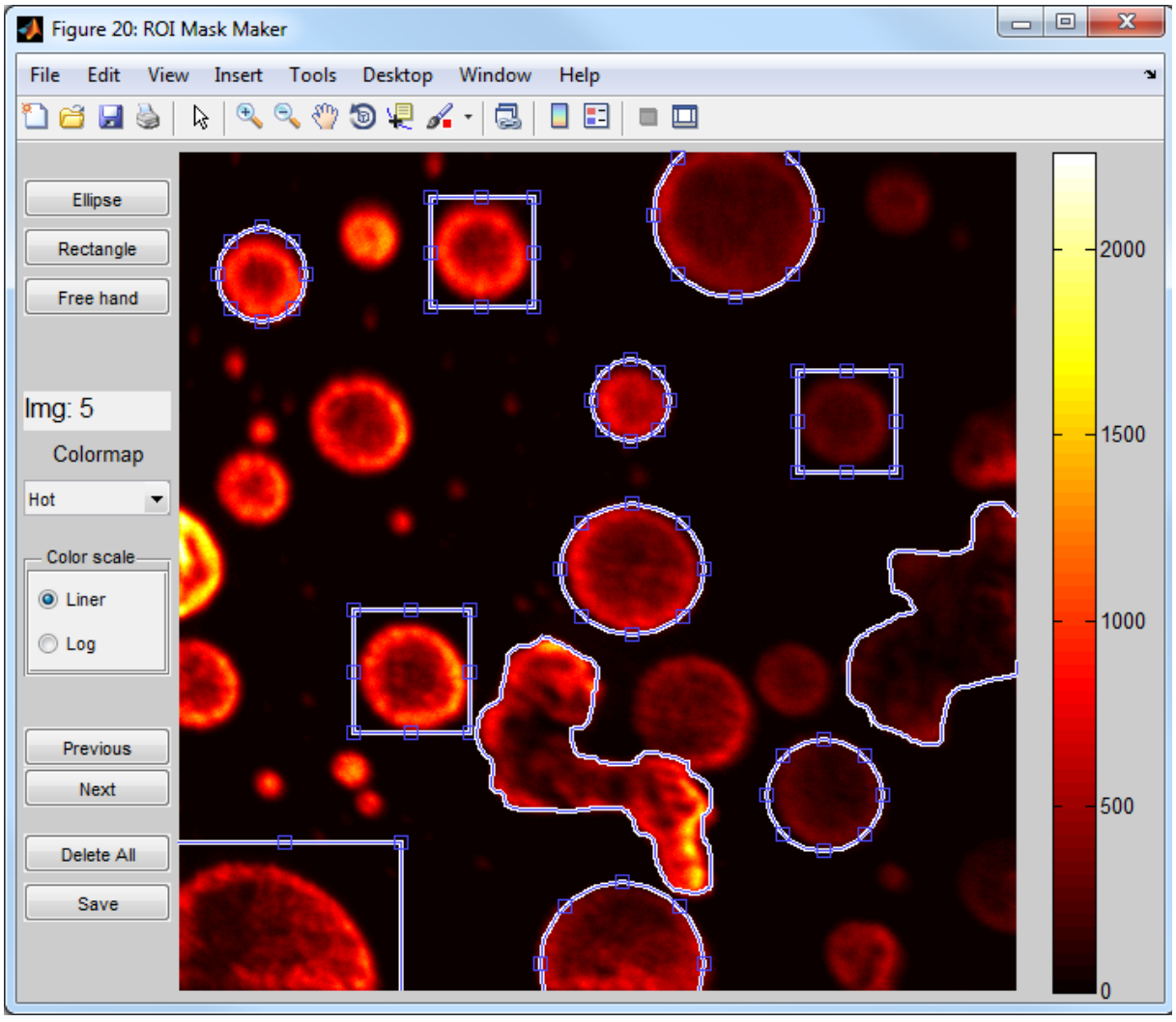

Figure A-18. ROI mask maker.

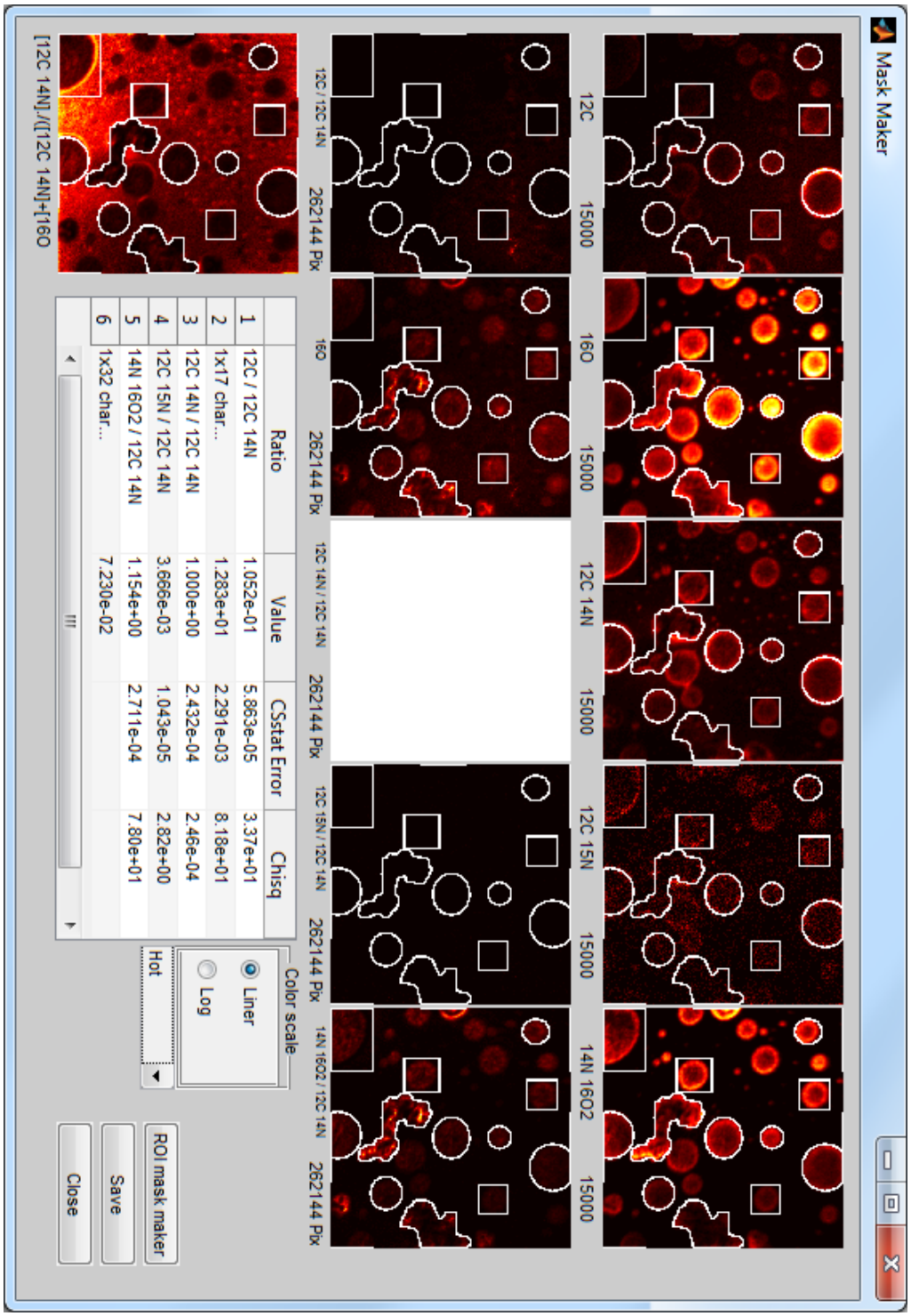

Figure A-19. ROI mask previewer.

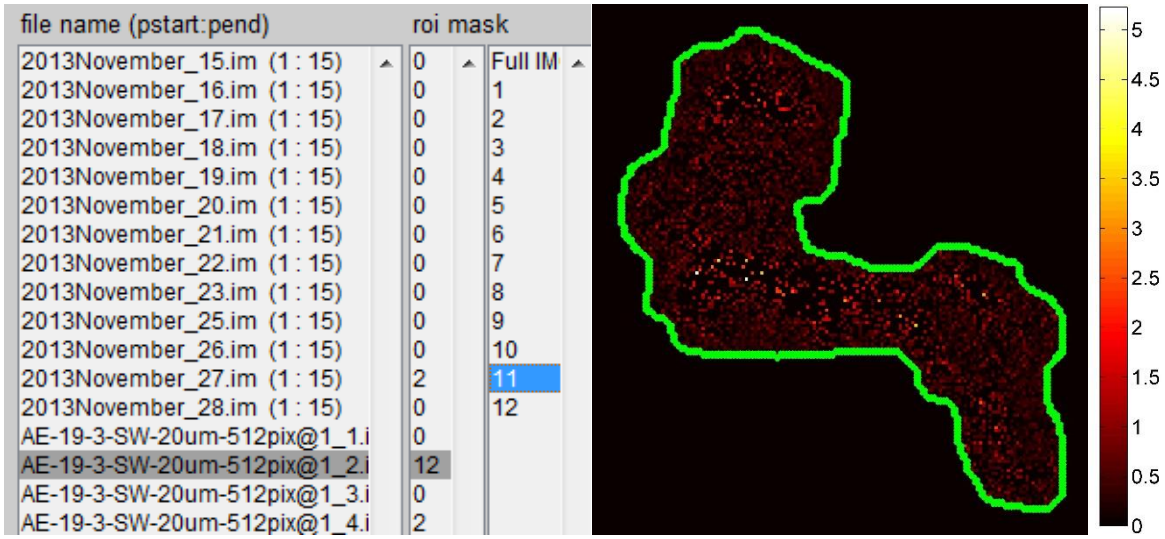

Figure A-20. An example of ROI mask setting result. Left figure shows the number of masks in selected im file and each mask can be selected and used for the calculations. Right figure is the secondary ion image ratio of $^{12}C^{15}N^{-}/^{12}C^{14}N^{-}$ of mask No. 11.

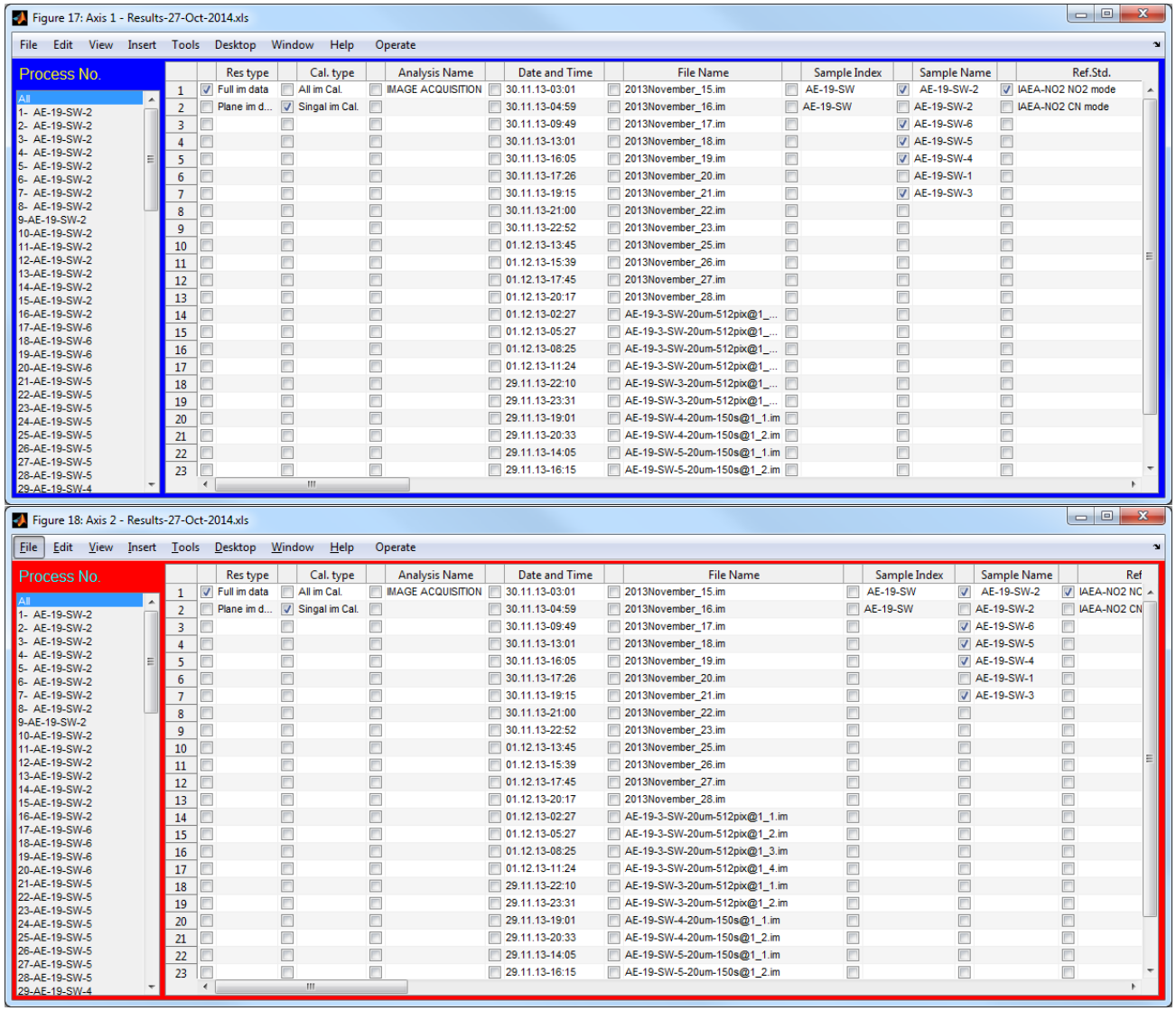

Figure A-21. Two results data filter. Interfaces in blue and red color are controls for the blue and red axes in figure A-22.

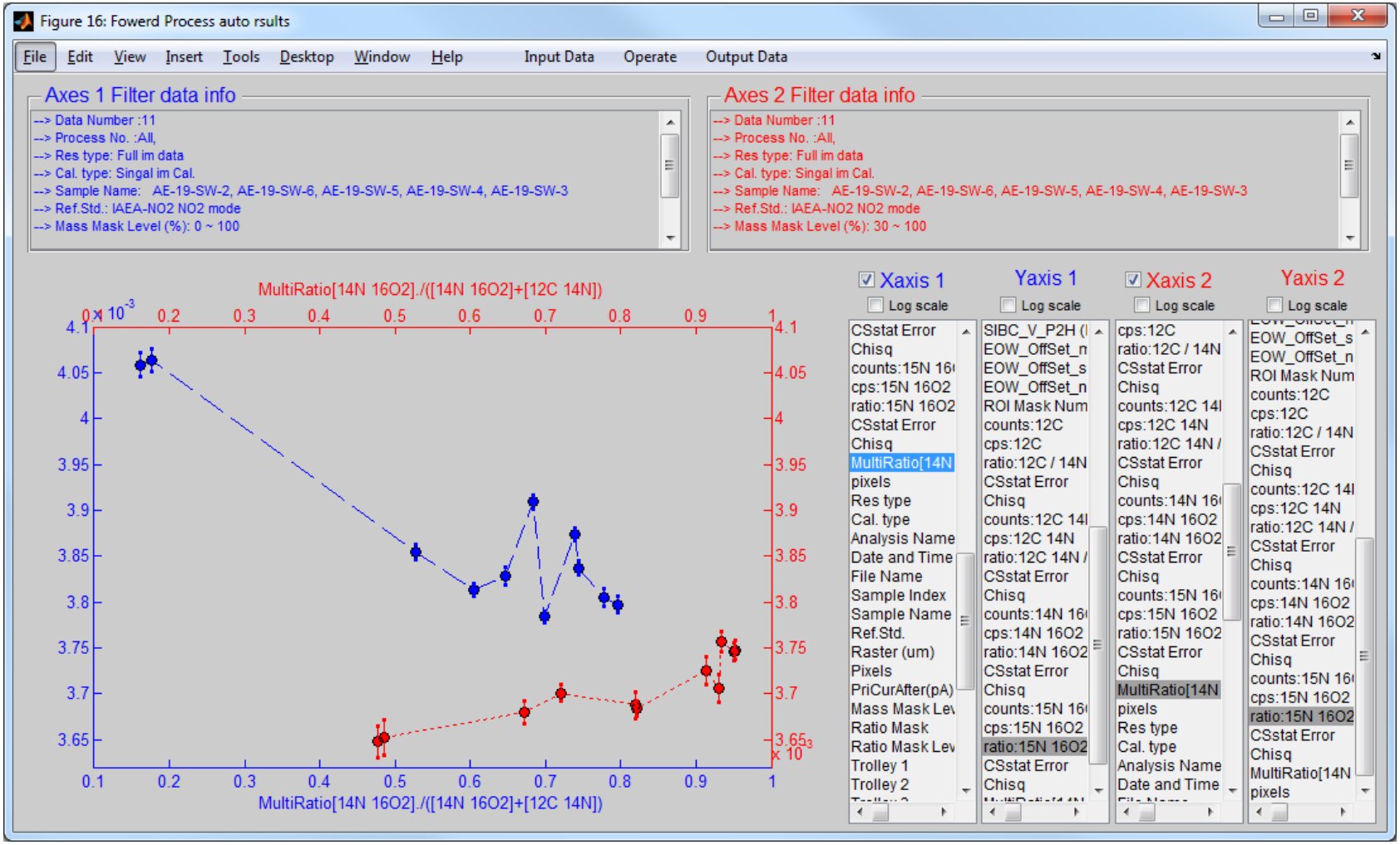

Figure A-22. Results data browser.

B Details of all analysis spots on bulk standards, isotope ratio measured by $^{15}N^{16}O_2^-$ / $^{14}N^{16}O_2^-$

Analysis no.	$n(^{15}N^{16}O_2^-)$ / $n(^{14}N^{16}O_2^-)$	1 σ	ion $^{14}N^{16}O_2^-$ (cps)	IMF (‰)	1 σ	Pre - sputtering Time (s)	$n(^{14}N^{16}O_2^-)$ / $n(Cs^+)$
August 2012 <SampleName:USGS35-NaNO3> <Raster:2.0>							
EXP-4@10_1	0.003739	0.000012	26554	14.4	3.3	135.2	1.8673E-03
EXP-4@10_2	0.003721	0.000011	30050	9.5	3.0	135.2	2.1096E-03
EXP-4@10_3	0.003733	0.000011	29280	12.8	3.1	135.2	2.0560E-03
EXP-4@10_4	0.003728	0.000012	27020	11.4	3.2	135.2	1.8987E-03
EXP-4@10_5	0.003723	0.000012	26496	10.0	3.3	135.2	1.8619E-03
EXP-4@10_6	0.003708	0.000016	13979	6.0	4.5	135.2	9.8301E-04
EXP-4@10_7	0.003713	0.000012	28411	7.3	3.1	135.2	2.0003E-03
EXP-4@10_8	0.003726	0.000011	31560	10.9	3.0	135.2	2.2215E-03
EXP-4@10_9	0.003712	0.000010	35887	7.1	2.8	135.2	2.5127E-03
EXP-4@10_10	0.003722	0.000011	33321	9.8	2.9	135.2	2.3325E-03
EXP-4@10_11	0.003730	0.000012	27970	11.9	3.2	135.2	1.9698E-03
EXP-4@10_12	0.003701	0.000011	33510	4.1	2.9	135.2	2.3691E-03
EXP-4@10_13	0.003701	0.000011	32293	4.1	2.9	135.2	2.2858E-03
EXP-4@10_14	0.003706	0.000011	31264	5.4	3.0	135.2	2.2237E-03
EXP-4@10_15	0.003720	0.000012	28137	9.2	3.2	135.2	2.0087E-03
EXP-4@10_16	0.003714	0.000011	28797	7.6	3.1	135.2	2.0609E-03
EXP-4@10_17	0.003717	0.000012	26942	8.4	3.2	135.2	1.9239E-03
EXP-4@10_18	0.003732	0.000011	31485	12.5	3.0	135.2	2.2390E-03
EXP-4@10_19	0.003720	0.000010	35827	9.2	2.8	135.2	2.5496E-03
EXP-4@10_20	0.003735	0.000011	33922	13.3	2.9	135.2	2.4176E-03
EXP-4@13_1	0.003724	0.000011	33922	10.3	2.9	135.2	2.2379E-03
EXP-4@13_2	0.003723	0.000011	32552	10.0	2.9	135.2	2.1510E-03
EXP-4@13_3	0.003764	0.000011	32139	21.2	3.0	135.2	2.1232E-03
EXP-4@13_4	0.003709	0.000011	29798	6.2	3.1	135.2	1.9734E-03
EXP-4@13_5	0.003717	0.000011	29912	8.4	3.1	135.2	1.9992E-03
EXP-4@13_6	0.003694	0.000013	21899	2.2	3.6	135.2	1.4738E-03
EXP-4@13_7	0.003727	0.000009	50208	11.1	2.4	135.2	3.3939E-03
EXP-4@13_8	0.003719	0.000011	31288	9.0	3.0	135.2	2.1219E-03
EXP-4@13_9	0.003718	0.000010	39206	8.7	2.7	135.2	2.6638E-03
EXP-4@13_10	0.003733	0.000011	31560	12.8	3.0	135.2	2.1478E-03
EXP-4@13_11	0.003719	0.000011	29125	9.0	3.1	135.2	1.9844E-03
EXP-4@13_12	0.003718	0.000010	36778	8.7	2.8	135.2	2.5105E-03
EXP-4@13_13	0.003715	0.000011	32139	7.9	2.9	135.2	2.2021E-03
EXP-4@13_14	0.003702	0.000010	34654	4.3	2.8	135.2	2.3750E-03

Analysis no.	$n(^{15}N^{16}O_2^-)$ / $n(^{14}N^{16}O_2^-)$	1 σ	ion $^{14}N^{16}O_2^-$ (cps)	IMF (‰)	1 σ	Pre - sputtering Time (s)	$n(^{14}N^{16}O_2^-)$ / $n(Cs^+)$
EXP-4@13_15	0.003706	0.000011	32139	5.4	2.9	135.2	2.2147E-03
EXP-4@13_16	0.003723	0.000011	31190	10.0	3.0	135.2	2.1579E-03
EXP-4@13_17	0.003714	0.000011	34061	7.6	2.9	135.2	2.3605E-03
EXP-4@13_18	0.003721	0.000011	33977	9.5	2.9	135.2	2.3659E-03
EXP-4@13_19	0.003738	0.000010	34855	14.1	2.8	135.2	2.4305E-03
EXP-4@13_20	0.003709	0.000010	40367	6.2	2.6	135.2	2.8149E-03
EXP-4@6_1	0.003716	0.000018	11117	8.1	5.0	98.3	7.4147E-04
EXP-4@6_2	0.003721	0.000015	15999	9.5	4.2	98.3	1.0632E-03
EXP-4@6_3	0.003732	0.000014	19622	12.5	3.8	98.3	1.3013E-03
EXP-4@6_4	0.003717	0.000014	20144	8.4	3.7	98.3	1.3362E-03
EXP-4@6_5	0.003737	0.000018	11899	13.8	4.9	98.3	7.9165E-04
EXP-4@6_6	0.003717	0.000019	10998	8.4	5.0	98.3	7.3390E-04
EXP-4@6_7	0.003684	0.000014	20439	-0.5	3.7	98.3	1.3711E-03
EXP-4@6_8	0.003741	0.000014	18238	14.9	3.9	98.3	1.2206E-03
EXP-4@6_9	0.003722	0.000014	18957	9.8	3.8	98.3	1.2644E-03
EXP-4@6_10	0.003752	0.000016	14877	17.9	4.4	98.3	9.9732E-04
EXP-4@6_11	0.003765	0.000016	14749	21.4	4.4	98.3	9.9701E-04
EXP-4@6_12	0.003749	0.000015	16309	17.1	4.2	98.3	1.1029E-03
EXP-4@6_13	0.003728	0.000016	14615	11.4	4.4	98.3	9.8863E-04
EXP-4@6_14	0.003745	0.000018	11253	16.0	5.0	98.3	7.6582E-04
EXP-4@6_15	0.003721	0.000020	9097	9.5	5.5	98.3	6.2057E-04
EXP-4@6_16	0.003709	0.000020	9234	6.2	5.5	98.3	6.3001E-04
EXP-4@6_17	0.003770	0.000021	8674	22.8	5.7	98.3	5.9295E-04
EXP-4@6_18	0.003706	0.000012	25602	5.4	3.3	98.3	1.7530E-03
EXP-4@6_19	0.003736	0.000013	21615	13.6	3.6	98.3	1.4848E-03
EXP-4@6_20	0.003724	0.000013	22471	10.3	3.5	98.3	1.5418E-03
August 2012 <SampleName:InHouse-NaNO3> <Raster:2.0>							
EXP-4@11_1	0.003790	0.000011	35058	14.2	2.8	135.2	2.4967E-03
EXP-4@11_2	0.003758	0.000010	41468	5.6	2.6	135.2	2.9640E-03
EXP-4@11_3	0.003768	0.000010	39692	8.3	2.6	135.2	2.8462E-03
EXP-4@11_4	0.003753	0.000010	39483	4.3	2.6	135.2	2.8396E-03
EXP-4@11_5	0.003777	0.000010	35058	10.7	2.8	135.2	2.5307E-03
EXP-4@11_6	0.003762	0.000011	31020	6.7	3.0	135.2	2.2470E-03
EXP-4@11_7	0.003790	0.000011	31190	14.2	3.0	135.2	2.2633E-03
EXP-4@11_8	0.003785	0.000011	34511	12.8	2.8	135.2	2.5037E-03
EXP-4@11_9	0.003780	0.000010	37315	11.5	2.7	135.2	2.7050E-03
EXP-4@11_10	0.003792	0.000010	38061	14.7	2.7	135.2	2.7612E-03
EXP-4@11_11	0.003783	0.000010	37379	12.3	2.7	135.2	2.7273E-03
EXP-4@11_12	0.003787	0.000010	40511	13.4	2.6	135.2	2.9678E-03
EXP-4@11_13	0.003763	0.000010	38932	7.0	2.7	135.2	2.8571E-03
EXP-4@11_14	0.003765	0.000010	35439	7.5	2.8	135.2	2.6041E-03
EXP-4@11_15	0.003769	0.000011	32840	8.6	2.9	135.2	2.4143E-03
EXP-4@11_16	0.003745	0.000012	28603	2.1	3.1	135.2	2.1124E-03

Analysis no.	$n(^{15}N^{16}O_2^-)$ / $n(^{14}N^{16}O_2^-)$	1 σ	ion $^{14}N^{16}O_2^-$ (cps)	IMF (‰)	1 σ	Pre - sputtering Time (s)	$n(^{14}N^{16}O_2^-)$ / $n(Cs^+)$
EXP-4@11_17	0.003772	0.000011	32242	9.4	2.9	135.2	2.3848E-03
EXP-4@11_18	0.003787	0.000010	36038	13.4	2.8	135.2	2.6662E-03
EXP-4@11_19	0.003788	0.000010	35233	13.6	2.8	135.2	2.6146E-03
EXP-4@11_20	0.003790	0.000010	36069	14.2	2.8	135.2	2.6828E-03
EXP-4@4_1	0.003799	0.000011	34597	16.6	2.8	98.3	2.3465E-03
EXP-4@4_2	0.003803	0.000011	33674	17.7	2.9	98.3	2.2460E-03
EXP-4@4_3	0.003812	0.000010	38359	20.1	2.7	98.3	2.5685E-03
EXP-4@4_4	0.003832	0.000011	35410	25.4	2.8	98.3	2.3726E-03
EXP-4@4_5	0.003809	0.000010	36622	19.3	2.8	98.3	2.4578E-03
EXP-4@4_6	0.003809	0.000010	36966	19.3	2.7	98.3	2.4936E-03
EXP-4@4_7	0.003817	0.000011	35262	21.4	2.8	98.3	2.3759E-03
EXP-4@4_8	0.003803	0.000010	36591	17.7	2.8	98.3	2.4625E-03
EXP-4@4_9	0.003800	0.000010	35827	16.9	2.8	98.3	2.4128E-03
EXP-4@4_10	0.003798	0.000011	34201	16.3	2.8	98.3	2.3097E-03
EXP-4@4_11	0.003808	0.000011	33133	19.0	2.9	98.3	2.2464E-03
EXP-4@4_12	0.003834	0.000011	33867	26.0	2.9	98.3	2.2999E-03
EXP-4@4_13	0.003793	0.000011	35029	15.0	2.8	98.3	2.3906E-03
EXP-4@4_14	0.003817	0.000010	36746	21.4	2.8	98.3	2.5178E-03
EXP-4@4_15	0.003807	0.000011	35204	18.7	2.8	98.3	2.4270E-03
EXP-4@4_16	0.003790	0.000010	35528	14.2	2.8	98.3	2.4674E-03
EXP-4@4_17	0.003821	0.000010	35887	22.5	2.8	98.3	2.5079E-03
EXP-4@4_18	0.003783	0.000010	36966	12.3	2.7	98.3	2.5845E-03
EXP-4@4_19	0.003796	0.000010	37315	15.8	2.7	98.3	2.6152E-03
EXP-4@4_20	0.003809	0.000010	36935	19.3	2.7	98.3	2.5935E-03
EXP-4@5_1	0.003803	0.000010	38094	17.7	2.7	98.3	2.7056E-03
EXP-4@5_2	0.003787	0.000010	36591	13.4	2.8	98.3	2.6135E-03
EXP-4@5_3	0.003784	0.000010	39798	12.6	2.6	98.3	2.8601E-03
EXP-4@5_4	0.003798	0.000010	42810	16.3	2.5	98.3	3.0888E-03
EXP-4@5_5	0.003812	0.000009	43405	20.1	2.5	98.3	3.1473E-03
EXP-4@5_6	0.003769	0.000010	36653	8.6	2.7	98.3	2.6604E-03
EXP-4@5_7	0.003777	0.000010	37156	10.7	2.7	98.3	2.7016E-03
EXP-4@5_8	0.003785	0.000010	36069	12.8	2.8	98.3	2.6082E-03
EXP-4@5_9	0.003791	0.000011	33894	14.5	2.9	98.3	2.4565E-03
EXP-4@5_10	0.003801	0.000011	33811	17.1	2.9	98.3	2.4714E-03
EXP-4@5_11	0.003774	0.000011	34398	9.9	2.8	98.3	2.5205E-03
EXP-4@5_12	0.003785	0.000010	37411	12.8	2.7	98.3	2.7379E-03
EXP-4@5_13	0.003784	0.000010	40331	12.6	2.6	98.3	2.9702E-03
EXP-4@5_14	0.003804	0.000010	36903	17.9	2.7	98.3	2.7240E-03
EXP-4@5_15	0.003804	0.000010	36191	17.9	2.8	98.3	2.6728E-03
EXP-4@5_16	0.003820	0.000009	47665	22.2	2.4	98.3	3.5327E-03
EXP-4@5_17	0.003817	0.000010	38426	21.4	2.7	98.3	2.8772E-03
EXP-4@5_18	0.003802	0.000010	39171	17.4	2.7	98.3	2.9620E-03
EXP-4@5_19	0.003785	0.000010	39069	12.8	2.7	98.3	2.9868E-03
EXP-4@5_20	0.003799	0.000010	36903	16.6	2.7	98.3	2.8369E-03

August 2012 <SampleName:InHouse-NaNO3> <Raster:5.0>

Analysis no.	$n(^{15}N^{16}O_2^-)$ / $n(^{14}N^{16}O_2^-)$	1 σ	ion $^{14}N^{16}O_2^-$ (cps)	IMF (‰)	1 σ	Pre - sputtering Time (s)	$n(^{14}N^{16}O_2^-)$ / $n(Cs^+)$
EXP-4@3_1	0.003757	0.000009	45353	5.4	2.5	491.5	3.1893E-03
EXP-4@3_2	0.003749	0.000010	37029	3.2	2.7	491.5	2.6172E-03
EXP-4@3_3	0.003756	0.000010	38594	5.1	2.7	491.5	2.7371E-03
EXP-4@3_4	0.003761	0.000010	40475	6.4	2.6	491.5	2.8782E-03
EXP-4@3_5	0.003784	0.000010	37156	12.6	2.7	491.5	2.6775E-03
EXP-4@3_6	0.003754	0.000010	38293	4.5	2.7	491.5	2.8280E-03
EXP-4@3_7	0.003758	0.000010	40511	5.6	2.6	491.5	3.0514E-03
EXP-4@3_8	0.003751	0.000010	39206	3.7	2.6	491.5	2.9902E-03
EXP-4@3_9	0.003745	0.000010	39309	2.1	2.6	491.5	3.0330E-03
EXP-4@3_10	0.003744	0.000010	38359	1.9	2.7	491.5	2.9995E-03
EXP-4@3_11	0.003750	0.000010	40729	3.5	2.6	491.5	3.2228E-03
EXP-4@3_12	0.003754	0.000010	41170	4.5	2.6	491.5	3.2791E-03
EXP-4@3_13	0.003766	0.000010	41845	7.8	2.6	491.5	3.3660E-03
EXP-4@3_14	0.003740	0.000009	44509	0.8	2.5	491.5	3.6142E-03
EXP-4@3_15	0.003769	0.000009	47527	8.6	2.4	491.5	3.8798E-03
EXP-4@3_16	0.003742	0.000009	46890	1.3	2.4	491.5	3.8581E-03
EXP-4@3_17	0.003749	0.000009	44467	3.2	2.5	491.5	3.6827E-03
EXP-4@3_18	0.003738	0.000009	46532	0.3	2.4	491.5	3.8746E-03
EXP-4@3_19	0.003732	0.000009	47389	-1.3	2.4	491.5	3.9836E-03
EXP-4@3_20	0.003736	0.000013	23394	-0.3	3.4	491.5	3.9320E-03
August 2012 <SampleName:IAEA-KNO3> <Raster:2.0>							
EXP-4@12_1	0.003773	0.000010	42150	21.7	2.6	135.2	2.8114E-03
EXP-4@12_2	0.003744	0.000010	40620	13.8	2.6	135.2	2.7186E-03
EXP-4@12_3	0.003758	0.000010	39171	17.6	2.7	135.2	2.6259E-03
EXP-4@12_4	0.003737	0.000010	37283	11.9	2.7	135.2	2.5103E-03
EXP-4@12_5	0.003752	0.000010	35558	16.0	2.8	135.2	2.3986E-03
EXP-4@12_6	0.003754	0.000010	37315	16.5	2.7	135.2	2.5159E-03
EXP-4@12_7	0.003751	0.000010	38127	15.7	2.7	135.2	2.5677E-03
EXP-4@12_8	0.003760	0.000009	43405	18.1	2.5	135.2	2.9205E-03
EXP-4@12_9	0.003756	0.000009	44177	17.1	2.5	135.2	2.9779E-03
EXP-4@12_10	0.003749	0.000009	44844	15.2	2.5	135.2	3.0186E-03
EXP-4@12_11	0.003759	0.000009	45698	17.9	2.5	135.2	3.0962E-03
EXP-4@12_12	0.003773	0.000009	45140	21.7	2.5	135.2	3.0627E-03
EXP-4@12_13	0.003765	0.000010	42073	19.5	2.6	135.2	2.8660E-03
EXP-4@12_14	0.003752	0.000010	40547	16.0	2.6	135.2	2.7724E-03
EXP-4@12_15	0.003753	0.000010	37315	16.2	2.7	135.2	2.5532E-03
EXP-4@12_16	0.003743	0.000009	42536	13.5	2.6	135.2	2.9132E-03
EXP-4@12_17	0.003767	0.000010	41430	20.0	2.6	135.2	2.8381E-03
EXP-4@12_18	0.003791	0.000009	46090	26.5	2.5	135.2	3.1640E-03
EXP-4@12_19	0.003766	0.000009	43166	19.8	2.6	135.2	2.9730E-03
EXP-4@12_20	0.003757	0.000009	43007	17.3	2.6	135.2	2.9720E-03
EXP-4@7_1	0.003742	0.000011	33811	13.3	2.9	98.3	2.3167E-03
EXP-4@7_2	0.003743	0.000011	34257	13.5	2.9	98.3	2.3684E-03

Analysis no.	$n(^{15}N^{16}O_2^-)$ / $n(^{14}N^{16}O_2^-)$	1 σ	ion $^{14}N^{16}O_2^-$ (cps)	IMF (‰)	1 σ	Pre - sputtering Time (s)	$n(^{14}N^{16}O_2^-)$ / $n(Cs^+)$
EXP-4@7_3	0.003730	0.000011	33106	10.0	2.9	98.3	2.3008E-03
EXP-4@7_4	0.003753	0.000011	31044	16.2	3.0	98.3	2.1643E-03
EXP-4@7_5	0.003734	0.000012	25932	11.1	3.3	98.3	1.8113E-03
EXP-4@7_6	0.003734	0.000011	30923	11.1	3.0	98.3	2.1641E-03
EXP-4@7_7	0.003768	0.000010	37897	20.3	2.7	98.3	2.6547E-03
EXP-4@7_8	0.003764	0.000010	38594	19.2	2.7	98.3	2.7127E-03
EXP-4@7_9	0.003746	0.000009	42889	14.4	2.6	98.3	3.0167E-03
EXP-4@7_10	0.003739	0.000009	42381	12.5	2.6	98.3	2.9789E-03
EXP-4@7_11	0.003754	0.000010	39939	16.5	2.7	98.3	2.7998E-03
EXP-4@7_12	0.003752	0.000010	40367	16.0	2.6	98.3	2.8318E-03
EXP-4@7_13	0.003756	0.000010	37315	17.1	2.7	98.3	2.6222E-03
EXP-4@7_14	0.003770	0.000010	35087	20.9	2.8	98.3	2.4638E-03
EXP-4@7_15	0.003749	0.000011	30189	15.2	3.0	98.3	2.1133E-03
EXP-4@7_16	0.003755	0.000011	29866	16.8	3.1	98.3	2.0831E-03
EXP-4@7_17	0.003753	0.000010	37315	16.2	2.7	98.3	2.5952E-03
EXP-4@7_18	0.003773	0.000009	42849	21.7	2.6	98.3	2.9716E-03
EXP-4@7_19	0.003751	0.000009	43365	15.7	2.5	98.3	3.0117E-03
EXP-4@7_20	0.003750	0.000010	42112	15.4	2.6	98.3	2.9254E-03
EXP-4@8_1	0.003763	0.000010	38594	19.0	2.7	135.2	2.5706E-03
EXP-4@8_2	0.003757	0.000011	33729	17.3	2.9	135.2	2.2497E-03
EXP-4@8_3	0.003760	0.000011	34483	18.1	2.9	135.2	2.3089E-03
EXP-4@8_4	0.003758	0.000011	34625	17.6	2.9	135.2	2.3212E-03
EXP-4@8_5	0.003754	0.000011	31936	16.5	3.0	135.2	2.1473E-03
EXP-4@8_6	0.003756	0.000010	36840	17.1	2.8	135.2	2.4845E-03
EXP-4@8_7	0.003772	0.000010	37540	21.4	2.7	135.2	2.5381E-03
EXP-4@8_8	0.003782	0.000010	40331	24.1	2.7	135.2	2.7313E-03
EXP-4@8_9	0.003753	0.000010	39309	16.2	2.7	135.2	2.6547E-03
EXP-4@8_10	0.003774	0.000009	44136	21.9	2.5	135.2	2.9731E-03
EXP-4@8_11	0.003787	0.000009	44467	25.5	2.5	135.2	2.9968E-03
EXP-4@8_12	0.003774	0.000009	42771	21.9	2.6	135.2	2.8945E-03
EXP-4@8_13	0.003775	0.000010	41281	22.2	2.6	135.2	2.8074E-03
EXP-4@8_14	0.003766	0.000010	39413	19.8	2.7	135.2	2.6885E-03
EXP-4@8_15	0.003769	0.000010	36872	20.6	2.8	135.2	2.5205E-03
EXP-4@8_16	0.003781	0.000010	38260	23.8	2.7	135.2	2.6135E-03
EXP-4@8_17	0.003764	0.000010	40584	19.2	2.6	135.2	2.7820E-03
EXP-4@8_18	0.003748	0.000009	43007	14.9	2.6	135.2	2.9510E-03
EXP-4@8_19	0.003761	0.000009	47989	18.4	2.4	135.2	3.2952E-03
EXP-4@8_20	0.003802	0.000010	43007	29.5	2.6	135.2	2.9558E-03
August 2012 <SampleName:IAEA-KNO3> <Raster:5.0>							
EXP-4@9_1	0.003743	0.000011	31386	13.5	3.0	516.1	2.1572E-03
EXP-4@9_2	0.003688	0.000019	10866	-1.4	5.0	516.1	7.4949E-04
EXP-4@9_3	0.003762	0.000021	8498	18.7	5.8	516.1	5.8849E-04
EXP-4@9_4	0.003752	0.000023	7235	16.0	6.2	516.1	5.0173E-04

Analysis no.	$n(^{15}N^{16}O_2^-)$ / $n(^{14}N^{16}O_2^-)$	1 σ	ion $^{14}N^{16}O_2^-$ (cps)	IMF (‰)	1 σ	Pre - sputtering Time (s)	$n(^{14}N^{16}O_2^-)$ / $n(Cs^+)$
EXP-4@9_5	0.003711	0.000025	6299	4.9	6.6	516.1	4.3823E-04
EXP-4@9_6	0.003781	0.000026	5703	23.8	7.0	516.1	4.0092E-04
EXP-4@9_7	0.003712	0.000024	6653	5.1	6.5	516.1	4.6920E-04
EXP-4@9_8	0.003726	0.000020	9253	8.9	5.5	516.1	6.5498E-04
EXP-4@9_9	0.003704	0.000018	11639	3.0	4.9	516.1	8.2622E-04
EXP-4@9_10	0.003726	0.000017	13697	8.9	4.5	516.1	9.7834E-04
EXP-4@9_11	0.003695	0.000018	12246	0.5	4.8	516.1	8.7833E-04
EXP-4@9_12	0.003701	0.000020	9198	2.2	5.5	516.1	6.6203E-04
EXP-4@9_13	0.003758	0.000025	6342	17.6	6.7	516.1	4.5825E-04
EXP-4@9_14	0.003763	0.000029	4477	19.0	7.9	516.1	3.2336E-04
EXP-4@9_15	0.003736	0.000033	3527	11.6	8.9	516.1	2.5574E-04
EXP-4@9_16	0.003693	0.000035	3167	0.0	9.3	516.1	2.3016E-04
EXP-4@9_17	0.003728	0.000029	4418	9.5	7.9	516.1	3.2155E-04
EXP-4@9_18	0.003763	0.000027	5119	19.0	7.4	516.1	3.7391E-04
EXP-4@9_19	0.003701	0.000024	6382	2.2	6.6	516.1	4.6779E-04
EXP-4@9_20	0.003748	0.000021	8529	14.9	5.7	516.1	6.2625E-04
September 2012 <SampleName:USGS35-NaNO3> <Raster:2.0>							
EXP-5@11_20	0.003673	0.000011	32448	-3.5	2.9	135.2	2.2041E-03
EXP-5@11_1	0.003679	0.000014	20595	-1.9	3.7	135.2	1.4276E-03
EXP-5@11_2	0.003711	0.000014	20068	6.8	3.7	135.2	1.3914E-03
EXP-5@11_3	0.003693	0.000013	23174	1.9	3.5	135.2	1.6041E-03
EXP-5@11_4	0.003698	0.000013	22757	3.3	3.5	135.2	1.5696E-03
EXP-5@11_5	0.003696	0.000011	28949	2.7	3.1	135.2	1.9882E-03
EXP-5@11_6	0.003669	0.000013	20833	-4.6	3.6	135.2	1.4295E-03
EXP-5@11_7	0.003688	0.000012	27318	0.5	3.2	135.2	1.8722E-03
EXP-5@11_8	0.003683	0.000011	28906	-0.8	3.1	135.2	1.9792E-03
EXP-5@11_9	0.003709	0.000011	30947	6.2	3.0	135.2	2.1175E-03
EXP-5@11_10	0.003690	0.000011	29147	1.1	3.1	135.2	1.9882E-03
EXP-5@11_11	0.003708	0.000012	24717	6.0	3.4	135.2	1.6845E-03
EXP-5@11_12	0.003698	0.000012	26325	3.3	3.3	135.2	1.7920E-03
EXP-5@11_13	0.003719	0.000011	30899	9.0	3.0	135.2	2.0989E-03
EXP-5@11_14	0.003706	0.000013	23586	5.4	3.4	135.2	1.6025E-03
EXP-5@11_15	0.003701	0.000013	22058	4.1	3.6	135.2	1.4987E-03
EXP-5@11_16	0.003692	0.000015	16208	1.6	4.1	135.2	1.0994E-03
EXP-5@11_17	0.003691	0.000012	27060	1.4	3.2	135.2	1.8411E-03
EXP-5@11_18	0.003692	0.000012	27358	1.6	3.2	135.2	1.8588E-03
EXP-5@11_19	0.003698	0.000011	33922	3.3	2.9	135.2	2.3048E-03
September 2012 <SampleName:USGS35-NaNO3> <Raster:5.0>							
EXP-5@12_1	0.003656	0.000010	37411	-8.1	2.7	491.5	2.4798E-03
EXP-5@12_2	0.003661	0.000008	55247	-6.8	2.2	491.5	3.6300E-03
EXP-5@12_3	0.003664	0.000008	52960	-6.0	2.3	491.5	3.4853E-03
EXP-5@12_4	0.003684	0.000008	57624	-0.5	2.2	491.5	3.7905E-03

Analysis no.	$n(^{15}N^{16}O_2^-)$ / $n(^{14}N^{16}O_2^-)$	1 σ	ion $^{14}N^{16}O_2^-$ (cps)	IMF (‰)	1 σ	Pre - sputtering Time (s)	$n(^{14}N^{16}O_2^-)$ / $n(Cs^+)$
EXP-5@12_5	0.003682	0.000008	63144	-1.1	2.1	491.5	4.1592E-03
EXP-5@12_6	0.003680	0.000008	61152	-1.6	2.1	491.5	4.0280E-03
EXP-5@12_7	0.003670	0.000008	63426	-4.3	2.1	491.5	4.1873E-03
EXP-5@12_8	0.003682	0.000008	57076	-1.1	2.2	491.5	3.7758E-03
EXP-5@12_9	0.003679	0.000008	52744	-1.9	2.3	491.5	3.4932E-03
EXP-5@12_10	0.003677	0.000008	63853	-2.4	2.1	491.5	4.2424E-03
EXP-5@12_11	0.003716	0.000009	43809	8.1	2.5	491.5	2.9107E-03
EXP-5@12_12	0.003687	0.000008	58367	0.3	2.2	491.5	3.8709E-03
EXP-5@12_13	0.003683	0.000008	62377	-0.8	2.1	491.5	4.1217E-03
EXP-5@12_14	0.003686	0.000008	58998	0.0	2.2	491.5	3.8958E-03
EXP-5@12_15	0.003670	0.000008	58430	-4.3	2.2	491.5	3.8496E-03
EXP-5@12_16	0.003675	0.000008	65383	-3.0	2.1	491.5	4.3106E-03
EXP-5@12_17	0.003676	0.000008	62793	-2.7	2.1	491.5	4.1371E-03
EXP-5@12_18	0.003684	0.000007	70233	-0.5	2.0	491.5	4.6377E-03
EXP-5@12_19	0.003678	0.000008	61624	-2.2	2.1	491.5	4.0738E-03
EXP-5@12_20	0.003708	0.000014	18922	6.0	3.8	491.5	1.2515E-03
EXP-5@15_1	0.003686	0.000008	53014	0.0	2.3	491.5	3.7884E-03
EXP-5@15_2	0.003666	0.000008	57624	-5.4	2.2	491.5	4.1199E-03
EXP-5@15_3	0.003675	0.000008	55886	-3.0	2.2	491.5	3.9878E-03
EXP-5@15_4	0.003679	0.000008	57994	-1.9	2.2	491.5	4.1362E-03
EXP-5@15_5	0.003668	0.000008	61152	-4.9	2.1	491.5	4.3550E-03
EXP-5@15_6	0.003663	0.000008	59703	-6.2	2.1	491.5	4.2383E-03
EXP-5@15_7	0.003669	0.000008	64720	-4.6	2.1	491.5	4.5778E-03
EXP-5@15_8	0.003672	0.000008	65680	-3.8	2.0	491.5	4.6378E-03
EXP-5@15_9	0.003679	0.000007	67899	-1.9	2.0	491.5	4.7794E-03
EXP-5@15_10	0.003664	0.000008	64285	-6.0	2.1	491.5	4.5239E-03
EXP-5@15_11	0.003676	0.000007	66814	-2.7	2.0	491.5	4.6951E-03
EXP-5@15_12	0.003695	0.000008	66661	2.4	2.0	491.5	4.6697E-03
EXP-5@15_13	0.003667	0.000007	67821	-5.2	2.0	491.5	4.7578E-03
EXP-5@15_14	0.003674	0.000007	72863	-3.3	1.9	491.5	5.1214E-03
EXP-5@15_15	0.003668	0.000008	62377	-4.9	2.1	491.5	4.3833E-03
EXP-5@15_16	0.003687	0.000007	68293	0.3	2.0	491.5	4.7921E-03
EXP-5@15_17	0.003688	0.000007	67664	0.5	2.0	491.5	4.7525E-03
EXP-5@15_18	0.003681	0.000007	67743	-1.4	2.0	491.5	4.7512E-03
EXP-5@15_19	0.003682	0.000007	68293	-1.1	2.0	491.5	4.7898E-03
EXP-5@15_20	0.003694	0.000007	68214	2.2	2.0	491.5	4.7796E-03
September 2012 <SampleName:USGS35-NaNO3> <Raster:10.0>							
EXP-5@18_1	0.003681	0.000006	94665	-1.4	1.7	1474.6	6.4274E-03
EXP-5@18_2	0.003686	0.000011	29981	0.0	3.0	1474.6	2.0285E-03
EXP-5@18_3	0.003690	0.000007	80577	1.1	1.9	1474.6	5.4241E-03
EXP-5@18_4	0.003687	0.000006	89229	0.3	1.8	1474.6	5.9926E-03
EXP-5@18_5	0.003684	0.000006	103064	-0.5	1.6	1474.6	6.9234E-03
EXP-5@18_6	0.003685	0.000007	87025	-0.3	1.8	1474.6	5.8459E-03

Analysis no.	$n(^{15}N^{16}O_2^-)$ / $n(^{14}N^{16}O_2^-)$	1 σ	ion $^{14}N^{16}O_2^-$ (cps)	IMF (‰)	1 σ	Pre - sputtering Time (s)	$n(^{14}N^{16}O_2^-)$ / $n(Cs^+)$
EXP-5@18_7	0.003691	0.000006	97707	1.4	1.7	1474.6	6.6401E-03
EXP-5@18_8	0.003689	0.000006	98525	0.8	1.7	1474.6	6.7397E-03
EXP-5@18_9	0.003697	0.000007	83923	3.0	1.8	1474.6	5.6663E-03
EXP-5@18_10	0.003682	0.000008	58808	-1.1	2.2	1474.6	3.9495E-03
EXP-5@18_11	0.003684	0.000006	89229	-0.5	1.8	1474.6	5.9733E-03
EXP-5@18_12	0.003690	0.000006	103064	1.1	1.6	1474.6	6.8663E-03
EXP-5@21_1	0.003683	0.000010	37637	-0.8	2.7	1966.1	2.5394E-03
EXP-5@21_2	0.003653	0.000014	19906	-9.0	3.7	1966.1	1.3174E-03
EXP-5@21_3	0.003676	0.000011	32396	-2.7	2.9	1966.1	2.1402E-03
EXP-5@21_4	0.003679	0.000009	44467	-1.9	2.5	1966.1	2.9788E-03
EXP-5@21_5	0.003681	0.000009	46399	-1.4	2.4	1966.1	3.1204E-03
EXP-5@21_6	0.003663	0.000009	46266	-6.2	2.4	1966.1	3.0620E-03
EXP-5@21_7	0.003657	0.000009	46980	-7.9	2.4	1966.1	3.0862E-03
EXP-5@21_8	0.003683	0.000009	43809	-0.8	2.5	1966.1	2.8656E-03
EXP-5@21_9	0.003663	0.000009	42343	-6.2	2.5	1966.1	2.7548E-03
EXP-5@21_10	0.003671	0.000009	44509	-4.1	2.5	1966.1	2.8777E-03
EXP-5@21_11	0.003678	0.000009	41845	-2.2	2.6	1966.1	2.7013E-03
EXP-5@21_12	0.003667	0.000010	38966	-5.2	2.7	1966.1	2.5071E-03
September 2012 <SampleName:InHouse-NaNO3> <Raster:5.0>							
EXP-5@16_1	0.003724	0.000008	61964	-3.5	2.1	491.5	4.0477E-03
EXP-5@16_2	0.003744	0.000008	65457	1.9	2.0	491.5	4.3048E-03
EXP-5@16_3	0.003722	0.000007	70315	-4.0	2.0	491.5	4.6097E-03
EXP-5@16_4	0.003737	0.000007	70481	0.0	2.0	491.5	4.6436E-03
EXP-5@16_5	0.003724	0.000007	68214	-3.5	2.0	491.5	4.5571E-03
EXP-5@16_6	0.003718	0.000007	71487	-5.1	1.9	491.5	4.7867E-03
EXP-5@16_7	0.003718	0.000007	71318	-5.1	2.0	491.5	4.7754E-03
EXP-5@16_8	0.003727	0.000007	67664	-2.7	2.0	491.5	4.5256E-03
EXP-5@16_9	0.003737	0.000007	72863	0.0	1.9	491.5	4.8744E-03
EXP-5@16_10	0.003739	0.000007	69091	0.5	2.0	491.5	4.6189E-03
EXP-5@16_11	0.003717	0.000007	68293	-5.4	2.0	491.5	4.5697E-03
EXP-5@16_12	0.003727	0.000007	72776	-2.7	1.9	491.5	4.8641E-03
EXP-5@16_13	0.003725	0.000007	72084	-3.2	1.9	491.5	4.8145E-03
EXP-5@16_14	0.003722	0.000007	69334	-4.0	2.0	491.5	4.6255E-03
EXP-5@16_15	0.003719	0.000007	70068	-4.8	2.0	491.5	4.6713E-03
EXP-5@16_16	0.003735	0.000008	67044	-0.5	2.0	491.5	4.4697E-03
EXP-5@16_17	0.003724	0.000007	69091	-3.5	2.0	491.5	4.6009E-03
EXP-5@16_18	0.003737	0.000007	69415	0.0	2.0	491.5	4.6172E-03
EXP-5@16_19	0.003721	0.000007	69577	-4.3	2.0	491.5	4.6238E-03
EXP-5@16_20	0.003719	0.000007	70647	-4.8	2.0	491.5	4.6895E-03
September 2012 <SampleName:InHouse-NaNO3> <Raster:10.0>							
EXP-5@19_12	0.003657	0.000010	38459	-21.4	2.6	1474.6	2.4555E-03

Analysis no.	$n(^{15}N^{16}O_2^-)$ / $n(^{14}N^{16}O_2^-)$	1 σ	ion $^{14}N^{16}O_2^-$ (cps)	IMF (‰)	1 σ	Pre - sputtering Time (s)	$n(^{14}N^{16}O_2^-)$ / $n(Cs^+)$
EXP-5@19_1	0.003731	0.000006	97843	-1.6	1.7	1474.6	6.4303E-03
EXP-5@19_2	0.003724	0.000006	96234	-3.5	1.7	1474.6	6.3503E-03
EXP-5@19_3	0.003735	0.000007	84247	-0.5	1.8	1474.6	5.5418E-03
EXP-5@19_4	0.003735	0.000006	102479	-0.5	1.6	1474.6	6.7244E-03
EXP-5@19_5	0.003735	0.000006	95838	-0.5	1.7	1474.6	6.2702E-03
EXP-5@19_6	0.003713	0.000006	94665	-6.4	1.7	1474.6	6.1796E-03
EXP-5@19_7	0.003714	0.000007	83815	-6.2	1.8	1474.6	5.4591E-03
EXP-5@19_8	0.003711	0.000007	76668	-7.0	1.9	1474.6	4.9858E-03
EXP-5@19_9	0.003717	0.000006	94023	-5.4	1.7	1474.6	6.1089E-03
EXP-5@19_10	0.003712	0.000007	84902	-6.7	1.8	1474.6	5.4930E-03
EXP-5@19_11	0.003682	0.000007	68056	-14.7	2.0	1474.6	4.3837E-03
September 2012 <SampleName:IAEA-KNO3> <Raster:2.0>							
EXP-5@10_1	0.003732	0.000011	29912	10.6	3.1	135.2	2.0399E-03
EXP-5@10_2	0.003737	0.000011	29191	11.9	3.1	135.2	1.9973E-03
EXP-5@10_3	0.003743	0.000011	30329	13.5	3.0	135.2	2.0815E-03
EXP-5@10_4	0.003732	0.000011	30259	10.6	3.0	135.2	2.0787E-03
EXP-5@10_5	0.003739	0.000011	32216	12.5	2.9	135.2	2.2152E-03
EXP-5@10_6	0.003753	0.000011	31659	16.2	3.0	135.2	2.1790E-03
EXP-5@10_7	0.003762	0.000010	35233	18.7	2.8	135.2	2.4267E-03
EXP-5@10_8	0.003743	0.000010	36344	13.5	2.8	135.2	2.5109E-03
EXP-5@10_9	0.003761	0.000010	37995	18.4	2.7	135.2	2.6256E-03
EXP-5@10_10	0.003742	0.000010	37061	13.3	2.7	135.2	2.5647E-03
EXP-5@10_11	0.003732	0.000010	35707	10.6	2.8	135.2	2.4769E-03
EXP-5@10_12	0.003736	0.000010	35351	11.6	2.8	135.2	2.4563E-03
EXP-5@10_13	0.003742	0.000010	34769	13.3	2.8	135.2	2.4135E-03
EXP-5@10_14	0.003733	0.000010	35439	10.8	2.8	135.2	2.4607E-03
EXP-5@10_15	0.003717	0.000011	34201	6.5	2.9	135.2	2.3735E-03
EXP-5@10_16	0.003721	0.000011	34483	7.6	2.8	135.2	2.3908E-03
EXP-5@10_17	0.003728	0.000010	37572	9.5	2.7	135.2	2.6088E-03
EXP-5@10_18	0.003747	0.000010	36436	14.6	2.8	135.2	2.5269E-03
EXP-5@10_19	0.003733	0.000010	37897	10.8	2.7	135.2	2.6244E-03
EXP-5@10_20	0.003738	0.000010	36467	12.2	2.8	135.2	2.5272E-03
September 2012 <SampleName:IAEA-KNO3> <Raster:5.0>							
EXP-5@13_1	0.003718	0.000009	46576	6.8	2.4	491.5	3.0889E-03
EXP-5@13_2	0.003692	0.000009	46002	-0.3	2.5	491.5	3.0515E-03
EXP-5@13_3	0.003714	0.000009	50812	5.7	2.3	491.5	3.3759E-03
EXP-5@13_4	0.003688	0.000009	50609	-1.4	2.3	491.5	3.3586E-03
EXP-5@13_5	0.003711	0.000009	49959	4.9	2.4	491.5	3.3231E-03
EXP-5@13_6	0.003709	0.000009	51686	4.3	2.3	491.5	3.4450E-03
EXP-5@13_7	0.003707	0.000008	52637	3.8	2.3	491.5	3.5124E-03
EXP-5@13_8	0.003714	0.000009	50660	5.7	2.3	491.5	3.3836E-03
EXP-5@13_9	0.003713	0.000009	52424	5.4	2.3	491.5	3.4974E-03

Analysis no.	$n(^{15}N^{16}O_2^-)$ / $n(^{14}N^{16}O_2^-)$	1 σ	ion $^{14}N^{16}O_2^-$ (cps)	IMF (‰)	1 σ	Pre - sputtering Time (s)	$n(^{14}N^{16}O_2^-)$ / $n(Cs^+)$
EXP-5@13_10	0.003721	0.000008	61692	7.6	2.1	491.5	4.1185E-03
EXP-5@13_11	0.003717	0.000008	56596	6.5	2.2	491.5	3.7940E-03
EXP-5@13_12	0.003708	0.000008	56298	4.1	2.2	491.5	3.8038E-03
EXP-5@13_13	0.003718	0.000008	58618	6.8	2.2	491.5	3.9809E-03
EXP-5@13_14	0.003704	0.000008	54002	3.0	2.3	491.5	3.6776E-03
EXP-5@13_15	0.003712	0.000008	54225	5.1	2.3	491.5	3.6851E-03
EXP-5@13_16	0.003698	0.000008	54337	1.4	2.3	491.5	3.6875E-03
EXP-5@13_17	0.003710	0.000008	59574	4.6	2.2	491.5	4.0326E-03
EXP-5@13_18	0.003694	0.000008	54113	0.3	2.3	491.5	3.6579E-03
EXP-5@13_19	0.003716	0.000008	55536	6.2	2.2	491.5	3.7540E-03
EXP-5@13_20	0.003704	0.000008	59445	3.0	2.2	491.5	4.0108E-03
EXP-5@14_20	0.003701	0.000009	49080	2.2	2.4	491.5	3.5220E-03
EXP-5@14_1	0.003705	0.000009	43526	3.2	2.5	491.5	3.0990E-03
EXP-5@14_2	0.003696	0.000009	50812	0.8	2.3	491.5	3.6284E-03
EXP-5@14_3	0.003705	0.000009	49566	3.2	2.4	491.5	3.5463E-03
EXP-5@14_4	0.003695	0.000008	52852	0.5	2.3	491.5	3.7880E-03
EXP-5@14_5	0.003715	0.000009	42928	6.0	2.5	491.5	3.0798E-03
EXP-5@14_6	0.003694	0.000009	51169	0.3	2.3	491.5	3.6710E-03
EXP-5@14_7	0.003657	0.000009	45525	-9.7	2.5	491.5	3.2701E-03
EXP-5@14_8	0.003708	0.000009	49176	4.1	2.4	491.5	3.5411E-03
EXP-5@14_9	0.003707	0.000009	44384	3.8	2.5	491.5	3.1960E-03
EXP-5@14_10	0.003720	0.000009	45310	7.3	2.5	491.5	3.2547E-03
EXP-5@14_11	0.003693	0.000008	53014	0.0	2.3	491.5	3.8071E-03
EXP-5@14_12	0.003691	0.000009	48036	-0.5	2.4	491.5	3.4488E-03
EXP-5@14_13	0.003713	0.000009	51843	5.4	2.3	491.5	3.7267E-03
EXP-5@14_14	0.003704	0.000009	50158	3.0	2.4	491.5	3.6127E-03
EXP-5@14_15	0.003699	0.000009	45654	1.6	2.5	491.5	3.2818E-03
EXP-5@14_16	0.003699	0.000009	44219	1.6	2.5	491.5	3.1849E-03
EXP-5@14_17	0.003709	0.000009	48506	4.3	2.4	491.5	3.4929E-03
EXP-5@14_18	0.003706	0.000009	51324	3.5	2.3	491.5	3.6930E-03
EXP-5@14_19	0.003709	0.000009	48223	4.3	2.4	491.5	3.4614E-03
September 2012 <SampleName:IAEA-KNO3> <Raster:10.0>							
EXP-5@17_1	0.003696	0.000010	41618	0.8	2.6	1474.6	2.7327E-03
EXP-5@17_2	0.003707	0.000009	44717	3.8	2.5	1474.6	2.9243E-03
EXP-5@17_3	0.003706	0.000010	39103	3.5	2.7	1474.6	2.5463E-03
EXP-5@17_4	0.003709	0.000009	42614	4.3	2.6	1474.6	2.7669E-03
EXP-5@17_5	0.003701	0.000009	46755	2.2	2.4	1474.6	3.0277E-03
EXP-5@17_6	0.003706	0.000009	43972	3.5	2.5	1474.6	2.8405E-03
EXP-5@17_7	0.003716	0.000009	45055	6.2	2.5	1474.6	2.9002E-03
EXP-5@17_8	0.003709	0.000010	39939	4.3	2.6	1474.6	2.5714E-03
EXP-5@17_9	0.003683	0.000010	39552	-2.7	2.6	1474.6	2.5415E-03
EXP-5@17_10	0.003681	0.000010	40547	-3.2	2.6	1474.6	2.5991E-03
EXP-5@17_11	0.003694	0.000009	45268	0.3	2.5	1474.6	2.8991E-03

Analysis no.	$n(^{15}N^{16}O_2^-)$ / $n(^{14}N^{16}O_2^-)$	1 σ	ion $^{14}N^{16}O_2^-$ (cps)	IMF (‰)	1 σ	Pre - sputtering Time (s)	$n(^{14}N^{16}O_2^-)$ / $n(Cs^+)$
EXP-5@17_12	0.003708	0.000009	42653	4.1	2.6	1474.6	2.7233E-03
EXP-5@20_1	0.003717	0.000013	22189	6.5	3.5	1966.1	1.5951E-03
EXP-5@20_2	0.003681	0.000013	21572	-3.2	3.6	1966.1	1.5488E-03
EXP-5@20_3	0.003692	0.000013	21089	-0.3	3.6	1966.1	1.5167E-03
EXP-5@20_4	0.003712	0.000012	27682	5.1	3.2	1966.1	1.9835E-03
EXP-5@20_5	0.003688	0.000012	27601	-1.4	3.2	1966.1	1.9704E-03
EXP-5@20_6	0.003708	0.000012	26611	4.1	3.2	1966.1	1.8919E-03
EXP-5@20_7	0.003700	0.000012	28475	1.9	3.1	1966.1	2.0200E-03
EXP-5@20_8	0.003705	0.000013	22788	3.2	3.5	1966.1	1.6071E-03
EXP-5@20_9	0.003725	0.000012	28053	8.7	3.2	1966.1	1.9728E-03
EXP-5@20_10	0.003680	0.000012	28347	-3.5	3.1	1966.1	1.9801E-03
EXP-5@20_11	0.003689	0.000011	29235	-1.1	3.1	1966.1	2.0348E-03
EXP-5@20_12	0.003703	0.000011	33294	2.7	2.9	1966.1	2.3045E-03
October 2012 <SampleName:USGS35-NaNO3> <Raster:2.0>							
EXP-6@2_1	0.003679	0.000015	17507	-1.9	4.0	61.4	1.2202E-03
EXP-6@2_2	0.003695	0.000015	16780	2.4	4.1	61.4	1.1671E-03
EXP-6@2_3	0.003675	0.000019	10237	-3.0	5.2	61.4	7.1267E-04
EXP-6@2_4	0.003667	0.000021	8233	-5.2	5.8	61.4	5.7275E-04
EXP-6@2_5	0.003682	0.000014	19696	-1.1	3.7	61.4	1.3652E-03
EXP-6@2_6	0.003680	0.000013	21021	-1.6	3.6	61.4	1.4551E-03
EXP-6@2_7	0.003682	0.000018	11694	-1.1	4.9	61.4	8.0909E-04
EXP-6@2_8	0.003697	0.000015	16373	3.0	4.1	61.4	1.1315E-03
EXP-6@2_9	0.003684	0.000014	18739	-0.5	3.8	61.4	1.2952E-03
EXP-6@2_10	0.003658	0.000015	17163	-7.6	4.0	61.4	1.1883E-03
EXP-6@2_11	0.003664	0.000016	14797	-6.0	4.3	61.4	1.0230E-03
EXP-6@2_12	0.003742	0.000020	9329	15.2	5.5	61.4	6.4481E-04
EXP-6@2_13	0.003673	0.000015	16026	-3.5	4.2	61.4	1.1104E-03
EXP-6@2_14	0.003691	0.000017	12477	1.4	4.7	61.4	8.6367E-04
EXP-6@2_15	0.003688	0.000017	13287	0.5	4.6	61.4	9.1995E-04
EXP-6@2_16	0.003713	0.000020	9210	7.3	5.5	61.4	6.3781E-04
EXP-6@2_17	0.003942	0.000025	6701	69.5	6.6	61.4	4.6308E-04
EXP-6@2_18	0.003758	0.000037	2745	19.5	10.1	61.4	1.8960E-04
EXP-6@2_19	0.003741	0.000026	5866	14.9	6.9	61.4	4.0539E-04
EXP-6@2_20	0.003757	0.000029	4459	19.3	8.0	61.4	3.0804E-04
EXP-6@3_1	0.003795	0.000026	5631	29.6	7.1	61.4	3.3437E-04
EXP-6@3_2	0.003726	0.000023	7084	10.9	6.3	61.4	4.3132E-04
EXP-6@3_3	0.003685	0.000017	12434	-0.3	4.7	61.4	7.6863E-04
EXP-6@3_4	0.003690	0.000025	5984	1.1	6.8	61.4	3.7289E-04
EXP-6@3_5	0.003720	0.000019	10256	9.2	5.2	61.4	6.4295E-04
EXP-6@3_6	0.003669	0.000016	15457	-4.6	4.2	61.4	9.7366E-04
EXP-6@3_7	0.003695	0.000015	16656	2.4	4.1	61.4	1.0505E-03
EXP-6@3_8	0.003668	0.000015	16965	-4.9	4.0	61.4	1.0721E-03

Analysis no.	$n(^{15}N^{16}O_2^-)$ / $n(^{14}N^{16}O_2^-)$	1 σ	ion $^{14}N^{16}O_2^-$ (cps)	IMF (‰)	1 σ	Pre - sputtering Time (s)	$n(^{14}N^{16}O_2^-)$ / $n(Cs^+)$
EXP-6@3_9	0.003709	0.000017	12459	6.2	4.7	61.4	7.8907E-04
EXP-6@3_10	0.003706	0.000016	15603	5.4	4.2	61.4	9.9034E-04
EXP-6@3_11	0.003710	0.000016	14991	6.5	4.3	61.4	9.5335E-04
EXP-6@3_12	0.003647	0.000017	12812	-10.6	4.6	61.4	8.1584E-04
EXP-6@3_13	0.003700	0.000018	11143	3.8	5.0	61.4	7.1050E-04
EXP-6@3_14	0.003680	0.000016	14475	-1.6	4.4	61.4	9.2421E-04
EXP-6@3_15	0.003682	0.000015	16618	-1.1	4.1	61.4	1.0643E-03
EXP-6@3_16	0.003688	0.000017	12948	0.5	4.6	61.4	8.3050E-04
EXP-6@3_17	0.003669	0.000017	12728	-4.6	4.7	61.4	8.1860E-04
EXP-6@3_18	0.003680	0.000018	12174	-1.6	4.8	61.4	7.8590E-04
EXP-6@3_19	0.003666	0.000019	10668	-5.4	5.1	61.4	6.9345E-04
EXP-6@3_20	0.003664	0.000020	9218	-6.0	5.5	61.4	6.0200E-04
EXP-6@7_1	0.003705	0.000036	2906	5.2	9.8	86	2.0506E-04
EXP-6@7_2	0.003746	0.000036	2975	16.3	9.7	86	2.1041E-04
EXP-6@7_3	0.003833	0.000036	2949	39.9	9.9	86	2.0910E-04
EXP-6@7_4	0.003649	0.000030	4228	-10.0	8.1	86	3.0072E-04
EXP-6@7_5	0.003807	0.000044	2053	32.8	11.8	86	1.4609E-04
EXP-6@7_6	0.003728	0.000035	3066	11.4	9.6	86	2.1851E-04
EXP-6@7_7	0.003742	0.000041	2279	15.2	11.1	86	1.6244E-04
EXP-6@7_8	0.003723	0.000042	2177	10.0	11.3	86	1.5520E-04
EXP-6@7_9	0.003680	0.000036	2822	-1.6	9.9	86	2.0101E-04
EXP-6@7_10	0.003843	0.000044	2006	42.6	12.0	86	1.4299E-04
EXP-6@7_11	0.003810	0.000046	1838	33.6	12.5	86	1.3095E-04
EXP-6@7_12	0.003829	0.000047	1794	38.8	12.7	86	1.2802E-04
EXP-6@7_13	0.003843	0.000048	1669	42.6	13.2	86	1.1888E-04
EXP-6@7_14	0.003848	0.000055	1300	44.0	14.9	86	9.2694E-05
EXP-6@7_15	0.003840	0.000063	994	41.8	17.0	86	7.0720E-05
EXP-6@7_16	0.003823	0.000065	916	37.2	17.7	86	6.5310E-05
EXP-6@7_17	0.003899	0.000071	788	57.8	19.3	86	5.6105E-05
EXP-6@7_18	0.003747	0.000049	1610	16.5	13.2	86	1.1460E-04
EXP-6@7_19	0.003770	0.000043	2113	22.8	11.6	86	1.5043E-04
EXP-6@7_20	0.003766	0.000049	1582	21.7	13.4	86	1.1262E-04
October 2012 <SampleName:USGS35-NaNO3> <Raster:5.0>							
EXP-6@10_1	0.003663	0.000016	14694	-6.2	4.3	847.9	1.0376E-03
EXP-6@10_2	0.003683	0.000021	8790	-0.8	5.6	847.9	6.2203E-04
EXP-6@10_3	0.003705	0.000026	5631	5.2	7.0	847.9	3.9817E-04
EXP-6@10_4	0.003672	0.000015	17083	-3.8	4.0	847.9	1.2148E-03
EXP-6@10_5	0.003686	0.000017	13342	0.0	4.6	847.9	9.4807E-04
EXP-6@10_6	0.003675	0.000021	8270	-3.0	5.8	847.9	5.8981E-04
EXP-6@10_7	0.003710	0.000020	9048	6.5	5.6	847.9	6.4655E-04
EXP-6@10_8	0.003717	0.000021	8732	8.4	5.7	847.9	6.2398E-04
EXP-6@10_9	0.003723	0.000024	6382	10.0	6.6	847.9	4.5754E-04
EXP-6@10_10	0.003757	0.000032	3740	19.3	8.7	847.9	2.6828E-04

Analysis no.	$n(^{15}N^{16}O_2^-)$ / $n(^{14}N^{16}O_2^-)$	1 σ	ion $^{14}N^{16}O_2^-$ (cps)	IMF (‰)	1 σ	Pre - sputtering Time (s)	$n(^{14}N^{16}O_2^-)$ / $n(Cs^+)$
EXP-6@10_11	0.003708	0.000042	2160	6.0	11.4	847.9	1.5494E-04
EXP-6@10_12	0.003763	0.000031	3985	20.9	8.4	847.9	2.8605E-04
EXP-6@10_13	0.003693	0.000034	3311	1.9	9.2	847.9	2.3823E-04
EXP-6@10_14	0.003731	0.000037	2765	12.2	10.1	847.9	1.9871E-04
EXP-6@10_15	0.003759	0.000047	1761	19.8	12.7	847.9	1.2658E-04
EXP-6@10_16	0.003793	0.000031	4146	29.0	8.3	847.9	2.9907E-04
EXP-6@10_17	0.003699	0.000040	2372	3.5	10.8	847.9	1.7111E-04
EXP-6@10_18	0.003727	0.000042	2192	11.1	11.3	847.9	1.5820E-04
EXP-6@10_19	0.003830	0.000054	1347	39.1	14.6	847.9	9.7136E-05
EXP-6@10_20	0.003802	0.000033	3610	31.5	8.9	847.9	2.6093E-04
October 2012 <SampleName:InHouse-NaNO3> <Raster:2.0>							
EXP-6@1_1	0.003727	0.000010	38160	-2.7	2.7	61.4	2.7209E-03
EXP-6@1_2	0.003706	0.000010	37930	-8.3	2.7	61.4	2.7052E-03
EXP-6@1_3	0.003722	0.000010	39798	-4.0	2.6	61.4	2.8356E-03
EXP-6@1_4	0.003737	0.000010	40620	0.0	2.6	61.4	2.9020E-03
EXP-6@1_5	0.003733	0.000009	43687	-1.1	2.5	61.4	3.1189E-03
EXP-6@1_6	0.003732	0.000010	38661	-1.3	2.7	61.4	2.7668E-03
EXP-6@1_7	0.003737	0.000009	42498	0.0	2.5	61.4	3.0406E-03
EXP-6@1_8	0.003723	0.000010	42073	-3.7	2.5	61.4	3.0110E-03
EXP-6@1_9	0.003740	0.000010	42035	0.8	2.6	61.4	3.0105E-03
EXP-6@1_10	0.003713	0.000010	38898	-6.4	2.6	61.4	2.7844E-03
EXP-6@1_11	0.003722	0.000010	38762	-4.0	2.6	61.4	2.7809E-03
EXP-6@1_12	0.003725	0.000010	34568	-3.2	2.8	61.4	2.4763E-03
EXP-6@1_13	0.003731	0.000010	37283	-1.6	2.7	61.4	2.6774E-03
EXP-6@1_14	0.003740	0.000010	37219	0.8	2.7	61.4	2.6702E-03
EXP-6@1_15	0.003726	0.000010	35558	-2.9	2.8	61.4	2.5554E-03
EXP-6@1_16	0.003724	0.000010	34826	-3.5	2.8	61.4	2.5034E-03
EXP-6@1_17	0.003730	0.000011	34173	-1.9	2.8	61.4	2.4589E-03
EXP-6@1_18	0.003701	0.000011	30636	-9.6	3.0	61.4	2.2066E-03
EXP-6@1_19	0.003721	0.000012	26573	-4.3	3.2	61.4	1.9163E-03
EXP-6@1_20	0.003738	0.000013	24326	0.3	3.4	61.4	1.7577E-03
EXP-6@8_1	0.003722	0.000010	40839	-4.0	2.6	86	2.8546E-03
EXP-6@8_2	0.003736	0.000010	40620	-0.3	2.6	86	2.8291E-03
EXP-6@8_3	0.003734	0.000010	40010	-0.8	2.6	86	2.7773E-03
EXP-6@8_4	0.003710	0.000010	41656	-7.2	2.6	86	2.8951E-03
EXP-6@8_5	0.003720	0.000010	39103	-4.5	2.6	86	2.7137E-03
EXP-6@8_6	0.003712	0.000010	38459	-6.7	2.7	86	2.6634E-03
EXP-6@8_7	0.003704	0.000010	40511	-8.8	2.6	86	2.7995E-03
EXP-6@8_8	0.003719	0.000009	43405	-4.8	2.5	86	2.9959E-03
EXP-6@8_9	0.003720	0.000009	45225	-4.5	2.5	86	3.1223E-03
EXP-6@8_10	0.003710	0.000009	45225	-7.2	2.4	86	3.1149E-03
EXP-6@8_11	0.003714	0.000009	43850	-6.2	2.5	86	3.0159E-03
EXP-6@8_12	0.003718	0.000009	42692	-5.1	2.5	86	2.9467E-03

Analysis no.	$n(^{15}N^{16}O_2^-)$ / $n(^{14}N^{16}O_2^-)$	1 σ	ion $^{14}N^{16}O_2^-$ (cps)	IMF (‰)	1 σ	Pre - sputtering Time (s)	$n(^{14}N^{16}O_2^-)$ / $n(Cs^+)$
EXP-6@8_13	0.003713	0.000010	40985	-6.4	2.6	86	2.8242E-03
EXP-6@8_14	0.003715	0.000010	38796	-5.9	2.6	86	2.6791E-03
EXP-6@8_15	0.003711	0.000011	33053	-7.0	2.9	86	2.2835E-03
EXP-6@8_16	0.003703	0.000012	25803	-9.1	3.2	86	1.7826E-03
EXP-6@8_17	0.003681	0.000011	30143	-15.0	3.0	86	2.0820E-03
EXP-6@8_18	0.003711	0.000011	33811	-7.0	2.8	86	2.3398E-03
EXP-6@8_19	0.003716	0.000010	40403	-5.6	2.6	86	2.7894E-03
EXP-6@8_20	0.003703	0.000010	41356	-9.1	2.6	86	2.8592E-03
October 2012 <SampleName:InHouse-NaNO3> <Raster:5.0>							
EXP-6@14_1	0.003718	0.000007	75367	-5.1	1.9	368.6	5.0675E-03
EXP-6@14_2	0.003721	0.000007	73125	-4.3	1.9	368.6	4.9293E-03
EXP-6@14_3	0.003711	0.000007	71998	-7.0	1.9	368.6	4.8556E-03
EXP-6@14_4	0.003708	0.000008	64793	-7.8	2.0	368.6	4.3849E-03
EXP-6@14_5	0.003706	0.000007	73213	-8.3	1.9	368.6	4.9627E-03
EXP-6@14_6	0.003709	0.000007	69253	-7.5	2.0	368.6	4.6867E-03
EXP-6@14_7	0.003710	0.000007	70481	-7.2	2.0	368.6	4.7709E-03
EXP-6@14_8	0.003701	0.000007	77332	-9.6	1.9	368.6	5.2444E-03
EXP-6@14_9	0.003710	0.000007	79473	-7.2	1.8	368.6	5.4034E-03
EXP-6@14_10	0.003721	0.000007	72689	-4.3	1.9	368.6	4.9456E-03
EXP-6@14_11	0.003711	0.000007	73566	-7.0	1.9	368.6	4.9983E-03
EXP-6@14_12	0.003721	0.000007	71403	-4.3	2.0	368.6	4.8468E-03
EXP-6@14_13	0.003712	0.000007	79972	-6.7	1.8	368.6	5.4310E-03
EXP-6@14_14	0.003720	0.000007	74639	-4.5	1.9	368.6	5.0831E-03
EXP-6@14_15	0.003698	0.000007	72342	-10.4	1.9	368.6	4.9336E-03
EXP-6@14_16	0.003711	0.000008	63639	-7.0	2.1	368.6	4.3299E-03
EXP-6@14_17	0.003724	0.000007	69172	-3.5	2.0	368.6	4.7108E-03
EXP-6@14_18	0.003714	0.000007	77141	-6.2	1.9	368.6	5.2695E-03
EXP-6@14_19	0.003711	0.000007	74639	-7.0	1.9	368.6	5.1057E-03
EXP-6@14_20	0.003715	0.000007	73389	-5.9	1.9	368.6	5.0297E-03
EXP-6@9_1	0.003702	0.000009	43809	-9.4	2.5	847.9	3.0124E-03
EXP-6@9_2	0.003708	0.000008	55305	-7.8	2.2	847.9	3.8200E-03
EXP-6@9_3	0.003732	0.000008	53068	-1.3	2.3	847.9	3.6672E-03
EXP-6@9_4	0.003719	0.000009	50965	-4.8	2.3	847.9	3.5185E-03
EXP-6@9_5	0.003730	0.000008	54732	-1.9	2.2	847.9	3.7733E-03
EXP-6@9_6	0.003720	0.000008	53450	-4.5	2.3	847.9	3.6944E-03
EXP-6@9_7	0.003716	0.000008	57809	-5.6	2.2	847.9	4.0005E-03
EXP-6@9_8	0.003721	0.000008	58744	-4.3	2.2	847.9	4.0730E-03
EXP-6@9_9	0.003710	0.000008	57502	-7.2	2.2	847.9	3.9887E-03
EXP-6@9_10	0.003717	0.000009	49566	-5.4	2.3	847.9	3.4489E-03
EXP-6@9_11	0.003722	0.000009	47573	-4.0	2.4	847.9	3.3134E-03
EXP-6@9_12	0.003716	0.000008	60093	-5.6	2.1	847.9	4.1854E-03
EXP-6@9_13	0.003732	0.000008	57747	-1.3	2.2	847.9	4.0144E-03
EXP-6@9_14	0.003733	0.000008	54846	-1.1	2.2	847.9	3.8246E-03
EXP-6@9_15	0.003714	0.000008	54903	-6.2	2.2	847.9	3.8442E-03

Analysis no.	$n(^{15}N^{16}O_2^-)$ / $n(^{14}N^{16}O_2^-)$	1 σ	ion $^{14}N^{16}O_2^-$ (cps)	IMF (‰)	1 σ	Pre - sputtering Time (s)	$n(^{14}N^{16}O_2^-)$ / $n(Cs^+)$
EXP-6@9_16	0.003727	0.000009	49322	-2.7	2.4	847.9	3.4567E-03
EXP-6@9_17	0.003712	0.000008	56715	-6.7	2.2	847.9	3.9710E-03
EXP-6@9_18	0.003722	0.000008	53946	-4.0	2.2	847.9	3.7835E-03
EXP-6@9_19	0.003714	0.000008	57624	-6.2	2.2	847.9	4.0435E-03
EXP-6@9_20	0.003709	0.000008	58744	-7.5	2.1	847.9	4.1340E-03
October 2012 <SampleName:IAEA-KNO3> <Raster:2.0>							
EXP-6@4_1	0.003685	0.000009	44054	-2.2	2.5	61.4	2.8822E-03
EXP-6@4_2	0.003713	0.000011	30707	5.4	3.0	61.4	2.0136E-03
EXP-6@4_3	0.003696	0.000009	43047	0.8	2.5	61.4	2.8227E-03
EXP-6@4_4	0.003693	0.000010	34769	0.0	2.8	61.4	2.3021E-03
EXP-6@4_5	0.003702	0.000010	39069	2.4	2.7	61.4	2.6263E-03
EXP-6@4_6	0.003688	0.000011	29912	-1.4	3.0	61.4	2.0187E-03
EXP-6@4_7	0.003695	0.000010	34511	0.5	2.8	61.4	2.3339E-03
EXP-6@4_8	0.003689	0.000011	33321	-1.1	2.9	61.4	2.2581E-03
EXP-6@4_9	0.003700	0.000011	31461	1.9	3.0	61.4	2.1385E-03
EXP-6@4_10	0.003677	0.000011	32396	-4.3	2.9	61.4	2.2068E-03
EXP-6@4_11	0.003690	0.000011	32526	-0.8	2.9	61.4	2.2156E-03
EXP-6@4_12	0.003697	0.000011	32012	1.1	2.9	61.4	2.1898E-03
EXP-6@4_13	0.003698	0.000011	34005	1.4	2.9	61.4	2.3273E-03
EXP-6@4_14	0.003695	0.000010	35351	0.5	2.8	61.4	2.4193E-03
EXP-6@4_15	0.003691	0.000010	37864	-0.5	2.7	61.4	2.5950E-03
EXP-6@4_16	0.003693	0.000011	32293	0.0	2.9	61.4	2.2158E-03
EXP-6@4_17	0.003684	0.000010	37995	-2.4	2.7	61.4	2.6200E-03
EXP-6@4_18	0.003684	0.000010	40875	-2.4	2.6	61.4	2.8213E-03
EXP-6@4_19	0.003684	0.000010	37540	-2.4	2.7	61.4	2.5966E-03
EXP-6@4_20	0.003683	0.000009	44054	-2.7	2.5	61.4	3.0479E-03
EXP-6@5_1	0.003690	0.000010	36560	-0.8	2.7	86	2.5342E-03
EXP-6@5_2	0.003684	0.000010	35351	-2.4	2.8	86	2.4616E-03
EXP-6@5_3	0.003662	0.000010	35617	-8.4	2.8	86	2.4861E-03
EXP-6@5_4	0.003688	0.000010	36653	-1.4	2.7	86	2.5547E-03
EXP-6@5_5	0.003701	0.000010	35528	2.2	2.8	86	2.4745E-03
EXP-6@5_6	0.003673	0.000010	38426	-5.4	2.7	86	2.6757E-03
EXP-6@5_7	0.003706	0.000010	39903	3.5	2.6	86	2.7786E-03
EXP-6@5_8	0.003693	0.000010	39240	0.0	2.7	86	2.7337E-03
EXP-6@5_9	0.003680	0.000010	37156	-3.5	2.7	86	2.5891E-03
EXP-6@5_10	0.003679	0.000010	41281	-3.8	2.6	86	2.8766E-03
EXP-6@5_11	0.003695	0.000010	35767	0.5	2.8	86	2.4941E-03
EXP-6@5_12	0.003670	0.000010	36529	-6.2	2.7	86	2.5479E-03
EXP-6@5_13	0.003698	0.000010	36998	1.4	2.7	86	2.5836E-03
EXP-6@5_14	0.003687	0.000010	36221	-1.6	2.8	86	2.5270E-03
EXP-6@5_15	0.003689	0.000010	37864	-1.1	2.7	86	2.6435E-03
EXP-6@5_16	0.003698	0.000010	34884	1.4	2.8	86	2.4390E-03
EXP-6@5_17	0.003700	0.000010	37767	1.9	2.7	86	2.6450E-03

Analysis no.	$n(^{15}N^{16}O_2^-)$ / $n(^{14}N^{16}O_2^-)$	1 σ	ion $^{14}N^{16}O_2^-$ (cps)	IMF (‰)	1 σ	Pre - sputtering Time (s)	$n(^{14}N^{16}O_2^-)$ / $n(Cs^+)$
EXP-6@5_18	0.003686	0.000010	35087	-1.9	2.8	86	2.4602E-03
EXP-6@5_19	0.003701	0.000010	37572	2.2	2.7	86	2.6383E-03
EXP-6@5_20	0.003679	0.000010	36966	-3.8	2.7	86	2.5914E-03
EXP-6@6_1	0.003705	0.000011	33922	3.2	2.9	86	2.3576E-03
EXP-6@6_2	0.003696	0.000010	36282	0.8	2.8	86	2.5078E-03
EXP-6@6_3	0.003697	0.000010	35797	1.1	2.8	86	2.4784E-03
EXP-6@6_4	0.003685	0.000010	35677	-2.2	2.8	86	2.4748E-03
EXP-6@6_5	0.003711	0.000011	32526	4.9	2.9	86	2.2579E-03
EXP-6@6_6	0.003690	0.000010	34540	-0.8	2.8	86	2.3931E-03
EXP-6@6_7	0.003696	0.000011	33729	0.8	2.9	86	2.3408E-03
EXP-6@6_8	0.003703	0.000010	37897	2.7	2.7	86	2.6238E-03
EXP-6@6_9	0.003686	0.000010	34370	-1.9	2.8	86	2.3745E-03
EXP-6@6_10	0.003699	0.000010	38094	1.6	2.7	86	2.6362E-03
EXP-6@6_11	0.003686	0.000010	36715	-1.9	2.7	86	2.5408E-03
EXP-6@6_12	0.003707	0.000010	35737	3.8	2.8	86	2.4760E-03
EXP-6@6_13	0.003713	0.000010	36282	5.4	2.8	86	2.5138E-03
EXP-6@6_14	0.003682	0.000010	35000	-3.0	2.8	86	2.4290E-03
EXP-6@6_15	0.003699	0.000011	32293	1.6	2.9	86	2.2460E-03
EXP-6@6_16	0.003698	0.000010	36038	1.4	2.8	86	2.5106E-03
EXP-6@6_17	0.003694	0.000010	35917	0.3	2.8	86	2.5064E-03
EXP-6@6_18	0.003684	0.000009	44384	-2.4	2.5	86	3.1032E-03
EXP-6@6_19	0.003705	0.000010	40547	3.2	2.6	86	2.8397E-03
EXP-6@6_20	0.003703	0.000009	42928	2.7	2.5	86	3.0137E-03
October 2012 <SampleName:IAEA-KNO3> <Raster:5.0>							
EXP-6@11_1	0.003679	0.000012	27744	-3.8	3.2	847.9	4.0273E-05
EXP-6@11_2	0.003685	0.000011	32165	-2.2	2.9	847.9	2.2729E-03
EXP-6@11_3	0.003687	0.000011	32037	-1.6	2.9	847.9	2.2617E-03
EXP-6@11_4	0.003676	0.000010	37897	-4.6	2.7	847.9	2.6943E-03
EXP-6@11_5	0.003670	0.000010	40045	-6.2	2.6	847.9	2.8694E-03
EXP-6@11_6	0.003673	0.000010	35707	-5.4	2.8	847.9	2.5680E-03
EXP-6@11_7	0.003679	0.000009	42692	-3.8	2.5	847.9	3.1049E-03
EXP-6@11_8	0.003679	0.000009	41845	-3.8	2.6	847.9	3.0810E-03
EXP-6@11_9	0.003679	0.000010	37188	-3.8	2.7	847.9	2.7492E-03
EXP-6@11_10	0.003695	0.000012	27970	0.5	3.1	847.9	2.0662E-03
EXP-6@11_11	0.003687	0.000010	34229	-1.6	2.8	847.9	2.5336E-03
EXP-6@11_12	0.003679	0.000010	38560	-3.8	2.7	847.9	2.8535E-03
EXP-6@11_13	0.003672	0.000009	50710	-5.7	2.3	847.9	3.7375E-03
EXP-6@11_14	0.003677	0.000010	37251	-4.3	2.7	847.9	2.7365E-03
EXP-6@11_15	0.003678	0.000009	47389	-4.1	2.4	847.9	3.4901E-03
EXP-6@11_16	0.003680	0.000009	44095	-3.5	2.5	847.9	3.2499E-03
EXP-6@11_17	0.003691	0.000009	42381	-0.5	2.6	847.9	3.1244E-03
EXP-6@11_18	0.003693	0.000009	47252	0.0	2.4	847.9	3.4791E-03
EXP-6@11_19	0.003682	0.000010	39448	-3.0	2.6	847.9	2.9074E-03

Analysis no.	$n(^{15}N^{16}O_2^-)$ / $n(^{14}N^{16}O_2^-)$	1 σ	ion $^{14}N^{16}O_2^-$ (cps)	IMF (‰)	1 σ	Pre - sputtering Time (s)	$n(^{14}N^{16}O_2^-)$ / $n(Cs^+)$
EXP-6@11_20	0.003700	0.000010	38160	1.9	2.7	847.9	2.8146E-03
EXP-6@12_1	0.003692	0.000011	33106	-0.3	2.9	368.6	2.3999E-03
EXP-6@12_2	0.003676	0.000010	38426	-4.6	2.7	368.6	2.7704E-03
EXP-6@12_3	0.003687	0.000009	44054	-1.6	2.5	368.6	3.1722E-03
EXP-6@12_4	0.003667	0.000010	35737	-7.0	2.8	368.6	2.5695E-03
EXP-6@12_5	0.003657	0.000010	38293	-9.7	2.7	368.6	2.7486E-03
EXP-6@12_6	0.003686	0.000009	44801	-1.9	2.5	368.6	3.2110E-03
EXP-6@12_7	0.003673	0.000010	40765	-5.4	2.6	368.6	2.9203E-03
EXP-6@12_8	0.003668	0.000009	41769	-6.8	2.6	368.6	2.9878E-03
EXP-6@12_9	0.003689	0.000009	49566	-1.1	2.4	368.6	3.5428E-03
EXP-6@12_10	0.003684	0.000009	42112	-2.4	2.6	368.6	3.0064E-03
EXP-6@12_11	0.003689	0.000010	39974	-1.1	2.6	368.6	2.8510E-03
EXP-6@12_12	0.003684	0.000010	39483	-2.4	2.6	368.6	2.8132E-03
EXP-6@12_13	0.003701	0.000009	46890	2.2	2.4	368.6	3.3304E-03
EXP-6@12_14	0.003695	0.000009	43647	0.5	2.5	368.6	3.0993E-03
EXP-6@12_15	0.003663	0.000010	37963	-8.1	2.7	368.6	2.6969E-03
EXP-6@12_16	0.003671	0.000010	37219	-6.0	2.7	368.6	2.6448E-03
EXP-6@12_17	0.003674	0.000010	41505	-5.1	2.6	368.6	2.9493E-03
EXP-6@12_18	0.003686	0.000009	45310	-1.9	2.5	368.6	3.2221E-03
EXP-6@12_19	0.003684	0.000009	42732	-2.4	2.5	368.6	3.0380E-03
EXP-6@12_20	0.003683	0.000010	40584	-2.7	2.6	368.6	2.8874E-03
January 2013 <SampleName:USGS35-NaNO3> <Raster:2.0>							
EXP-8@3_1	0.003669	0.000010	40949	-4.6	2.6	184.3	3.0497E-03
EXP-8@3_2	0.003675	0.000010	39413	-3.0	2.6	184.3	2.9459E-03
EXP-8@3_3	0.003685	0.000010	40188	-0.3	2.6	184.3	3.0076E-03
EXP-8@3_4	0.003662	0.000010	41207	-6.5	2.6	184.3	3.0974E-03
EXP-8@3_5	0.003686	0.000009	43126	0.0	2.5	184.3	3.2492E-03
EXP-8@3_6	0.003686	0.000009	48554	0.0	2.4	184.3	3.6648E-03
EXP-8@3_7	0.003671	0.000009	48506	-4.1	2.4	184.3	3.6726E-03
EXP-8@3_8	0.003679	0.000009	51634	-1.9	2.3	184.3	3.9064E-03
EXP-8@3_9	0.003677	0.000009	50009	-2.4	2.4	184.3	3.7649E-03
EXP-8@3_10	0.003675	0.000009	50358	-3.0	2.3	184.3	3.8049E-03
EXP-8@6_1	0.003667	0.000010	38127	-5.2	2.7	245.8	2.7489E-03
EXP-8@6_2	0.003664	0.000010	36809	-6.0	2.7	245.8	2.6697E-03
EXP-8@6_3	0.003664	0.000010	39448	-6.0	2.6	245.8	2.8718E-03
EXP-8@6_4	0.003676	0.000010	39552	-2.7	2.6	245.8	2.8895E-03
EXP-8@6_5	0.003667	0.000009	41693	-5.2	2.6	245.8	3.0505E-03
EXP-8@6_6	0.003675	0.000009	43607	-3.0	2.5	245.8	3.2034E-03
EXP-8@6_7	0.003671	0.000009	44342	-4.1	2.5	245.8	3.2673E-03
EXP-8@6_8	0.003681	0.000009	44384	-1.4	2.5	245.8	3.2770E-03
EXP-8@6_9	0.003663	0.000009	43285	-6.2	2.5	245.8	3.1967E-03
EXP-8@6_10	0.003683	0.000009	44054	-0.8	2.5	245.8	3.2634E-03

Analysis no.	$n(^{15}N^{16}O_2^-)$ / $n(^{14}N^{16}O_2^-)$	1 σ	ion $^{14}N^{16}O_2^-$ (cps)	IMF (‰)	1 σ	Pre - sputtering Time (s)	$n(^{14}N^{16}O_2^-)$ / $n(Cs^+)$
January 2013 <SampleName:USGS35-NaNO3> <Raster:5.0>							
EXP-8@11_1	0.003664	0.000009	45915	-6.0	2.4	1536	3.2319E-03
EXP-8@11_2	0.003653	0.000009	46134	-9.0	2.4	1536	3.2387E-03
EXP-8@11_3	0.003659	0.000009	45568	-7.3	2.5	1536	3.2029E-03
EXP-8@11_4	0.003666	0.000009	48936	-5.4	2.4	1536	3.4579E-03
EXP-8@11_5	0.003654	0.000008	52424	-8.7	2.3	1536	3.9538E-03
EXP-8@11_6	0.003676	0.000010	40439	-2.7	2.6	1536	3.0786E-03
EXP-8@11_7	0.003671	0.000008	53891	-4.1	2.3	1536	3.8520E-03
EXP-8@11_8	0.003688	0.000009	51375	0.5	2.3	1536	3.6427E-03
EXP-8@11_9	0.003671	0.000009	51169	-4.1	2.3	1536	3.6237E-03
EXP-8@11_10	0.003664	0.000009	51582	-6.0	2.3	1536	3.6645E-03
EXP-8@9_1	0.003643	0.000008	53122	-11.7	2.3	1155.1	3.9910E-03
EXP-8@9_2	0.003669	0.000008	56596	-4.6	2.2	1155.1	4.2707E-03
EXP-8@9_3	0.003661	0.000008	55132	-6.8	2.2	1155.1	4.1884E-03
EXP-8@9_4	0.003663	0.000008	55536	-6.2	2.2	1155.1	4.1907E-03
EXP-8@9_5	0.003685	0.000008	56417	-0.3	2.2	1155.1	4.2352E-03
EXP-8@9_6	0.003660	0.000007	71572	-7.1	2.0	1155.1	5.4106E-03
EXP-8@9_7	0.003667	0.000008	61624	-5.2	2.1	1155.1	4.7000E-03
EXP-8@9_8	0.003668	0.000008	60884	-4.9	2.1	1155.1	4.6705E-03
EXP-8@9_9	0.003667	0.000008	61353	-5.2	2.1	1155.1	4.9489E-03
EXP-8@9_10	0.003665	0.000008	57076	-5.7	2.2	1155.1	4.6167E-03
January 2013 <SampleName:InHouse-NaNO3> <Raster:2.0>							
EXP-8@4_1	0.003738	0.000011	31068	0.3	3.0	184.3	2.4112E-03
EXP-8@4_2	0.003727	0.000012	25207	-2.7	3.3	184.3	1.9454E-03
EXP-8@4_3	0.003734	0.000012	25475	-0.8	3.3	184.3	1.9667E-03
EXP-8@4_4	0.003725	0.000012	25154	-3.2	3.3	184.3	1.9475E-03
EXP-8@4_5	0.003744	0.000013	23731	1.9	3.4	184.3	1.8393E-03
EXP-8@4_6	0.003753	0.000011	30494	4.3	3.0	184.3	2.3692E-03
EXP-8@4_7	0.003727	0.000011	33977	-2.7	2.8	184.3	2.6349E-03
EXP-8@4_8	0.003735	0.000010	35145	-0.5	2.8	184.3	2.7125E-03
EXP-8@4_9	0.003742	0.000011	34625	1.3	2.8	184.3	2.6837E-03
EXP-8@4_10	0.003730	0.000010	36008	-1.9	2.8	184.3	2.7968E-03
EXP-8@7_1	0.003754	0.000012	26099	4.5	3.2	245.8	1.9890E-03
EXP-8@7_2	0.003733	0.000013	23142	-1.1	3.4	245.8	1.7716E-03
EXP-8@7_3	0.003741	0.000013	21212	1.1	3.6	245.8	1.6336E-03
EXP-8@7_4	0.003733	0.000013	22560	-1.1	3.5	245.8	1.7467E-03
EXP-8@7_5	0.003726	0.000013	23221	-2.9	3.4	245.8	1.8017E-03
EXP-8@7_6	0.003748	0.000011	29593	2.9	3.0	245.8	2.2840E-03
EXP-8@7_7	0.003745	0.000011	30779	2.1	3.0	245.8	2.3506E-03
EXP-8@7_8	0.003731	0.000011	31461	-1.6	2.9	245.8	2.3957E-03
EXP-8@7_9	0.003730	0.000011	33647	-1.9	2.8	245.8	2.5642E-03

Analysis no.	$n(^{15}N^{16}O_2^-)$ / $n(^{14}N^{16}O_2^-)$	1 σ	ion $^{14}N^{16}O_2^-$ (cps)	IMF (‰)	1 σ	Pre - sputtering Time (s)	$n(^{14}N^{16}O_2^-)$ / $n(Cs^+)$
EXP-8@7_10	0.003739	0.000011	31264	0.5	3.0	245.8	2.3895E-03
January 2013 <SampleName:InHouse-NaNO3> <Raster:5.0>							
EXP-8@10_1	0.003708	0.000012	25729	-7.8	3.2	1155.1	2.0081E-03
EXP-8@10_2	0.003715	0.000013	23894	-5.9	3.4	1155.1	1.8820E-03
EXP-8@10_3	0.003721	0.000012	24444	-4.3	3.3	1155.1	1.9279E-03
EXP-8@10_4	0.003738	0.000013	23861	0.3	3.4	1155.1	1.8866E-03
EXP-8@10_5	0.003708	0.000012	24838	-7.8	3.3	1155.1	1.9681E-03
EXP-8@10_6	0.003704	0.000012	26439	-8.8	3.2	1155.1	2.1012E-03
EXP-8@10_7	0.003718	0.000011	29147	-5.1	3.1	1155.1	2.3343E-03
EXP-8@10_8	0.003712	0.000012	28179	-6.7	3.1	1155.1	2.2717E-03
EXP-8@10_9	0.003731	0.000011	29235	-1.6	3.1	1155.1	2.3543E-03
EXP-8@10_10	0.003713	0.000011	29235	-6.4	3.0	1155.1	2.3426E-03
EXP-8@12_1	0.003703	0.000014	18491	-9.1	3.8	1536	1.3198E-03
EXP-8@12_2	0.003702	0.000015	15821	-9.4	4.1	1536	1.1248E-03
EXP-8@12_3	0.003694	0.000016	15698	-11.5	4.1	1536	1.1117E-03
EXP-8@12_4	0.003711	0.000015	15883	-7.0	4.1	1536	1.1259E-03
EXP-8@12_5	0.003723	0.000015	16589	-3.7	4.1	1536	1.1800E-03
EXP-8@12_6	0.003720	0.000014	19561	-4.5	3.7	1536	1.3893E-03
EXP-8@12_7	0.003703	0.000013	21629	-9.1	3.5	1536	1.5384E-03
EXP-8@12_8	0.003707	0.000013	21198	-8.0	3.6	1536	1.5167E-03
EXP-8@12_9	0.003721	0.000013	21103	-4.3	3.6	1536	1.5106E-03
EXP-8@12_10	0.003712	0.000013	21502	-6.7	3.6	1536	1.5411E-03
EXP-8@14_1	0.003728	0.000011	29798	-2.4	3.0	1536	1.9980E-03
EXP-8@14_2	0.003729	0.000012	26458	-2.1	3.2	1536	1.7761E-03
EXP-8@14_3	0.003752	0.000012	25675	4.0	3.3	1536	1.7315E-03
EXP-8@14_4	0.003743	0.000012	25656	1.6	3.3	1536	1.7363E-03
EXP-8@14_5	0.003717	0.000012	24960	-5.4	3.3	1536	1.7455E-03
EXP-8@14_6	0.003717	0.000011	30329	-5.4	3.0	1536	2.1114E-03
EXP-8@14_7	0.003712	0.000011	32973	-6.7	2.9	1536	2.2058E-03
EXP-8@14_8	0.003725	0.000011	32683	-3.2	2.9	1536	2.1854E-03
EXP-8@14_9	0.003722	0.000011	32999	-4.0	2.9	1536	2.2224E-03
EXP-8@14_10	0.003722	0.000011	32319	-4.0	2.9	1536	2.1806E-03
EXP-8@15_1	0.003727	0.000011	32474	-2.7	2.9	1155.1	2.2095E-03
EXP-8@15_2	0.003733	0.000012	28390	-1.1	3.1	1155.1	1.9507E-03
EXP-8@15_3	0.003720	0.000012	28625	-4.5	3.1	1155.1	1.9828E-03
EXP-8@15_4	0.003708	0.000011	28732	-7.8	3.1	1155.1	1.9997E-03
EXP-8@15_5	0.003715	0.000011	29548	-5.9	3.0	1155.1	2.0664E-03
EXP-8@15_6	0.003715	0.000011	32683	-5.9	2.9	1155.1	2.2955E-03
EXP-8@15_7	0.003728	0.000010	34826	-2.4	2.8	1155.1	2.4603E-03
EXP-8@15_8	0.003722	0.000010	35469	-4.0	2.8	1155.1	2.5179E-03
EXP-8@15_9	0.003694	0.000010	35857	-11.5	2.7	1155.1	2.5548E-03

Analysis no.	$n(^{15}N^{16}O_2^-)$ / $n(^{14}N^{16}O_2^-)$	1 σ	ion $^{14}N^{16}O_2^-$ (cps)	IMF (‰)	1 σ	Pre - sputtering Time (s)	$n(^{14}N^{16}O_2^-)$ / $n(Cs^+)$
EXP-8@15_10	0.003727	0.000012	25101	-2.7	3.3	1155.1	1.7937E-03
January 2013 <SampleName:IAEA-KNO3> <Raster:2.0>							
EXP-8@2_10	0.003717	0.000010	38193	6.5	2.7	184.3	2.8157E-03
EXP-8@2_1	0.003700	0.000011	34005	1.9	2.9	184.3	2.4874E-03
EXP-8@2_2	0.003710	0.000010	39240	4.6	2.7	184.3	2.8761E-03
EXP-8@2_3	0.003702	0.000010	35978	2.4	2.8	184.3	2.6370E-03
EXP-8@2_4	0.003717	0.000010	35647	6.5	2.8	184.3	2.6193E-03
EXP-8@2_5	0.003709	0.000010	37604	4.3	2.7	184.3	2.9894E-03
EXP-8@2_6	0.003702	0.000010	39833	2.4	2.6	184.3	3.1528E-03
EXP-8@2_7	0.003746	0.000010	37540	14.4	2.7	184.3	2.7473E-03
EXP-8@2_8	0.003712	0.000010	37734	5.1	2.7	184.3	2.7519E-03
EXP-8@2_9	0.003696	0.000010	40985	0.8	2.6	184.3	3.0063E-03
EXP-8@5_1	0.003698	0.000011	33456	1.4	2.9	245.8	2.3544E-03
EXP-8@5_2	0.003724	0.000012	28539	8.4	3.1	245.8	2.0050E-03
EXP-8@5_3	0.003709	0.000012	26981	4.3	3.2	245.8	1.8983E-03
EXP-8@5_4	0.003722	0.000012	27378	7.9	3.2	245.8	1.9314E-03
EXP-8@5_5	0.003731	0.000012	27439	10.3	3.2	245.8	1.9380E-03
EXP-8@5_6	0.003706	0.000011	31461	3.5	3.0	245.8	2.2318E-03
EXP-8@5_7	0.003709	0.000011	33106	4.3	2.9	245.8	2.3600E-03
EXP-8@5_8	0.003721	0.000011	32683	7.6	2.9	245.8	2.3321E-03
EXP-8@5_9	0.003706	0.000010	35588	3.5	2.8	245.8	2.5406E-03
EXP-8@5_10	0.003743	0.000011	34625	13.5	2.8	245.8	2.4780E-03
January 2013 <SampleName:IAEA-KNO3> <Raster:5.0>							
EXP-8@13_1	0.003693	0.000012	25030	0.0	3.3	1536	1.6076E-03
EXP-8@13_2	0.003694	0.000013	23796	0.3	3.4	1536	1.5444E-03
EXP-8@13_3	0.003700	0.000012	24614	1.9	3.4	1536	1.6140E-03
EXP-8@13_4	0.003706	0.000012	26212	3.5	3.3	1536	1.7297E-03
EXP-8@13_5	0.003703	0.000011	32191	2.7	2.9	1536	2.1252E-03
EXP-8@13_6	0.003685	0.000012	25511	-2.2	3.3	1536	1.6973E-03
EXP-8@13_7	0.003690	0.000012	27621	-0.8	3.2	1536	1.8491E-03
EXP-8@13_8	0.003713	0.000010	39448	5.4	2.7	1536	2.6420E-03
EXP-8@13_9	0.003689	0.000012	27459	-1.1	3.2	1536	1.8248E-03
EXP-8@13_10	0.003708	0.000012	26805	4.1	3.2	1536	1.7773E-03
EXP-8@8_1	0.003688	0.000014	19806	-1.4	3.7	1155.1	1.4732E-03
EXP-8@8_2	0.003693	0.000015	16858	0.0	4.1	1155.1	1.2539E-03
EXP-8@8_3	0.003709	0.000015	17651	4.3	4.0	1155.1	1.3013E-03
EXP-8@8_4	0.003714	0.000014	18314	5.7	3.9	1155.1	1.3591E-03
EXP-8@8_5	0.003694	0.000015	16761	0.3	4.1	1155.1	1.2596E-03
EXP-8@8_6	0.003689	0.000013	21474	-1.1	3.6	1155.1	1.6183E-03
EXP-8@8_7	0.003702	0.000013	21799	2.4	3.6	1155.1	1.6488E-03

Analysis no.	$n(^{15}N^{16}O_2^-)$ / $n(^{14}N^{16}O_2^-)$	1 σ	ion $^{14}N^{16}O_2^-$ (cps)	IMF (‰)	1 σ	Pre - sputtering Time (s)	$n(^{14}N^{16}O_2^-)$ / $n(Cs^+)$
EXP-8@8_8	0.003690	0.000013	22441	-0.8	3.5	1155.1	1.7151E-03
EXP-8@8_9	0.003728	0.000014	20648	9.5	3.7	1155.1	1.5873E-03
EXP-8@8_10	0.003701	0.000013	22234	2.2	3.5	1155.1	1.6873E-03
July 2013 <SampleName:IAEA-KNO3> <Raster:5.0>							
Press10-IAEA-200s@1_1	0.003682	0.000010	28590	-14.7	2.7	196.6	6.4278E-04
Press10-IAEA-200s@1_2	0.003668	0.000009	34821	-18.5	2.5	196.6	7.8599E-04
Press10-IAEA-200s@1_3	0.003686	0.000009	33598	-13.6	2.5	196.6	7.5974E-04
Press10-IAEA-200s@1_4	0.003690	0.000009	36420	-12.6	2.4	196.6	8.2802E-04
Press10-IAEA-200s@1_5	0.003675	0.000009	37084	-16.6	2.4	196.6	8.4310E-04
Press10-IAEA-200s@1_6	0.003691	0.000008	44152	-12.3	2.2	196.6	1.0020E-03
Press10-IAEA-200s@1_7	0.003694	0.000009	35942	-11.5	2.5	196.6	8.1569E-04
Press10-IAEA-200s@1_8	0.003683	0.000009	39148	-14.5	2.3	196.6	8.8721E-04
press10-IAEA-500s@1_1	0.003690	0.000011	25712	-12.6	2.9	503.8	5.8095E-04
press10-IAEA-500s@1_2	0.003685	0.000011	26874	-13.9	2.8	503.8	6.0697E-04
press10-IAEA-500s@1_3	0.003681	0.000011	24777	-15.0	2.9	503.8	5.5817E-04
press10-IAEA-500s@1_4	0.003683	0.000011	24376	-14.5	3.0	503.8	5.4653E-04
press10-IAEA-500s@1_5	0.003696	0.000010	27451	-11.0	2.8	503.8	6.1353E-04
press10-IAEA-500s@1_6	0.003675	0.000009	36420	-16.6	2.4	503.8	8.1367E-04
press10-IAEA-500s@1_7	0.003692	0.000011	23966	-12.0	3.0	503.8	5.3491E-04
press10-IAEA-500s@1_8	0.003682	0.000010	27838	-14.7	2.8	503.8	6.2218E-04
press4-IAEA-KNO3-100S@1_1	0.003676	0.000006	80040	-16.3	1.6	98.3	1.7826E-03
press4-IAEA-KNO3-100S@1_2	0.003673	0.000006	77949	-17.1	1.7	98.3	1.7360E-03
press4-IAEA-KNO3-100S@1_3	0.003681	0.000006	82923	-15.0	1.6	98.3	1.8482E-03
press4-IAEA-KNO3-100S@1_4	0.003682	0.000006	85838	-14.7	1.6	98.3	1.9110E-03
press4-IAEA-KNO3-100S@1_5	0.003685	0.000006	82334	-13.9	1.6	98.3	1.8304E-03
press4-IAEA-KNO3-100S@1_6	0.003676	0.000006	93980	-16.3	1.5	98.3	2.0881E-03
USGS35-200s@1_1	0.003674	0.000021	7132	-5.1	5.6	196.6	1.5661E-04
USGS35-200s@1_2	0.003665	0.000020	7756	-7.6	5.9	196.6	1.6555E-04
USGS35-200s@1_3	0.003686	0.000023	5914	-1.9	6.1	196.6	1.2615E-04
USGS35-200s@1_4	0.003686	0.000020	7675	-1.9	5.4	196.6	1.6723E-04
USGS35-200s@1_5	0.003659	0.000019	7931	-9.2	5.4	196.6	1.7324E-04
USGS35-200s@1_6	0.003690	0.000020	7560	-0.8	5.4	196.6	1.6554E-04
USGS35-200s@1_7	0.003659	0.000020	7852	-9.2	6.8	196.6	1.7226E-04
USGS35-200s@1_8	0.003641	0.000018	9275	-14.1	4.9	196.6	2.0401E-04
USGS35-200s@1_9	0.003663	0.000022	6089	-8.1	6.0	196.6	1.3422E-04
USGS35-200s@1_10	0.003667	0.000019	8754	-7.0	5.7	196.6	1.9299E-04
USGS35-500s@1_1	0.003669	0.000020	7162	-6.5	5.5	503.8	1.6422E-04
USGS35-500s@1_2	0.003661	0.000019	8084	-8.7	5.8	503.8	1.8547E-04
USGS35-500s@1_3	0.003667	0.000022	6438	-7.0	6.4	503.8	1.4782E-04
USGS35-500s@1_4	0.003674	0.000021	6874	-5.1	6.3	503.8	1.5821E-04

Analysis no.	$n(^{15}N^{16}O_2^-)$ / $n(^{14}N^{16}O_2^-)$	1 σ	ion $^{14}N^{16}O_2^-$ (cps)	IMF (‰)	1 σ	Pre - sputtering Time (s)	$n(^{14}N^{16}O_2^-)$ / $n(Cs^+)$
USGS35-500s@1_5	0.003659	0.000022	6108	-9.2	6.3	503.8	1.4090E-04
USGS35-500s@1_6	0.003672	0.000020	7223	-5.7	6.2	503.8	1.6709E-04
USGS35-500s@1_7	0.003657	0.000020	7229	-9.7	5.5	503.8	1.6737E-04
USGS35-500s@1_8	0.003673	0.000021	6776	-5.4	5.7	503.8	1.5679E-04
USGS35-100s@3_1	0.003668	0.000020	7479	-6.8	5.6	98.3	1.6085E-04
USGS35-100s@3_2	0.003669	0.000018	9209	-6.5	5.1	98.3	1.9867E-04
USGS35-100s@3_3	0.003632	0.000019	8204	-16.5	6.2	98.3	1.7699E-04
USGS35-100s@3_4	0.003645	0.000018	8709	-13.0	6.0	98.3	1.8867E-04
USGS35-100s@3_5	0.003662	0.000020	7387	-8.4	6.3	98.3	1.6009E-04
USGS35-100s@3_6	0.003638	0.000019	8538	-14.9	5.3	98.3	1.8518E-04
USGS35-100s@3_7	0.003648	0.000019	8215	-12.2	6.0	98.3	1.7832E-04
USGS35-100s@3_8	0.003634	0.000019	8193	-16.0	6.0	98.3	1.7777E-04
USGS35-100s@3_9	0.003654	0.000017	10102	-10.6	4.7	98.3	2.1921E-04
USGS35-100s@3_10	0.003702	0.000018	9183	2.4	6.2	98.3	1.9947E-04
July 2013 <SampleName:In-house NaNO3> <Raster:5.0>							
IAEA-KNO3-100s@1_1	0.003709	0.000015	12721	-7.5	4.1	98.3	2.9494E-04
IAEA-KNO3-100s@1_2	0.003728	0.000015	13173	-2.4	4.1	98.3	3.0606E-04
IAEA-KNO3-100s@1_3	0.003704	0.000015	12995	-8.8	4.1	98.3	3.0131E-04
IAEA-KNO3-100s@1_4	0.003691	0.000015	14348	-12.3	3.9	98.3	3.3302E-04
IAEA-KNO3-100s@1_5	0.003718	0.000015	13682	-5.1	4.0	98.3	3.1763E-04
IAEA-KNO3-100s@1_6	0.003708	0.000014	14793	-7.8	3.8	98.3	3.4355E-04
IAEA-KNO3-100s@1_7	0.003696	0.000015	13794	-11.0	4.0	98.3	3.2114E-04
IAEA-KNO3-100s@1_8	0.003682	0.000015	13851	-14.7	3.9	98.3	3.2232E-04
IAEA-KNO3-100s@1_9	0.003695	0.000014	14520	-11.2	3.9	98.3	3.3833E-04
IAEA-KNO3-100s@1_10	0.003690	0.000014	14704	-12.6	3.8	98.3	3.4254E-04
IAEA-KNO3-200s@1_1	0.003682	0.000013	16969	-14.7	3.6	196.6	3.5838E-04
IAEA-KNO3-200s@1_2	0.003716	0.000014	15092	-5.6	3.8	196.6	3.1908E-04
IAEA-KNO3-200s@1_3	0.003683	0.000014	16014	-14.5	3.7	196.6	3.3853E-04
IAEA-KNO3-200s@1_4	0.003706	0.000014	16571	-8.3	3.6	196.6	3.5095E-04
IAEA-KNO3-200s@1_5	0.003671	0.000014	16258	-17.7	3.6	196.6	3.4477E-04
IAEA-KNO3-200s@1_6	0.003707	0.000014	15934	-8.0	3.7	196.6	3.3873E-04
IAEA-KNO3-200s@1_7	0.003715	0.000014	15630	-5.9	3.7	196.6	3.3213E-04
IAEA-KNO3-200s@1_8	0.003688	0.000014	16300	-13.1	3.6	196.6	3.4662E-04
IAEA-KNO3-1000s@2_1	0.003729	0.000015	12735	-2.1	4.1	1007.6	2.7127E-04
IAEA-KNO3-1000s@2_2	0.003720	0.000016	12352	-4.5	4.2	1007.6	2.6282E-04
IAEA-KNO3-1000s@2_3	0.003708	0.000015	12763	-7.8	4.1	1007.6	2.7158E-04
IAEA-KNO3-1000s@2_4	0.003709	0.000016	12325	-7.5	4.2	1007.6	2.6239E-04
IAEA-KNO3-1000s@2_5	0.003705	0.000015	13166	-8.6	4.1	1007.6	2.8109E-04
IAEA-KNO3-1000s@2_6	0.003707	0.000015	13054	-8.0	4.1	1007.6	2.7849E-04
IAEA-KNO3-1000s@2_7	0.003724	0.000015	13572	-3.5	4.0	1007.6	2.8987E-04
IAEA-KNO3-1000s@2_8	0.003679	0.000015	13363	-15.5	4.0	1007.6	2.8567E-04
IAEA-KNO3-1000s@2_9	0.003721	0.000015	12706	-4.3	4.1	1007.6	2.7179E-04
IAEA-KNO3-1000s@2_10	0.003759	0.000016	12756	5.9	4.2	1007.6	2.7286E-04

Analysis no.	$n(^{15}N^{16}O_2^-)$ / $n(^{14}N^{16}O_2^-)$	1 σ	ion $^{14}N^{16}O_2^-$ (cps)	IMF (‰)	1 σ	Pre - sputtering Time (s)	$n(^{14}N^{16}O_2^-)$ / $n(Cs^+)$
IAEA-KNO3-500S@1_1	0.003701	0.000016	12032	-9.6	4.2	503.8	2.5750E-04
IAEA-KNO3-500S@1_2	0.003710	0.000017	10285	-7.2	4.6	503.8	2.2000E-04
IAEA-KNO3-500S@1_3	0.003684	0.000016	11806	-14.2	4.3	503.8	2.5291E-04
IAEA-KNO3-500S@1_4	0.003704	0.000016	12045	-8.8	4.2	503.8	2.5798E-04
IAEA-KNO3-500S@1_5	0.003690	0.000015	12566	-12.6	4.1	503.8	2.6979E-04
IAEA-KNO3-500S@1_6	0.003700	0.000015	12785	-9.9	4.1	503.8	2.7419E-04
IAEA-KNO3-500S@1_7	0.003704	0.000016	12393	-8.8	4.2	503.8	2.6553E-04
IAEA-KNO3-500S@1_8	0.003704	0.000016	12531	-8.8	4.2	503.8	2.6869E-04
IAEA-KNO3-500S@1_9	0.003702	0.000015	12622	-9.4	4.1	503.8	2.7049E-04
IAEA-KNO3-500S@1_10	0.003708	0.000017	11032	-7.8	4.4	503.8	2.3664E-04
July 2013 <SampleName: USGS35> <Raster:5.0>							
new-USGS35-100s@1_2	0.003631	0.000007	55273	-14.9	2.0	98.3	1.2293E-03
new-USGS35-100s@1_3	0.003650	0.000007	54952	-9.8	2.0	98.3	1.2212E-03
new-USGS35-100s@1_4	0.003644	0.000007	60515	-11.4	1.9	98.3	1.3459E-03
new-USGS35-100s@1_5	0.003645	0.000007	57943	-11.1	1.9	98.3	1.2895E-03
new-USGS35-100s@1_6	0.003656	0.000007	59639	-8.1	1.9	98.3	1.3277E-03
new-USGS35-100s@1_1	0.003638	0.000009	36697	-13.0	2.4	98.3	8.1378E-04
new-USGS35-1000s@1_2	0.003620	0.000012	22244	-17.9	3.1	1007.6	4.9648E-04
new-USGS35-1000s@1_3	0.003650	0.000011	23729	-9.8	3.0	1007.6	5.2899E-04
new-USGS35-1000s@1_4	0.003669	0.000011	26421	-4.6	2.9	1007.6	5.8900E-04
new-USGS35-1000s@1_5	0.003647	0.000011	27005	-10.6	2.9	1007.6	6.0238E-04
new-USGS35-1000s@1_1	0.003615	0.000012	20790	-19.3	3.2	1007.6	4.6284E-04
August 2013 <SampleName: USGS35> <Raster:5.0>							
IAEA-KNO3-500S@1_1	0.003643	0.000024	5157	-13.5	6.5	503.8	1.1517E-04
IAEA-KNO3-500S@1_2	0.003648	0.000022	6312	-12.2	5.9	503.8	1.4135E-04
IAEA-KNO3-500S@1_3	0.003666	0.000020	7362	-7.3	5.5	503.8	1.6483E-04
IAEA-KNO3-500S@1_4	0.003695	0.000022	6146	0.5	6.0	503.8	1.3789E-04
IAEA-KNO3-500S@1_5	0.003675	0.000022	6094	-4.9	6.0	503.8	1.3682E-04
IAEA-KNO3-500S@1_6	0.003680	0.000024	5436	-3.5	6.4	503.8	1.2226E-04
IAEA-KNO3-500S@1_7	0.003626	0.000023	5379	-18.1	6.4	503.8	1.2124E-04
IAEA-KNO3-500S@1_8	0.003656	0.000023	5636	-10.0	6.2	503.8	1.2699E-04
IAEA-KNO3-500S-2@1_1	0.003719	0.000037	2178	7.0	10.1	503.8	4.9229E-05
IAEA-KNO3-500S-2@1_2	0.003672	0.000028	3912	-5.7	7.5	503.8	8.8627E-05
IAEA-KNO3-500S-2@1_3	0.003711	0.000038	2154	4.9	10.2	503.8	4.8989E-05
IAEA-KNO3-500S-2@1_4	0.003716	0.000038	2099	6.2	10.3	503.8	4.7805E-05
IAEA-KNO3-500S-2@1_5	0.003682	0.000034	2659	-3.0	9.1	503.8	6.0668E-05
IAEA-KNO3-500S-2@1_6	0.003678	0.000034	2525	-4.1	9.3	503.8	5.7798E-05
IAEA-KNO3-500S-2@1_7	0.003671	0.000029	3522	-6.0	7.9	503.8	8.0753E-05
IAEA-KNO3-500S-2@1_8	0.003682	0.000031	3095	-3.0	8.4	503.8	7.1073E-05

Analysis no.	$n(^{15}N^{16}O_2^-)$ / $n(^{14}N^{16}O_2^-)$	1 σ	ion $^{14}N^{16}O_2^-$ (cps)	IMF (‰)	1 σ	Pre - sputtering Time (s)	$n(^{14}N^{16}O_2^-)$ / $n(Cs^+)$
IAEA-KNO3-200S@1_1	0.003641	0.000023	5684	-14.1	6.2	208.9	1.2823E-04
IAEA-KNO3-200S@1_2	0.003622	0.000016	10873	-19.2	4.5	208.9	2.4558E-04
IAEA-KNO3-200S@1_3	0.003639	0.000019	7821	-14.6	5.3	208.9	1.7667E-04
IAEA-KNO3-200S@1_4	0.003660	0.000017	10565	-8.9	4.6	208.9	2.3900E-04
IAEA-KNO3-200S@1_5	0.003629	0.000015	13226	-17.3	4.1	208.9	2.9926E-04
IAEA-KNO3-200S@1_6	0.003663	0.000015	13084	-8.1	4.1	208.9	2.9675E-04
IAEA-KNO3-200S@1_7	0.003633	0.000015	12559	-16.2	4.2	208.9	2.8547E-04
IAEA-KNO3-200S@1_8	0.003672	0.000018	8998	-5.7	4.9	208.9	2.0429E-04
IAEA-KNO3-200S-3@1_1	0.003715	0.000021	7094	6.0	5.6	196.6	1.6427E-04
IAEA-KNO3-200S-3@1_2	0.003691	0.000021	7144	-0.5	5.6	196.6	1.6538E-04
IAEA-KNO3-200S-3@1_3	0.003664	0.000019	8388	-7.9	5.1	196.6	1.9409E-04
IAEA-KNO3-200S-3@1_4	0.003692	0.000020	7924	-0.3	5.3	196.6	1.8355E-04
IAEA-KNO3-200S-3@1_5	0.003679	0.000019	8721	-3.8	5.0	196.6	2.0163E-04
IAEA-KNO3-200S-3@1_6	0.003674	0.000019	8766	-5.1	5.0	196.6	2.0275E-04
IAEA-KNO3-200S-3@1_7	0.003668	0.000018	8774	-6.8	5.0	196.6	2.0331E-04
IAEA-KNO3-200S-3@1_8	0.003635	0.000018	8815	-15.7	5.0	196.6	2.0476E-04
IAEA-KNO3-500S-3@1_1	0.003695	0.000023	5561	0.5	6.3	503.8	1.2973E-04
IAEA-KNO3-500S-3@1_2	0.003693	0.000022	6250	0.0	5.9	503.8	1.4593E-04
IAEA-KNO3-500S-3@1_3	0.003849	0.000023	6139	42.2	6.1	503.8	1.4307E-04
IAEA-KNO3-500S-3@1_3	0.003681	0.000024	5428	-3.2	6.4	503.8	1.2649E-04
IAEA-KNO3-500S-3@1_1	0.003694	0.000036	2278	0.3	9.9	503.8	5.3140E-05
IAEA-KNO3-500S-3@1_4	0.003696	0.000023	5764	0.8	6.2	503.8	1.3408E-04
IAEA-KNO3-500S-3@1_5	0.003701	0.000018	9744	2.2	4.8	503.8	2.2639E-04
IAEA-KNO3-500S-3@1_6	0.003673	0.000019	8013	-5.4	5.2	503.8	1.8608E-04
IAEA-KNO3-500S-3@1_7	0.003710	0.000023	5772	4.6	6.2	503.8	1.3411E-04
IAEA-KNO3-500S-3@1_8	0.003669	0.000022	6451	-6.5	5.8	503.8	1.5025E-04
September 2013 <SampleName: IAEA-NO-3> <Raster:5.0>							
P4-NO2-IAEA-KNO3-200S@1_1	0.003721	0.000010	29776	7.6	2.7	196.6	6.6878E-04
P4-NO2-IAEA-KNO3-200S@1_2	0.003716	0.000010	31895	6.2	2.6	196.6	7.2937E-04
P4-NO2-IAEA-KNO3-200S@1_3	0.003715	0.000010	32554	6.0	2.6	196.6	7.4415E-04
P4-NO2-IAEA-KNO3-200S@1_4	0.003705	0.000010	32554	3.2	2.6	196.6	7.4520E-04
P4-NO2-IAEA-KNO3-200S@1_5	0.003714	0.000010	28023	5.7	2.8	196.6	6.4148E-04
P4-NO2-IAEA-KNO3-200S@1_6	0.003709	0.000012	20308	4.3	3.3	196.6	4.6610E-04
P4-NO2-IAEA-KNO3-200S@1_7	0.003704	0.000010	30213	3.0	2.7	196.6	6.9330E-04
P4-NO2-IAEA-KNO3-200S@1_8	0.003709	0.000010	31200	4.3	2.7	196.6	7.1609E-04
P4-NO2-IAEA-KNO3-200S@1_9	0.003705	0.000010	28977	3.2	2.8	196.6	6.6600E-04
P4-NO2-IAEA-KNO3-200S@1_10	0.003715	0.000010	30714	6.0	2.7	196.6	7.0765E-04
P4-NO2-IAEA-KNO3-200S@1_11	0.003714	0.000010	28686	5.7	2.8	196.6	6.6347E-04
P4-NO2-IAEA-KNO3-200S@1_12	0.003693	0.000010	30423	0.0	2.7	196.6	7.0696E-04
P4-NO2-IAEA-KNO3-200S@1_13	0.003728	0.000011	26917	9.5	2.9	196.6	6.2821E-04
P4-NO2-IAEA-KNO3-200S@1_14	0.003722	0.000013	19063	7.9	3.4	196.6	4.4591E-04
P4-NO2-IAEA-KNO3-200S@1_15	0.003721	0.000010	27769	7.6	2.8	196.6	6.5143E-04

Analysis no.	$n(^{15}N^{16}O_2^-)$ / $n(^{14}N^{16}O_2^-)$	1 σ	ion $^{14}N^{16}O_2^-$ (cps)	IMF (‰)	1 σ	Pre - sputtering Time (s)	$n(^{14}N^{16}O_2^-)$ / $n(Cs^+)$
September 2013 <SampleName: USGS35> <Raster:5.0>							
P4-NO2-USGS35-200sn@1_1	0.003662	0.000007	59279	-6.5	1.9	196.6	1.3064E-03
P4-NO2-USGS35-200sn@1_2	0.003680	0.000008	48868	-1.6	2.1	196.6	1.0795E-03
P4-NO2-USGS35-200sn@1_3	0.003666	0.000008	53086	-5.4	2.0	196.6	1.1767E-03
P4-NO2-USGS35-200sn@1_4	0.003672	0.000008	52070	-3.8	2.1	196.6	1.1622E-03
P4-NO2-USGS35-200sn@1_5	0.003676	0.000008	48975	-2.7	2.1	196.6	1.0953E-03
P4-NO2-USGS35-200sn@1_6	0.003665	0.000007	62480	-5.7	1.9	196.6	1.3998E-03
P4-NO2-USGS35-200sn@1_7	0.003670	0.000007	67311	-4.3	1.8	196.6	1.5110E-03
P4-NO2-USGS35-200sn@1_8	0.003666	0.000007	65863	-5.4	1.8	196.6	1.4843E-03
September 2013 <SampleName: In-house NaNO3> <Raster:5.0>							
P4-NO2-INHOUSE-NaNO3-200S1@1_1	0.003731	0.000008	44198	-1.6	2.2	196.6	9.9884E-04
P4-NO2-INHOUSE-NaNO3-200S1@1_2	0.003727	0.000008	47300	-2.7	2.1	196.6	1.0692E-03
P4-NO2-INHOUSE-NaNO3-200S1@1_3	0.003749	0.000009	41266	3.2	2.3	196.6	9.3407E-04
P4-NO2-INHOUSE-NaNO3-200S1@1_4	0.003728	0.000008	48708	-2.4	2.1	196.6	1.1061E-03
P4-NO2-INHOUSE-NaNO3-200S1@1_5	0.003737	0.000009	41266	0.0	2.3	196.6	9.3800E-04
P4-NO2-INHOUSE-NaNO3-200S1@1_6	0.003720	0.000009	39072	-4.5	2.4	196.6	8.8973E-04
P4-NO2-INHOUSE-NaNO3-200S1@1_7	0.003743	0.000009	41558	1.6	2.3	196.6	9.4750E-04
October 2013 <SampleName: IAEA-NO-3> <Raster:5.0>							
IAEA-KNO3-NO2-100S@1_1	0.003670	0.000008	49626	-6.2	2.1	98.3	1.0121E-03
IAEA-KNO3-NO2-100S@1_2	0.003683	0.000007	54319	-2.7	2.0	98.3	1.1126E-03
IAEA-KNO3-NO2-100S@1_3	0.003696	0.000008	52904	0.8	2.0	98.3	1.0945E-03
IAEA-KNO3-NO2-100S@1_4	0.003679	0.000007	56518	-3.8	2.0	98.3	1.1791E-03
IAEA-KNO3-NO2-100S@1_5	0.003701	0.000008	50741	2.2	2.1	98.3	1.0609E-03
IAEA-KNO3-NO2-100S@1_6	0.003677	0.000008	52484	-4.3	2.0	98.3	1.0964E-03
IAEA-KNO3-NO2-100S@1_7	0.003679	0.000008	52425	-3.8	2.0	98.3	1.0943E-03
IAEA-KNO3-NO2-100S@1_8	0.003674	0.000007	55338	-5.1	2.0	98.3	1.1539E-03
IAEA-KNO3-NO2-100S@2_1	0.003685	0.000008	51544	-2.2	2.1	98.3	1.0446E-03
IAEA-KNO3-NO2-100S@2_2	0.003677	0.000007	55402	-4.3	2.0	98.3	1.1283E-03
IAEA-KNO3-NO2-100S@2_4	0.003677	0.000007	55858	-4.3	2.0	98.3	1.1441E-03
IAEA-KNO3-NO2-100S@2_5	0.003676	0.000007	60367	-4.6	1.9	98.3	1.2312E-03
IAEA-KNO3-NO2-100S@2_6	0.003674	0.000007	57258	-5.1	2.0	98.3	1.1669E-03
IAEA-KNO3-NO2-100S@2_7	0.003683	0.000007	59567	-2.7	1.9	98.3	1.2137E-03
IAEA-KNO3-NO2-100S@2_8	0.003681	0.000007	55662	-3.2	2.0	98.3	1.1329E-03

Analysis no.	$n(^{15}N^{16}O_2^-)$ / $n(^{14}N^{16}O_2^-)$	1 σ	ion $^{14}N^{16}O_2^-$ (cps)	IMF (‰)	1 σ	Pre - sputtering Time (s)	$n(^{14}N^{16}O_2^-)$ / $n(Cs^+)$
IAEA-KNO3-NO2-100S@2_9	0.003674	0.000007	54445	-5.1	2.0	98.3	1.1096E-03
IAEA-KNO3-NO2-100S@2_10	0.003675	0.000007	57736	-4.9	2.0	98.3	1.1785E-03
IAEA-KNO3-NO2-100S@2_11	0.003698	0.000008	49846	1.4	2.1	98.3	1.0199E-03
IAEA-KNO3-NO2-100S@2_12	0.003670	0.000007	61260	-6.2	1.9	98.3	1.2570E-03
IAEA-KNO3-NO2-100S@2_13	0.003695	0.000009	33812	0.5	2.6	98.3	6.9760E-04
IAEA-KNO3-NO2-100S@2_14	0.003684	0.000010	28210	-2.4	2.8	98.3	5.8499E-04
IAEA-KNO3-NO2-100S@2_15	0.003682	0.000010	29347	-3.0	2.7	98.3	6.1171E-04
IAEA-KNO3-NO2-100S@2_16	0.003693	0.000007	58012	0.0	2.0	98.3	1.2128E-03
AP1-IAEA-KNO3-NO2-100S@1_1	0.003672	0.000008	49736	-5.7	2.1	98.3	1.0685E-03
AP1-IAEA-KNO3-NO2-100S@1_2	0.003685	0.000007	57530	-2.2	2.0	98.3	1.2401E-03
AP1-IAEA-KNO3-NO2-100S@1_3	0.003670	0.000007	57874	-6.2	1.9	98.3	1.2516E-03
AP1-IAEA-KNO3-NO2-100S@1_4	0.003657	0.000007	56385	-9.7	2.0	98.3	1.2243E-03
AP1-IAEA-KNO3-NO2-100S@1_5	0.003669	0.000007	58570	-6.5	1.9	98.3	1.2754E-03
AP1-IAEA-KNO3-NO2-100S@1_6	0.003660	0.000007	57326	-8.9	2.0	98.3	1.2512E-03
AP1-IAEA-KNO3-NO2-100S@1_7	0.003662	0.000007	61335	-8.4	1.9	98.3	1.3371E-03
AP1-IAEA-KNO3-NO2-100S@1_8	0.003671	0.000007	60074	-6.0	1.9	98.3	1.3092E-03
October 2013 <SampleName: USGS35> <Raster:5.0>							
USGS35-NaNO3-NO2-100S@1_1	0.003650	0.000012	19760	-9.8	3.3	98.3	4.0379E-04
USGS35-NaNO3-NO2-100S@1_2	0.003671	0.000012	20322	-4.1	3.3	98.3	4.1566E-04
USGS35-NaNO3-NO2-100S@1_3	0.003619	0.000012	21585	-18.2	3.2	98.3	4.4219E-04
USGS35-NaNO3-NO2-100S@1_4	0.003615	0.000012	21711	-19.3	3.2	98.3	4.4486E-04
USGS35-NaNO3-NO2-100S@1_5	0.003622	0.000014	15110	-17.4	3.8	98.3	3.0911E-04
USGS35-NaNO3-NO2-100S@1_6	0.003649	0.000015	13166	-10.0	4.1	98.3	2.6914E-04
USGS35-NaNO3-NO2-100S@1_7	0.003657	0.000014	14538	-7.9	3.9	98.3	2.9772E-04
USGS35-NaNO3-NO2-100S@1_8	0.003647	0.000014	16156	-10.6	3.7	98.3	3.3200E-04
USGS35-NANO3-NO2-100S@2_1	0.003642	0.000007	68009	-11.9	1.8	98.3	1.5064E-03
USGS35-NANO3-NO2-100S@2_2	0.003640	0.000007	66284	-12.5	1.8	98.3	1.4560E-03
USGS35-NANO3-NO2-100S@2_3	0.003648	0.000006	71194	-10.3	1.8	98.3	1.5450E-03
USGS35-NANO3-NO2-100S@2_4	0.003641	0.000006	72920	-12.2	1.7	98.3	1.5648E-03
USGS35-NANO3-NO2-100S@2_5	0.003642	0.000007	69529	-11.9	1.8	98.3	1.6937E-03
USGS35-NANO3-NO2-100S@2_6	0.003628	0.000006	72145	-15.7	1.7	98.3	1.7385E-03
USGS35-NANO3-NO2-100S@2_7	0.003643	0.000006	76671	-11.7	1.7	98.3	1.5586E-03
USGS35-NANO3-NO2-100S@2_8	0.003653	0.000006	79928	-9.0	1.7	98.3	1.6260E-03
October 2013 <SampleName: In-house NaNO3> <Raster:5.0>							
InHouse-NaNO3-NO2-100S@1_1	0.003709	0.000007	67485	-7.5	1.8	98.3	1.3843E-03
InHouse-NaNO3-NO2-100S@1_2	0.003703	0.000007	60515	-9.1	1.9	98.3	1.2373E-03
InHouse-NaNO3-NO2-100S@1_3	0.003738	0.000007	62947	0.3	1.9	98.3	1.2831E-03
InHouse-NaNO3-NO2-100S@1_4	0.003704	0.000007	68097	-8.8	1.8	98.3	1.3826E-03
InHouse-NaNO3-NO2-100S@1_5	0.003706	0.000007	70262	-8.3	1.8	98.3	1.4232E-03
InHouse-NaNO3-NO2-100S@1_6	0.003710	0.000006	74710	-7.2	1.7	98.3	1.5120E-03
InHouse-NaNO3-NO2-100S@1_7	0.003698	0.000006	71858	-10.4	1.7	98.3	1.4517E-03

Analysis no.	$n(^{15}N^{16}O_2^-)$ / $n(^{14}N^{16}O_2^-)$	1 σ	ion $^{14}N^{16}O_2^-$ (cps)	IMF (‰)	1 σ	Pre - sputtering Time (s)	$n(^{14}N^{16}O_2^-)$ / $n(Cs^+)$
InHouse-NaNO3-NO2-100S@1_8	0.003682	0.000006	73608	-14.7	1.7	98.3	1.4886E-03
InHouse-NaNO3-NO2-100S@1_9	0.003684	0.000006	73509	-14.2	1.7	98.3	1.4837E-03
InHouse-NaNO3-NO2-100S@1_10	0.003724	0.000007	69529	-3.5	1.8	98.3	1.4034E-03
InHouse-NaNO3-NO2-100S@1_11	0.003714	0.000007	67746	-6.2	1.8	98.3	1.3681E-03
InHouse-NaNO3-NO2-100S@1_12	0.003690	0.000007	70913	-12.6	1.7	98.3	1.4346E-03
InHouse-NaNO3-NO2-100S@1_13	0.003692	0.000006	75629	-12.0	1.7	98.3	1.5333E-03
InHouse-NaNO3-NO2-100S@1_14	0.003707	0.000006	79705	-8.0	1.6	98.3	1.6209E-03
InHouse-NaNO3-NO2-100S@1_15	0.003687	0.000006	73214	-13.4	1.7	98.3	1.4862E-03
InHouse-NaNO3-NO2-100S@1_16	0.003691	0.000006	71858	-12.3	1.7	98.3	1.4582E-03
AP1-InHouse-KNO3-NO2-100S@1_1	0.003634	0.000009	37297	-27.6	2.4	98.3	7.4289E-04
AP1-InHouse-KNO3-NO2-100S@1_2	0.003653	0.000007	54635	-22.5	2.0	98.3	1.0788E-03
AP1-InHouse-KNO3-NO2-100S@1_3	0.003654	0.000007	54132	-22.2	2.0	98.3	1.0649E-03
AP1-InHouse-KNO3-NO2-100S@1_4	0.003640	0.000008	42325	-26.0	2.2	98.3	8.3701E-04
AP1-InHouse-KNO3-NO2-100S@1_5	0.003639	0.000008	44014	-26.2	2.2	98.3	8.7591E-04
AP1-InHouse-KNO3-NO2-100S@1_6	0.003645	0.000008	41474	-24.6	2.3	98.3	8.2697E-04
AP1-InHouse-KNO3-NO2-100S@1_7	0.003641	0.000009	40935	-25.7	2.3	98.3	8.1637E-04
AP1-InHouse-KNO3-NO2-100S@1_8	0.003640	0.000008	42804	-26.0	2.2	98.3	8.5377E-04
AP1-InHouse-KNO3-NO2-100S@1_9	0.003643	0.000008	42672	-25.2	2.2	98.3	8.4876E-04
AP1-InHouse-KNO3-NO2-100S@1_10	0.003643	0.000008	44944	-25.2	2.2	98.3	8.9067E-04
December 2013 <SampleName: IAEA-NO-3> <Raster:5.0>							
IAEA-NaNO3-100s@1_1	0.003672	0.000008	41727	-5.7	2.3	98.3	9.5807E-04
IAEA-NaNO3-100s@1_2	0.003627	0.000008	42672	-17.9	2.3	98.3	9.8018E-04
IAEA-NaNO3-100s@1_3	0.003628	0.000008	48337	-17.6	2.1	98.3	1.1101E-03
IAEA-NaNO3-100s@1_4	0.003679	0.000008	43695	-3.8	2.2	98.3	1.0053E-03
IAEA-NaNO3-100s@1_5	0.003675	0.000008	44198	-4.9	2.2	98.3	1.0183E-03
IAEA-NaNO3-100s@1_6	0.003666	0.000009	36282	-7.3	2.5	98.3	8.3662E-04
IAEA-NaNO3-100s@1_7	0.003668	0.000010	32818	-6.8	2.6	98.3	7.5704E-04
IAEA-NaNO3-100s@1_8	0.003635	0.000008	43741	-15.7	2.2	98.3	1.0086E-03
IAEA-KNO3-1-150S@1_1	0.003681	0.000019	8354	-3.2	5.1	147.5	1.7593E-04
IAEA-KNO3-1-150S@1_2	0.003699	0.000022	6370	1.6	5.9	147.5	1.3477E-04
IAEA-KNO3-1-150S@1_3	0.003668	0.000020	7434	-6.8	5.4	147.5	1.5590E-04
IAEA-KNO3-1-150S@1_4	0.003692	0.000017	10178	-0.3	4.7	147.5	2.1125E-04
IAEA-KNO3-1-150S@1_5	0.003679	0.000017	9957	-3.8	4.7	147.5	2.0762E-04
IAEA-KNO3-1-150S@1_6	0.003653	0.000017	10817	-10.8	4.5	147.5	2.2659E-04
IAEA-KNO3-1-150S@1_7	0.003653	0.000016	11692	-10.8	4.3	147.5	2.4520E-04
IAEA-KNO3-1-150S@1_8	0.003671	0.000015	13714	-6.0	4.0	147.5	2.8786E-04
IAEA-KNO3-1-150S@1_9	0.003683	0.000015	13294	-2.7	4.1	147.5	2.7936E-04
IAEA-KNO3-1-150S@1_10	0.003694	0.000015	13471	0.3	4.1	147.5	2.8386E-04
IAEA-KNO3-1-150S@1_11	0.003654	0.000016	11488	-10.6	4.4	147.5	2.4262E-04
IAEA-KNO3-1-150S@1_12	0.003674	0.000021	6860	-5.1	5.7	147.5	1.4504E-04
December 2013 <SampleName: In-house NaNO3> <Raster:5.0>							

Analysis no.	$n(^{15}N^{16}O_2^-)$ / $n(^{14}N^{16}O_2^-)$	1 σ	ion $^{14}N^{16}O_2^-$ (cps)	IMF (‰)	1 σ	Pre - sputtering Time (s)	$n(^{14}N^{16}O_2^-)$ / $n(Cs^+)$
InHouse-NaNO3-1-150S@1_1	0.003712	0.000006	77842	-6.7	1.7	147.5	1.5636E-03
InHouse-NaNO3-1-150S@1_2	0.003720	0.000006	82217	-4.5	1.6	147.5	1.6568E-03
InHouse-NaNO3-1-150S@1_3	0.003704	0.000006	77306	-8.8	1.7	147.5	1.5687E-03
InHouse-NaNO3-1-150S@1_4	0.003711	0.000006	80040	-7.0	1.6	147.5	1.6353E-03
InHouse-NaNO3-1-150S@1_5	0.003718	0.000006	77627	-5.1	1.7	147.5	1.5958E-03
InHouse-NaNO3-1-150S@1_6	0.003706	0.000006	74106	-8.3	1.7	147.5	1.5311E-03
InHouse-NaNO3-1-150S@1_7	0.003717	0.000006	73509	-5.4	1.7	147.5	1.5269E-03
InHouse-NaNO3-1-150S@1_8	0.003705	0.000006	79260	-8.6	1.7	147.5	1.6548E-03
P2013Nov-InHouse-NaNO3-1-150S@1_1	0.003730	0.000007	58641	-1.9	1.9	147.5	1.2447E-03
P2013Nov-InHouse-NaNO3-1-150S@1_2	0.003744	0.000008	50854	1.9	2.1	147.5	1.0841E-03
P2013Nov-InHouse-NaNO3-1-150S@1_3	0.003732	0.000007	57530	-1.3	1.9	147.5	1.2289E-03
P2013Nov-InHouse-NaNO3-1-150S@1_4	0.003723	0.000008	52965	-3.7	2.0	147.5	1.1331E-03
P2013Nov-InHouse-NaNO3-1-150S@1_5	0.003728	0.000007	55080	-2.4	2.0	147.5	1.1793E-03
P2013Nov-InHouse-NaNO3-1-150S@1_6	0.003735	0.000008	53574	-0.5	2.0	147.5	1.1492E-03
P2013Nov-InHouse-NaNO3-1-150S@1_7	0.003733	0.000007	64624	-1.1	1.8	147.5	1.3896E-03
P2013Nov-InHouse-NaNO3-1-150S@1_8	0.003742	0.000007	59208	1.3	1.9	147.5	1.2715E-03
P2013Nov-InHouse-NaNO3-1-150S@1_9	0.003746	0.000006	78930	2.4	1.7	147.5	1.6972E-03
P2013Nov-InHouse-NaNO3-1-150S@1_10	0.003749	0.000007	67398	3.2	1.8	147.5	1.4637E-03
P2013Nov-InHouse-NaNO3-1-150S@1_11	0.003742	0.000007	68808	1.3	1.8	147.5	1.5021E-03
P2013Nov-InHouse-NaNO3-1-150S@1_12	0.003735	0.000007	60589	-0.5	1.9	147.5	1.3301E-03
P2013Nov-InHouse-NaNO3-1-150S@1_13	0.003734	0.000007	61789	-0.8	1.9	147.5	1.3572E-03
P2013Nov-InHouse-NaNO3-1-150S@1_14	0.003721	0.000007	61561	-4.3	1.9	147.5	1.3478E-03
P2013Nov-InHouse-NaNO3-1-150S@1_15	0.003727	0.000007	64138	-2.7	1.8	147.5	1.4028E-03
P2013Nov-InHouse-NaNO3-1-150S@2_1	0.003720	0.000010	33085	-4.5	2.6	147.5	7.3324E-04
P2013Nov-InHouse-NaNO3-1-150S@2_2	0.003745	0.000009	33936	2.1	2.5	147.5	7.5669E-04
P2013Nov-InHouse-NaNO3-1-150S@2_3	0.003734	0.000010	29149	-0.8	2.7	147.5	6.5277E-04

Analysis no.	$n(^{15}N^{16}O_2^-)$ / $n(^{14}N^{16}O_2^-)$	1 σ	ion $^{14}N^{16}O_2^-$ (cps)	IMF (‰)	1 σ	Pre - sputtering Time (s)	$n(^{14}N^{16}O_2^-)$ / $n(Cs^+)$
P2013Nov-InHouse-NaNO3-1-150S@2_4	0.003731	0.000010	32008	-1.6	2.6	147.5	7.2135E-04
P2013Nov-InHouse-NaNO3-1-150S@2_6	0.003732	0.000009	35841	-1.3	2.5	147.5	8.1225E-04
P2013Nov-InHouse-NaNO3-1-150S@2_7	0.003738	0.000010	32583	0.3	2.6	147.5	7.3945E-04
P2013Nov-InHouse-NaNO3-1-150S@2_8	0.003725	0.000009	40487	-3.2	2.3	147.5	9.2475E-04

C Details of all analysis spots on aerosol-like mixture standards, isotope ratio measured by $^{15}N^{16}O_2^-$ / $^{14}N^{16}O_2^-$

Analysis no.	$^{16}O^-$ (cps)	$^{12}C^{14}N^-$ (cps)	$^{14}N^{16}O_2^-$ (cps)	n($^{15}N^{16}O_2^-$) / n($^{14}N^{16}O_2^-$)	1 σ	f*	f
Nuclepore filter, potassium nitrate + glucose							
Mask level 0 %							
2014January_9	110518	13833	61249	0.003655	0.000006	0.357	0.816
2014January_10	89551	17341	61663	0.003642	0.000006	0.408	0.781
2014January_14	51782	9374	29262	0.003645	0.000008	0.361	0.757
2014January_15	55863	11431	33535	0.003645	0.000008	0.375	0.746
AE-19-4-uncle-75p-no2@1_2	21484	6925	7538	0.003595	0.000016	0.260	0.521
AE-19-4-uncle-75p-no2@1_3	33226	8204	10277	0.003582	0.000014	0.236	0.556
AE-19-3-uncle-75p-NO2@1_1	48430	10323	13277	0.003564	0.000012	0.215	0.563
AE-19-3-uncle-75p-NO2@1_2	62923	10875	18446	0.003588	0.000010	0.227	0.629
AE-19-3-uncle-75p-NO2@1_3	46451	10548	14141	0.003602	0.000012	0.233	0.573
AE-19-3-uncle-75p-NO2@1_4	46331	9348	14252	0.003633	0.000012	0.235	0.604
AE-19-3-uncle-75p-NO2@1_5	50737	9428	15637	0.003610	0.000011	0.236	0.624
AE-19-3-uncle-75p-NO2@1_6	33221	8942	9775	0.003594	0.000014	0.227	0.522
AE-19-3-uncle-75p-NO2@1_7	87641	13741	22393	0.003626	0.000009	0.204	0.620
AE-19-3-uncle-75p-NO2@1_8	44091	9333	11406	0.003618	0.000013	0.206	0.550
Mask level 10 %							
2014January_9	111799	13889	61884	0.003655	0.000006	0.356	0.817
2014January_10	90278	17396	62133	0.003642	0.000006	0.408	0.781
2014January_14	66343	10007	36231	0.003646	0.000009	0.353	0.784
2014January_15	59832	11640	35749	0.003647	0.000008	0.374	0.754
AE-19-4-uncle-75p-no2@1_2	65341	10311	24775	0.003609	0.000017	0.275	0.706
AE-19-4-uncle-75p-no2@1_3	77560	11790	24230	0.003583	0.000014	0.238	0.673
AE-19-3-uncle-75p-NO2@1_1	121918	16931	33116	0.003573	0.000013	0.214	0.662
AE-19-3-uncle-75p-NO2@1_2	126901	15523	37044	0.003594	0.000011	0.226	0.705
AE-19-3-uncle-75p-NO2@1_3	101820	15702	30844	0.003605	0.000012	0.232	0.663
AE-19-3-uncle-75p-NO2@1_4	118133	14784	36898	0.003639	0.000012	0.238	0.714
AE-19-3-uncle-75p-NO2@1_5	112657	13405	34380	0.003622	0.000012	0.234	0.719
AE-19-3-uncle-75p-NO2@1_6	99454	14518	30185	0.003609	0.000015	0.233	0.675
AE-19-3-uncle-75p-NO2@1_7	134211	17278	34104	0.003627	0.000009	0.203	0.664
AE-19-3-uncle-75p-NO2@1_8	116090	14749	30311	0.003620	0.000014	0.207	0.673
Mask level 20 %							
2014January_9	126761	14411	68540	0.003658	0.000006	0.351	0.826
2014January_10	102585	18137	69268	0.003642	0.000006	0.403	0.792
2014January_14	116017	11378	55978	0.003654	0.000011	0.325	0.831

Analysis no.	$^{16}O^-$ (cps)	$^{12}C^{14}N^-$ (cps)	$^{14}N^{16}O_2^-$ (cps)	$n(^{15}N^{16}O_2^-) / n(^{14}N^{16}O_2^-)$	1 σ	f*	f
2014January_15	76380	12351	43950	0.003647	0.000008	0.365	0.781
AE-19-4-uncle-75p-no2@1_2	86759	11575	32583	0.003615	0.000019	0.273	0.738
AE-19-4-uncle-75p-no2@1_3	98088	13056	29896	0.003585	0.000015	0.234	0.696
AE-19-3-uncle-75p-NO2@1_1	152715	18419	40290	0.003570	0.000014	0.209	0.686
AE-19-3-uncle-75p-NO2@1_2	152358	16850	43529	0.003592	0.000011	0.222	0.721
AE-19-3-uncle-75p-NO2@1_3	130471	17871	38126	0.003607	0.000013	0.226	0.681
AE-19-3-uncle-75p-NO2@1_4	144038	16191	44266	0.003640	0.000013	0.235	0.732
AE-19-3-uncle-75p-NO2@1_5	141831	14591	42176	0.003623	0.000012	0.229	0.743
AE-19-3-uncle-75p-NO2@1_6	136586	16984	40063	0.003610	0.000017	0.227	0.702
AE-19-3-uncle-75p-NO2@1_7	155937	18555	38909	0.003631	0.000010	0.200	0.677
AE-19-3-uncle-75p-NO2@1_8	151583	16694	38412	0.003627	0.000015	0.202	0.697
Mask level 30 %							
2014January_9	157163	14924	80442	0.003663	0.000006	0.339	0.844
2014January_10	128354	18997	82803	0.003645	0.000007	0.392	0.813
2014January_14	165376	11697	74519	0.003662	0.000015	0.311	0.864
2014January_15	104447	13148	55799	0.003647	0.000009	0.348	0.809
AE-19-4-uncle-75p-no2@1_2	104753	12470	39031	0.003601	0.000020	0.271	0.758
AE-19-4-uncle-75p-no2@1_3	115332	14057	33973	0.003583	0.000016	0.228	0.707
AE-19-3-uncle-75p-NO2@1_1	179248	18824	46269	0.003569	0.000015	0.205	0.711
AE-19-3-uncle-75p-NO2@1_2	173337	17546	48263	0.003592	0.000011	0.218	0.733
AE-19-3-uncle-75p-NO2@1_3	151809	18713	42698	0.003604	0.000014	0.220	0.695
AE-19-3-uncle-75p-NO2@1_4	163270	16752	49110	0.003646	0.000013	0.231	0.746
AE-19-3-uncle-75p-NO2@1_5	165099	15167	47748	0.003635	0.000013	0.224	0.759
AE-19-3-uncle-75p-NO2@1_6	162731	18466	46522	0.003611	0.000018	0.222	0.716
AE-19-3-uncle-75p-NO2@1_7	170889	19174	41805	0.003630	0.000010	0.197	0.686
AE-19-3-uncle-75p-NO2@1_8	176473	17496	43358	0.003627	0.000015	0.197	0.712
Silicon wafer, potassium nitrate + glucose							
Mask level 0 %							
2013November_15		33364	6282	0.004074	0.000013		0.158
2013November_16		31632	6788	0.004068	0.000012		0.176
AE-19-SW-3-20um-512pix@1_1		15239	23414	0.003814	0.000007		0.607
AE-19-SW-3-20um-512pix@1_2		11428	12832	0.003854	0.000009		0.530
AE-19-SW-4-20um-150s@1_1		5321	9878	0.003828	0.000010		0.650
AE-19-SW-4-20um-150s@1_2		10775	25250	0.003785	0.000006		0.702
AE-19-SW-5-20um-150s@1_1		2808	11150	0.003797	0.000009		0.799
AE-19-SW-5-20um-150s@1_2		3090	10727	0.003814	0.000010		0.777
AE-19-SW-6-20um-512@1_1		296	22463	0.003878	0.000007		0.987
AE-19-SW-6-20um-512@1_2		282	15340	0.003909	0.000008		0.982
AE-19-SW-6-20um-512@1_3		255	18769	0.003838	0.000007		0.987

Analysis no.	$^{16}O^-$ (cps)	$^{12}C^{14}N^-$ (cps)	$^{14}N^{16}O_2^-$ (cps)	$n(^{15}N^{16}O_2^-) / n(^{14}N^{16}O_2^-)$	1 σ	f*	f
Mask level 10 %							
2013November_15		79914	34661	0.003701	0.000014		0.302
2013November_16		104403	35853	0.003730	0.000013		0.255
AE-19-SW-3-20um-512pix@1_1		33976	71827	0.003730	0.000007		0.680
AE-19-SW-3-20um-512pix@1_2		39569	74571	0.003721	0.000009		0.654
AE-19-SW-4-20um-150s@1_1		18339	61554	0.003707	0.000011		0.771
AE-19-SW-4-20um-150s@1_2		22908	79344	0.003711	0.000006		0.777
AE-19-SW-5-20um-150s@1_1		8056	51002	0.003739	0.000010		0.864
AE-19-SW-5-20um-150s@1_2		8041	54377	0.003724	0.000010		0.871
AE-19-SW-6-20um-512@1_1		477	156079	0.003747	0.000007		0.997
AE-19-SW-6-20um-512@1_2		598	113741	0.003775	0.000008		0.995
AE-19-SW-6-20um-512@1_3		467	130520	0.003737	0.000008		0.996
Mask level 20 %							
2013November_15		75124	49932	0.003675	0.000015		0.399
2013November_16		95357	57345	0.003674	0.000015		0.375
AE-19-SW-3-20um-512pix@1_1		44567	104796	0.003716	0.000007		0.702
AE-19-SW-3-20um-512pix@1_2		53030	107737	0.003697	0.000010		0.671
AE-19-SW-4-20um-150s@1_1		23869	97955	0.003697	0.000013		0.804
AE-19-SW-4-20um-150s@1_2		29326	123381	0.003691	0.000007		0.808
AE-19-SW-5-20um-150s@1_1		11512	92150	0.003734	0.000012		0.889
AE-19-SW-5-20um-150s@1_2		10146	94644	0.003721	0.000012		0.903
AE-19-SW-6-20um-512@1_1		547	237240	0.003745	0.000009		0.998
AE-19-SW-6-20um-512@1_2		658	183328	0.003758	0.000010		0.996
AE-19-SW-6-20um-512@1_3		523	220896	0.003738	0.000009		0.998
Mask level 30 %							
2013November_15		69641	62210	0.003651	0.000018		0.472
2013November_16		80155	75364	0.003658	0.000019		0.485
AE-19-SW-3-20um-512pix@1_1		53206	136231	0.003703	0.000009		0.720
AE-19-SW-3-20um-512pix@1_2		65790	134737	0.003683	0.000013		0.672
AE-19-SW-4-20um-150s@1_1		27395	125743	0.003687	0.000015		0.821
AE-19-SW-4-20um-150s@1_2		32960	156720	0.003682	0.000009		0.827
AE-19-SW-5-20um-150s@1_1		15157	154115	0.003722	0.000015		0.911
AE-19-SW-5-20um-150s@1_2		11679	144149	0.003713	0.000014		0.925
AE-19-SW-6-20um-512@1_1		602	305583	0.003749	0.000010		0.998
AE-19-SW-6-20um-512@1_2		659	245370	0.003755	0.000011		0.997
AE-19-SW-6-20um-512@1_3		561	293696	0.003745	0.000010		0.998

APPENDIX C

Analysis no.	$^{16}O^-$ (cps)	$^{12}C^{14}N^-$ (cps)	$^{14}N^{16}O_2^-$ (cps)	$n(^{15}N^{16}O_2^-) / n(^{14}N^{16}O_2^-)$	1 σ	f*	f
Carbon caot bulk samples, potassium nitrate							
Mask level 0 %							
carbon-IAEA-150planes@1_1	471644	23925	17930	0.003659	0.000006	0.037	0.428
carbon-IAEA-150planes@1_2	455386	25059	18427	0.003685	0.000006	0.039	0.424
carbon-IAEA-150planes@1_3	396223	23145	22106	0.003700	0.000006	0.053	0.489
carbon-IAEA-150planes@1_4	186462	13797	18484	0.003732	0.000006	0.090	0.573
Mask level 10 %							
carbon-IAEA-150planes@1_1	630756	18415	31825	0.003655	0.000007	0.048	0.633
carbon-IAEA-150planes@1_2	623693	17493	33053	0.003677	0.000007	0.050	0.654
carbon-IAEA-150planes@1_3	520212	15861	34289	0.003697	0.000006	0.062	0.684
carbon-IAEA-150planes@1_4	252764	11204	30654	0.003728	0.000007	0.108	0.732
Mask level 20 %							
carbon-IAEA-150planes@1_1	721472	25068	45017	0.003657	0.000008	0.059	0.642
carbon-IAEA-150planes@1_2	731410	26988	48394	0.003684	0.000008	0.062	0.642
carbon-IAEA-150planes@1_3	617608	22726	50636	0.003700	0.000007	0.076	0.690
carbon-IAEA-150planes@1_4	291225	15131	43242	0.003736	0.000008	0.129	0.741
Mask level 30 %							
carbon-IAEA-150planes@1_1	791425	32220	57418	0.003671	0.000010	0.068	0.641
carbon-IAEA-150planes@1_2	795577	35819	61260	0.003687	0.000010	0.071	0.631
carbon-IAEA-150planes@1_3	658070	30125	64028	0.003703	0.000009	0.089	0.680
carbon-IAEA-150planes@1_4	310969	19195	53612	0.003730	0.000009	0.147	0.737

D Details of all analysis spots on aerosol-like mixture standards, isotope ratio measured by $^{12}C^{15}N^-$ / $^{12}C^{14}N^-$

Analysis no.	ion $^{12}C^{14}N^-$ (cps)	n($^{12}C^{15}N^-$) / n($^{12}C^{14}N^-$)	1 σ	ion $^{14}N^{16}O_2^-$ (cps)	f
Nuclepore filter, sodium nitrate + glucose					
Mask level 0 %					
February2015_31	3309	0.003667	0.000027	8111	0.710
February2015_32	4259	0.003639	0.000024	9360	0.687
February2015_33	4703	0.003602	0.000023	10340	0.687
February2015_38@1_1	3287	0.003637	0.000014	6037	0.647
February2015_38@1_2	387	0.003551	0.000040	244	0.387
February2015_38@1_3	2756	0.003641	0.000015	4089	0.597
February2015_38@1_4	4370	0.003624	0.000012	6845	0.610
February2015_38@1_5	4045	0.003617	0.000012	4723	0.539
February2015_38@1_6	3787	0.003630	0.000013	5363	0.586
February2015_38@1_7	5408	0.003652	0.000011	6256	0.536
February2015_40@1_3	2524	0.003649	0.000016	328	0.115
February2015_40@1_4	2946	0.003635	0.000014	127	0.041
February2015_40@1_5	3610	0.003648	0.000013	192	0.051
February2015_40@1_6	3133	0.003634	0.000014	129	0.039
Mask level 10 %					
February2015_31	3459	0.003667	0.000032	10941	0.760
February2015_32	4319	0.003624	0.000027	11832	0.733
February2015_33	4994	0.003588	0.000025	13239	0.726
February2015_37@1_5	5875	0.003587	0.000073	549	0.085
February2015_38@1_1	3869	0.003636	0.000017	10698	0.734
February2015_38@1_3	2847	0.003639	0.000026	10930	0.793
February2015_38@1_4	4917	0.003615	0.000015	12128	0.711
February2015_38@1_5	4598	0.003620	0.000018	9823	0.681
February2015_38@1_6	4233	0.003607	0.000018	11401	0.729
February2015_38@1_7	5948	0.003659	0.000016	13145	0.688
February2015_40@1_1	2850	0.003680	0.000040	422	0.129
February2015_40@1_3	2928	0.003719	0.000065	5605	0.657
February2015_40@1_4	3774	0.003619	0.000031	597	0.137
February2015_40@1_5	3781	0.003626	0.000039	1190	0.239
February2015_40@1_6	3676	0.003575	0.000040	846	0.187
Mask level 20 %					
February2015_31	3440	0.003637	0.000036	13123	0.792
February2015_32	4194	0.003630	0.000030	13609	0.764

Analysis no.	ion $^{12}C^{14}N^-$ (cps)	$n(^{12}C^{15}N^-) / n(^{12}C^{14}N^-)$	1 σ	ion $^{14}N^{16}O_2^-$ (cps)	f
February2015_33	4960	0.003613	0.000029	15637	0.759
February2015_38@1_1	4066	0.003635	0.000020	13674	0.771
February2015_38@1_3	2891	0.003640	0.000032	14588	0.835
February2015_38@1_4	5010	0.003611	0.000019	15866	0.760
February2015_38@1_5	4833	0.003626	0.000023	13817	0.741
February2015_38@1_6	4313	0.003612	0.000023	15123	0.778
February2015_38@1_7	5965	0.003669	0.000023	18529	0.756
Mask level 30 %					
February2015_31	3391	0.003623	0.000043	15622	0.822
February2015_32	3939	0.003636	0.000036	15723	0.800
February2015_33	4843	0.003615	0.000034	18503	0.793
February2015_38@1_1	4092	0.003634	0.000025	16750	0.804
February2015_38@1_3	2931	0.003636	0.000040	18033	0.860
February2015_38@1_4	4863	0.003633	0.000025	19516	0.801
February2015_38@1_5	4916	0.003640	0.000030	17509	0.781
February2015_38@1_6	4238	0.003617	0.000029	18764	0.816
February2015_38@1_7	5536	0.003647	0.000037	23625	0.810
Silicon wafer, sodimu nitrate + glucose					
Mask level 0 %					
February2015_7	31047	0.003683	0.000009	51	0.002
February2015_8	28748	0.003661	0.000009	79	0.003
February2015_9	20338	0.003668	0.000011	42	0.002
February2015_10	5147	0.003672	0.000022	6826	0.570
February2015_11	6636	0.003687	0.000019	3644	0.354
February2015_12	3723	0.003620	0.000013	691	0.156
February2015_12@1_1	4286	0.003650	0.000012	1025	0.193
February2015_12@1_2	3428	0.003640	0.000013	560	0.140
February2015_12@1_3	2144	0.003662	0.000017	255	0.106
February2015_12@1_4	3059	0.003596	0.000014	524	0.146
February2015_13	2525	0.003610	0.000031	2925	0.537
February2015_14	3475	0.003638	0.000027	5083	0.594
February2015_15	3595	0.003626	0.000026	2844	0.442
February2015_16	2140	0.003568	0.000034	4639	0.684
February2015_17	2989	0.003603	0.000029	4939	0.623
February2015_18	2978	0.003630	0.000029	4321	0.592
Mask level 10 %					
February2015_7	74268	0.003716	0.000025	313	0.004
February2015_8	67811	0.003711	0.000016	326	0.005
February2015_9	44932	0.003605	0.000018	136	0.003
February2015_10	3410	0.003702	0.000040	14843	0.813
February2015_11	5910	0.003756	0.000039	12079	0.671
February2015_12	8518	0.003635	0.000030	7846	0.479

Analysis no.	ion $^{12}C^{14}N^-$ (cps)	$n(^{12}C^{15}N^-) / n(^{12}C^{14}N^-)$	1 σ	ion $^{14}N^{16}O_2^-$ (cps)	f
February2015_12@1_1	9174	0.003654	0.000026	9662	0.513
February2015_12@1_2	9135	0.003653	0.000032	7821	0.461
February2015_12@1_3	5652	0.003693	0.000048	4754	0.457
February2015_12@1_4	4593	0.003575	0.000040	5770	0.557
February2015_13	4437	0.003653	0.000051	13271	0.749
February2015_14	4411	0.003652	0.000041	14680	0.769
February2015_15	5924	0.003708	0.000044	12521	0.679
February2015_16	2149	0.003591	0.000048	9261	0.812
February2015_17	3523	0.003593	0.000044	13532	0.793
February2015_18	3804	0.003540	0.000045	13351	0.778
Mask level 20 %					
February2015_7	80298	0.003730	0.000041	495	0.006
February2015_8	84412	0.003743	0.000026	551	0.006
February2015_9	57287	0.003700	0.000031	247	0.004
February2015_10	2727	0.003700	0.000048	16403	0.857
February2015_11	4703	0.003766	0.000048	14034	0.749
February2015_12	6229	0.003638	0.000044	10910	0.636
February2015_12@1_1	6896	0.003628	0.000036	12953	0.652
February2015_12@1_2	6805	0.003629	0.000045	10852	0.614
February2015_12@1_3	4742	0.003618	0.000069	7333	0.607
February2015_12@1_4	3561	0.003586	0.000059	7919	0.690
February2015_13	3771	0.003672	0.000059	14808	0.797
February2015_14	3809	0.003635	0.000047	16798	0.815
February2015_15	5092	0.003685	0.000050	13906	0.732
February2015_16	1895	0.003543	0.000056	10778	0.850
February2015_17	3068	0.003553	0.000051	15390	0.834
February2015_18	3449	0.003553	0.000053	16100	0.824
Mask level 30 %					
February2015_7	78844	0.003753	0.000057	573	0.007
February2015_8	84476	0.003699	0.000042	661	0.008
February2015_9	56952	0.003732	0.000046	334	0.006
February2015_10	2226	0.003678	0.000056	17855	0.889
February2015_11	3846	0.003791	0.000059	15954	0.806
February2015_12	4136	0.003646	0.000067	13112	0.760
February2015_12@1_1	4411	0.003617	0.000053	15514	0.779
February2015_12@1_2	4713	0.003546	0.000067	13350	0.739
February2015_12@1_3	3493	0.003565	0.000102	9831	0.738
February2015_12@1_4	2935	0.003623	0.000084	9551	0.765
February2015_13	3226	0.003736	0.000069	16505	0.837
February2015_14	3218	0.003664	0.000055	18512	0.852
February2015_15	4390	0.003701	0.000058	15330	0.777
February2015_16	1667	0.003543	0.000065	12191	0.880
February2015_17	2659	0.003581	0.000058	16798	0.863
February2015_18	3045	0.003542	0.000061	18122	0.856

Analysis no.	ion $^{12}C^{14}N^-$ (cps)	$n(^{12}C^{15}N^-) / n(^{12}C^{14}N^-)$	1 σ	ion $^{14}N^{16}O_2^-$ (cps)	f
Nuclepore filter, potassium nitrate + glucose					
Mask level 0 %					
2014January_34	11940	0.003582	0.000008	35547	0.749
2014January_35	10212	0.003614	0.000008	26323	0.721
2014January_36	10441	0.003598	0.000008	18003	0.633
2014January_38@1_1	12512	0.003590	0.000008	17454	0.582
2014January_38@1_2	15141	0.003615	0.000007	20928	0.580
Mask level 10 %					
2014January_34	12350	0.003581	0.000008	39067	0.760
2014January_35	11690	0.003607	0.000009	34295	0.746
2014January_36	13277	0.003587	0.000012	38795	0.745
2014January_38@1_1	17611	0.003596	0.000009	28091	0.614
2014January_38@1_2	18030	0.003615	0.000008	30969	0.632
Mask level 20 %					
2014January_34	13230	0.003577	0.000009	48269	0.785
2014January_35	13186	0.003604	0.000011	45968	0.777
2014January_36	14036	0.003584	0.000013	49279	0.778
2014January_38@1_1	19709	0.003596	0.000010	35719	0.644
2014January_38@1_2	19524	0.003614	0.000010	38806	0.665
Mask level 30 %					
2014January_34	13915	0.003573	0.000013	60640	0.813
2014January_35	14344	0.003607	0.000015	58918	0.804
2014January_36	14420	0.003579	0.000016	57513	0.800
2014January_38@1_1	19588	0.003591	0.000013	44082	0.692
2014January_38@1_2	19292	0.003611	0.000013	48117	0.714
Silicon wafer, potassium nitrate + glucose					
Mask level 0 %					
2013November_19	4012	0.003679	0.000010	17272	0.812
2013November_20	6045	0.003655	0.000012	24063	0.799
2013November_21	5608	0.003646	0.000011	19607	0.778
2013November_22	8158	0.003640	0.000009	12523	0.606
2013November_23	5898	0.003597	0.000011	9099	0.607
2013November_25	16189	0.003623	0.000007	4583	0.219
2013November_26	7423	0.003642	0.000010	1876	0.201
2013November_27	38210	0.003632	0.000004	635	0.016
2013November_28	39758	0.003640	0.000003	3766	0.085
AE-19-3-SW-20um-512pix@1_1	2506	0.003647	0.000013	1911	0.433
AE-19-3-SW-20um-512pix@1_2	6542	0.003669	0.000008	6897	0.513
AE-19-3-SW-20um-512pix@1_3	5347	0.003679	0.000009	3980	0.426

Analysis no.	ion $^{12}C^{14}N^-$ (cps)	$n(^{12}C^{15}N^-)$ / $n(^{12}C^{14}N^-)$	1 σ	ion $^{14}N^{16}O_2^-$ (cps)	f
Mask level 10 %					
2013November_19	7414	0.003674	0.000016	73082	0.908
2013November_20	12440	0.003628	0.000018	78324	0.863
2013November_21	12777	0.003612	0.000014	66555	0.839
2013November_22	21533	0.003647	0.000013	55586	0.721
2013November_23	14140	0.003585	0.000014	32264	0.695
2013November_25	55739	0.003621	0.000009	23654	0.296
2013November_26	26552	0.003613	0.000015	12039	0.311
2013November_27	128603	0.003664	0.000009	8854	0.063
2013November_28	124579	0.003645	0.000005	23351	0.156
AE-19-3-SW-20um-512pix@1_1	9289	0.003694	0.000024	13743	0.597
AE-19-3-SW-20um-512pix@1_2	23358	0.003654	0.000013	43546	0.651
AE-19-3-SW-20um-512pix@1_3	20164	0.003680	0.000014	24097	0.544
Mask level 20 %					
2013November_19	7925	0.003634	0.000025	122645	0.939
2013November_20	16845	0.003592	0.000029	154020	0.902
2013November_21	15487	0.003614	0.000018	104758	0.871
2013November_22	29460	0.003650	0.000018	93662	0.761
2013November_23	19906	0.003576	0.000017	51602	0.722
2013November_25	60453	0.003611	0.000013	38921	0.390
2013November_26	30336	0.003600	0.000026	23005	0.431
2013November_27	128821	0.003656	0.000012	12479	0.087
2013November_28	136628	0.003652	0.000006	31513	0.185
AE-19-3-SW-20um-512pix@1_1	12352	0.003612	0.000040	23362	0.654
AE-19-3-SW-20um-512pix@1_2	27575	0.003644	0.000021	69656	0.716
AE-19-3-SW-20um-512pix@1_3	24302	0.003654	0.000023	38161	0.611
Mask level 30 %					
2013November_19	8004	0.003628	0.000043	182966	0.958
2013November_20	20221	0.003613	0.000039	216351	0.915
2013November_21	15833	0.003586	0.000025	153125	0.906
2013November_22	33518	0.003640	0.000024	123655	0.787
2013November_23	26400	0.003599	0.000022	75915	0.742
2013November_25	62161	0.003589	0.000018	53536	0.462
2013November_26	28026	0.003542	0.000038	29774	0.515
2013November_27	127918	0.003664	0.000014	16353	0.112
2013November_28	144531	0.003655	0.000007	39217	0.211
AE-19-3-SW-20um-512pix@1_1	12882	0.003716	0.000068	28308	0.687
AE-19-3-SW-20um-512pix@1_2	29473	0.003683	0.000036	94997	0.763
AE-19-3-SW-20um-512pix@1_3	27262	0.003608	0.000037	50287	0.648